



# Contribution to electromagnetic energy harvesting for wireless autonomous devices

Yuwei Zhou

## ► To cite this version:

Yuwei Zhou. Contribution to electromagnetic energy harvesting for wireless autonomous devices. Engineering Sciences [physics]. UNIVERSITE DE NANTES, 2013. English. NNT : ED503-203 . tel-01104855

HAL Id: tel-01104855

<https://hal.science/tel-01104855>

Submitted on 19 Jan 2015

**HAL** is a multi-disciplinary open access archive for the deposit and dissemination of scientific research documents, whether they are published or not. The documents may come from teaching and research institutions in France or abroad, or from public or private research centers.

Public Domain

L'archive ouverte pluridisciplinaire **HAL**, est destinée au dépôt et à la diffusion de documents scientifiques de niveau recherche, publiés ou non, émanant des établissements d'enseignement et de recherche français ou étrangers, des laboratoires publics ou privés.

# Thèse de Doctorat

# Yuwei ZHOU

Mémoire présenté en vue de l'obtention  
**du grade de Docteur de l'Université de Nantes**  
Sous le label de l'Université Nantes Angers Le Mans

Discipline : Electronique  
Spécialité : Télécommunications  
Laboratoire : IETR UMR 6164

Soutenance le 31 octobre 2013

École doctorale Sciences et Technologies de l'Information et Mathématiques (STIM)  
Thèse N° ED503-203

## Contribution à la récupération de l'énergie électromagnétique ambiante pour les objets communicants autonomes

### JURY

Président :	<b>M. Benoit GIFFARD</b> , Professeur, Faculté des Sciences et Techniques, Université de Nantes
Rapporteurs :	<b>M. Jean Lou DUBARD</b> , Professeur, Université de Nice Sophia Antipolis
	<b>M. Fabien NDAGIJIMANA</b> , Professeur, INPG Grenoble
Examinateurs :	<b>M. Eduardo MOTTA-CRUZ</b> , Ingénieur/HDR, Bouygues Telecom, Nantes
Directeur de Thèse :	<b>M. Tchanguiz RAZBAN</b> , Professeur, Ecole polytechnique de l'université de Nantes
Co-encadrant :	<b>M. Bruno FROPIER</b> , Maître de Conférences, IUT de la Roche s/Yon



# *Acknowledgements*

One of the joys of completion is to look over the journey past and remember all the professors, friends, and family who have helped and supported me along this long but fulfilling road.

I would like to express my heartfelt gratitude to my supervisors, Professor Tchanguiz RAZBAN and Professor Bruno FROPPIER, for providing me with the opportunity to complete my PhD thesis at the University of Nantes. They are not only mentors but dear friends. They have been actively interested in my work and have always been available to advise me. I am grateful for their encouragement, patience, motivation, enthusiasm, and immense knowledge in the field of microwave passive components and RF circuit design, antennas and propagation, and their applications in wireless communications.

I also would like to thank the members of my PhD committee, Professor Jean Lou DUBARD, Professor Fabien NDAGIJIMANA, Professor Benoit GUIFFARD, and Professor Eduardo MOTTA-CRUZ, who have provided encouraging and constructive feedback. It is not an easy task to review a thesis. I am grateful for helping to shape and guide the direction of the work with their thoughtful and instructive comments.

For this thesis, some layout realisation and experiments are essential. I gratefully acknowledge the assistance of many colleagues at IETR and Polytech' Nantes, especially Guillaume LIRZIN and Marc BRUNET, for the fabrication and measurements.

In the process of layout design and modelization, I met some problems about circuit simulation. I sent my questions to Agilent EEsof EDA and received their valuable responses. So I thanks to the engineers in the department of Technical Support Engineer and Trainer, Franz KUSIDLO and Haim SPIEGEL, for offering suggestions on works in progress and their generous support.

I am thankful to my friends in the University of Nantes for all the great times that we have shared. And I would like to thank my old friends in China for the happiest memories in the past.

This last word of acknowledgement I have saved is for my family because of their love, support, and sacrifices. Without their selfless dedication, I would not

have been living a life in France. Owing to the studying experience abroad, I am on the way to make my dream come true.

# Contents

<b>Acknowledgements</b>	<b>i</b>
<b>List of Figures</b>	<b>vii</b>
<b>List of Tables</b>	<b>xv</b>
<b>1 Introduction</b>	<b>1</b>
1.1 Background of energy harvesting . . . . .	1
1.1.1 Thermoelectric generator . . . . .	2
1.1.2 Mechanical resonator . . . . .	2
1.1.3 Photovoltaic cell . . . . .	3
1.1.4 RF sensor . . . . .	3
1.1.5 Implantable or wearable sensor . . . . .	3
1.2 Motivation . . . . .	4
1.3 Preliminary analysis of rectifying process . . . . .	6
1.3.1 Rectifying principle . . . . .	7
1.3.2 Diode model . . . . .	12
1.3.3 Impact of diode parameters . . . . .	20
<b>2 State of The Art</b>	<b>29</b>
2.1 Configuration of rectennas . . . . .	29
2.2 From series diode rectifier to bridge rectifier . . . . .	31
2.3 Compact bridge rectifier with no via-hole connection . . . . .	32
2.4 Dual-diode rectenna with harmonic-rejecting design . . . . .	34
2.5 Stacked rectenna with radial stubs . . . . .	35
2.6 Circularly polarized rectenna with unbalanced circular slots . . . . .	37
2.7 Harmonic-rejecting circular-sector rectenna . . . . .	38
2.8 Rectifier with high Q resonators . . . . .	39
2.9 Spiral rectenna for surrounding energy harvesting . . . . .	40
2.10 Dual-frequency for energy harvesting at low power levels . . . . .	41
2.11 Conclusion of the art state . . . . .	42
<b>3 RF/DC Conversion</b>	<b>45</b>

---

3.1	Power range . . . . .	45
3.2	Design for high power levels . . . . .	47
3.2.1	Choice of the diode . . . . .	47
3.2.2	Choice of the load . . . . .	47
3.2.3	Realisation and measurement . . . . .	49
3.2.4	Analysis of matching circuits . . . . .	51
3.2.5	Sensitivity of the matching circuit . . . . .	55
3.3	Design for low power levels . . . . .	58
3.3.1	Choice of the diode and the load . . . . .	58
3.3.2	Design of matching circuits . . . . .	59
3.3.3	Comparison among different circuits . . . . .	65
3.3.4	Investigation in the simulation model . . . . .	67
3.4	Research to increase the efficiency . . . . .	71
3.4.1	Choice of lumped components . . . . .	71
3.4.2	Layout and realisation . . . . .	72
3.4.3	DC voltage and conversion efficiency . . . . .	73
3.5	Power management . . . . .	75
3.5.1	DC modelization . . . . .	75
3.5.2	MPPT . . . . .	79
3.6	Conclusion of the design of rectifying circuit . . . . .	80
<b>4</b>	<b>Antenna Design for Energy Harvesting</b>	<b>83</b>
4.1	Characteristics of antennas . . . . .	83
4.1.1	Microwave transmission equation . . . . .	83
4.1.2	Emitting antenna . . . . .	85
4.1.3	Description of the received power . . . . .	88
4.2	Patch antenna . . . . .	90
4.2.1	Dimension of the patch . . . . .	91
4.2.2	Impedance of the patch . . . . .	93
4.2.3	Frequency response of the patch . . . . .	95
4.2.4	Radiation patterns and gain . . . . .	95
4.3	Monopole antenna . . . . .	98
4.3.1	Prototype of the monopole . . . . .	99
4.3.2	Frequency response of the monopole . . . . .	100
4.3.3	Radiation patterns and gain . . . . .	101
4.4	Monopole with a shorting pin . . . . .	103
4.4.1	Prototype of the modified monopole . . . . .	104
4.4.2	Frequency response of the modified monopole . . . . .	105
4.4.3	Radiation patterns and gain . . . . .	105
4.4.4	Analysis of the received power . . . . .	108
4.5	Conclusion of the antenna design . . . . .	110
<b>5</b>	<b>Combination and Integration of Rectenna</b>	<b>113</b>
5.1	Design for high power levels . . . . .	113

5.1.1	Rectenna experiment . . . . .	113
5.1.2	Rectifying circuit with HSMS-2820 . . . . .	114
5.2	Design for low power levels . . . . .	117
5.2.1	Rectifying circuit with HSMS-2860 . . . . .	117
5.2.2	Measurement in an anechoic chamber . . . . .	118
5.3	Rectenna integration . . . . .	121
5.3.1	Integrated monopole rectenna: rectenna I . . . . .	122
5.3.2	Integration of DC loop: rectenna II . . . . .	123
5.3.3	Anechoic chamber experiment . . . . .	124
5.4	Rectenna with high efficiency . . . . .	127
5.4.1	Rectifying circuit with HSMS-2850 . . . . .	128
5.4.2	Integrated rectenna with HSMS-2850: rectenna III . . . . .	129
5.4.3	Integrated rectenna with new DC loop: rectenna IV . . . . .	130
5.4.4	DC voltage and equivalent efficiency . . . . .	131
5.5	Conclusion of rectenna design . . . . .	134
<b>6</b>	<b>Conclusion and Perspective</b>	<b>137</b>
6.1	Conclusion . . . . .	137
6.2	Perspective . . . . .	140
<b>Bibliography</b>		<b>143</b>
<b>Résumé en français</b>		<b>155</b>



# List of Figures

1.1	Schematic of the power harvesting system . . . . .	1
1.2	Equivalent model of Schottky diode without parasitic package . . . . .	7
1.3	Half-wave rectification . . . . .	10
1.4	Scheme of a rectifying circuit . . . . .	10
1.5	Prototype of a rectifying circuit with single serial diode . . . . .	11
1.6	Cross-section of Schottky diode . . . . .	12
1.7	Equivalent circuit model of diode chip . . . . .	12
1.8	Metal-semiconductor junction . . . . .	13
1.9	DC simulation of diode models . . . . .	17
1.10	Comparison of diode models in DC simulation . . . . .	17
1.11	Schematic current-voltage characteristic of Schottky diode HSMS-2860 . . . . .	18
1.12	S-parameter simulation of diode models: (a)Vendor model; (b)SPICE model; (c)SPICE model with package parasitics . . . . .	19
1.13	Comparison of diode models in S-parameter simulation . . . . .	19
1.14	Schematic of the simulated model considering zero-bias junction capacitance . . . . .	20
1.15	Efficiency comparison in terms of zero-bias junction capacitance . .	21
1.16	Schematic of the simulated model considering series ohmic resistance	22
1.17	Efficiency comparison in terms of series ohmic resistance . . . . .	22
1.18	Efficiency comparison in terms of saturation current . . . . .	23
1.19	Efficiency comparison in terms of junction potential . . . . .	23
1.20	Efficiency comparison in terms of emission coefficient . . . . .	24
1.21	Efficiency comparison in terms of grading coefficient . . . . .	24
1.22	Efficiency comparison in terms of breakdown voltage . . . . .	25
1.23	Efficiency comparison among Schottky diode HSMS-2810, HSMS-2820, HSMS-2850, and HSMS-2860 . . . . .	25
2.1	Topologies of rectennas . . . . .	30
2.2	Serial and bridge rectifiers designed by H. Takhedmit . . . . .	31
2.3	Compact bridge rectifier designed by H. Takhedmit . . . . .	32
2.4	Impedance schema of diodes $D_1-D_4$ . . . . .	33
2.5	Geometry of dual-diode rectenna (dimensions in mm) designed by H. Takhedmit . . . . .	34
2.6	Layout of the stacked rectenna designed by J. A. G. Akkermans . .	36

2.7	Antenna and rectifying circuit configuration and the photographs of proposed rectenna designed by T. C. Yo. Geometry parameters for the CP antenna are: W=60, L=60, R <sub>p</sub> =15.5, F <sub>r</sub> =6.5, d <sub>1</sub> =5.2, r <sub>1</sub> =5.2, d <sub>2</sub> =8.3, r <sub>2</sub> =2.3, h <sub>1</sub> =1.6, h <sub>1</sub> =0.8 (Dimension:mm) . . . . .	37
2.8	Schematic and photograph of doubler rectifier with 3rd harmonic rejection radial stub designed by T. C. Yo . . . . .	38
2.9	Rectenna with a microstrip circular-sector antenna designed by J. Y. Park . . . . .	39
2.10	Equivalent circuit with 24 MHz crystal resonator Q <sub>C</sub> and two HSMS-286x diodes from Agilent for the rectification, designed by T. Ungan . . . . .	39
2.11	Rectenna prototype with spiral antenna designed by D. Bouchouicha . . . . .	40
2.12	Dual-frequency rectenna designed by Z. Saddi . . . . .	41
3.1	Series diode circuit with matching circuit . . . . .	45
3.2	S parameters and efficiencies for given designs of different power levels . . . . .	46
3.3	Effective efficiency versus the transmitted power in terms of load resistance . . . . .	48
3.4	Input impedance of 10 dBm design versus the transmitted power . . . . .	48
3.5	Configuration of a rectifying circuit designed for 10 dBm . . . . .	49
3.6	Frequency response of a rectifying circuit designed for 10 dBm . . . . .	49
3.7	DC output voltage of 10 dBm design versus the input power . . . . .	50
3.8	Conversion efficiency of 10 dBm design versus the input power . . . . .	50
3.9	Scheme of single stub matching circuit . . . . .	52
3.10	Frequency response of circuits with single stub matched for 10 dBm . . . . .	52
3.11	Power response of circuits with single stub matched at 2.45 GHz . . . . .	52
3.12	S parameter variation of the design with single stub matching circuit . . . . .	53
3.13	Scheme of tapered line matching circuit . . . . .	53
3.14	Frequency response of circuits with tapered line matched for 10 dBm . . . . .	54
3.15	Power response of circuits with tapered line matched at 2.45 GHz . . . . .	54
3.16	S parameter variation of the design with tapered line matching circuit . . . . .	54
3.17	Fabricated rectifying circuits with some different details . . . . .	55
3.18	Frequency response simulated (red curve) and measured (blue curve) with more precise layouts . . . . .	56
3.19	Measured output DC voltage of 10 dBm design for precise layout . . . . .	57
3.20	Measured conversion efficiency of 10 dBm design for precise layout . . . . .	57
3.21	<i>design 1</i> : rectifying circuit with single stub matching circuit . . . . .	59
3.22	Return loss of a rectifying circuit with single stub . . . . .	60
3.23	Measured DC voltage of rectifying circuits with single stub: <i>design 1</i> forward diode (cyan curve); <i>design 1r</i> reverse diode (magenta curve) . . . . .	60
3.24	Measured conversion efficiency of rectifying circuits with single stub: <i>design 1</i> forward diode (cyan curve); <i>design 1r</i> reverse diode (magenta curve) . . . . .	61
3.25	<i>design 2</i> : rectifying circuit with radial stubs low pass filter . . . . .	61
3.26	Return loss of a rectifying circuit with radial stubs low pass filter . . . . .	62

3.27	Measured DC voltage of rectifying circuits with radial stubs low pass filter: <i>design 2</i> forward diode (black curve); <i>design 2r</i> reverse diode (red curve) . . . . .	63
3.28	Measured conversion efficiency of rectifying circuits with single stub: <i>design 2</i> forward diode (black curve); <i>design 2r</i> reverse diode (red curve) . . . . .	63
3.29	<i>design 3</i> : rectifying circuit with compact structure . . . . .	64
3.30	Return loss of a rectifying circuit with compact structure . . . . .	64
3.31	Measured DC voltage of rectifying circuits with compact structure: <i>design 3</i> forward diode (green curve); <i>design 3r</i> reverse diode (blue curve) . . . . .	65
3.32	Measured conversion efficiency of rectifying circuits with compact structure: <i>design 3</i> forward diode (green curve); <i>design 3r</i> reverse diode (blue curve) . . . . .	65
3.33	DC voltage comparison of rectifying circuit configurations . . . . .	66
3.34	Efficiency comparison of rectifying circuit configurations . . . . .	66
3.35	Configuration of a rectifying circuit designed for -20 dBm . . . . .	68
3.36	Post-simulated and measured return loss of the rectifying circuit designed for -20 dBm against the frequency . . . . .	69
3.37	Post-simulated and measured return loss of the rectifying circuit designed for -20 dBm against the input power . . . . .	69
3.38	Post-simulated and measured DC output voltage of the rectifying circuit . . . . .	70
3.39	Post-simulated and measured conversion efficiency of the rectifying circuit . . . . .	70
3.40	Configuration of a rectifying circuit with HSMS-2850 . . . . .	72
3.41	Simulated and measured frequency response of the rectifying circuit with HSMS-2850 . . . . .	72
3.42	Simulated and measured DC voltage of the rectifying circuit with HSMS-2850 . . . . .	73
3.43	Simulated and measured conversion efficiency of the rectifying circuit with HSMS-2850 . . . . .	74
3.44	Simulated conversion efficiency of the rectifying circuit with HSMS-2850 against the length of $L_3$ . . . . .	74
3.45	Simulated conversion efficiency of the rectifying circuit with HSMS-2850 against the load . . . . .	75
3.46	Single serial diode configuration of rectifying circuits . . . . .	75
3.47	Simulated DC current-voltage curves of diodes HSMS-2860 for different power levels . . . . .	76
3.48	Simulated efficiencies of diodes HSMS-2860 in terms of load resistances for different power levels . . . . .	77
3.49	Simulated DC current-voltage curves of diodes HSMS-2850 for different power levels . . . . .	78
3.50	Simulated efficiencies of diodes HSMS-2850 in terms of load resistances for different power levels . . . . .	78

---

4.1	Experimental set-up of an antenna . . . . .	83
4.2	Scheme of antenna measurements . . . . .	84
4.3	Emitting horn antenna . . . . .	85
4.4	Measured gain of the emitting horn antenna . . . . .	87
4.5	Power density versus range . . . . .	90
4.6	Microstrip patch antenna . . . . .	91
4.7	Top view of patch antenna . . . . .	92
4.8	Equivalent circuit of rectangular patch antenna . . . . .	93
4.9	Configuration of the patch . . . . .	94
4.10	Simulated and measured return loss of the patch . . . . .	95
4.11	Simulated radiation patterns of E-plane and H-plane in co-polarization (red line) and cross-polarization (green line) of the patch . . . . .	96
4.12	Measured radiation patterns of E-plane and H-plane in co-polarization (red line) and cross-polarization (green line) of the patch . . . . .	96
4.13	Radiation patterns of the patch with frequency sweep . . . . .	97
4.14	Simulated 3D gain of the patch . . . . .	98
4.15	Configuration of the monopole . . . . .	99
4.16	Simulated and measured return loss of the monopole . . . . .	100
4.17	Simulated (red line) and measured (blue line) radiation patterns of the monopole . . . . .	101
4.18	Radiation patterns of the monopole with frequency sweep . . . . .	102
4.19	Measured gain of the monopole . . . . .	103
4.20	Simulated 3D gain of the monopole . . . . .	103
4.21	Configuration of the monopole with a shorting pin . . . . .	104
4.22	Simulated and measured return loss of the monopole with a shorting pin . . . . .	105
4.23	Simulated (red line) and measured (blue line) radiation patterns of the monopole with a shorting pin . . . . .	106
4.24	Radiation patterns of the modified monopole with frequency sweep	107
4.25	Measured gain of the monopole with a shorting pin . . . . .	107
4.26	Simulated 3D gain of the monopole with a shorting pin . . . . .	108
4.27	Measured received power of the monopole with a shorting pin against the frequency . . . . .	109
4.28	Measured received power of the monopole with a shorting pin against the rotation angle . . . . .	109
5.1	Rectenna experiment set-up with a movable position . . . . .	113
5.2	Modified rectifying circuit with a patch antenna . . . . .	115
5.3	Output DC voltage of the rectenna integrated with a patch . . . . .	115
5.4	Conversion efficiency of the rectenna integrated with a patch . . . . .	116
5.5	Output DC voltage of the rectenna integrated with a patch against power densities . . . . .	116
5.6	Conversion efficiency of the rectenna integrated with a patch against power densities . . . . .	117
5.7	Experimental set-up of the rectifying circuit with the antenna . . . . .	118

5.8	Antenna shelf . . . . .	119
5.9	Vout comparison between the rectifying circuit and the circuit with the monopole . . . . .	119
5.10	Efficiency comparison between the rectifying circuit and the circuit with the monopole . . . . .	120
5.11	Output DC voltage of the rectifying circuit with the antenna against the rotation angle . . . . .	121
5.12	Conversion efficiency of the rectifying circuit with the antenna against the rotation angle . . . . .	121
5.13	Configuration of the rectenna I . . . . .	122
5.14	Configuration of the rectenna II . . . . .	124
5.15	Experimental set-up of a rectenna . . . . .	124
5.16	Measured DC voltage of the rectennas I and II against the power density at 0° . . . . .	125
5.17	Equivalent efficiency of the rectennas I and II against the power density at 0° . . . . .	125
5.18	Measured DC voltage of the rectennas I and II against the power density at -90° . . . . .	126
5.19	Equivalent efficiency of the rectennas I and II against the power density at -90° . . . . .	127
5.20	Rectifying circuit with HSMS-2850 connected with the modified monopole . . . . .	128
5.21	Configuration of the rectenna III . . . . .	129
5.22	Configuration of the rectenna IV . . . . .	130
5.23	Measured DC voltage of the rectennas III and IV against the power density at 0° . . . . .	131
5.24	Equivalent efficiency of the rectennas III and IV against the power density at 0° . . . . .	132
5.25	Equivalent efficiency of the rectennas III and IV against the incident power at 0° . . . . .	132
5.26	Measured DC voltage of the rectennas III and IV against the rota- tion angle . . . . .	133
5.27	Equivalent efficiency of the rectennas III and IV against the rotation angle . . . . .	133
6.1	Conversion efficiency of rectifying circuits in Epoxy and in Arlon . .	140
6.2	Conversion efficiency of circuits in Epoxy and in Arlon against the equivalent power density with 3 dBi antenna . . . . .	140
6.3	Schéma du système de récupération d'énergie . . . . .	155
6.4	Modèle électrique d'une diode Schottky avec les éléments parasites du boîtier . . . . .	158
6.5	Schéma d'un circuit de redressement . . . . .	161
6.6	Schéma d'un circuit redresseur de diode série . . . . .	162
6.7	Circuit de redressement pour les niveaux de puissance élevés . .	164

6.8	$S_{11}$ en fonction de la fréquence pour la conception de niveaux de puissance élevés . . . . .	164
6.9	Tension DC de sortie pour la conception de niveaux de puissance élevés . . . . .	165
6.10	Rendement mesuré et simulé pour la conception de niveaux de puissance élevés . . . . .	165
6.11	Circuit de redressement pour la conception de faibles niveaux de puissance . . . . .	166
6.12	$S_{11}$ en fonction de la fréquence pour la conception de faibles niveaux de puissance . . . . .	167
6.13	$S_{11}$ en fonction de la puissance pour la conception de faibles niveaux de puissance . . . . .	168
6.14	Tension DC de sortie pour la conception de faibles niveaux de puissance . . . . .	168
6.15	Rendement mesuré et simulé pour la conception de faibles niveaux de puissance . . . . .	169
6.16	Circuit de redressement pour la conception à haute efficacité . . . . .	170
6.17	$S_{11}$ en fonction de la fréquence pour la conception à haute efficacité	171
6.18	Tension DC de sortie pour la conception à haute efficacité . . . . .	171
6.19	Rendement mesuré et simulé pour la conception à haute efficacité .	172
6.20	Rendement simulé en fonction de la longueur $L3$ . . . . .	172
6.21	Rendement simulé en fonction de la résistance de charge . . . . .	173
6.22	Antenne patch rectangulaire . . . . .	174
6.23	$S_{11}$ en fonction de la fréquence pour l'antenne patch . . . . .	174
6.24	Les diagrammes de rayonnement simulés sur le plan E et sur le plan H en co-polarisation (courbe rouge) et en polarisation croisée (courbe verte) pour l'antenne patch . . . . .	175
6.25	Les diagrammes de rayonnement mesurés dans le plan E et dans le plan H en co-polarisation (courbe rouge) et en polarisation croisée (courbe verte) pour l'antenne patch . . . . .	176
6.26	Les diagrammes de rayonnement en fonction de la fréquence et de l'angle de rotation pour l'antenne patch . . . . .	176
6.27	Antenne monopôle . . . . .	177
6.28	$S_{11}$ simulé et mesuré d'antenne monopôle . . . . .	178
6.29	Les diagrammes de rayonnement simulés (courbe rouge) et mesurés (courbe bleue) d'antenne monopôle . . . . .	178
6.30	Les diagrammes de rayonnement en fonction de la fréquence et de l'angle de rotation pour l'antenne monopôle . . . . .	179
6.31	Gain mesuré de l'antenne monopôle . . . . .	180
6.32	Antenne monopôle court-circuitée . . . . .	180
6.33	$S_{11}$ simulé et mesuré d'antenne monopôle court-circuitée . . . . .	181
6.34	Les diagrammes de rayonnement simulés (courbe rouge) et mesurés (courbe bleue) d'antenne monopôle court-circuitée . . . . .	181
6.35	Les diagrammes de rayonnement en fonction de la fréquence et de l'angle de rotation pour l'antenne monopôle court-circuitée . . . . .	182

6.36 Gain mesuré de l'antenne monopôle court-circuitée . . . . .	183
6.37 Rectenna pour des niveaux de puissance élevés . . . . .	184
6.38 Montage expérimental de la rectenna avec une position mobile . . . . .	184
6.39 Tension DC de sortie de la rectenna pour les niveaux de puissance élevés . . . . .	185
6.40 Rendement mesuré et simulé de la rectenna pour les niveaux de puissance élevés . . . . .	185
6.41 Rectenna I pour les faibles niveaux de puissance . . . . .	186
6.42 Rectenna II pour les faibles niveaux de puissance . . . . .	187
6.43 Tension DC de sortie des rectennas I et II en fonction de la densité de puissance à 0° . . . . .	188
6.44 Rendement équivalent des rectennas I et II en fonction de la densité de puissance à 0° . . . . .	188
6.45 Tension DC de sortie des rectennas I et II en fonction de la densité de puissance à -90° . . . . .	189
6.46 Rendement équivalent des rectennas I et II en fonction de la densité de puissance à -90° . . . . .	190
6.47 Rectenna III à haute efficacité . . . . .	190
6.48 Rectenna IV à haute efficacité . . . . .	191
6.49 Tension DC de sortie des rectennas III et IV en fonction de la densité de puissance à 0° . . . . .	192
6.50 Rendement équivalent des rectennas III et IV en fonction de la densité de puissance à 0° . . . . .	193
6.51 Tension DC de sortie des rectennas III et IV en fonction de l'angle de rotation . . . . .	193
6.52 Rendement équivalent des rectennas III et IV en fonction de l'angle de rotation . . . . .	194



# List of Tables

1.1	Typical parameters of Schottky diode HSMS-28xx . . . . .	26
1.2	Typical parameters of other Schottky diodes . . . . .	27
2.1	Reference of rectenna design . . . . .	43
3.1	Comparison of rectifying circuits designed for 10 dBm . . . . .	58
3.2	Comparison of rectifying circuits designed for -20 dBm . . . . .	67
4.1	IDPH-2018 specifications . . . . .	86
5.1	Measured results of rectenna design . . . . .	135
6.1	Comparison of rectenna designs . . . . .	139
6.2	Les paramètres typiques des diodes Schottky de la série HSMS-28xx	160
6.3	Les résultats mesurés des rectennas . . . . .	194
6.4	Comparaison des rectennas . . . . .	196



*Dedicated to whom I love and who loves me, especially  
my parents...*



# Chapter 1

## Introduction

### 1.1 Background of energy harvesting

People have searched for some ways to obtain the energy from nature resources, such as thermal effect, mechanical vibration, photovoltaic cells, and electromagnetic energy receivers, as shown in Fig. 1.1. These methods have provided efficient and practical solutions to consumer, industrial, and military needs.

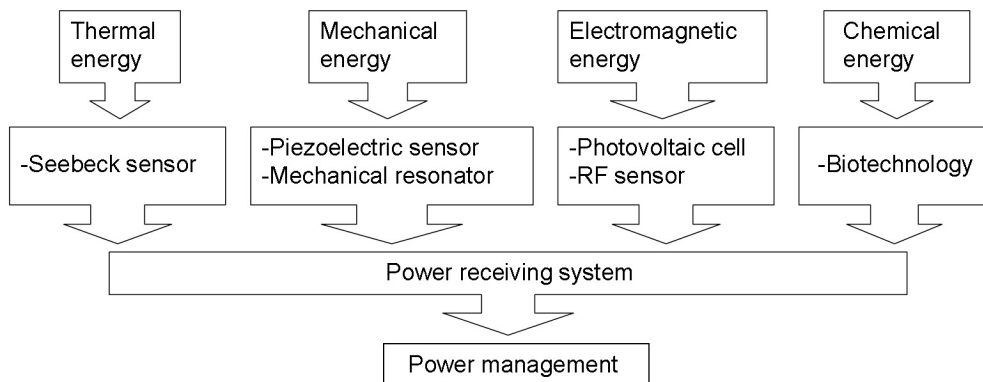


FIGURE 1.1: Schematic of the power harvesting system

The search for new energy harvesting devices is driven by sensor networks and green communications. The autonomous sensors exchange their data cooperatively through the network to a main location thanks to the technology of energy self-sufficiency at the terminals. The energy harvesting is needed to increase the lifetime of the sensor and to minimize the energy impact of the communication [1, 2].

### 1.1.1 Thermoelectric generator

Thermoelectric power generation presents many advantages including solid-state operation with no moving parts, long life-times, no emission of toxic gases, and high reliability [3]. The drawbacks of existing thermoelectric generators are low efficiency and large size. A new generation of nano-structured thermoelectric energy harvesters has been introduced by companies such as Micropelt offering the promise to greatly increase thermoelectric efficiency. As a result, there is new interest in the commercial field with automakers looking at thermoelectric as a replacement for alternators thereby improving fuel efficiency. In this scenario, the thermoelectric generator could be wrapped around a car's exhaust pipe to harvest the waste heat and produce electricity [4].

### 1.1.2 Mechanical resonator

Mechanical energy harvesting devices produce electricity from vibration, mechanical stress and strain of the surface sensor [5]. Mechanical vibrations cause the mass component to move and oscillate. This kinetic energy can be converted into electrical energy via an electromagnetic field, such as the strain on a piezoelectric material. Most vibration-powered systems rely on resonance to work, which implies there is a peak frequency and the system derives most of its energy at this frequency [6].

The main device in mechanical energy harvesting is the piezoelectric device. Piezoelectric energy harvesting converts mechanical energy to electrical energy by straining a piezoelectric material [7]. Strain or deformation in a piezoelectric material causes charge separation across the device, producing an electric field, and consequently a voltage drop proportional to the stress is applied. The oscillating system is typically a cantilever-beam structure with a mass at the unattached end of the lever, since it provides higher strain for a given input force. The voltage produced varies with time and strain, effectively producing an irregular AC signal. Piezoelectric energy conversion produces relatively higher voltage and power levels than the electromagnetic system [8].

Apart from piezoelectric sensors, mechanical energy harvesting can rely on natural sources from the environment such as wind and water flow. At large scale, windmills and turbines are well documented and can operate near the maximum

theoretical power. This is not the case for miniature devices which operate at a much higher speed [9].

### 1.1.3 Photovoltaic cell

Ambient light can be used by photovoltaic cells to produce electricity either indoors or outdoors. Photovoltaic energy conversion is considered to be a mature integrated circuit-compatible technology with potentially long life-times and higher output power levels than other energy-harvesting mechanisms [10]. Photovoltaic cells are exploited across a wide range of size scales area and power levels. The challenge is to conform to small surface area and its output power which strongly depends on environmental conditions, for example, on varying light intensity. Additionally, for different indoor light source, different emission spectra affect the conversion efficiency for a given apparent light level [11].

### 1.1.4 RF sensor

A large number of potential RF sources exist in metropolitan environments, such as broadcast radio and TV, mobile telephony, and wireless networks. It is beneficial to collect parts of these disparate sources and convert them into useful energy. The conversion of electromagnetic energy is based upon a special type of rectifying antenna which is used to directly convert microwave energy into DC electricity. This device can operate 24 hours per day and even in an embedded device. A simple rectenna can be constructed from a Schottky diode placed between antennas and loads. In laboratory environments, rectennas are highly efficient for converting microwave energy to DC electricity [12, 13]. However, the energy levels actually are so low that present electronic devices are difficult to be supplied [14].

### 1.1.5 Implantable or wearable sensor

The biological body moves and radiates heat continuously. For an instance, the human body at rest is emitting about 100 watts into the environment. It is possible to capture some of this energy by power wearable electronics. Two methods include active and passive energy harvesting methods. The active powering of

electronic devices takes place when the user of the electronic product is required to perform a specific task that they would not normally carry out. The passive powering of electronic devices harvests energy from everyday actions the user, such as walking, breathing, body heat, blood pressure, and finger motion [15].

While energy harvesting from human body may be useful as a supplemental power source, the current research in this field tries to combine existing techniques to create more efficient power generators. A number of efforts have been funded to harvest energy from leg and arm motion, shoe impacts, blood pressure for low level power, and implantable or wearable sensors [16, 17]. The need is to improve the energy generation capabilities of individual techniques.

## 1.2 Motivation

The technology of energy self-sufficiency has received an increasing attention in the field of power supplying for wireless devices [18]. Rectennas (Rectifying antennas) give a reliable way to increase the life-time of network sensors and to minimize the energy impact of wireless devices. A rectenna usually consists of a receiving antenna and a rectifying circuit. It is capable of capturing the microwave energy from surrounding environments and converting the electromagnetic energy into useful DC energy.

The existing designs of rectennas are mostly applicable with high conversion efficiency for high power levels at frequency bands of ISM (Industry, Scientific, and Medical) or GSM (Global System for Mobile) [19]. These rectennas participate in the application of microwave power transmission. First of all, DC electrical power is converted into RF power by power generators. The RF power is then transmitted through space to some distant point by antennas. Finally the power is collected and converted into DC power at the receiving point by rectennas [20].

The overall efficiency of energy transmission system is necessarily the product of the individual efficiencies associated with the energy emitting, receiving, and converting processes of the system. The usability depends upon efficient conversion technology as well as upon aperture-to-aperture transfer efficiency. The modern free-space power transmission needs to achieve the combined objectives of high efficiency, low cost, high reliability, and low mass at the transmitting and receiving ends of the system [21].

For example, an efficient rectenna based on a dual Schottky diodes converter and harmonic-rejecting configuration at 2.45 GHz exhibits an efficiency of 83 % at  $0.31 \text{ mW/cm}^2$  [22]. Another design is a CP (Circularly Polarized) high-gain high-efficiency rectenna array in a coplanar stripline circuit. Each antenna has CP gain of 11 dB and each rectenna element achieves RF-to-DC conversion efficiency of 81 % at 5.71 GHz [23].

However, high levels of power density are not available everywhere. In the field of power transmission from a base station, the attenuation of microwave energy is inevitable for a long distance. Besides, human activities exist at low power densities in respect of the health standard.

According to the ICNIRP (International Commission on Non-Ionizing Radiation Protection) exposure guidelines, power densities are limited to  $0.45 \text{ mW/cm}^2$  ( $41 \text{ V/m}$ ) at 900 MHz and  $0.9 \text{ mW/cm}^2$  ( $58 \text{ V/m}$ ) at 1.8 GHz for mobile phone base station frequencies, and  $1 \text{ mW/cm}^2$  ( $61 \text{ V/m}$ ) at the microwave oven frequency 2.45 GHz [24, 25]. Announced by WHO (World Health Organization), typical maximum public exposure levels are  $10 \mu\text{W/cm}^2$  ( $6 \text{ V/m}$ ) for TV and radio transmitters and for mobile phone base stations,  $20 \mu\text{W/cm}^2$  for radars, and  $50 \mu\text{W/cm}^2$  for microwave ovens [26]. The investigation of electric field in practical cases is between  $0.14 \text{ V/m}$  ( $5.2 \text{ nW/cm}^2$ ) and  $3 \text{ V/m}$  ( $2.4 \mu\text{W/cm}^2$ ) as shown in the COPIC newsletters and articles [27].

Under this condition, the device of power harvesting for low power levels is restricted by the diode behaviour. For an instance, the rectifier with a high Q crystal quartz resonator can achieve DC voltage 1 V and conversion efficiency more than 22 % for the power level -30 dBm but at a medium wave frequency 24 MHz [28]. Another example is a spiral rectenna with conversion efficiency 0.7 % at the power power density  $3.55 \text{ nW/cm}^2$  at 1.85 GHz [29]. All in all, the rectenna design succeeds in high efficiency at high power densities and low efficiency for low power levels. With the research of power density in an ambient environment, we found that in the aim of increasing the life-time of wireless devices without a specific RF beam, a rectenna with splendid efficiency at low power densities is necessary.

In this thesis, we present a study of Schottky diode rectenna for RF energy harvesting systems. The radiating part is a narrowband patch antenna or a broadband monopole antenna. Integrated with the antenna on a PCB (Printed Circuit

Board), rectifying circuits are proposed with single Schottky diode for RF-DC conversion. Matching circuits are optimised to improve the power at fundamental frequency transferring inside the diode and to reject harmonic signals. The parameters which determine the rectenna performance have been simulated in Agilent ADS (Advanced Design System) and Ansoft HFSS (High Frequency Structure Simulator).

Our rectennas can be used in point-to-point power transmission of high energy levels and power supplying far away from centralized power sources. Besides, these rectennas are suitable for power harvesting from surrounding environments at ISM frequencies, such as Wi-Fi, Bluetooth, and ZigBee networks. Batteries of wireless devices are recharged by rectennas which captures RF energy from ambient radiation sources at low power densities.

### **1.3 Preliminary analysis of rectifying process**

The rectenna was invented by W. C. Brown and has been used for various applications such as the microwave power helicopter and the receiving array for solar power satellites [30, 31]. It is one of the most important components in microwave power transmission system. The main objective of the rectenna design is to obtain high conversion efficiency. The first approach is to collect maximum RF power. The second one is to convert the captured energy into DC energy efficiently.

The key to improve RF-to-DC conversion efficiency is the rectifying circuit. The typical circuit includes a Schottky diode [32, 33], an input matching circuit, an output low pass filter, and a load resistor. The performance of the circuit is determined by the non-linear process of Schottky diodes, by the barrier losses, and by the series resistance loss [34–36]. It is difficult to predict the rectenna system optimized for the maximum conversion efficiency. Some theoretical methods have been studied to analyse the converting process in the time domain [37] and in the frequency domain.

### 1.3.1 Rectifying principle

The non-linear behaviour of Schottky diodes is performed due to two elements of the equivalent model, a junction resistance  $R_j$  and a junction capacitor  $C_d$ , as presented in Fig. 1.2. These two elements are non-linear, so as the series resistance  $R_s$ . But  $R_s$  is generally considered as linear resistance because of its small variation under forward bias [38].

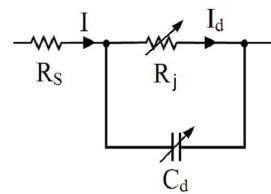


FIGURE 1.2: Equivalent model of Schottky diode without parasitic package

$C_d$  is the function of  $V_d$  which is the voltage at two ends of  $R_j$ .

$$C_d \propto V_d^{-1/2} \quad (1.1)$$

Suppose that the component  $V_d$  is driven by a RF power generator in form of a sinusoidal voltage and the phase shift is zero.

$$V_d = V_0 \cos(\omega t + \varphi) \xrightarrow{\varphi=0} V_d = V_0 \cos(\omega t) \quad (1.2)$$

where  $V_0$  is the maximum value of the sinusoidal voltage.

The current  $I_d$ , passing through the junction resistance  $R_j$ , is given as follows.

$$I_d = I_s (e^{\frac{qV_d}{NkT}} - 1) \quad (1.3)$$

where  $I_s$  is the saturation current (typically  $1 \times 10^{-12}$  A).

$q$  is the charge of electron ( $1.6 \times 10^{-19}$  Coulomb).

$k$  is Boltzmann's constant ( $1.38 \times 10^{-23}$  JK $^{-1}$ ).

$T$  is the junction temperature in Kelvins.

$N$  is the emission coefficient (typically between 1 and 2). It depends on the fabrication process and semiconductor material. In many cases, it is assumed to be approximately equal to 1. The factor is added to account for imperfect junctions as observed in real transistors.

Suppose that  $\frac{q}{NkT}$  is one constant value  $a$ , then the equation (1.3) is simplified.

$$I_d = I_s(e^{aV_d} - 1) \quad (1.4)$$

The equation above is transformed by the Taylor series [39].

$$I_d = aI_s V_0 \cos(\omega t) + \frac{a^2 I_s V_0^2}{2!} \cos^2(\omega t) + \frac{a^3 I_s V_0^3}{3!} \cos^3(\omega t) + \frac{a^4 I_s V_0^4}{4!} \cos^4(\omega t) + \dots \quad (1.5)$$

Then the equation above is deformed by mathematical methods.

$$\begin{aligned} I_d = & \frac{a^2 I_s V_0^2}{2 \cdot 2!} + \frac{3 \cdot a^4 I_s V_0^4}{8 \cdot 4!} + \left( aI_s V_0 + \frac{3 \cdot a^3 I_s V_0^3}{4 \cdot 3!} \right) \cos(\omega t) + \left( \frac{a^2 I_s V_0^2}{2 \cdot 2!} + \frac{a^4 I_s V_0^4}{2 \cdot 4!} \right) \cos(2\omega t) \\ & + \frac{a^3 I_s V_0^3}{4 \cdot 3!} \cos(3\omega t) + \frac{a^4 I_s V_0^4}{8 \cdot 4!} \cos(4\omega t) \dots \end{aligned} \quad (1.6)$$

The current  $I_d$  is expressed by the equation (1.7).

$$\begin{aligned}
I_d = & \underbrace{\frac{a^2 I_s V_0^2}{2 \cdot 2!} + \frac{3 \cdot a^4 I_s V_0^4}{8 \cdot 4!}}_{\text{DC}} + \underbrace{(a I_s V_0 + \frac{a^3 I_s V_0^3}{4 \cdot 2!}) \cos(2\pi f t)}_{f_1} + \underbrace{(\frac{a^2 I_s V_0^2}{2 \cdot 2!} + \frac{a^4 I_s V_0^4}{2 \cdot 4!})}_{f_2=2f_1} \\
& \cdot \cos(2\pi \cdot 2f t) + \underbrace{\frac{a^3 I_s V_0^3}{4!} \cos(2\pi \cdot 3f t)}_{f_3=3f_1} + \underbrace{\frac{a^4 I_s V_0^4}{8 \cdot 4!} \cos(2\pi \cdot 4f t)}_{f_4=4f_1} \dots
\end{aligned} \tag{1.7}$$

According to the spectrum analysis of currents and voltages through diodes, currents are distributed at DC, fundamental frequency, and harmonic frequencies. Suppose the thermal voltage  $kT/q$  is 26 mV at the room temperature, a non-linearity coefficient equals 1, and  $V_0$  is 1 V, then DC signal and the second harmonic are dominant in the equation of  $I_d$ . That is to say, the generation of harmonics exists. In details, DC component is 34.07 % of the total current value. The first and second harmonics are 7.05 % and 45.31 % of the total current respectively. The third and fourth harmonics are 2.34 % and 11.24 % of the total current.

A good behaviour of RF/DC conversion is obtained if RF filters are used to block signals at the fundamental frequency and at high order harmonics from transmitting to the load. Harmonic signals can be reflected and rectified again in a new conversion cycle [40]. The conversion efficiency increases consequently owing to the rectification process of signals at the fundamental frequency as well as the harmonics.

The common scenario in AC-to-DC conversion is a rectifier with a large smoothing capacitor which acts as a reservoir. After a peak of output voltages, the capacitor supplies currents to a load till the capacitor voltage falls to the value of next half-cycle of rectified voltages. At that point, rectifiers turn on again and deliver currents to the reservoir till a peak voltage is reached again. If the time constant is large in comparison to the period of the AC waveform, then a reasonable accurate approximation can be made by assuming that the capacitor voltage falls linearly. A useful assumption can be made if the ripple is small compared with the DC voltage. Then the capacitor is discharging all the way from one peak to the next [41, 42].

As we can see in Fig. 1.3, the half-wave rectifier is a simple type of rectifying circuits since it uses single diode. When the AC input is positive, the diode is

forward-biased and lets the current through. When the AC input is negative, the diode is reverse-biased and the diode does not let any current through. With the help of a large capacitor, the rectifier output yields DC voltage.

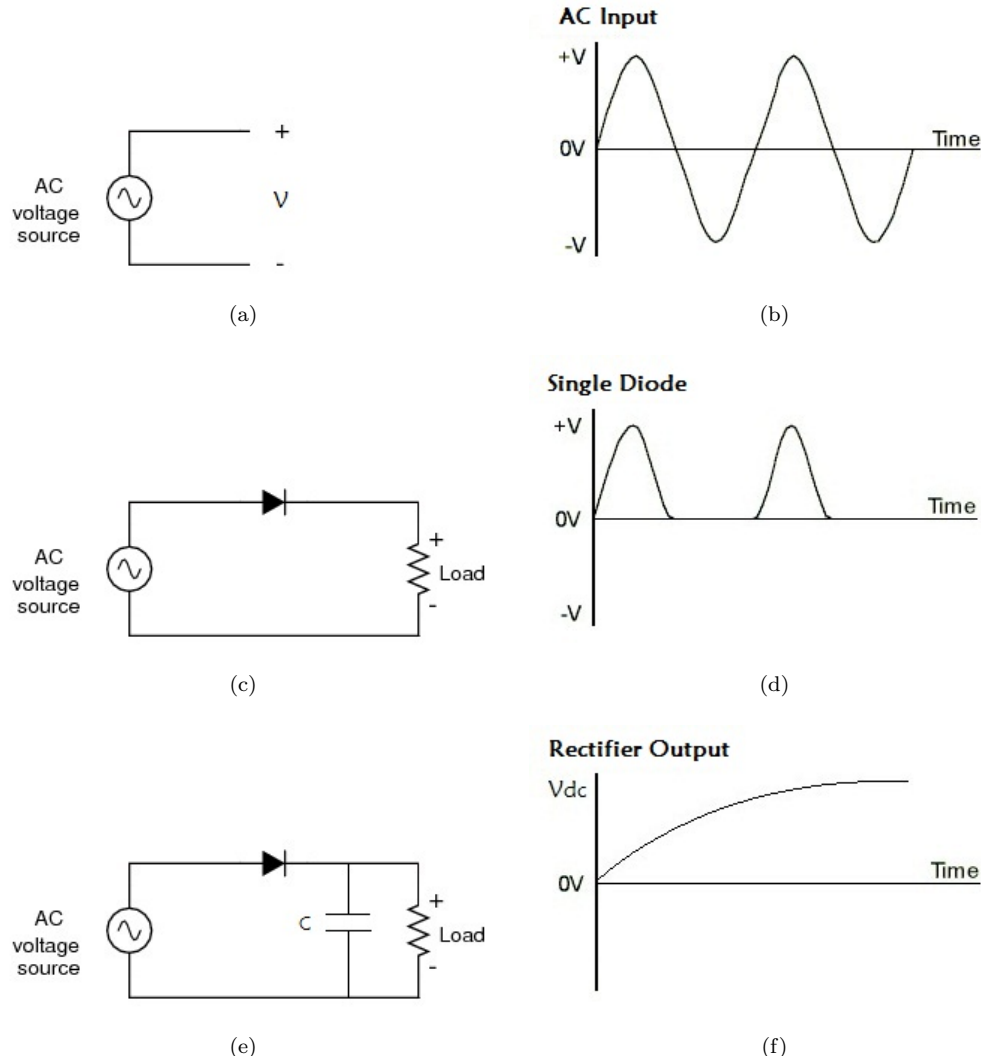


FIGURE 1.3: Half-wave rectification

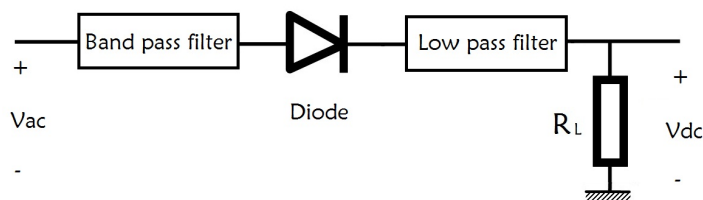


FIGURE 1.4: Scheme of a rectifying circuit

Generally rectifying circuits are composed by diodes, resistive loads, input band pass filter, and output low pass filter, as shown in Fig. 1.4. The input band pass filter rejects harmonics created by diodes. The output low pass filter prevents

harmonics going through the load and locks harmonic signals to participate a new rectifying cycle. In respect of conjugate matching, impedance matching circuits should be designed between receiving antennas and rectifying circuits in order to avoid the mismatch loss.

Take a single serial diode configuration for instance, as shown in Fig. 1.5.  $P_{in}$  is the output power from the sum of power sources.  $P_t$  is the power effectively inside the diode.  $P_r$  is the reflected power at the diode input.  $P_{DC}$  is the output DC power.

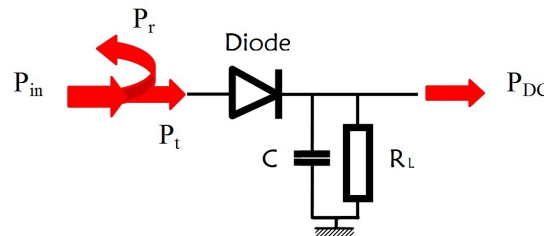


FIGURE 1.5: Prototype of a rectifying circuit with single serial diode

The efficiency of the overall system, noted by the global efficiency, is defined by the ratio of output DC power to input RF power [43].

$$\eta = \frac{P_{DC}}{P_{in}} \times 100\% = \frac{V_{DC}^2/R_L}{P_{in}} \times 100\% \quad (1.8)$$

The efficiency of the rectifying circuit, noted by the effective efficiency, is defined by the ration of output DC power to transmitted RF power [43].

$$\eta_{eff} = \frac{P_{DC}}{P_t} \times 100\% = \frac{V_{DC}^2/R_L}{P_t} \times 100\% \quad (1.9)$$

The effective efficiency is defined by taking into account an input mismatch. It is estimated regardless of mismatching loss. If an input band pass filter is well designed, the incident power from power sources transfers totally to the diode of rectifying circuits. In this case, the global efficiency can be high, which is close to the effective efficiency. In return, the global efficiency may be low due to the mismatch between the input impedance of diodes and the output impedance of power supply devices.

### 1.3.2 Diode model

The analysis of frequency components through Schottky diodes gives a description about the relationship between diode parameters and DC output. It proves that RF filters are needed for pure DC output and high conversion efficiency. Following the section of theoretical analysis, the physical prototype of Schottky diodes is depicted as well as the equivalent circuit model with parasitic packaged elements.

A Schottky diode consists of a metal-semiconductor barrier formed by deposition of a metal layer on a semiconductor [44]. A common type, the passivated diode, is shown in Fig. 1.6, along with its equivalent circuit in Fig. 1.7.

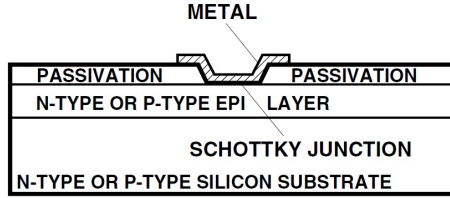


FIGURE 1.6: Cross-section of Schottky diode

$R_s$  is the parasitic series resistance of the diode, the sum of the bond-wire and lead-frame resistance, the resistance of the bulk layer of silicon, etc. RF energy coupled into  $R_s$  is lost as heat. Thus it does not contribute to the rectified output of the diode.  $C_d$  is the parasitic junction capacitance of the diode, controlled by the thickness of the epitaxial layer and the diameter of the Schottky contact.

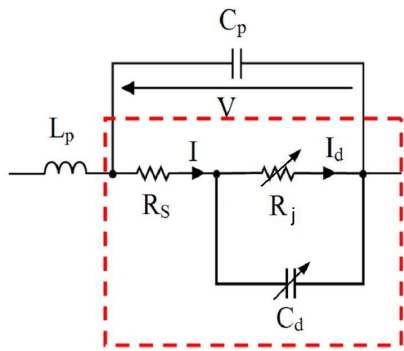


FIGURE 1.7: Equivalent circuit model of diode chip

The diode has a non-linear behaviour. As seen in Fig. 1.7, the characteristic of Schottky diodes mainly depends on two elements of the equivalent model, the

junction resistor  $R_j$  and the junction capacitor  $C_d$ .  $I_d$  is the current passing through the junction resistance  $R_j$  and  $V_d$  is the voltage at its two ends.  $L_p$  is the parasitic inductance.  $C_p$  is the parasitic capacitance.

The equation (1.3) describes the exact current through a diode, in terms of the voltage dropped across the junction, the temperature of the junction, and several physical constants.  $I_d$  is proportional to the saturation current  $I_s$ .  $I_s$  is the thermionic current from metal to semiconductor. It is related to the barrier height of the diode.  $I_s$  and  $R_s$  determine the DC characteristic of diodes.

The concept of barrier height of diodes is considered for the design of rectifying circuits, as shown in Fig. 1.8 [45]. A low barrier height metal has a low forward voltage drop and a large reverse leakage current. Conversely, a high barrier height metal has a large forward voltage drop and a small reverse leakage current. Therefore, it is desirable to have a Schottky diode which exhibits the forward characteristics of a low barrier height metal and the reverse characteristics of a high barrier height metal.

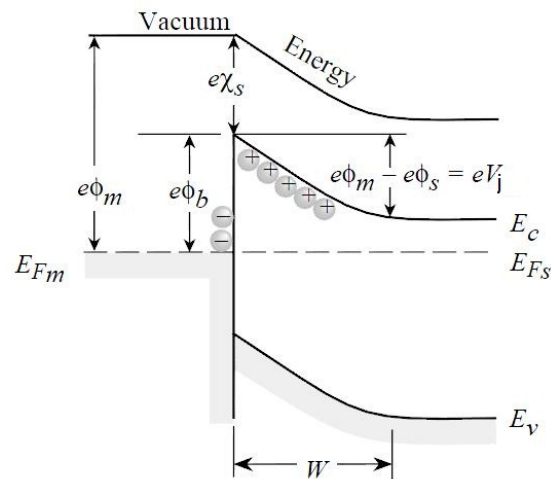


FIGURE 1.8: Metal-semiconductor junction

The thermal potential  $kT/q$  is about 26 mV at room temperature. Assuming the emission coefficient of 1, the diode equation is simplified to the equation (1.10).

$$I_d = I_s(e^{\frac{V_d}{0.026}} - 1) \quad (1.10)$$

The depletion layer is located between the metal and the semiconductor of Schottky diodes. The diode in reverse bias exhibits a depletion-layer capacitance, called a junction capacitance. The junction capacitance is proportional to the zero-bias junction capacitance, one of SPICE (Simulation Program with Integrated Circuit Emphasis) parameters [46].

$$C_d = C_{j0} \left(1 - \frac{V_d}{V_j}\right)^{-M} \quad (1.11)$$

where  $C_{j0}$  is the zero-bias junction capacitance (0.7 pF for HSMS-2820; 0.18 pF for HSMS-2850 and HSMS-2860).

$V_j$  is the junction potential (0.65 V for HSMS-2820 and HSMS-2860; 0.35 V for HSMS-2850).

$M$  is the grading coefficient (1/2 for an abrupt junction; 1/3 for a linearly graded junction).

Constructed by metal-semiconductor junction rather than P-N junction, Schottky diodes are characterized by fast switching time, low reverse-recovery time, low forward voltage drop, and low junction capacitance. The equivalent circuit model shows the junction capacitor parallel with the junction resistor. The distribution of electricity component depends on the impedances of this junction capacitor and the resistor. The diode with small junction capacitance converts much RF energy and thus has good rectifying performance.

Take the single diode configuration as an example. The conduction loss is calculated in terms of the current and the series resistance. The equation (1.12) indicates that the increment of  $R_s$  influences negatively the global efficiency of the circuit because of the increment of the conduction loss [47].  $T$  is a rectifying period.

$$P_{loss} = \frac{1}{T} \int_{\frac{T}{2}+t_0}^{t_0} R_s i_d^2(t) dt \quad (1.12)$$

In the application of rectifying circuits, fast switching time equates to high speed capability and lower forward voltage drop equates to less power dissipation

when conducting. Schottky diodes are well suited for high-frequency applications. Because the forward voltage is low, the reverse-recovery time is short, and the junction capacitance is small.

Based on Agilent ADS simulation approaches, such as SP (Scattering Parameter), LSSP (Large Signal Scattering Parameter), HBS (Harmonic Balance Simulation), and multiple parameter sweeps, the simulated model is built by taking into account an input mismatch. SP is used to characterize a passive RF component and establish the small-signal characteristics of a device at a specific bias and temperature. HBS is a frequency-domain analysis technique for simulating distortion in non-linear circuits and systems. LSSP is performed on non-linear circuits and thus includes non-linear effects such as gain compression and variations in power levels.

Assuming that all the power from energy sources participates in the rectification process, the global efficiency is close to the effective efficiency which is relative to the output DC voltage and the power going inside the diode. The transmitted power  $P_t$  can be calculated in terms of the reflection coefficient  $S_{11}$  and the incident power  $P_{in}$ , by the equation (1.13). The reflection coefficient is extracted from SP simulations for small signals as well as from LSSP simulations for power controlled designs.

$$P_t = (1 - |S_{11}|^2) \times P_{in} \quad (1.13)$$

Although SP and LSSP simulations extract scattering parameters for distributed components,  $S_{11}$  can also be calculated in terms of the input impedance  $Z_{in}$  by the equation (1.14). Besides, HBS is used with current probes, power probes, and wire labels for non-linear lumped components. By this way, return losses, DC outputs, and conversion efficiencies can be observed in the frequency domain and in the power domain by using simulating techniques including LSSP, HBS, and multiple parameter sweeps.

$$S_{11} = \frac{Z_{in} - Z_0}{Z_{in} + Z_0} \quad (1.14)$$

where  $Z_0$  is the reference impedance,  $50 \Omega$  in most cases.

$Z_{in}$  is the input impedance of rectifying circuits.

$$Z_{ink} = \frac{V_k}{I_k} \quad (1.15)$$

where  $Z_{ink}$  is the input impedance of rectifying circuits at DC, fundamental frequency, second harmonic, and high order harmonic frequencies. Since a diode operates in a non-linear process, voltage pins and current probes extract voltages  $V_k$  and currents  $I_k$  in terms of harmonic orders  $k$ .

Take the fundamental frequency as the reference. The input impedance is determined by its voltage and current at the diode input at the fundamental frequency. By the same token, the load resistance equals the ratio of the output DC voltage to its current.

$$Z_L = \frac{V_{dc}}{I_{dc}} \quad (1.16)$$

The input impedance of diodes is a complex value. ADS component library provides two types of diode model including the vendor model and the SPICE model. The vendor model is a non-linear model since the output changes as a function of an input power and a bias. This vendor model includes a specific configuration of diodes and its package. The high-frequency diode library consists of non-linear models representing 164 diodes from 7 manufacturers in ADS [48]. The diodes are available for selection from the schematic window. It acts as a black box which can not be pushed into hierarchy.

Another way to introduce commercial diodes into circuit simulations is the SPICE model. This model supplies values for a diode device. Most of needed values are given on the data sheet, for example Schottky diodes HSMS-28xx in Table 1.1. It specifies SPICE parameters which are calculated or extracted in the schematic window. By this way, the diode device can be built according to our requirement.

DC simulations of two models in Fig. 1.9 give the same result of current-voltage characteristic. It means that the hidden model in the vendor model is the standard diode model of ADS. As seen in Fig. 1.10, the blue curve represents the vendor model and the red curve represents the SPICE model. DC characteristics of these two models are perfectly fit.

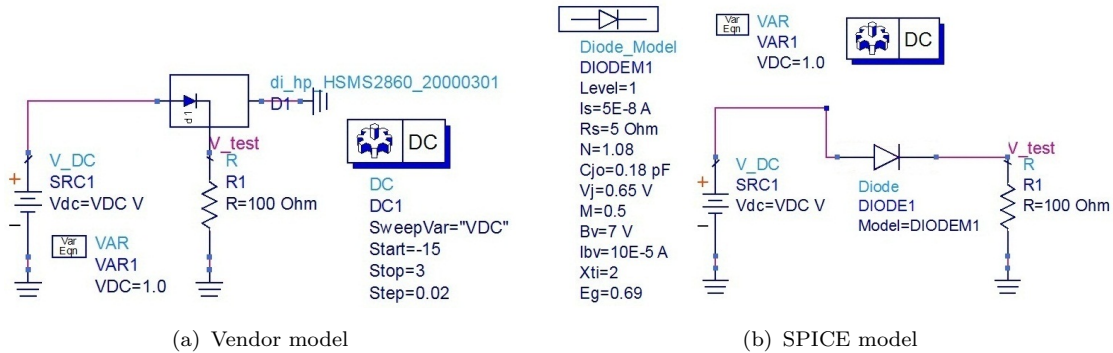


FIGURE 1.9: DC simulation of diode models

When the power supply offers DC voltages larger than the threshold voltage, diodes are turned on. At this moment, the diode export DC voltage and current. Otherwise, diodes are turned off. In this case, no electricity goes through the load. When the power supply offers negative voltages and the value is larger than the breakdown voltage of diodes, diodes are not in the normal situation of rectification.

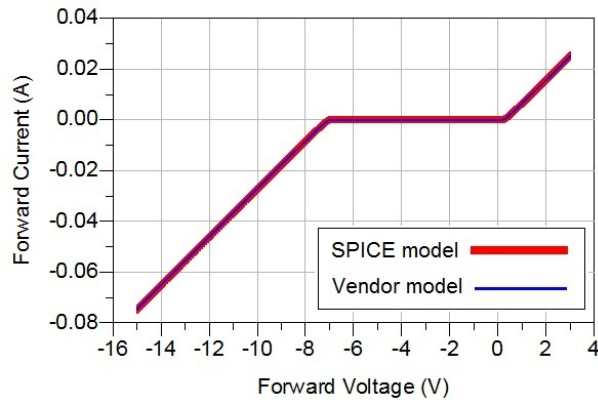


FIGURE 1.10: Comparison of diode models in DC simulation

A common type of diode test sets is a combination of a DC power supply, a resistor, a voltmeter, and an ampere-meter. The measurements of forward voltage drops, forward currents, reverse voltages, and reverse leakage currents, have been done with this equipment. The condition of diode circuits is determined by comparing its actual values under test with typical values obtained from the manufacturer's data sheets.

Fig. 1.11 shows the current-voltage characteristic of Schottky diode HSMS-2860. Here, the load resistance is  $100 \Omega$ . The forward voltage is only 0.35 V compared with 0.6 to 1.7 V for a normal silicon diode. DC characteristics of the SPICE model and the vendor model fit well. And they are similar to the current-voltage test of Schottky diode HSMS-2860. These figures all verify DC characteristics of Schottky diodes in the forward, reverse, and breakdown region.

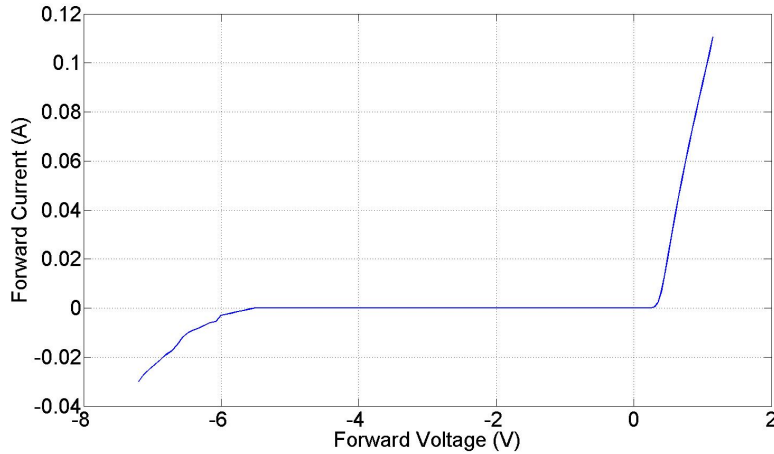


FIGURE 1.11: Schematic current-voltage characteristic of Schottky diode HSMS-2860

However, these models with zero-bias show different results in SP simulations in Fig. 1.12.  $C1$  and  $L1$  are the parasitic capacitance (0.08 pF) and inductance (2 nH). Their values are determined by parasitic elements of diode packages.

As shown in Fig. 1.13, the SPICE model by adding the equivalent circuit model of package parasitics is close to the vendor model. On the other hand, the vendor model contains the equivalent circuit with probably a few additional hidden components in the vendor library, which are provided and recompiled by the vendors. Therefore, the vendor model is similar to the measurement in practical cases. It is used to build the simulation schematic of rectifying circuits. Besides, the SPICE model also shows diode characteristics. It is simulated with the sweep of diode parameters in order to observe diode behaviours.

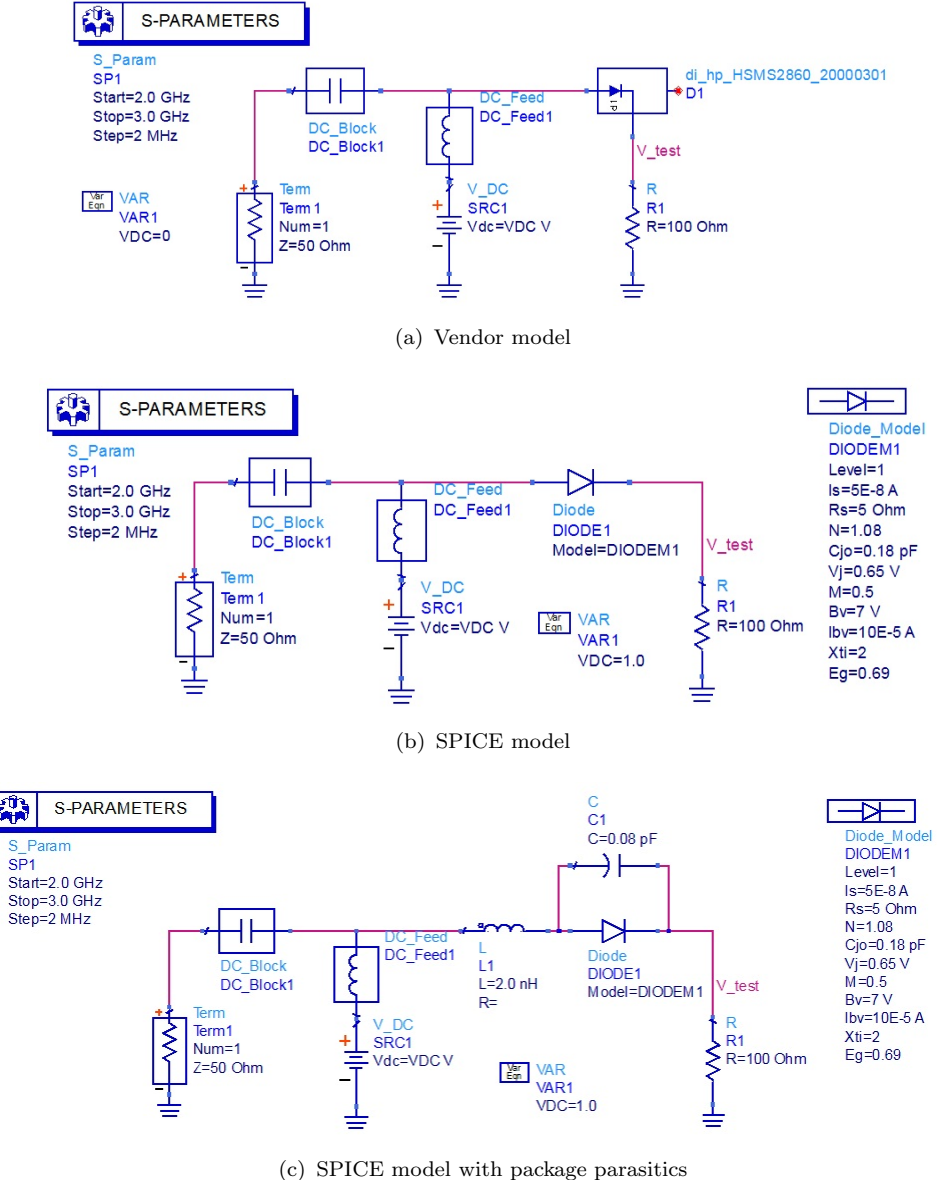


FIGURE 1.12: S-parameter simulation of diode models: (a)Vendor model; (b)SPICE model; (c)SPICE model with package parasitics

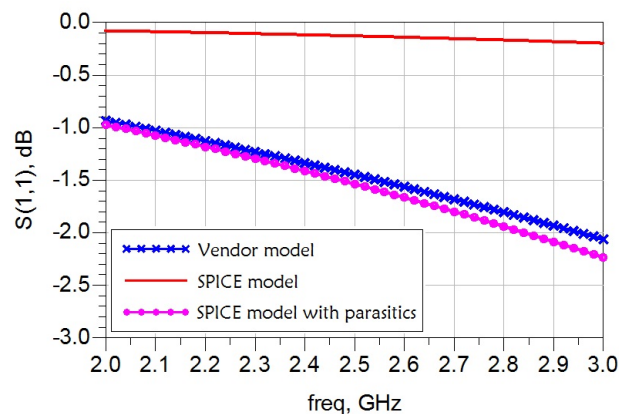


FIGURE 1.13: Comparison of diode models in S-parameter simulation

### 1.3.3 Impact of diode parameters

In purpose to find a diode that is suitable for a given application, the SPICE model is studied by setting SPICE parameters instead of the vendor model. Equivalent circuit models of package parasitic elements are not introduced in the simulated model at this point. The effective efficiency is studied in terms of some typical SPICE parameters, including the breakdown voltage, the zero-bias junction capacitance, the series resistance, and the saturation current.

Take SPICE parameters of HSMS-2820 as the reference. The simulated model is built in circuit simulations combined of HBS and multiple parameter sweeps in order to have a global view of efficiencies both in the frequency domain and in the power domain. The goal is to achieve best values of effective efficiencies in order to ameliorate the overall performance.

The schematic in Fig. 1.14 presents the circuit simulation with the SPICE model of diodes. The diode is connected in series to a capacitor and a load. The capacitance is large enough to export DC voltage, compared to the load resistance. A quarter-wavelength short stub is introduced at the diode input with the aim of DC loop structure based on Kirchhoff's circuit laws.

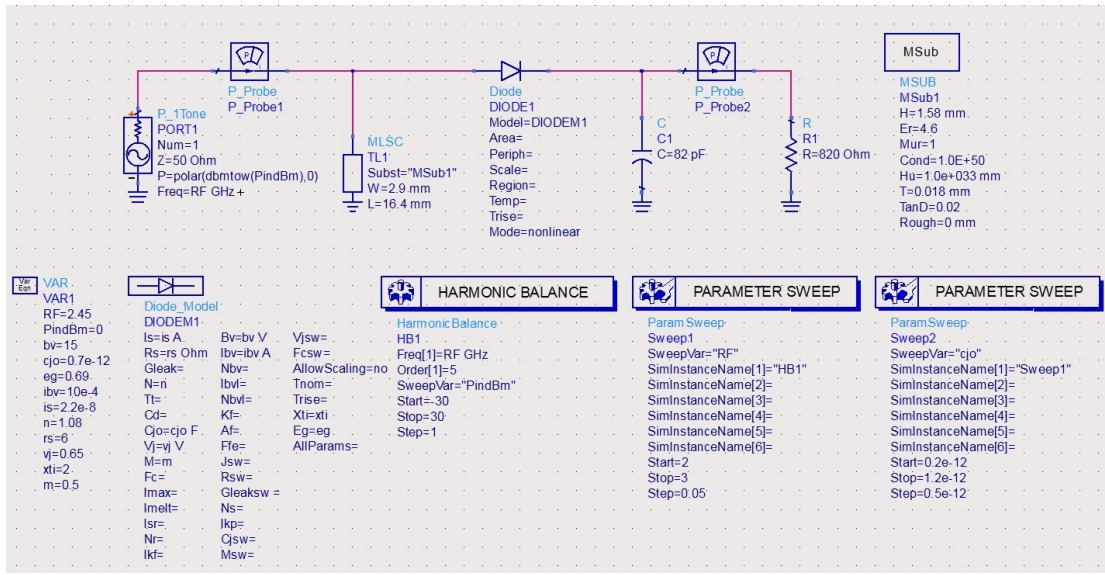


FIGURE 1.14: Schematic of the simulated model considering zero-bias junction capacitance

In order to determine the influence of each diode parameter inside the equivalent circuit model, the conversion efficiency is simulated corresponding to the

variation of SPICE parameters [49]. In each simulation, only one of these parameters is considered and others are set as the same as the reference HSMS-2820. Some equations are built to obtain the return loss in terms of voltages, currents, and input impedance. Thus the effective efficiency is calculated by taking into account an input mismatch. The simulated curves show the diode performance against the variation of SPICE parameters.

One of diode SPICE parameters, zero-bias junction capacitance, is simulated in a parameter sweep, as well as operating frequencies and input power levels. Fig. 1.15 displays the data of the simulated model by taking into account an input mismatch at ISM frequency 2.45 GHz. It shows that the diode with lower zero-bias junction capacitance  $C_{j0}$  has better efficiency. Thus it is more applicable for low power levels.

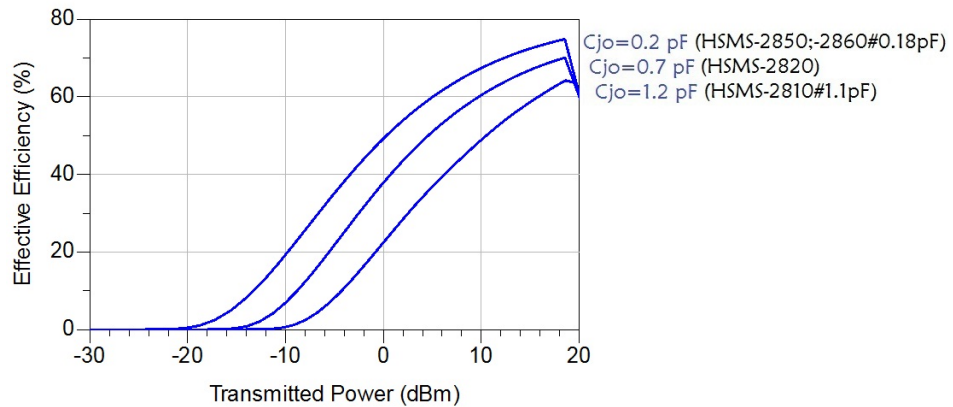


FIGURE 1.15: Efficiency comparison in terms of zero-bias junction capacitance

As we know, the series ohmic resistance contributes to the conduction loss. The smaller  $R_s$  is, the less the diode loss is, and then the better the efficiency is. The schematic is designed in Fig. 1.16. The series resistance is controlled by a parameter sweep controller, as well as operating frequencies and input power levels. Other SPICE parameters of Schottky diodes are kept as the same as the reference.

By taking into account an input mismatch, the simulated model is built based on the relation between the input power and the transmitted power by building equations in the data display window. Fig. 1.17 shows the comparison of effective efficiencies in terms of  $R_s$ . The diode with lower series resistance gives better efficiency. Aimed at the choice of diodes, the conduction loss is important, especially for high power levels.

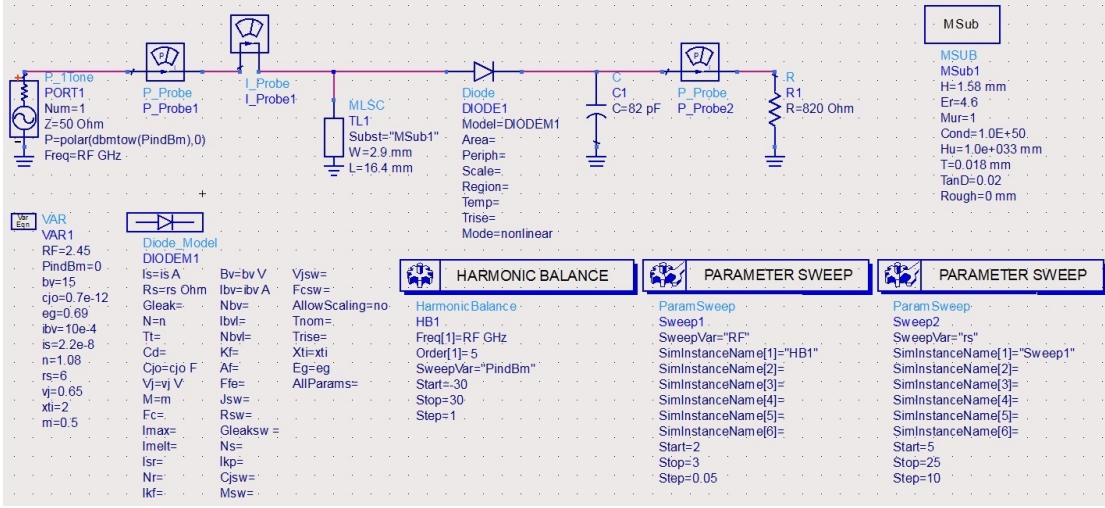


FIGURE 1.16: Schematic of the simulated model considering series ohmic resistance

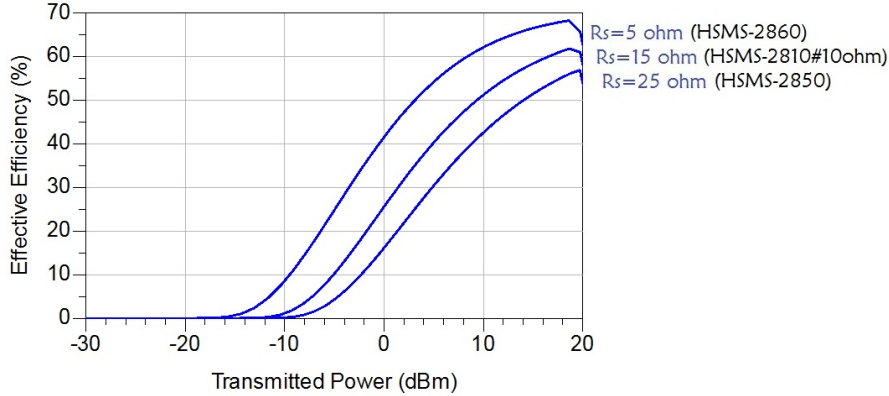


FIGURE 1.17: Efficiency comparison in terms of series ohmic resistance

By the same manner as the efficiency of simulated model against SPICE parameters, the efficiency curve in comparison of the saturation current is shown in Fig. 1.18. The diode with higher saturation current provides slightly better efficiency. This property is also verified by the analysis of equivalent circuit model of diodes.  $I_s$  depends on the barrier height of diodes. The diode with low barrier height owns low forward voltage drop and large reverse leakage current. Thus the application of low power levels needs the diode with high saturation current. The diode is easily turned on by small signals.

Other SPICE parameters are studied by this simulated model, such as the junction potential, the emission coefficient, the grading coefficient, and the breakdown voltage. The diode with larger junction potential obtains better efficiency, as shown in Fig. 1.19. Since the Schottky diodes mentioned above have the similar value of  $V_j$ , the influence on effective efficiencies is not obviously. Thus this

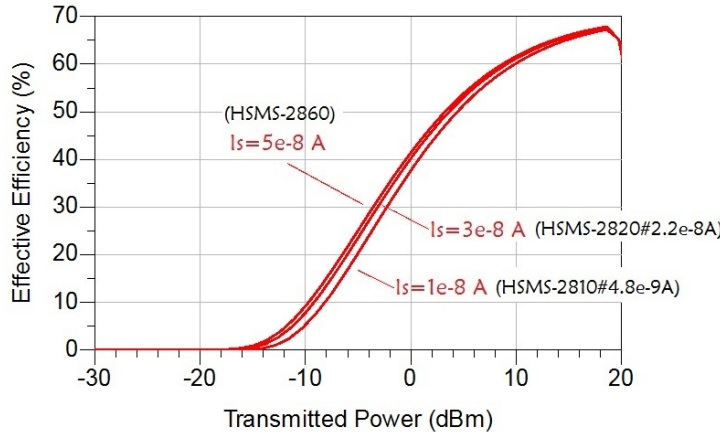


FIGURE 1.18: Efficiency comparison in terms of saturation current

parameter do not contribute much to the efficiency difference among these diodes.

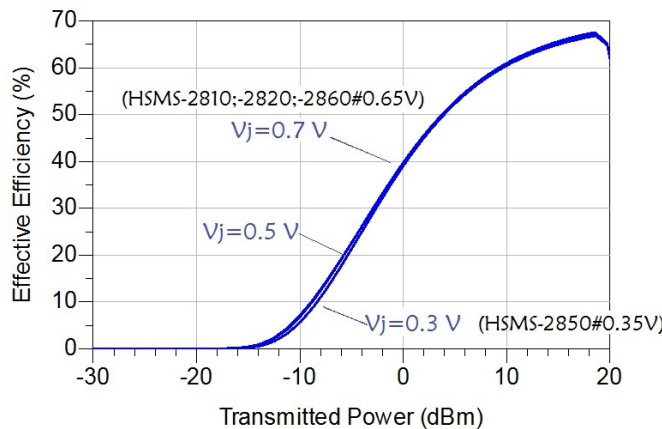


FIGURE 1.19: Efficiency comparison in terms of junction potential

The junction potential is from 0.35 V to 0.65 V for the diodes mentioned above. This parameter is used to define the diode model which is built by SPICE parameters. However, the forward voltage is a practical value corresponding to the forward current. It is not shown in the SPICE model.

The emission coefficient is determined by materials and the fabrication process. The factor of ideal diodes is 1. Emission coefficients of these diodes in the family HSMS-28xx are similar (1.06 for HSMS-2850; 1.08 for HSMS-2810, HSMS-2820, and HSMS-2860). Thus efficiencies have a little difference, as shown in Fig. 1.20. When this diode family is compared with other diodes, the diode with smaller emission coefficient gets better efficiency and it is more applicable for low power levels. The diode MA4E1317 mentioned below has larger value of  $N$  (1.5) and then lower effective efficiency.

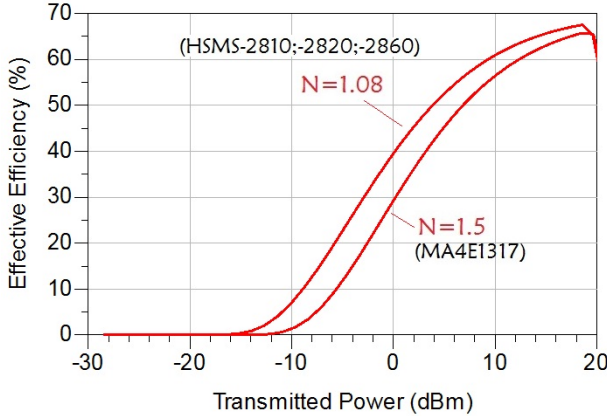


FIGURE 1.20: Efficiency comparison in terms of emission coefficient

The junction grading coefficient is related to the doping profile of the junction.  $M$  is 0.5 for an abrupt junction and 0.333 for a linearly graded junction. Grading coefficients of HSMS-28xx series are the same value (0.5). And other diodes mentioned below have very similar values of  $M$ . Thus there is a tiny difference of efficiencies, as presented in Fig. 1.21.

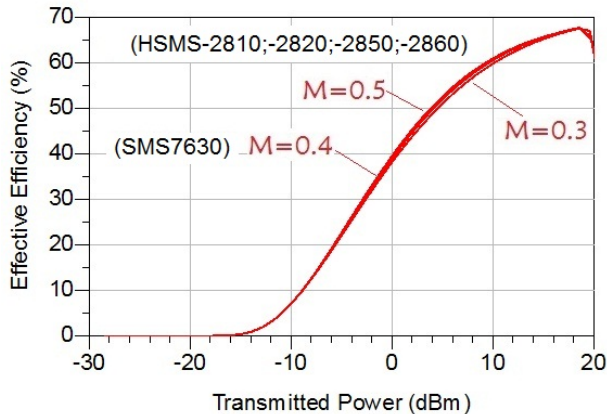


FIGURE 1.21: Efficiency comparison in terms of grading coefficient

Fig. 1.22 displays an interesting phenomenon. These modelling diodes own same SPICE parameters except the breakdown voltage and they has the same performance before diodes break down. The turning point of effective efficiency is only corresponding to the breakdown voltage.

The larger the breakdown voltage is, the higher power levels the diode is available for. The diode with smaller breakdown voltage operates no longer for very high power levels. Once the reverse voltage gets beyond the breakdown voltage, diodes can not operate normally. Under this circumstance, diode modelling simulations do not show diode characteristics in practical cases.

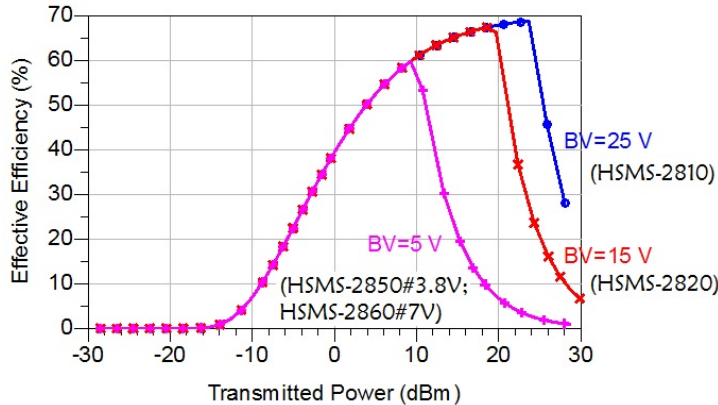


FIGURE 1.22: Efficiency comparison in terms of breakdown voltage

All the products in the HSMS-28xx family use the same diode chip but they differ only in package configurations. The HSMS-281x series features very low flicker noise. The HSMS-282x series is the best all-around choice for most applications, featuring low series resistance, low forward voltage at current levels, and good RF characteristics. The HSMS-285x is a family of zero bias detector diodes for small signal ( $P_{in} < -20$  dBm) applications at frequencies below 1.5 GHz.

At higher frequencies, the DC biased HSMS-286x should be considered. The HSMS-286x series is a high performance diode offering superior forward voltage and ultra-low capacitance. In large signal power or gain control applications ( $P_{in} > -20$  dBm), HSMS-282x and HSMS-286x products should be used. The HSMS-285x zero bias diode is not designed for large signal applications. Each series has a different set of characteristics, which can be compared most easily by consulting the SPICE parameters given on each data sheet.

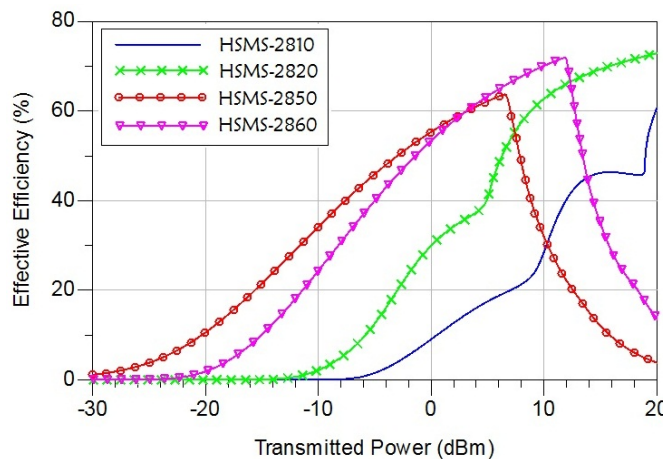


FIGURE 1.23: Efficiency comparison among Schottky diode HSMS-2810, HSMS-2820, HSMS-2850, and HSMS-2860

Diode Type	HSMS-2810	HSMS-2820	HSMS-2850	HSMS-2860
$BV(V)$	25	15	3.8	7
$I_{BV}(A)$	10E-5	10E-4	10E-4	10E-5
$C_{j0}(\text{pF})$	1.1	0.7	0.18	0.18
$E_G(\text{eV})$	0.69	0.69	0.69	0.69
$I_s(A)$	4.8E-9	2.2E-8	3E-6	5E-8
$N$	1.08	1.08	1.06	1.08
$R_s(\Omega)$	10	6	25	5
$V_j(V)$	0.65	0.65	0.35	0.65
$X_{TI}$	2	2	2	2
$M$	0.5	0.5	0.5	0.5
$V_f$	400mV ( $I_f=1\text{mA}$ ) 1V ( $I_f=35\text{mA}$ )	340mV( $I_f=1\text{mA}$ ) 0.5V( $I_f=10\text{mA}$ ) 0.7V( $I_f=30\text{mA}$ )	150mV ( $I_f=0.1\text{mA}$ ) 250mV ( $I_f=1\text{mA}$ )	350mV( $I_f=1\text{mA}$ ) 0.6V( $I_f=30\text{mA}$ )
Power Level	Low flicker noise	>-20dBm	<-20dBm	$P_{in} < -20\text{dBm}$ ( $\text{freq} > 1.5\text{GHz}$ ) $P_{in} > -20\text{dBm}$ ( $\text{freq} > 4\text{GHz}$ )
Frequency Band	RF	RF	<1.5GHz	915MHz-5.8GHz

TABLE 1.1: Typical parameters of Schottky diode HSMS-28xx

The diode vendor models are used in circuit simulation of effective efficiency by taking into account an input mismatch. The load is given as  $C = 82 \text{ pF}$  and  $R = 820 \Omega$ . Fig. 1.23 presents the effective efficiency against the transmitted power. HSMS-2820 produces high efficiency for high power levels. HSMS-2850 has good performance for low power levels. HSMS-2860 obtains high efficiency for medium power levels. In the aim of achieving the best efficiency, each diode should cooperate with its optimal load for given power levels.

Table 1.1 presents the typical parameters for Schottky diode HSMS-28xx [50].  $BV$  is the reverse breakdown voltage.  $I_{BV}$  is the current at the breakdown voltage.  $E_G$  is the band gap energy. Every solid has its own characteristic energy band structure. The band gap energy of semiconductors tends to decrease with increasing temperature.  $X_{TI}$  is the saturation-current temperature exponent (3 for P-N junction; 2 for Schottky).  $X_{TI}$  and  $E_G$  take part in defining the dependence of  $I_s$ .

$V_f$  is the forward voltage drop, which is corresponding to the forward current  $I_f$ . It is an important parameter that must be considered in diode simulations. The diode HSMS-2850 owns extremely small forward voltage (150 mV) and forward

Diode Type	SMS1546	SMS76210	SMS7630	MA4E1317
BV(V)	3	3	2	7
C <sub>j0</sub> (pF)	0.38	0.1	0.14	0.02
E <sub>G</sub> (eV)	0.69	0.69	0.69	0.69
I <sub>BV</sub> (A)	10E-5	10E-5	10E-4	10E-4
I <sub>s</sub> (A)	3E-7	4E-8	5E-6	10E-8
N	1.04	1.05	1.05	1.5
R <sub>s</sub> (Ω)	4	12	20	4
V <sub>j</sub> (V)	0.51	0.51	0.34	0.323
X <sub>TI</sub>	2	2	2	2
M	0.36	0.35	0.4	0.5
V <sub>f</sub>	200-270mV (I <sub>f</sub> =1mA)	260-320mV (I <sub>f</sub> =1mA)	60-120mV(I <sub>f</sub> =0.1mA) 135-240mV(I <sub>f</sub> =1mA)	700mV (I <sub>f</sub> =1mA)

TABLE 1.2: Typical parameters of other Schottky diodes

current (0.1 mA). Even in the condition of the forward current 1 mA, the forward voltage of HSMS-2850 is lower than HSMS-2810, HSMS-2820, and HSMS-2860. It means that HSMS-2850 can be turned on by the lowest power level. This diode may be the best choice for the application of very low power. But it is not advised for the frequency band that we desire.

In the bibliography study, other diodes [51, 52] are also taken into account by using the simulated model and the SPICE model. In comparison of SPICE parameters on the data sheets [53, 54], as presented in Table 1.2, HSMS-2820 is perfect for RF-to-DC conversion of high power levels due to small series resistance and large breakdown voltage. MA4E1317 and HSMS-2860 are both suited to constitute rectifying circuits for low power levels. But compared with MA4E1317, HSMS-2860 has larger saturation current, smaller emission coefficient, larger junction potential, and thus better efficiency.

These diodes from HSMS-28xx family are surface mount RF Schottky barrier diodes. They are all encapsulated in SOT-23 package. Thus it is interesting to design rectifying circuits for high power levels with HSMS-2820 and for low power levels with HSMS-2860 due to diode characteristics. HSMS-2850 owns very low forward voltage and it operates well in low power levels. In the following sections, rectifying circuits are designed with these diodes according to specific requirements.



# Chapter 2

## State of The Art

### 2.1 Configuration of rectennas

A rectenna contains an antenna and a rectifying circuit. The antenna collects the microwave power. The rectifying circuit converts the RF energy into useful DC energy. The conversion is done by a non-linear element, usually Schottky diode. Thus rectifying circuits have non-linear characteristics.

A rectifying circuit is made up of a combination of Schottky diodes, input RF filter, output capacitor, and resistive load. Generally, the input RF filter is a band pass filter which rejects harmonics created by diodes. Matching circuits are needed between the antenna and the rectifying circuit with the aim of minimizing the mismatch loss and ameliorating the overall efficiency.

Several configurations have been used to convert the microwave power into useful DC power, such as half bridge circuits [55] and whole bridge circuits [56]. According to the requirement of output DC voltage and conversion efficiency, single serial diode circuits [57, 58], single shunt diode circuits [59, 60], voltage doubler circuits [61], and multi-step voltage doubler circuits [62] have been considered, as shown in Fig. 2.1. All the configurations of rectifying circuits should be accurately optimized to maximize the conversion efficiency [63].

For a given incident power, the efficiency of rectifying circuits is altered by the conduction loss of diodes and the impedance mismatching, as well as the dielectric and metallic losses. The diode loss is inevitable. It is one of dominant factors for

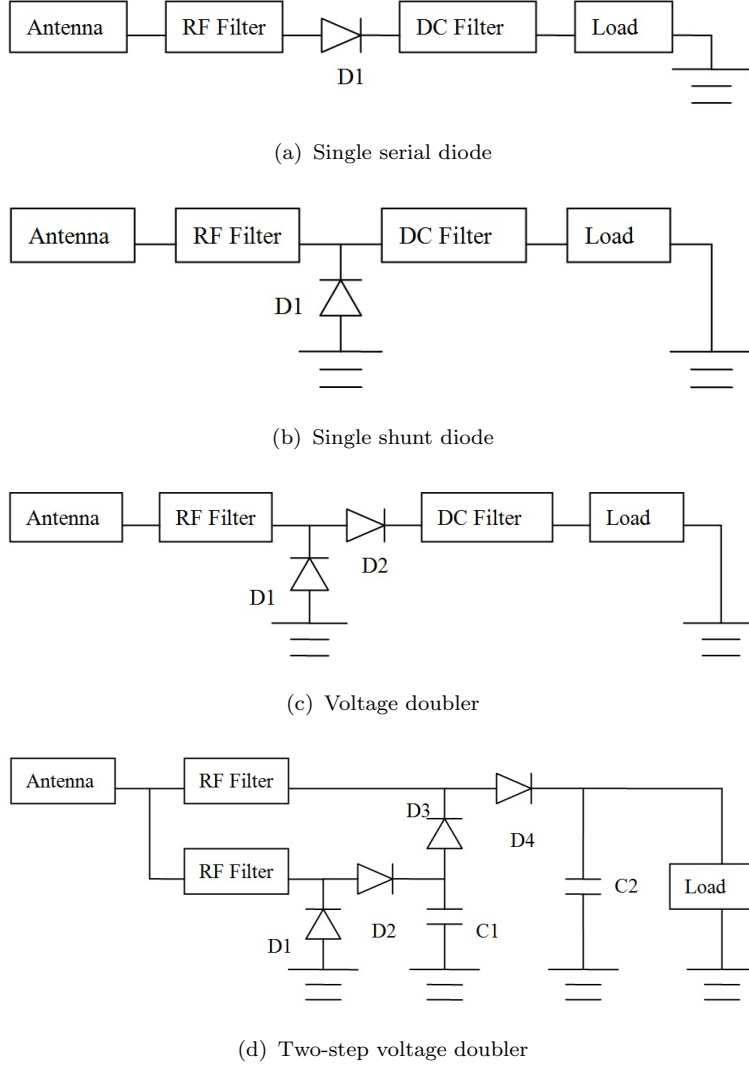


FIGURE 2.1: Topologies of rectennas

the rectification of either low power levels or high power levels. In addition, the efficiency of rectifying circuits affects the overall efficiency of rectennas.

Structures with single series or shunt diode have an advantage of minimizing the conduction loss introduced by diodes. The structure of voltage doubler obtains higher output DC voltage than the case of single diode under the same condition of input power levels. The voltage doubler has more diodes in parallel participating in the rectification process. It brings higher output DC voltage but it is not efficient due to more conduction loss. It is interesting to make a compromise between RF-DC conversion efficiency and DC output voltage.

We desire a rectifying circuit which gives high DC voltage and high efficiency even if incident power levels are low. So the single diode configuration is a good

choice owing to low conduction loss.

## 2.2 From series diode rectifier to bridge rectifier

A series diode circuit contains an input low pass filter dedicated to input matching and harmonics rejecting, and a quarter-wavelength radial stub which stops RF signal superimposed to the load. The rectification is done by Schottky diode HSMS-2860 characterized by a low parasitic capacitance  $C_{j0}$  of 0.18 pF and a low serial resistor  $R_s$  of 5  $\Omega$ . The load resistor is optimal to 1050  $\Omega$  with a 33 pF SMD shunt capacitor. As shown in Fig. 2.2(a), the serial diode rectifier obtained the max experimental efficiency of 73 % for 12 dBm RF power [64].

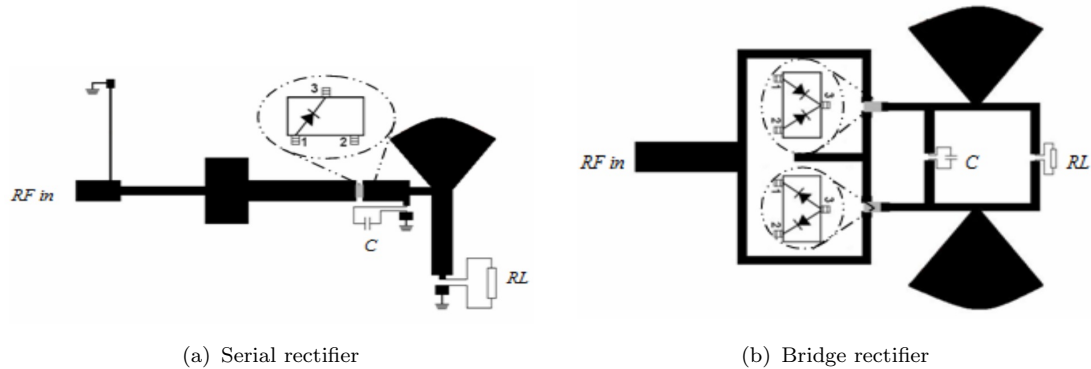


FIGURE 2.2: Serial and bridge rectifiers designed by H. Takhedmit

H. Takhedmit proposed a modified bridge rectifier based on an original structure of bridge rectifiers, as shown in Fig. 2.2(b). This circuit contains two radial stubs that act as RF short circuits to isolate RF and DC components at the output. A common anode HSMS-2863 and a common cathode HSMS-2864 with two Schottky diodes on same packages are soldered on the circuit. A quarter-wavelength open line between the two packages adjusts the RF-to-DC conversion efficiency accurately. A 10 k $\Omega$  resistor operates as the load with a 33 pF SMD shunt capacitor. The length between the diode and the output DC filter is tuned in order to cancel its capacitive reactance and to improve the diode efficiency. This compact structure obtains the maximal measured efficiency of 65 % for 12 dBm RF power [64].

## 2.3 Compact bridge rectifier with no via-hole connection

H. Takhedmit continued to use a compact structure of a common anode HSMS-2863 and a common cathode HSMS-2864, as shown in Fig. 2.3. The Schottky diodes are characterized by a low parasitic capacitance  $C_{j0}$  of 0.18 pF and a low serial resistance  $R_s$  of 5  $\Omega$ .

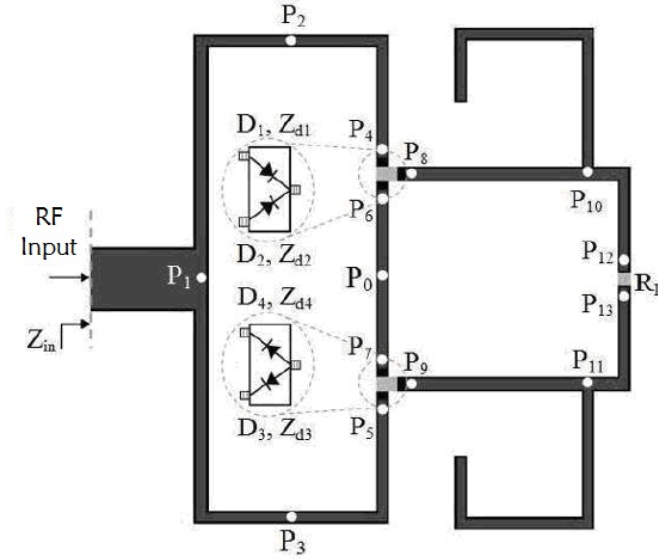


FIGURE 2.3: Compact bridge rectifier designed by H. Takhedmit

Due to the differential measurement of the voltage on the two side of the load  $R_L$ , via-hole connection is not necessary. The circuit contains two quarter-wavelength open stubs which act as RF short circuits to isolate DC and RF components (2.45 GHz, 7.35 GHz, etc.). The length between the diodes and the output DC filter is accurately optimized to maximize the conversion efficiency of the diodes by cancelling its capacitive reactance. This bridge rectifier achieves an RF-DC conversion efficiency of 61 % for 10 mW input power. When the power density is 0.15 mW/cm<sup>2</sup> the rectenna shows an efficiency of 52 % over an optimal resistive load of 1.50  $\Omega$  [65].

This paper gives an idea to simplify the study of the current and voltage across diodes in the time domain. The non-linear component  $I_d$  is considered in the electric equivalent model of Schottky diodes. If the voltage applied across the diode is larger than the threshold voltage, the diode gets through. If not, the diode is blocked and the current is nearly zero through the diode. In his design, as shown

in Fig. 2.4, two diodes  $D_1$  and  $D_3$  get through when the voltage is beyond the threshold voltage. Other two diodes  $D_2$  and  $D_4$  are blocked and do not participate in the conversion process. The impedances of diodes,  $Z_{d1}$  and  $Z_{d2}$ , are determined by the load  $R_L$  and input power  $P_{RF}$ .

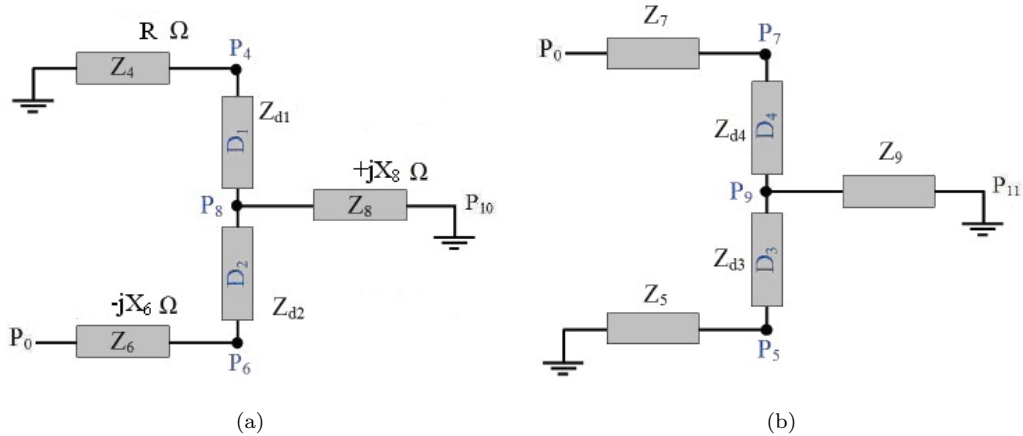


FIGURE 2.4: Impedance schema of diodes  $D_1$ - $D_4$

In order to maximize RF-DC conversion efficiency, it is necessary to transfer the maximum power  $P_{RF}$  into  $D_1$  and  $D_3$ . So the matching circuit should be designed in terms of the power level at  $P_4$  and  $P_5$ . The two diodes  $D_1$  and  $D_3$  are symmetric. Thus, they present the same impedance at 2.45 GHz. The diodes  $D_2$  and  $D_4$  are also the same dynamic impedance. The transmission line, between the diode  $D_1$  and the quarter-wavelength open stub, is ended at a short circuited point  $P_{10}$  which transforms imaginary inductive impedance at the point  $P_8$  for 2.45 GHz. And it also cancels the capacitance of  $D_1$ .

According to the derivation of the spectrum analysis of currents and voltages through diodes, currents and voltages at the odd order frequency components (2.45 GHz, 7.35 GHz, etc.) are out of phase. But currents and voltages at the even order frequency components (DC, 4.9 GHz, 9.8 GHz, etc.) are in phase. Due to the symmetric structure, the current components arrived at the point  $P_0$  for 2.45 GHz are out of phase, which generate an open circuited point. Thus, the impedance is imaginary at the point  $P_6$ .

All the impedance can be determined by the current probe and the voltage probe in ADS for a specific input power. The impedance calculation can be done in the frequency domain by both the amplitude and phase of currents and also voltages at 2.45 GHz. The length from the power divider  $P_1$  to  $P_4$  or  $P_1$  to  $P_5$  is chosen to assure the matching level for the RF input power.

Likewise, the power at the second harmonic frequency 4.9 GHz is generated by  $D_1$  and  $D_3$ , and it is trapped into a loop ( $P_1$ ,  $P_2$ ,  $P_0$ ,  $P_3$ , and  $P_1$ ). The symmetric structure sets up the short circuited points  $P_1$  and  $P_0$  at 4.9 GHz. The two points  $P_2$  and  $P_3$  are located half-wavelength away from  $P_1$ , so they are also short circuited. The total length of this loop is twice wavelength at 4.9 GHz. The impedance of each diode can be calculated by ADS, and the sum of four diode impedances is small enough to confine the second harmonic. In other word, the power at 4.9 GHz, generated by  $D_1$  and  $D_3$ , dissipates through  $D_2$  and  $D_4$ .

## 2.4 Dual-diode rectenna with harmonic-rejecting design

The bridge rectifier has been used to integrate with a patch antenna in order to realize a compact structure [22]. This compact structure with no via-hole connection is also used in a dual Schottky diodes converter, as presented in Fig. 2.5. The rectifier contains two folded quarter-wavelength open stubs which act as short circuits at the frequency of interest and isolate the resistive load  $R_L$ . Besides, the length  $L_7$  between the diode and the open stub is used to tune the reactance at the input of the diodes. The DC voltage is obtained by measuring the voltage difference between  $V_1$  and  $V_2$  across the resistor load, without reference to the RF ground plane. Therefore, there is no need for any via-holes.

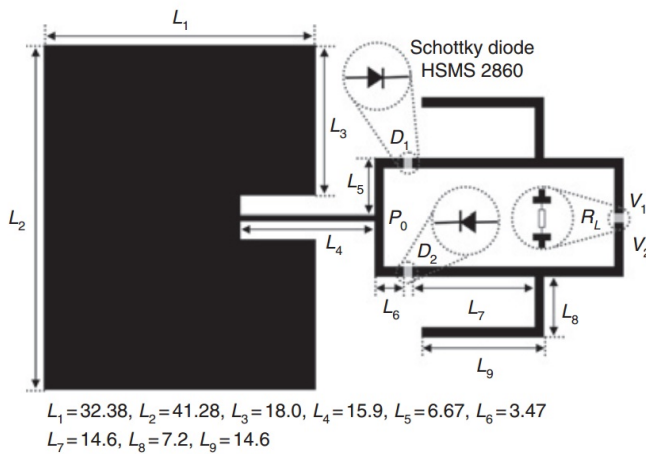


FIGURE 2.5: Geometry of dual-diode rectenna (dimensions in mm) designed by H. Takhedmit

The rectifying circuit is suitable for wireless sensor applications because no input low pass filter and no via-hole connection are required. The input LPF rejects harmonics created by the diodes and matches the rectifier to the antenna. It can be directly integrated on the radiating element by using harmonic-rejecting antennas.

The rectenna contains a linearly polarized rectangular patch antenna designed at 2.45 GHz. The optimized symmetric lines are chosen to match the input of the rectifier with the patch antenna at 2.45 GHz and 10 dBm input power. The power is yielded from the antenna and split into two separated equivalent RF components. The RF signals propagate in phase on both symmetrical and parallel microstrip lines towards the diodes  $D_1$  and  $D_2$ . Then they are partially converted into DC current with unwanted higher-order harmonics.

The diodes are localized on a null of current to minimize the power loss. In addition, the second harmonic is generated by the non-linear diode. Owing to the half-wavelength distance between the diodes at 4.9 GHz, it is distributed by a standing wave with a peak of current at the input of the circuit ( $P_0$ ) and confined inside the microstrip loop. There are no propagation effect towards the microstrip antenna or towards the resistive load, because no current exists at 4.9 GHz. Though there is a mismatch between the antenna and the rectifier at the third harmonic 7.35 GHz, the efficiency is not affected because it is greatly reduced. The rectenna exhibits a measured efficiency of 83 % at 0.31 mW/cm<sup>2</sup> [22].

## 2.5 Stacked rectenna with radial stubs

Two of the main design parameters of the rectenna are the dimensions and the conversion efficiency. J. A. G. Akkermans proposed a layered design with Schottky diode HSMS-2852 to acquire a small-area rectenna [66]. The backside of the patch antenna is used for the rectifying circuit. As a result, the ground plane of the antenna is also the ground plane of the rectifying circuit.

As presented in Fig. 2.6, radial stubs are placed between the antenna and the rectifier to prevent the harmonics from being re-radiated by the antenna. Because the harmonics of the operating frequency correspond closely to radiating modes of the patch antenna. Higher harmonics are not as significant as the first harmonic and they are excited by radial stubs. Between the rectifier and the load, two radial

stubs are also placed. These radial stubs prevent the harmonic signals from being dissipated in the load.

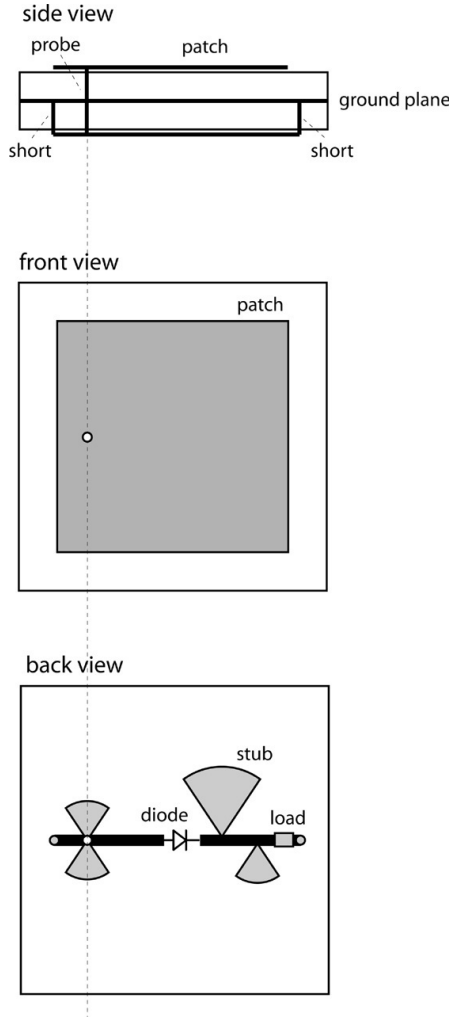


FIGURE 2.6: Layout of the stacked rectenna designed by J. A. G. Akkermans

The analytical models are employed to match the microstrip patch antenna and the rectifying circuit including the radial stubs. The conversion efficiency is maximized by choosing a probe position where the conversion efficiency of the Schottky diode is favourable. The layered rectenna is photo-etched from copper-clad FR4 material and allowed for a fast realization. The conversion efficiency is 52 % for 0 dBm ( $53.2 \mu\text{W}/\text{cm}^2$ ) input power at 2.45 GHz [67].

## 2.6 Circularly polarized rectenna with unbalanced circular slots

Different from the simple structure of rectangular patch, Fig. 2.7 shows a circular patch. This patch antenna is modified from linear polarization to circular polarization by unbalanced circular slots. This structure is adopted for size reduction and 2nd harmonic rejection. The slotted CP antenna has the advantages of compact size, circularly polarized characteristic, and second harmonic rejection property. Built on low cost FR4 substrate, the antenna has -10 dB return loss bandwidth of 137 MHz and 30 MHz CP bandwidth for 3 dB axial ratio [68].

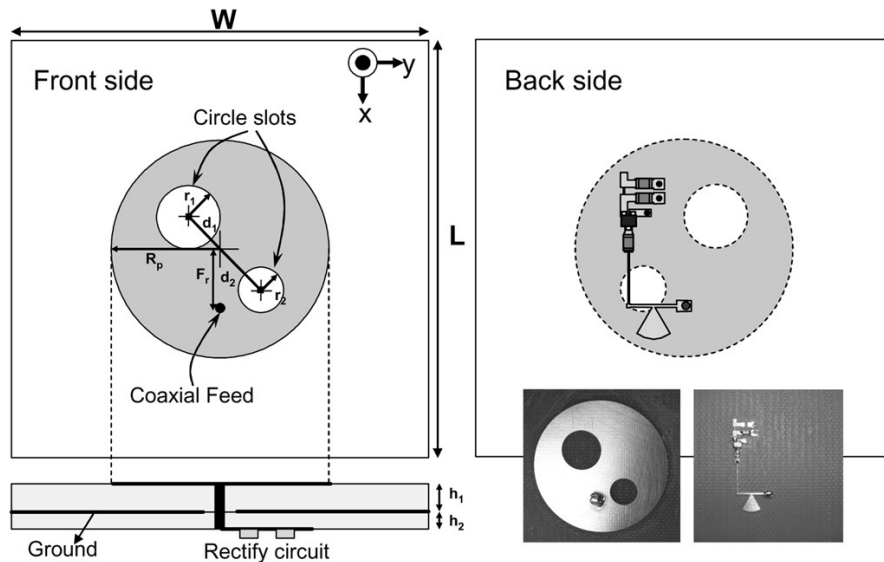


FIGURE 2.7: Antenna and rectifying circuit configuration and the photographs of proposed rectenna designed by T. C. Yo. Geometry parameters for the CP antenna are:  $W=60$ ,  $L=60$ ,  $R_p=15.5$ ,  $F_r=6.5$ ,  $d_1=5.2$ ,  $r_1=5.2$ ,  $d_2=8.3$ ,  $r_2=2.3$ ,  $h_1=1.6$ ,  $h_2=0.8$  (Dimension:mm)

When integrating circuits with the antenna, the transmission line may cause complicated layout schematic for antenna array applications. Besides, the nearby circuit may introduce coupling effects and affect antenna characteristics. To contribute a rectenna for RF-to-DC power conversion, the back side of the CP antenna is the doubler rectifier circuit with Schottky detector diode pair HSMS-282c and 3rd order harmonic rejection radial stub. By up to 3rd order harmonic rejection, the RF-to-DC conversion efficiency reaches 53 % and 75 % with 1  $k\Omega$  resistor load under ANSI/IEEE uncontrolled and controlled RF human exposure limit respectively [68].

As shown in Fig. 2.8, the voltage doubler provides at least twice DC output and includes half input impedance of the single diode rectifier. By the 2nd harmonics rejection CP antenna and the 3rd harmonic rejection stub, the harmonics generated by the non-linear diodes can be mostly suppressed for efficiency improvement and interference elimination. The unwanted RF signals leaking to load are also suppressed by the DC pass filter.

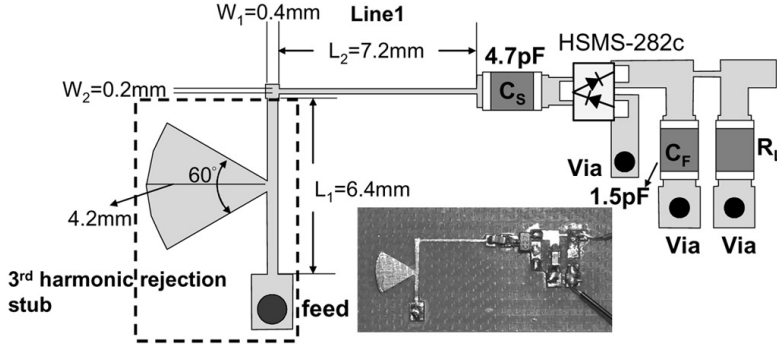


FIGURE 2.8: Schematic and photograph of doubler rectifier with 3rd harmonic rejection radial stub designed by T. C. Yo

T. C. Yo proposed a compact circular polarized rectenna with two unbalanced circular slots and harmonic-rejecting property. The 2nd harmonic rejection property originates from the two unbalanced circular slots and simplifies the design of rectify circuits. The doubler rectifier provides optimum DC voltage of 15.8 V and RF-DC conversion efficiency of 78 % at 16.5 mW/cm<sup>2</sup> incident power density.

## 2.7 Harmonic-rejecting circular-sector rectenna

Generally, a conventional patch antenna shows resonant frequencies at multiple harmonics. Radiation of harmonics is generated by a non-linear diode and needed to be prevented by using filters. J. Y. Park proposed a rectenna designed with microstrip harmonic-rejecting circular sector of 240°. He used an insert feeding method with a quarter-wavelength transformer at 2.4 GHz and an angle of 30° from the edge of the circular sector for impedance matching, as presented in Fig. 2.9. Compared to a conventional microstrip square-patch antenna, the circular sector antenna has a gain of 4.677 dBi. It exhibits high reflection coefficients at the second and the third harmonics.

The rectenna with integrated circular sector antenna eliminates a band pass filter placed between the antenna and the diode and produces high output power.

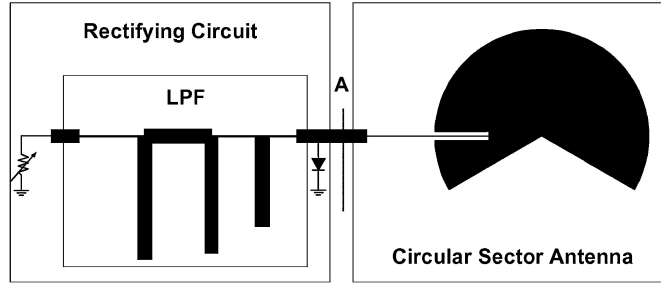


FIGURE 2.9: Rectenna with a microstrip circular-sector antenna designed by J. Y. Park

Moreover, a microstrip low pass filter completely blocks not only the fundamental frequency, but also the second and the third harmonics at the output of Schottky diode HSMS-2820. The efficiency is increased as the increment of input power. A maximum efficiency of 77.8 % is achieved with the load resistor of  $150 \Omega$  when the input power is 10 dBm ( $0.27 \text{ mW/cm}^2$ ) [69].

## 2.8 Rectifier with high Q resonators

Most approaches of rectenna circuits at the far field radiation rely either on RF power inputs ( $> -25 \text{ dBm}$ ) or have low efficiency ( $< 10 \%$ ) at  $-30 \text{ dBm}$  input power [28]. Since the transmitting power is restricted by law for the health standard, it is needed to rectify low ambient radiation energy to supply autonomous measurement systems. T. Uungan proposed a voltage double rectifier with high Q crystal quartz resonator at the resonant frequency 24 MHz, as shown in Fig. 2.10.

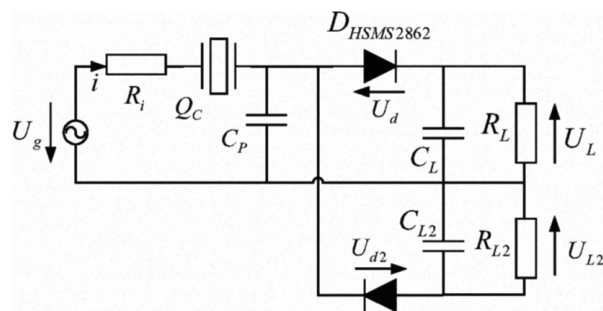


FIGURE 2.10: Equivalent circuit with 24 MHz crystal resonator  $Q_C$  and two HSMS-286x diodes from Agilent for the rectification, designed by T. Uungan

For a specific RF power and frequency, the output voltage is limited by the voltage sensitivity of the diode, the quality factor, and the efficiency of the system. The Q factor and the frequency stability of quartz resonators are much better

than what is achievable with integrated passives. The resonance circuit enables the passive voltage boosting proportional to its loaded Q. The sensitivity of the rectifier circuit is improved by maximizing the input voltage to the rectifier. This rectifier achieves a sensitivity of -30 dBm for DC output voltage of 1 V and an efficiency of more than 22 % [28].

## 2.9 Spiral rectenna for surrounding energy harvesting

The average of the surrounding RF power density in broadband (1 GHz to 3.5 GHz) is in the order of -12 dBm/m<sup>2</sup> (6.3 nW/cm<sup>2</sup>). The maximum of the RF power density is in 1.8 GHz to 1.9 GHz frequency band, that is around -14.5 dBm/m<sup>2</sup> (3.55 nW/cm<sup>2</sup>). Under this condition, D. Bouchouicha proposed spiral rectennas at 1.85 GHz and 2.45 GHz, as shown in Fig. 2.11 and measured it near a base station in an urban area.

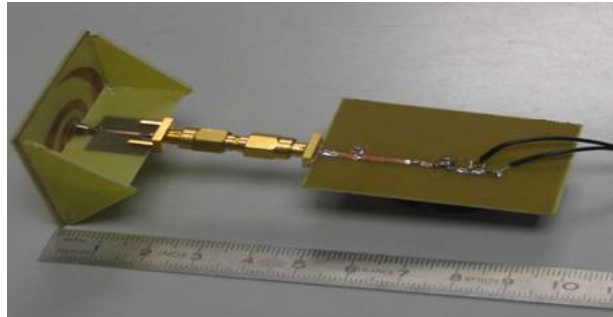


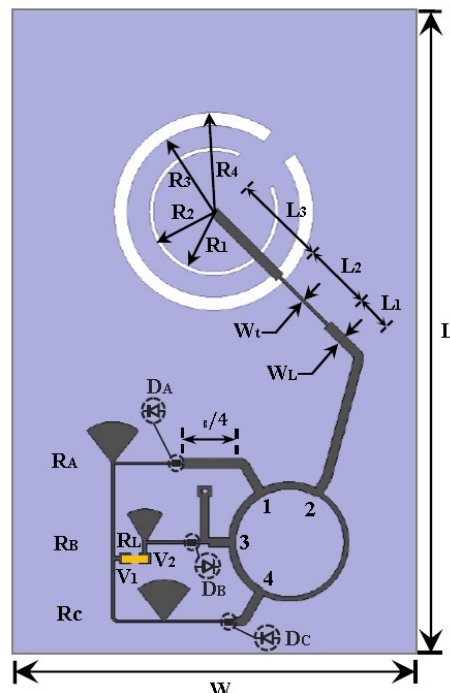
FIGURE 2.11: Rectenna prototype with spiral antenna designed by D. Bouchouicha

The efficiency of rectifying circuits is estimated to 0.7 % for a DC power reaching 1.2 nW over an optimum load of 18 kΩ when the RF power is around -38 dBm in the frequency range of 1.8 GHz to 1.9 GHz. The efficiency over a load of 7.4 kΩ is equal to 13 % with a DC power of 1.3 μW in the case of an input RF power equal to -20 dBm at 2.45 GHz [29].

In the measurements outdoor, the base station was situated at a height of 29 m from the ground and the rectenna was placed at 1.3 m from the ground. The average DC voltage reaches 8 mV for an equivalent power of 3.55 nW, whereas the maximum DC voltage reaches 42 mV which is equivalent to a dissipated DC power of 0.1 μW [29].

Because the measurement in urban RF power density conditions produces very low DC energy, the energy harvested is too low to supply an electronic application continuously. However, this energy can be stored for later utilization. The DC power at 1.85 GHz recovered by a rectenna at the distance of 100 m near a base station was about 0.5 pW to 100 nW with an average value around 3.5 nW [29]. An antenna arrays or a specific emitting source can be used to increase the DC power scavenging and to charge the micro batteries for wireless sensors.

## 2.10 Dual-frequency for energy harvesting at low power levels



$$\begin{aligned}
 R_1 &= 22.5; & R_2 &= 24; & R_3 &= 32; & R_4 &= 37; & L_1 &= 15.1; & L_2 &= 25.4; \\
 L_3 &= 34.5; & W_L &= 3.45; & W_i &= 1.2; & L &= 240; & W &= 150;
 \end{aligned}
 \quad (\text{dimensions en mm})$$

FIGURE 2.12: Dual-frequency rectenna designed by Z. Saddi

Rectennas are composed by antennas and RF-to-DC conversion circuits in the aim of harvesting the RF power and supplying electronic devices continuously. The dual-frequency rectenna is used to maximize the captured RF power. Z. Saddi proposed a rectenna based on a hybrid ring antenna and a antenna with double circular slots. The antenna is optimized with two circular slots on the ground plane

for the dual-frequency property, as presented in Fig. 2.12. Each slot contains a short circuit to generate the circular polarization.

Three converting circuits with Schottky diodes SMS7630 are printed on Arlon 25N substrate with  $\varepsilon_r = 3.4$ ,  $\tan\delta = 0.0025$ , and 1.524 mm thickness. The incident RF power comes from Port 2 and goes to Port 1 and 4 with  $180^\circ$  phase shift. And Port 3 includes all the signals between Port 1 and 4. The circuits  $R_A$  and  $R_C$  operate at 1.8 GHz and  $R_B$  at 2.45 GHz. Based on a hybrid ring, these circuits are serial and parallel in the rectifying system in order to optimize the output DC voltage and power. The rectifying system presents comparable performance at two frequencies 1.8 and 2.45 GHz. Due to the distortion at resonant frequencies, the measurement has been done at 1.8 and 2.35 GHz. This rectenna achieves the efficiency of 21 % when the received power is -20 dBm at 1.8 and 1.35 GHz, and the efficiency of 50 % when the RF power is -6 dBm[70].

## 2.11 Conclusion of the art state

The modern communication respects some standards of wireless devices. Since the power density in an urban environment is sufficient for the application of EM energy harvesting. Some laboratories are focus on this research to improve the life-time of small communication devices. Moreover, for the environment without or not enough ambient energy, microwave energy transmission is a reliable way to supply wireless devices, such as sensor networks.

As presented in Table 2.1, most existing designs of rectennas are applicable for high RF power inputs with good efficiency or low power levels with low efficiency owing to the behaviour of Schottky diodes. It is difficult to supply high levels of microwave energy in the far field due to the attenuation in free-space. Using a high Q crystal quartz resonator can overcome the restriction of power supplying. But the quartz resonant frequency is usually low instinctively. This kind of high Q resonator can not be used at ISM frequencies.

Our goals is to design a rectifying antenna suitable for wireless sensor applications. This radiating antenna is expected to be integrated with rectifying circuits. The approach is to study the electromagnetic distribution and the impedance inside the antenna and to design a feeding style in order to make the antenna well matching the input impedance of diodes inside rectifying circuits. In other words,

Design	Rectenna with unbalanced slots	Dual-diode rectifier	Circular-sector rectenna	Modified bridge rectifier
$\eta$	78%	83%	77.8%	52%
Incident power	16.5mW/cm <sup>2</sup>	0.31mW/cm <sup>2</sup>	0.27mW/cm <sup>2</sup>	0.15mW/cm <sup>2</sup>
Operating frequency	2.45GHz	2.45GHz	2.4GHz	2.45GHz
Common and difference	ISM, high power	ISM, high power	ISM, high power	ISM, high power
Design	Stacked rectenna	Dual-frequency rectenna	Rectifier with high Q resonators	Spiral rectenna
$\eta$	52%	10.5%	22%	0.7 %
Incident power	53.2 $\mu$ W/cm <sup>2</sup>	0.13 and 0.248 $\mu$ W/cm <sup>2</sup>	-30dBm	3.55nW/cm <sup>2</sup>
Operating frequency	2.45GHz	1.8 and 2.35GHz	24MHz	1.85GHz
Common and difference	ISM, medium power	GSM and ISM, low power	Medium wave, low power	GSM, low power

TABLE 2.1: Reference of rectenna design

diodes can be soldered inside or on the fringe of the antenna. It is necessary to consider the combination of antennas and rectifiers in a novel way. Once rectifying circuits are printed with antennas on the same side of PCD, microstrip circuits may affect radiation patterns of antennas. It brings the variation of resonant frequencies and the mismatch between antennas and rectifying circuits. A global analysis by coupling electromagnetic distribution and non-linear circuit simulation can be the breakthrough of this conception.



# Chapter 3

## RF/DC Conversion

Based on the rectification principle in Chapter 1 and the study of the art state in Chapter 2, we have designed some rectifying circuits, RF-to-DC converters. Unlike the operation property of antennas, we notice that rectifying circuits usually operate for a specific region of power levels due to diode characteristics.

2.45 GHz is considered at an operating frequency of our study. Because this frequency band is free for industrial, scientific and medical needs. Besides, it is not attenuated strongly in free-space even under some weather condition [71]. Thus, it is easy to realize a low-cost circuit and apply it for the application of power transmission between ground to ground.

### 3.1 Power range

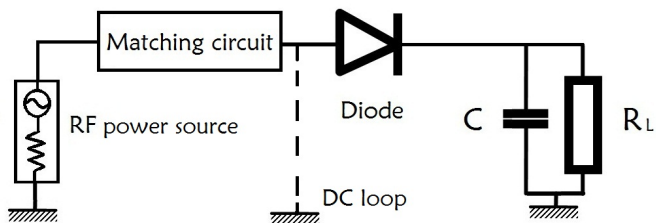


FIGURE 3.1: Series diode circuit with matching circuit

In order to maximise the efficiency value, the serial diode structure has been chosen, as shown in Fig. 3.1. We search for the border of high and low power levels. The power range can be defined by the worldwide standards, the investigation in practical cases, and also the diode behaviours.

On one hand, matching circuits are designed for different power levels [72, 73]. Two factors,  $S_{11}$  and conversion efficiency, are extracted to present the affect of matching levels on conversion efficiencies for the diode HSMS-2820.

For high power levels,  $P_{in} = 10$  dBm for example, the maximum efficiency point is inside the well matched power span ( $S_{11} < -10$  dB), as shown by the shaded area in Fig. 3.2(a). The matching circuit improves the RF-DC conversion efficiency. To the contrary, for the low power level,  $P_{in} = 0$  dBm for example, the maximum efficiency point is beyond the well matched power span, as shown by the shaded area in Fig. 3.2(b). In this case, the contribution of matching circuits to the conversion efficiency is negligible.

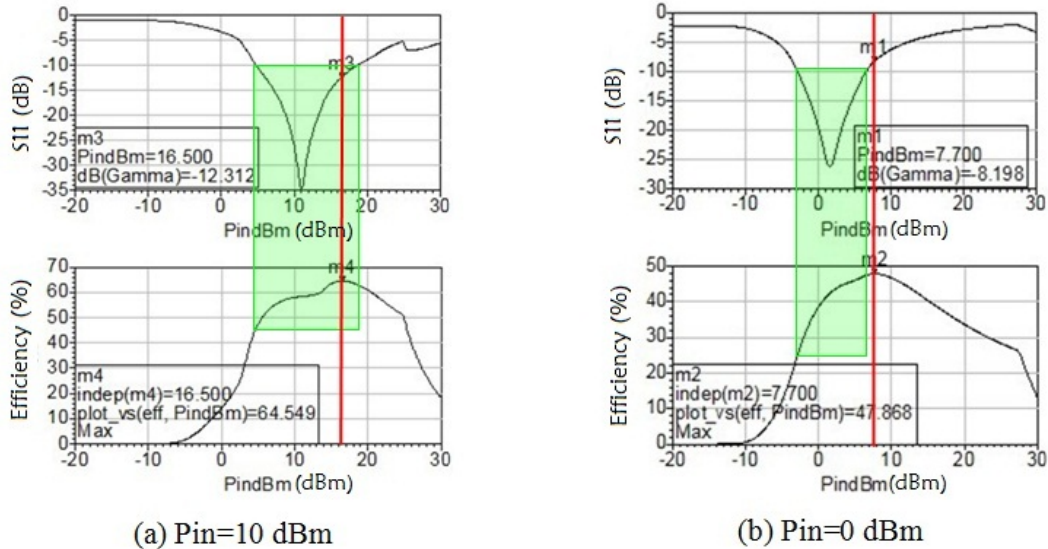


FIGURE 3.2: S parameters and efficiencies for given designs of different power levels

Consequently, high power levels can be noted as the region of  $P_{in} > 5$  dBm and matching circuits improve the efficiency till the limit of diodes. Low power levels can be noted as the region of  $P_{in} < 5$  dBm and the rectifying performance is mainly due to the diode behaviour, and partly owing to the matching levels. Approaches to design a matching circuit are different for each situation. Matching circuits are optimized based on scattering parameters less than -10 dB for the design of high power, and on efficiencies as high as possible for the design of low power.

On the other hand, we found the criteria that half maximum efficiency could define the border of high and low power levels. Take the diode HSMS-2850 for an

instance. As presented in Fig. 1.23, the border of high and low power levels is 5 dBm. This definition is also proved by the worldwide standards. The maximal power density in ICNIRP is  $0.5 \text{ mW/cm}^2$  which is equivalent to 10 dBm input power for a 2 dBi antenna. This value corresponds to the high power range. From WHO, a typical ambient power density is  $50 \mu\text{W/cm}^2$  which is equivalent to 0 dBm input power for a 2 dBi antenna. This value corresponds to the low power range. For other diodes in Fig. 1.23, the border of high and low power is -8 dBm for HSMS-2850 and -5 dBm for HSMS-2860. So we fix the border of high power and low power to 0 dBm. In practical cases, the power density is from  $5 \text{ nW/cm}^2$  to  $26 \mu\text{W/cm}^2$ . All the practical cases are in the low power range.

## 3.2 Design for high power levels

In the research of commercial diodes, existing packaged Schottky diodes are recommended for medium power levels with good conversion efficiency. A few diodes are suitable for very low power applications owing to diode characteristics. Our process of circuit design starts from high power levels, then goes to low power levels, finally gets high efficiency at low power densities.

### 3.2.1 Choice of the diode

The diode HSMS-2820, encapsulated in a SOT23 package, is optimized for zero-bias detector diodes in RF applications [44]. In addition, the parasitic series resistance of this product is low to  $6 \Omega$  involving low conduction loss of diodes and high efficiency of rectifying operation. Moreover, the breakdown voltage is high to 15 V involving high power output.

### 3.2.2 Choice of the load

Followed by the study of diodes, the choice of output load is done to get the best value of effective efficiency  $\eta_{eff}$ . By using HBS and LSSP simulations [74], the load resistance  $R_L$ , operating frequencies, and incident power levels are swept in the simulated model by taking into account an input mismatch. The results show the non-linear behaviour of diodes at different power levels. With the simulating

parameters, we made the load resistance vary and found out the highest efficiency located at the load between  $500 \Omega$  and  $1000 \Omega$ , as shown in Fig. 3.3.

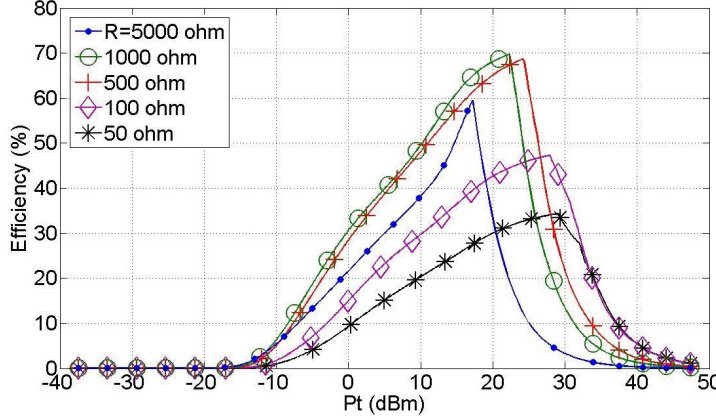


FIGURE 3.3: Effective efficiency versus the transmitted power in terms of load resistance

When the capacitor is greater than  $30 \text{ pF}$ , the capacitance increment does not influence the rectifying effect any more. The capacitor  $C$ , parallel with the load, is chosen as a value which is large enough to export continuous DC voltage.

Consequently, the rectifying circuit consists of a single Schottky diode HSMS-2820, a load resistor  $820 \Omega$ , and a parallel capacitor  $82 \text{ pF}$ . The maximum effective efficiency reaches  $70 \%$  when the input power is  $22 \text{ dBm}$ , although the conversion efficiency is low to  $23 \%$  without matching. The simulated results verify that matching circuits have great significance for the global efficiency.

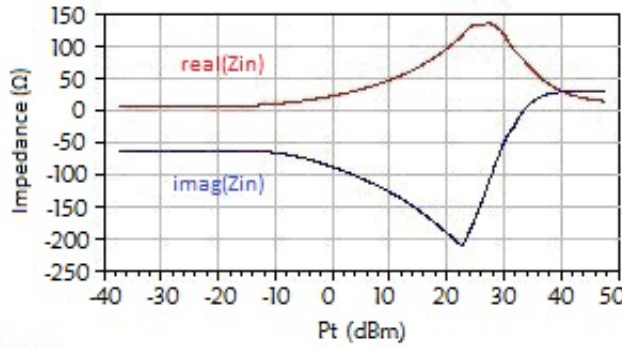


FIGURE 3.4: Input impedance of  $10 \text{ dBm}$  design versus the transmitted power

By means of the simultaneous frequency and power optimization, matching circuits are designed based on a conjugate matching technique between the input impedance of diodes and the reference impedance ( $50 \Omega$ ) so as to improve the global efficiency of rectifying circuits. As shown in Fig. 3.4, the input impedance

at the fundamental frequency (2.45 GHz) is variable for different power levels due to the non-linear behaviour of Schottky diodes.

### 3.2.3 Realisation and measurement

By using the Hybrid optimization in ADS, the double stubs matching circuit is designed corresponding to the input power 10 dBm at 2.45 GHz. As shown in Fig. 3.5, the matching circuit consists of two open stubs ( $L_4$ ,  $L_5$ ) and two microstrip lines ( $L_2$ ,  $L_3$ ) connecting these stubs and the diode. It transfers the input impedance of the rectifying part to  $50 \Omega$ . A quarter wavelength short-circuited stub is introduced next to a  $50 \Omega$  feeding line. It contributes to a DC loop (Via-hole  $P_2$  - Schottky diode - Load - Via-hole  $P_3$  - Ground plane) and also to harmonic-rejection [75]. Microstrip step components are considered to simulate discontinuity effects of different width of transmission lines.

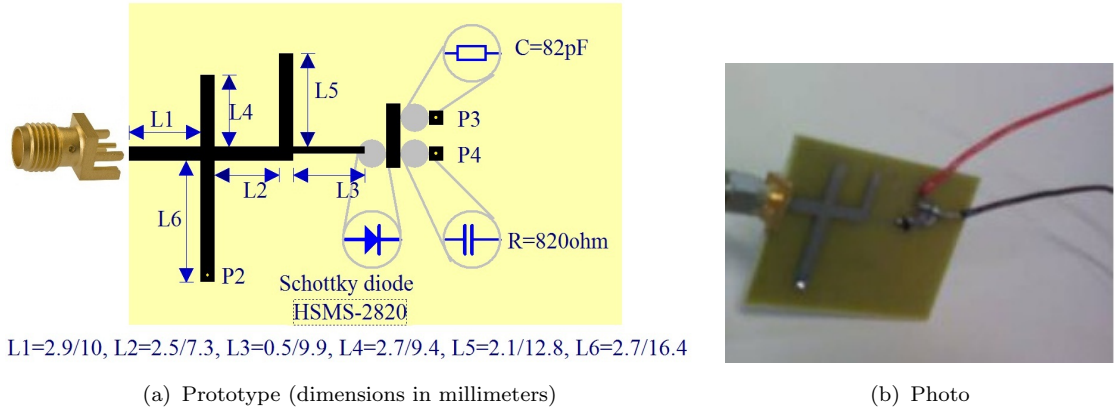


FIGURE 3.5: Configuration of a rectifying circuit designed for 10 dBm

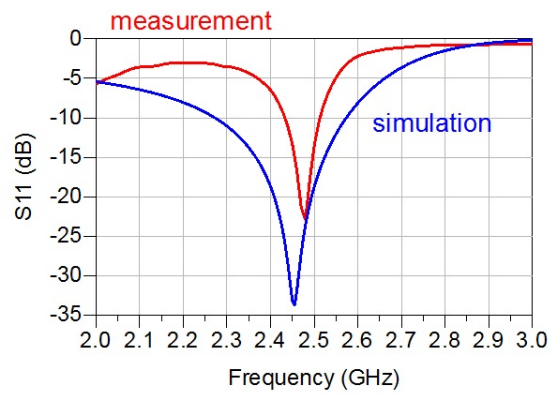


FIGURE 3.6: Frequency response of a rectifying circuit designed for 10 dBm

The circuit is printed on Bernier FR4 substrate with  $\epsilon_r = 4.6$  and 1.58 mm thickness. The return loss is measured by a network analyser. As shown in Fig. 3.6, the measured frequency response has a bandwidth of 80 MHz. The resonant frequency shifts to 2.48 GHz, compared with the simulated one (2.45 GHz). The difference between simulation and measurement is due to the difficulty of the diode modelization and the fabrication accuracy [76].

When the rectifying circuit is connected to a RF power generator, it converts the input power into DC energy. A voltmeter is used to measure DC voltage through the load. The DC output voltage increases till getting the maximum value about 11 V, as shown in Fig. 3.7. The turning point is caused by the breakdown voltage when the reverse bias voltage is beyond the peak inverse voltage. The diode can not continue to operate in the rectifying process after getting the breakdown voltage.

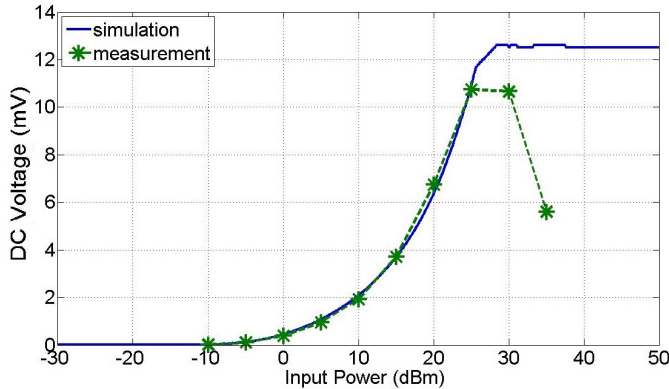


FIGURE 3.7: DC output voltage of 10 dBm design versus the input power

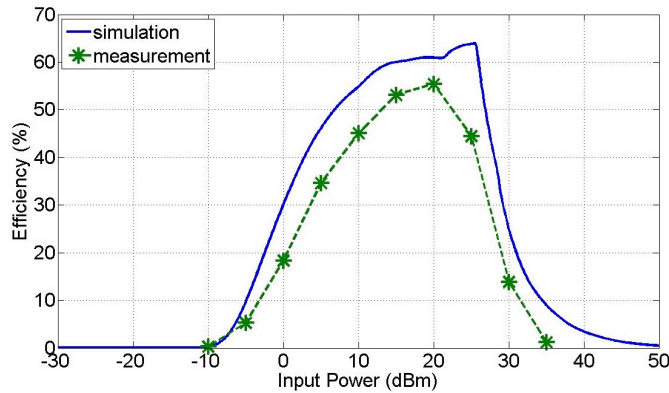


FIGURE 3.8: Conversion efficiency of 10 dBm design versus the input power

The conversion efficiency of rectifying circuits is calculated in terms of the measured DC voltage. It reaches 55 % compared to 65 % theoretically, as presented in Fig. 3.8. The matching circuit operates well. It improves the measured

efficiency close to the simulated one. The losses inside diodes and connectors may reduce the efficiency a bit. This study on a RF-DC rectifying circuit shows that the matching circuit is critical to a good performance.

### 3.2.4 Analysis of matching circuits

The matching circuit transfers the input impedance of rectifying circuits to match the antenna impedance and so improves power transmission from an antenna to a diode. A quarter-wavelength short stub, cooperating with the matching circuit, prevents harmonic signals generated by the rectification process. In the former work, the diode is matched by double stubs in a narrow bandwidth for a specific RF power. Other types of matching circuits, single stub and tapered line for instance, are also considered for the input power 10 dBm at a bandwidth around 2.45 GHz. Different configurations of matching circuits are designed to show the link between their physical limits and available power levels [77].

An approach of hierarchical parameter sweeps is used in ADS simulation. This method is based on scattering parameter simulation at operating frequencies. The sweeps of several parameters are combined into a hierarchical sweep plan. Due to the non-linear performance of diodes, the input impedance changes with the variation of input power levels. The harmonic balance simulation shows DC voltage and alternating voltages in the frequency domain, which include the fundamental frequency and harmonics of high orders.

The input impedance is calculated by the ratio between input voltage and input current at the fundamental frequency. Then the input impedance is sampled corresponding to different power levels. The index of real part and imaginary part of the input impedance is used to label each situation of operating frequencies and power levels. By this way, return losses can be presented both in the frequency domain and in the power domain. Different configurations of matching circuits provide various frequency response and power response.

For the single stub matching circuit, its structure is relative to several elements, including the length and width of a series microstrip line, and the length and width of a stub, as presented in Fig. 3.9.

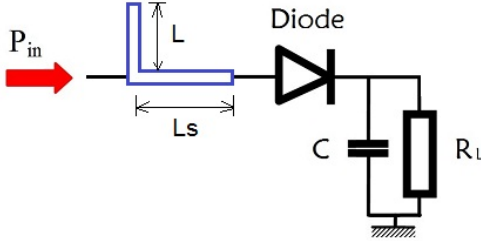


FIGURE 3.9: Scheme of single stub matching circuit

The relation between the physical dimension and the performance of matching circuits is obtained in the frequency domain, as shown in Fig. 3.10, and in the power domain, as shown in Fig. 3.11.

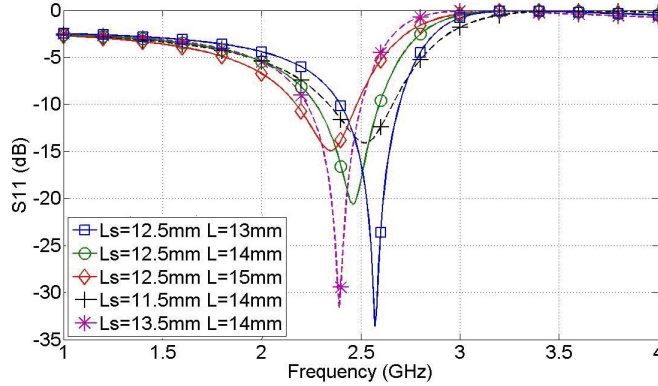


FIGURE 3.10: Frequency response of circuits with single stub matched for 10 dBm

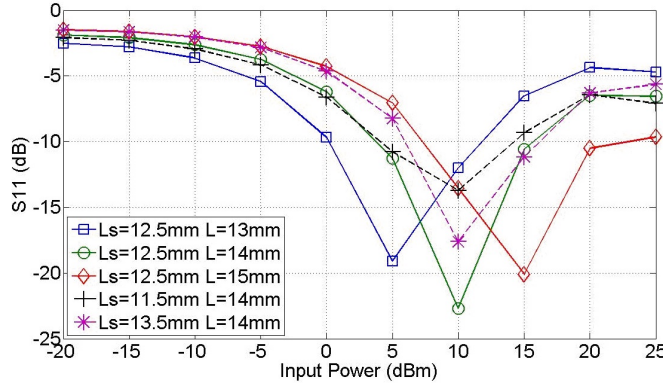


FIGURE 3.11: Power response of circuits with single stub matched at 2.45 GHz

The dimensions of microstrip lines control the frequency response, the power response, and the matching level. The electromagnetic energy flux depends on the microstrip dimension and the operating frequency. The frequency response is not sensitive to the width variation of microstrip lines. The well matched region stays the same and only matching levels vary. But it is sensitive to the length variation

and this sensitivity is high for a narrow microstrip line. The length ( $L_s$ ) of a series microstrip line determines the available range of power levels. And the length ( $L$ ) of a single stub affects the matching level.

Besides, Fig. 3.12 shows the matching level for the optimized design both in the frequency domain and at specified power levels. The figure shows that the matching circuit can control both the power bandwidth and the frequency bandwidth.

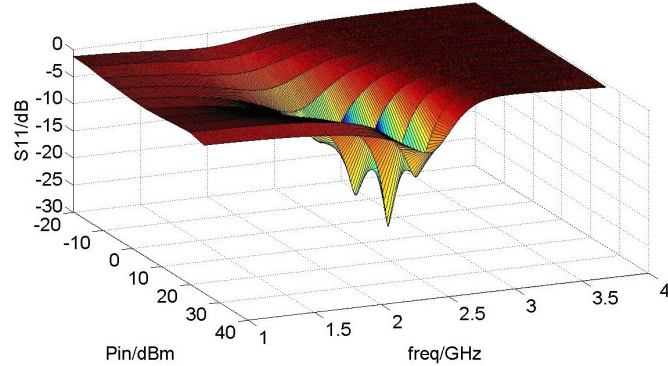


FIGURE 3.12: S parameter variation of the design with single stub matching circuit

A tapered-line matching network matches a real load impedance to a desired real input impedance using a continuously varying line characteristic impedance to realize a specified frequency response [78, 79]. By way of hierarchical parameter sweeps, the length of a tapered line, the input power, and the operating frequency are optimized. Take the exponential tapered line as an example, as shown in Fig. 3.13.

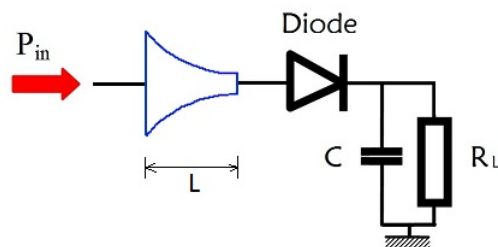


FIGURE 3.13: Scheme of tapered line matching circuit

As shown in Fig. 3.14, tapered line matching circuits provide a good way to get a broad frequency bandwidth. Higher power levels are easily matched by longer tapered lines, and in this case, the power span is larger, as shown in Fig. 3.15.

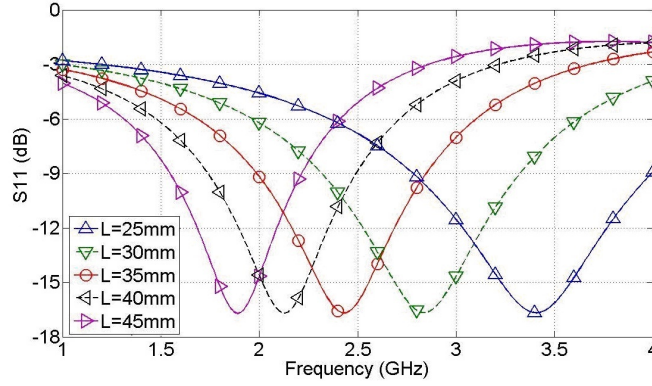


FIGURE 3.14: Frequency response of circuits with tapered line matched for 10 dBm

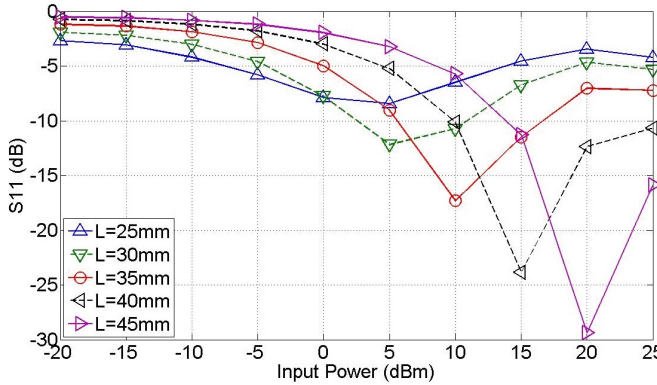


FIGURE 3.15: Power response of circuits with tapered line matched at 2.45 GHz

Meanwhile, Fig. 3.16 shows the matching level for the optimized design both in the frequency domain and at specified power levels. The tapered line matching circuit is capable of wider frequency bandwidth and larger span of input power levels than the single stub matching circuit. It is suitable for RF energy converting of high power levels.

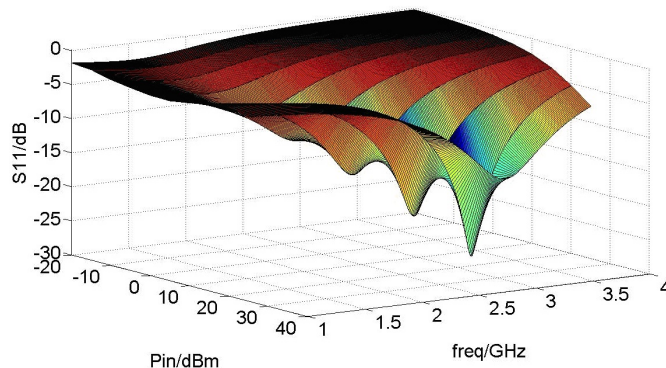


FIGURE 3.16: S parameter variation of the design with tapered line matching circuit

The analysis on a variety of matching circuit configurations brings more evidence to ameliorate the overall performance. The input impedance matching depends on both the non-linear behaviour of diodes against input power levels and the operational frequency affecting the electromagnetic field distribution on transmission lines [80]. The non-linear simulation of rectifying circuits and an analytic description of multiple dimensional parameters are the key to study the relation between the physical layout and the rectifying operation in the frequency domain and in the power domain.

### 3.2.5 Sensitivity of the matching circuit

The layout of double stubs has a little variation of resonant frequencies between simulated results and measured ones. We want to test different configurations of matching circuits in order to improve the process of simulation and realization. Four rectifying circuits were designed by ADS Hybrid optimization. The circuit consists of a Schottky diode HSMS-2820, a capacitor 82 pF, and a resistor 820  $\Omega$ . These circuits were analysed by HBS, LSSP, and other simulating techniques. Then they were realized on Bernier FR4 substrate with  $\epsilon_r = 4.6$  and 1.58 mm thickness, and tested by a network analyser.

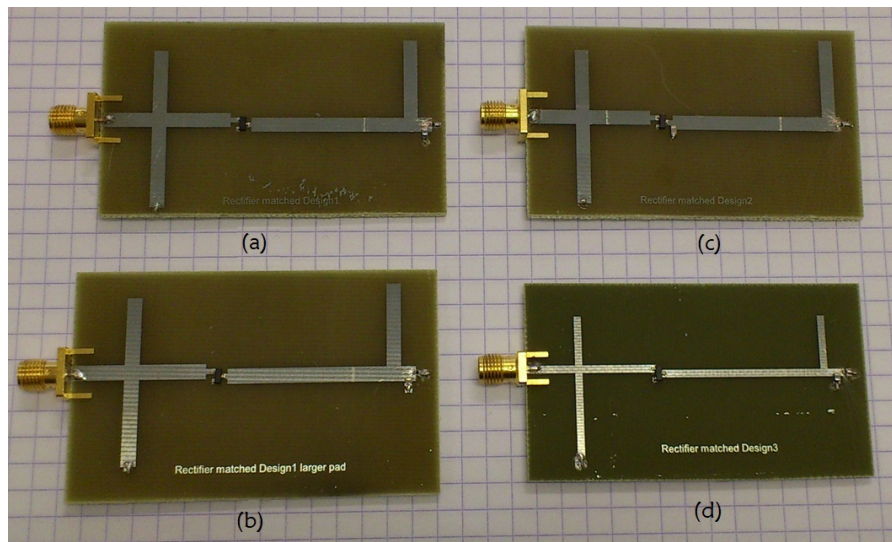


FIGURE 3.17: Fabricated rectifying circuits with some different details

Fig. 3.17 (a) is the *design 1* presenting a rectifying circuit with via-hole of 0.4 mm diameter and via-pad of a side length 0.8 mm. Fig. 3.17 (b) is the *design 1 big pad* presenting a circuit with via-hole of 0.6 mm diameter and via-pad of

a side length 1.5 mm. Fig. 3.17 (c) is the *design 2* showing a circuit with the capacitor near the diode. Fig. 3.17 (d) is the *design 3* showing a circuit printed on FR4  $h=0.8$  mm compared with the former cases ( $h=1.58$  mm).

In comparison of simulation and realization, the measured results agree well with the simulated curves, as shown in Fig. 3.18. The measured resonant frequencies are located around 2.45 GHz with a narrow bandwidth. The high order harmonics (4.9 GHz and 7.35 GHz for instance), generated by diodes, dissipate due to the matching circuit between the input port and the diode.

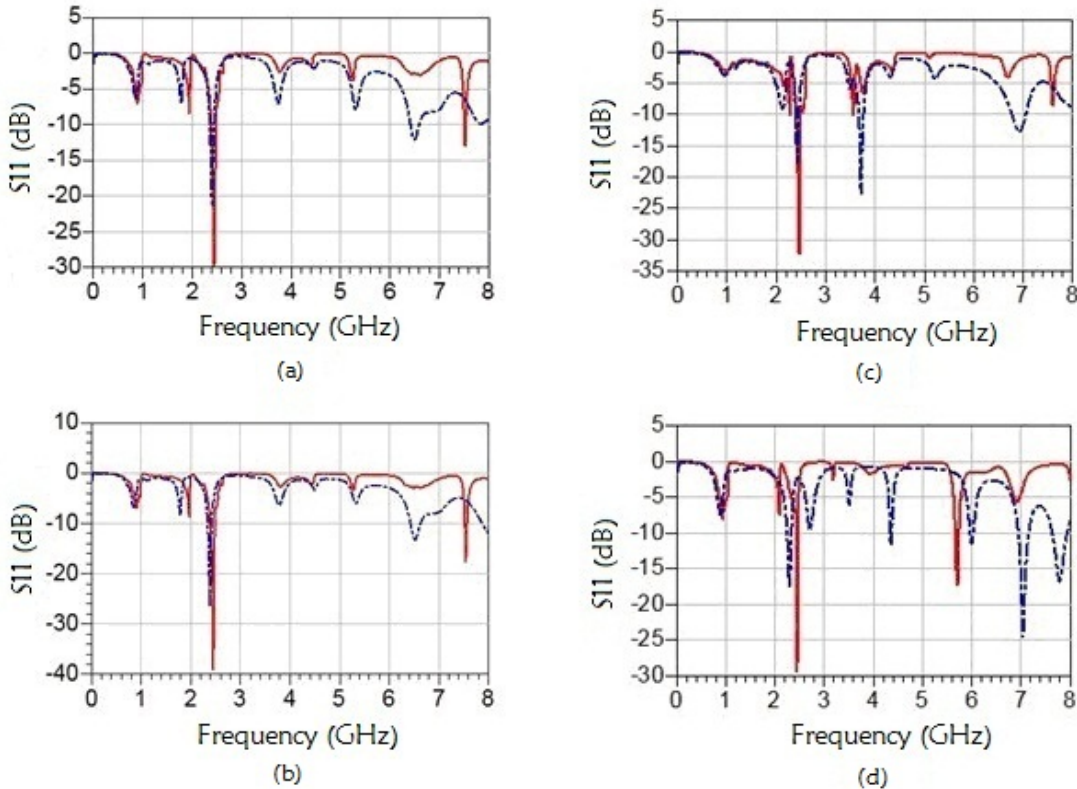


FIGURE 3.18: Frequency response simulated (red curve) and measured (blue curve) with more precise layouts

The simulating model of via-hole is an equivalent serial circuit of a resistance and an inductance. The smaller via-hole shows more inductance behaviour. The via-pad is introduced for precise simulations. Its size is not important, as shown in Fig. 3.18 (a) and (b). The capacitor, parallel with the load, is one part of the output low pass filter. The measured result, in Fig. 3.18 (a) and (c), proves that the circuit with the capacitor near the diode has a worse matching level than the circuit with the capacitor near the load. Fig. 3.18 (d) shows the frequency response is quite sensitive for microstrip lines of a narrow width.

Fig. 3.19 and Fig. 3.20 present the measurements of DC voltage and conversion efficiency. All the curves of output DC voltage have the similar shape. As the input power increases, the output DC voltage increases to more than 11 V and then diodes break down. Corresponding to the DC voltage, the conversion efficiency increases to more than 50 %. It achieves the maximum value before diodes break down.

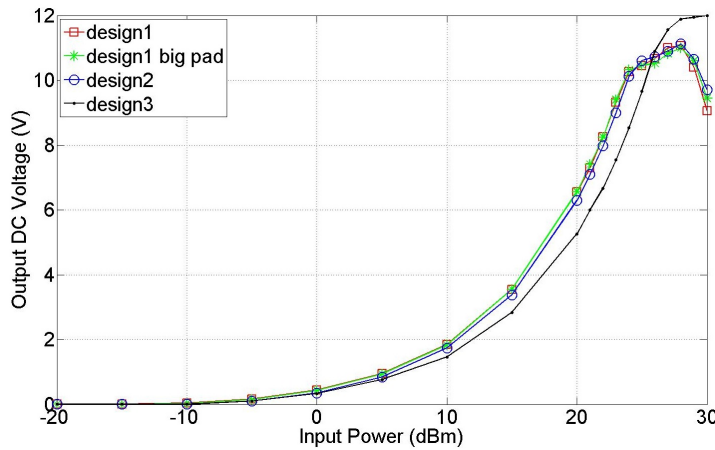


FIGURE 3.19: Measured output DC voltage of 10 dBm design for precise layout

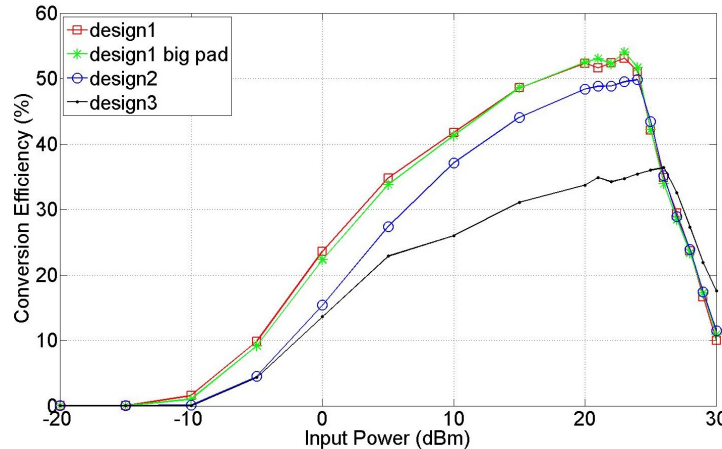


FIGURE 3.20: Measured conversion efficiency of 10 dBm design for precise layout

In the comparison of four rectifying circuits, as shown in Table 3.1, the serial diode configuration with precise via-hole (*design 1*) has a good performance. The matching circuits, such as double stubs and single stub, have the same function to improve the rectifying operation. The efficiency of other designs is not as good as the *design 1*. In the *design 2*, the capacitor is near the diode. The harmonics are generated by diodes and dissipated inside the capacitor. The *design 3* is printed

Rectifying Circuit	<i>design 1</i>	<i>design 1 big pad</i>	<i>design 2</i>	<i>design 3</i>
Resonant Frequency	2.4GHz	2.38GHz	2.42GHz	2.29GHz
$V_{dc}$ @10dBm	1.85V	1.84V	1.745V	1.46V
$V_{dc}$ Max	11.1V@28dBm	11V@28dBm	11.1V@28dBm	12V@30dBm
$Eff$ @10dBm	41.74%	41.29%	37.13%	26%
$Eff$ Max	53.1%@23dBm	54%@23dBm	49.5%@24dBm	36.4%@26dBm

TABLE 3.1: Comparison of rectifying circuits designed for 10 dBm

on the substrate with less height. This circuit owns higher technological sensitivity and higher loss.

### 3.3 Design for low power levels

Based on the study of rectifying circuits with Schottky diode HSMS-2820 for high power applications, obviously this diode is not suitable for low power levels less than -20 dBm. We propose another diode HSMS-2860 for the applications of low power levels.

#### 3.3.1 Choice of the diode and the load

According to SPICE parameters on the data sheet, HSMS-2860 owns large saturation current of 50 nA, small series resistance of  $5 \Omega$ , and small zero-bias junction capacitance of 0.18 pF [81]. It operates from 915 MHz to 5.8 GHz. Compared with other diodes, this diode will give better efficiency for low power levels at the operating frequency 2.45 GHz. Moreover, the diode with single serial diode configuration is sensitive to a weak signal owing to low threshold voltage of 0.35 V. It is suitable for energy harvesting applications at low power densities. However, as a result of low peak reverse voltage of 7 V, this diode should be kept working in low power levels in order to protect it from breaking down.

The load resistance is optimized for the best value of effective efficiency by taking into account an input mismatch. And the capacitor, parallel with the load, takes a suitable value to export continuous DC output.

### 3.3.2 Design of matching circuits

The matching circuit is simulated by the Hybrid Optimization in order to improve the rectification process. We propose three rectifying circuits with different configurations of matching circuit, such as single stub, as presented in Fig. 3.21, radial stubs in Fig. 3.25, and compact structure in Fig. 3.29. The single stub is simple and easily designed. The radial stub is beneficial for wide frequency band. Finally, the compact structure is used to integrate to antennas with the purpose of compact rectennas.

In addition, we use the co-simulation to improve the precision of the simulating model and take into account the loss and the coupling effect. The co-simulation means to combine momentum and circuit simulation from the schematic. Hence, the co-simulation gives an accurate expression of dielectric and metallic losses.

These rectifying circuits are printed on Bernier FR4 substrate with  $\varepsilon_r=4.6$  and 1.58 mm thickness. Each circuit contains a Schottky diode HSMS-2860 in a SOT23 package. Fig. 3.21 presents a rectifying circuit with single stub matching circuit. The length of microstrip line  $L2$  and the length of open stub  $L5$  are optimized for the impedance matching between the diode and the feed line  $L1$ .

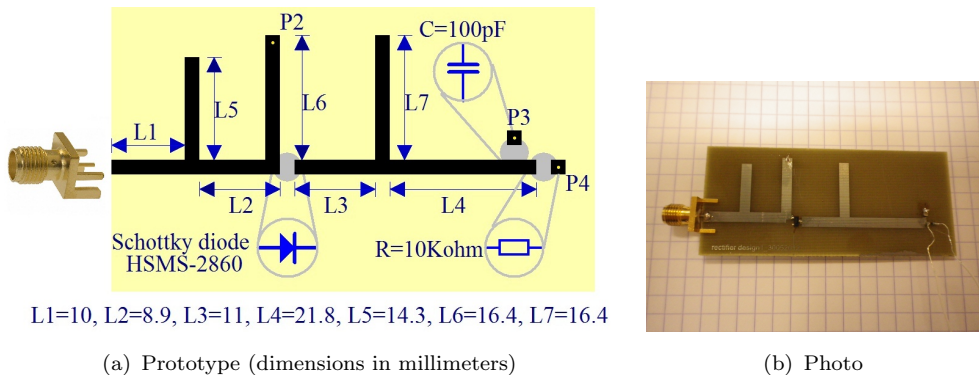


FIGURE 3.21: *design 1*: rectifying circuit with single stub matching circuit

A quarter-wavelength short stub  $L6$  is constructed for the DC loop (Via-hole  $P2$  - Schottky diode - Load - Via-hole  $P4$  - Ground plane). A low pass filter ( $L3$ ,  $L4$ , and  $L7$ ) is added between the diode and the load. It rejects the harmonics generated by diodes and locks the harmonics to join in a new rectifying period. The open stub  $L7$  is quart-wavelength at 2.45 GHz and dissipates the signal the fundamental frequency at the output. The value of resistive load is also optimized to 10 k $\Omega$  for obtaining the best efficiency.

As shown in Fig. 3.22, the measured results agree well with the simulated curves. The resonant frequency is located around 2.44 GHz with a narrow bandwidth. This circuit has a simple profile and it is easily fabricated for given resonant frequencies. However, the frequency response is quite sensitive to the dimensions of microstrip lines. The layout should be precisely designed to obtain the desired resonant frequency.

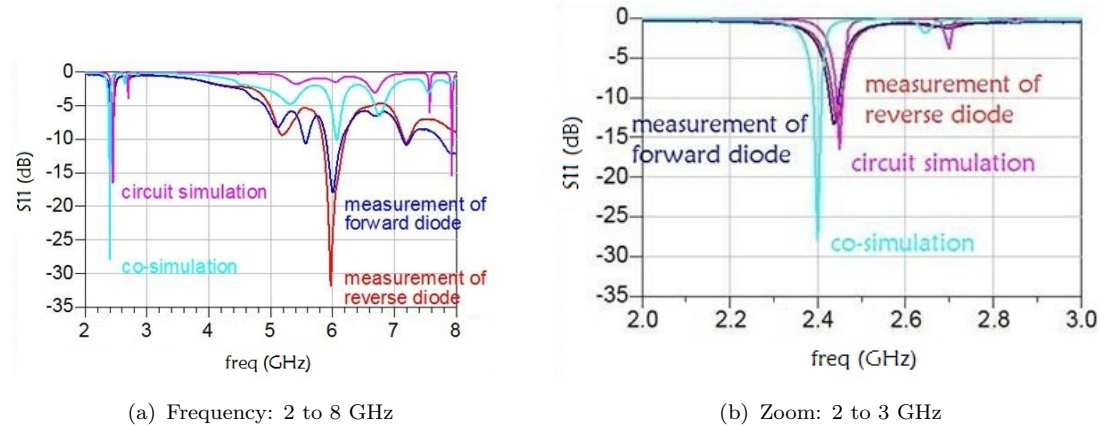


FIGURE 3.22: Return loss of a rectifying circuit with single stub

Furthermore, the diode acts as the equivalent non-linear circuit in the high frequency domain. Since input signals are the sinusoidal wave form, the single serial diode only operates in half-wave rectification no matter that the diode input is its anode or its cathode. Thus, frequency responses fit well between the diode circuit in the forward direction and the one in the reverse direction.

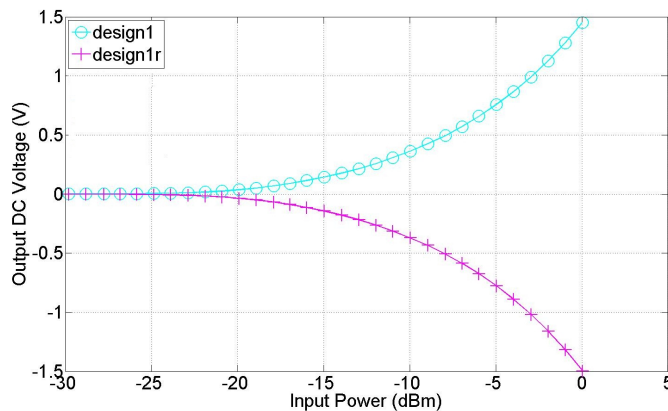


FIGURE 3.23: Measured DC voltage of rectifying circuits with single stub: *design 1* forward diode (cyan curve); *design 1r* reverse diode (magenta curve)

To characterize these rectifying circuits, output DC voltages are measured for various incident power at each resonant frequency, as presented in Fig. 3.23. The

design with single stub matching circuit has a good performance of DC output. The DC voltage of 36.2 mV is obtained over a load of  $10\text{ k}\Omega$  when the input power is -20 dBm. And the DC output increases with an increment of the incident power till 1.5 V for the input power of 0 dBm.

As shown in Fig. 3.24, the circuit with single stub matching circuit has an efficiency of 1.3 % when the input power is -20 dBm. The efficiency increases to 20.9 % for the input power of 0 dBm.

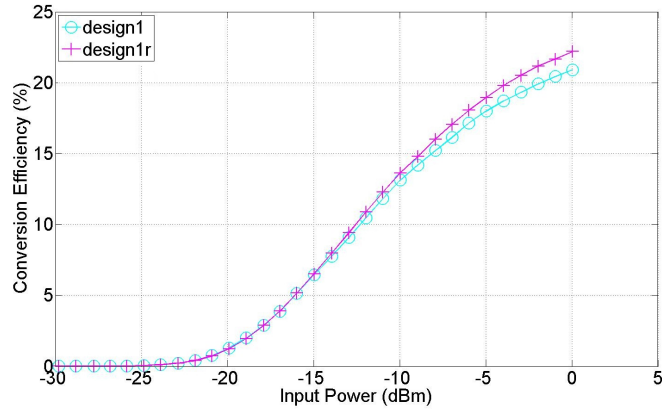


FIGURE 3.24: Measured conversion efficiency of rectifying circuits with single stub: *design 1* forward diode (cyan curve); *design 1r* reverse diode (magenta curve)

The design with single stub is narrowband. In order to widen the frequency bandwidth, a rectifying circuit with radial stubs low pass filter is presented in Fig. 3.25. The single stub matching circuit ( $L2$  and  $L7$ ) is used to match the diode and the feed line  $L1$ . A quarter-wavelength short stub  $L6$  constructs the DC loop (Via-hole  $P2$  - Schottky diode - Load - Via-hole  $P4$  - Ground plane).

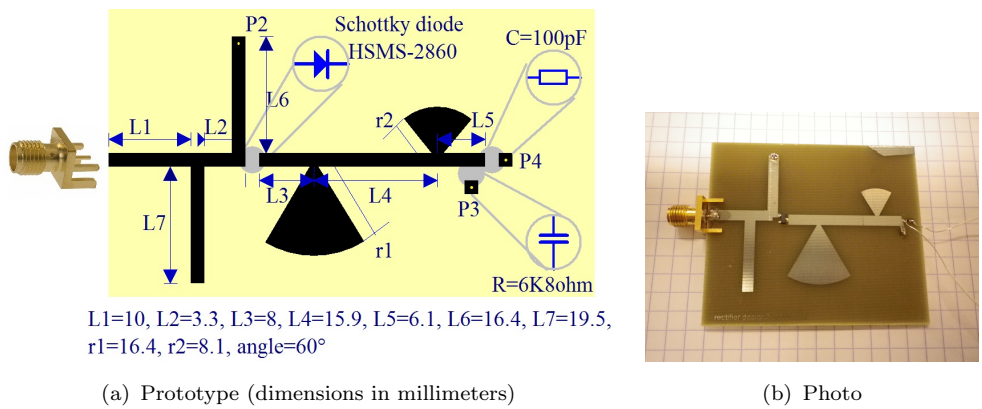


FIGURE 3.25: *design 2*: rectifying circuit with radial stubs low pass filter

The radial stubs low pass filter ( $L3$ ,  $L4$ ,  $L5$ , and radial stubs  $r1$ ,  $r2$ ) is used to prevent harmonics going through the load, and to increase the bandwidth in the frequency response. The radial stub  $r1$  is quart-wavelength at 2.45 GHz and dissipates the signal at the fundamental frequency. The radial stub  $r2$  is quart-wavelength at 4.9 GHz and rejects the signal at the second harmonic. The load is optimized to  $6800 \Omega$ .

The measured results show a little difference against the simulated curves, as presented in Fig. 3.26. The resonant frequency shifts to 2.48 GHz. Nevertheless, this circuit has a bandwidth of 30 MHz three times wider than the former design (10 MHz). The high order harmonics in measured curves are weak due to the outstanding feature of radial stubs between the diode and the load resistor.

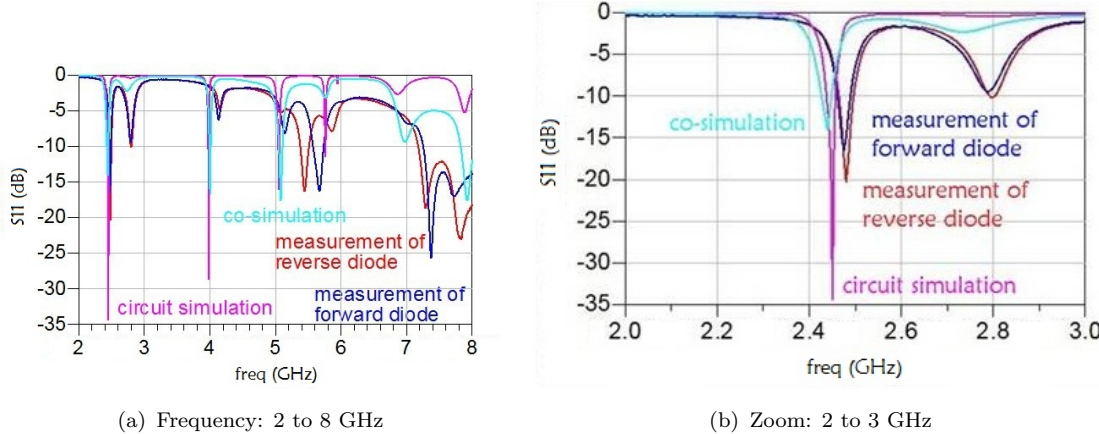


FIGURE 3.26: Return loss of a rectifying circuit with radial stubs low pass filter

The design with radial stubs low pass filter has DC voltage of 35.2 mV over a load of  $6800 \Omega$  when the input power is -20 dBm, as shown in Fig. 3.27. The DC voltage increases to 1.3 V at the power level of 0 dBm. The case of forward diode is the same as the one of reverse diode but in opposite polarity.

As shown in Fig. 3.28, the rectifying circuit with radial stubs low pass filter has a little better rectification performance. The conversion efficiency of 1.7 % is obtained when the input power is -20 dBm. And the efficiency increases with an increment of the incident power till 23 % for the input power of 0 dBm. The efficiency curve perfectly fit between the diode in forward direction and in reverse direction.

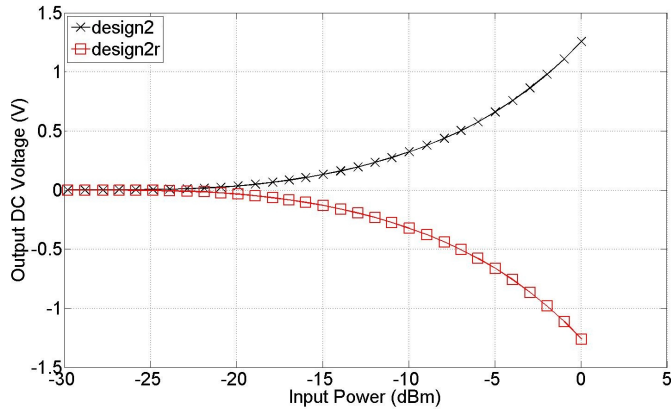


FIGURE 3.27: Measured DC voltage of rectifying circuits with radial stubs low pass filter: *design 2* forward diode (black curve); *design 2r* reverse diode (red curve)

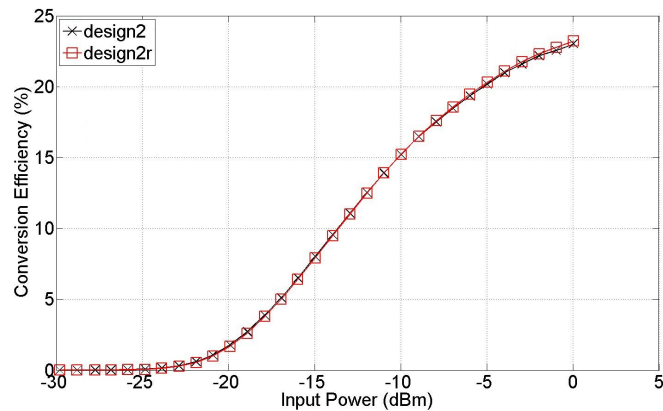
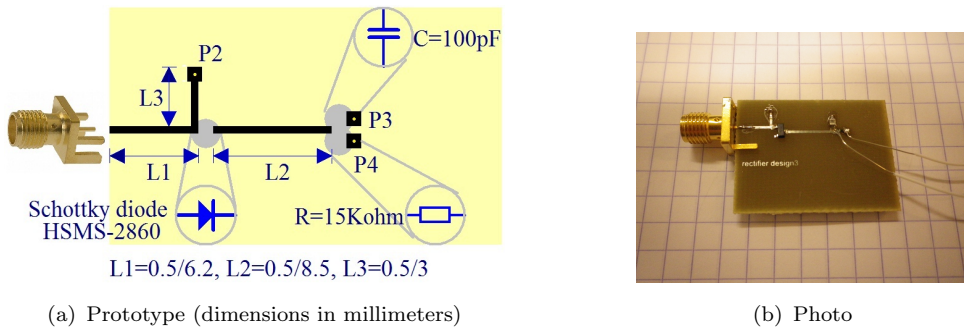


FIGURE 3.28: Measured conversion efficiency of rectifying circuits with single stub: *design 2* forward diode (black curve); *design 2r* reverse diode (red curve)

In order to minimize the surface of rectifying circuits, we designed a rectifying circuit with compact structure. As presented in Fig. 3.29, the matching circuit consists of microstrip lines  $L1$  and  $L3$ . The short stub  $L3$  also contributes to the DC loop (Via-hole  $P2$  - Schottky diode - Load - Via-hole  $P4$  - Ground plane). Besides, a microstrip  $L2$  connects diodes and loads with an optimal length for maximal efficiency. The physical dimensions are reduced by 69 %, compared with the circuit *design 1*.

As shown in Fig. 3.30, the resonant frequency shifts to 2.36 GHz. The variation between simulation and measurement is mainly due to the tolerance of the manufacturing process and the dielectric constant. And the frequency response is sensitive to the microstrip dimension, especially for the narrow width of transmission lines. Matching levels can be changed by a slight variation of its physical

FIGURE 3.29: *design 3*: rectifying circuit with compact structure

dimension owing to its large characteristic impedance.

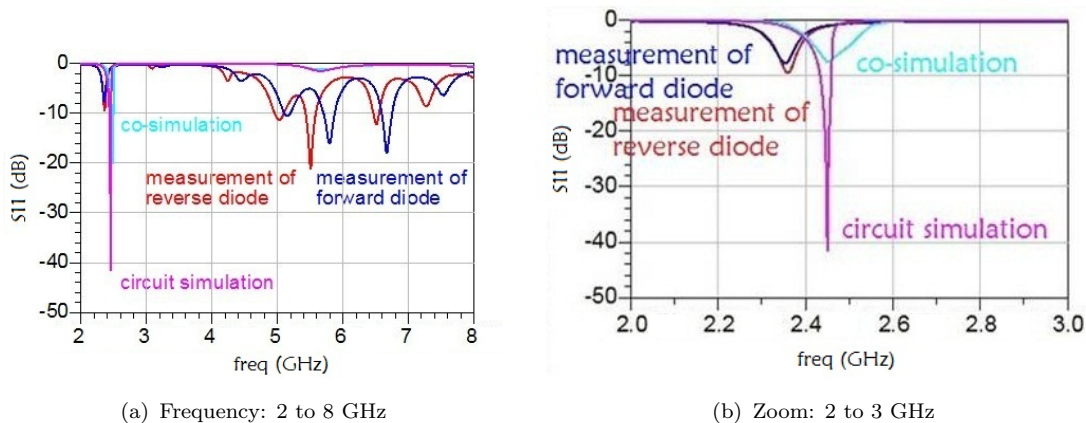


FIGURE 3.30: Return loss of a rectifying circuit with compact structure

As shown in Fig. 3.31, the design with compact structure has DC voltage of 20.5 mV over a load of  $15\text{ k}\Omega$  when the input power is -20 dBm. The DC voltage increases to 1.4 V as the incident power goes to 0 dBm. Fig. 3.32 shows that the circuit with compact structure has an efficiency of 0.3 % when the input power is -20 dBm. The efficiency goes up to 13.4 % at the power level of 0 dBm.

This rectifying circuit achieves size reduction at the cost of conversion efficiency. The matching level at its resonant frequency is not good but the DC output is considerable. The idea inspired by compact structures is considered to integrate the rectifying circuit to the antenna with an improvement on conversion efficiency.

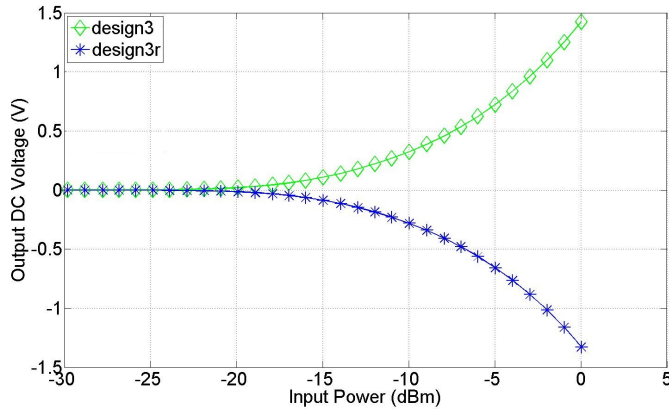


FIGURE 3.31: Measured DC voltage of rectifying circuits with compact structure: *design 3* forward diode (green curve); *design 3r* reverse diode (blue curve)

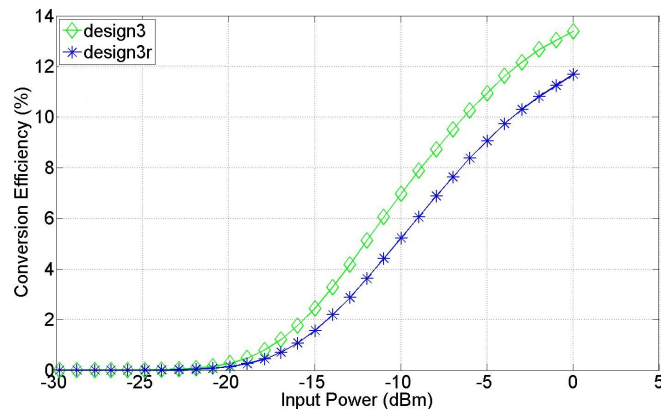


FIGURE 3.32: Measured conversion efficiency of rectifying circuits with compact structure: *design 3* forward diode (green curve); *design 3r* reverse diode (blue curve)

### 3.3.3 Comparison among different circuits

The *design 1*, a rectifying circuit with single stub matching circuit, has the desired resonant frequency and -10 dB return loss bandwidth of 10 MHz. The *design 2* with radial stubs low pass filter has wider bandwidth of 30 MHz owing to the good matching effect of low pass filter. The *design 3* with compact structure shows an advantage of size reduction at the cost of matching level.

As presented in Fig. 3.33, the *design 1* produces 36.2 mV over a load of 10 k $\Omega$  when the input power is -20 dBm. Under the same condition, the *design 2* produces 35.2 mV over a load of 6800  $\Omega$  and the *design 3* yields 20.5 mV over a load of 15 k $\Omega$ . When the incident power increases to 0 dBm, DC voltages of 1.45 V, 1.26 V, and 1.42 V are achieved respectively. The *design 1* has the best

output DC voltage. The single stub matching circuit operates to match the input impedance of diodes in a good matching level.

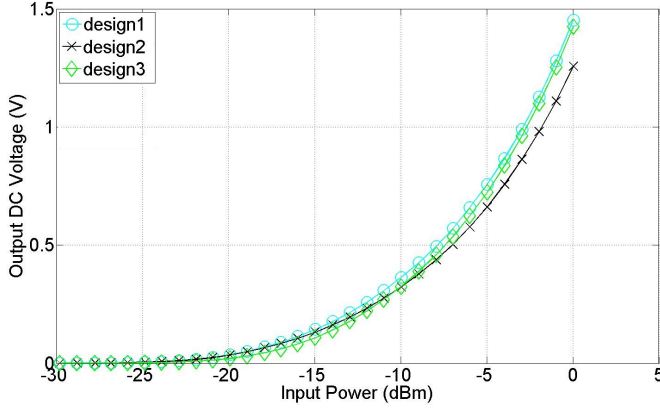


FIGURE 3.33: DC voltage comparison of rectifying circuit configurations

Fig. 3.34 shows the conversion efficiency on rectifying circuits with single stub, radial stubs, and compact structure. The efficiencies are 1.3 % on *design 1*, 1.7 % on *design 2*, and 0.3 % on *design 3* when the input power is -20 dBm. As incident power levels increase, the efficiency also increases. The efficiencies of 20.9 %, 23 %, and 13.4 % are obtained respectively at the power level of 0 dBm. The *design 2* yields the best conversion efficiency. The radial stubs low pass filter prevents harmonics going through the load. By this way, high order harmonics may reflect to diodes and participate in the rectification process.

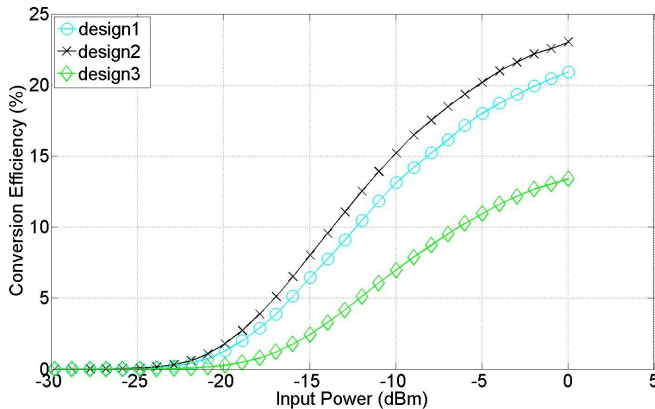


FIGURE 3.34: Efficiency comparison of rectifying circuit configurations

The procedure to design rectifying circuits begins with the choice of non-linear element and lumped components, such as diodes, capacitors, and resistors. Then the layout is designed in order to deal with the impedance match, to prevent harmonics, and to filter desired DC signals.

Rectifying Circuit	<i>design 1</i> (single stub)	<i>design 2</i> (radial stubs)	<i>design 3</i> (compact structure)
Physical Dimension	72mm×31mm	60mm×51mm	30mm×23mm
Load Resistance	10kΩ	6800Ω	15kΩ
Resonant Frequency	2.44GHz	2.48GHz	2.36GHz
Frequency Bandwidth (-10dB)	10MHz	30MHz	0
$V_{dc}$ @-20dBm	36.2mV	35.2mV	20.5mV
$V_{dc}$ @-10dBm	364mV	323mV	325mV
$V_{dc}$ @0dBm	1.45V	1.26V	1.42V
$Eff$ @-20dBm	1.3%	1.7%	0.3%
$Eff$ @-10dBm	13.1%	15.2%	7%
$Eff$ @0dBm	20.9%	23%	13.4%
Advantage	Simple profile, more sensitive to low power levels	Harmonic-rejecting, high conversion efficiency	Compact structure
Drawback	Distortion of high order harmonics	Area occupied	High sensitivity of narrow microstrip, low conversion efficiency

TABLE 3.2: Comparison of rectifying circuits designed for -20 dBm

As presented in Table 3.2, rectifying circuits *design 1* and *design 3* own larger resistive loads than *design 2* and they produce higher DC voltages but lower efficiencies. Considering the surface and the efficiency of each circuit, the *design 1* is the best choice. Moreover, matching techniques make an effort on the improvement of conversion efficiency. The efficiency may be limited by the characteristic of diodes. But the matching network influences the overall performance.

### 3.3.4 Investigation in the simulation model

We have designed rectifying circuits based on ADS simulation. Then the circuits have been realized and measured carefully. But there is a difference between simulation and measurement. In order to improve the simulating process, the performance of rectifying circuits was observed in terms of return loss, output DC voltage, and conversion efficiency. We also did the post-simulation after the measurement.

Take a rectifying circuit with single stub as an example. The circuit contains a serial Schottky diode HSMS-2860, an output load resistor, and a capacitor parallel with the load, as presented in Fig. 3.35. The circuit is printed on Bernier FR4 substrate with  $\epsilon_r = 4.6$  and 1.58 mm thickness.

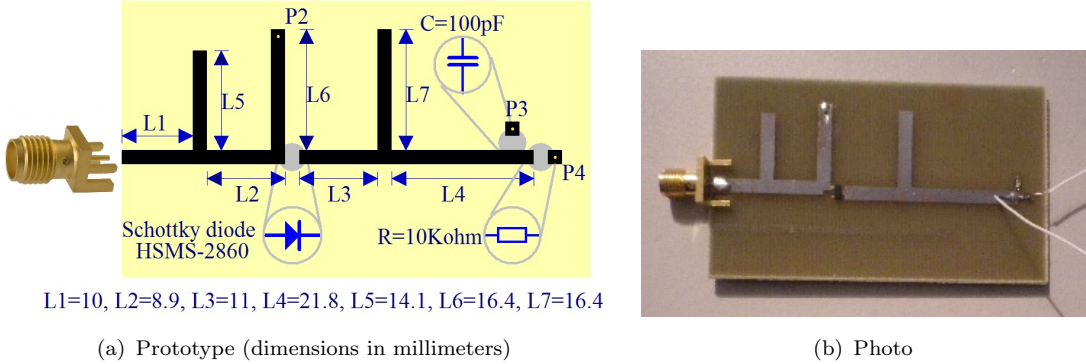


FIGURE 3.35: Configuration of a rectifying circuit designed for -20 dBm

By using ADS harmonic balance simulation and large signal scattering parameter, a capacitor of 100 pF is chosen to export continuous DC signal. The maximum power transfer theorem and DC modelization of rectifying circuits are studied to find an optimal load resistor of  $10 \text{ k}\Omega$  in the aim of obtaining a maximal efficiency.

A simple profile, single stub matching circuit,  $L2$  and  $L5$ , is optimised for an incident power of -20 dBm at 2.45 GHz by means of a criterion of best conversion efficiency in ADS Hybrid optimization. A short stub  $L6$  of quarter-wavelength is proposed at the input of the diode in order to constitute a DC loop and to reject harmonic signals generated by the rectification process. An output open stub  $L7$  of quarter-wavelength composes a low pass filter to prevent harmonic signals going through the load. Considering an open-end effect on a microstrip fringe and an equivalent inductance at a via-hole, some modelling methods improve the simulation accuracy.

The rectifying circuit were realised and tested by Rohde&Schwarz VNA. Then we characterized the parameters of this substrate Bernier FR4 and did the post-simulation after the measurement.  $\epsilon_r$  is 4.26 and  $\tan\delta$  is 0.013. By this way, the measured results agree well with the simulated curves. In the frequency response from 2 GHz to 3 GHz, as shown in Fig. 3.36, a resonant frequency is located around 2.45 GHz with a narrow bandwidth.

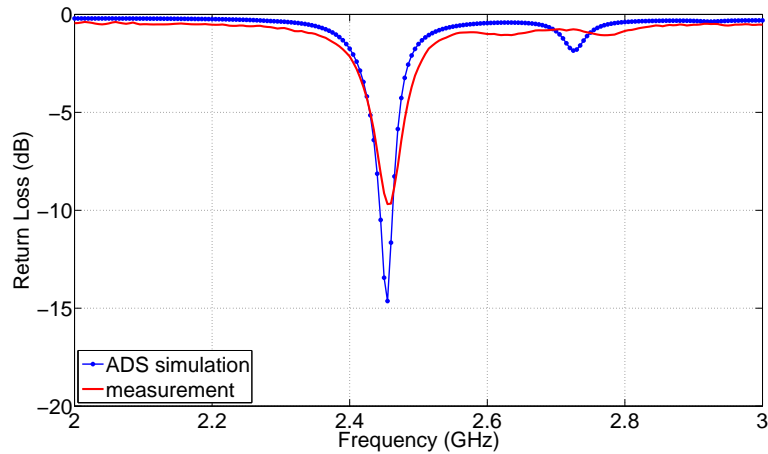


FIGURE 3.36: Post-simulated and measured return loss of the rectifying circuit designed for -20 dBm against the frequency

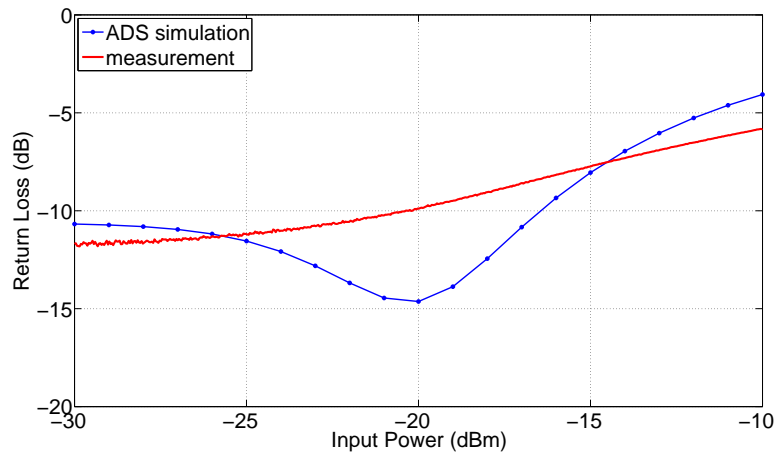


FIGURE 3.37: Post-simulated and measured return loss of the rectifying circuit designed for -20 dBm against the input power

In the power response from -30 dBm to -10 dBm, as shown in Fig. 3.37, a matching level is perfect when an input power is less than -20 dBm. The variation between simulated results and measured ones is mainly led by the limitation of diode modelization and the tolerance of manufacturing process.

The DC output shows the conversion performance of the rectifying circuit. When the input of this circuit is connected to a RF power generator, the output voltage is tested by a multimeter. As seen in Fig. 3.38, the measured DC voltages are 42.1 mV, 146.1 mV, and 338.8 mV, when the power levels are -20 dBm, -15 dBm, and -10 dBm, respectively.

As seen in Fig. 3.39, the measured efficiencies are 1.8 %, 6.7 %, and 11.5

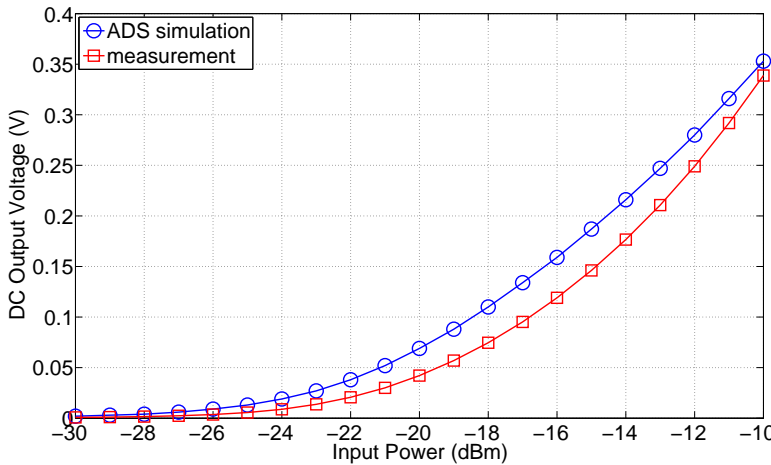


FIGURE 3.38: Post-simulated and measured DC output voltage of the rectifying circuit

% while  $P_{in} = -20$  dBm,  $-15$  dBm, and  $-10$  dBm, respectively. This conversion efficiency is low due to some reasons, including the diode loss, the dielectric loss, the metallic loss, the radiating loss, and the losses introduced by cables and connectors. They are the influential factors for such low power levels.

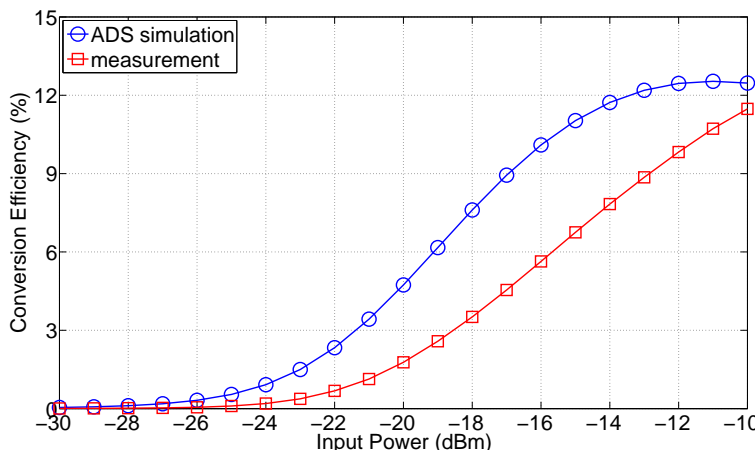


FIGURE 3.39: Post-simulated and measured conversion efficiency of the rectifying circuit

On the other hand, some RF energy, which is not efficiently transferred to receivers, is wasted. If 5 % to 10 % of it can be recycled to useful DC energy, this device contributes to lower costs and a cleaner environment.

## 3.4 Research to increase the efficiency

Rectifying circuits have been studied for high power levels and low power levels. The rectifying circuit with Schottky diode HSMS-2820 and double stubs matching circuit produces DC voltage of 11 V and conversion efficiency of 55 % when the input power is 20 dBm. On the other hand, the rectifying circuit with Schottky diode HSMS-2860 and single stub matching circuit yields DC voltage of 42.1 mV and conversion efficiency of 1.8 % while the incident power is -20 dBm.

These circuits can be applied in the application of power transmission in respect of the requirement of power levels. However, the rectifying circuit designed for low power levels produces low efficiency due to the characteristic of diodes. With the aim of high efficiency at low power densities, other designs have been considered for the application of energy harvesting.

### 3.4.1 Choice of lumped components

HSMS-285x family of zero bias Schottky detector diodes has been designed for use in small signal ( $P_{in} < -20$  dBm and  $freq < 1.5$  GHz) [82]. Even if the diode is not advised for out frequency band, it is adopted because of high sensitivity for low power levels.

The diode HSMS-2850 is encapsulated in a SOT23 package. It owns small zero-bias junction capacitance, large saturation current. Thus it takes fast switching time and operates efficiently. This diode with low barrier height has low junction potential and low forward voltage drop. The forward voltage is 150 mV when the forward current is 0.1 mA and 250 mV when  $I_f = 1$  mA. The speciality of low forward voltage is quite suitable for the design of low power levels. However, the diode has large series resistance. It means the conduction loss inside the diode is huge for high power levels. It is not recommended for high power applications.

By Hybrid optimization in ADS simulation, the rectifying circuit has been optimized for a good matching level around 2.45 GHz. At the same time, the load resistance is chosen as  $3\text{ k}\Omega$  for the best efficiency at the power level -20 dBm. The capacitor parallel with the load is 100 pF which is large enough for continuous DC output.

### 3.4.2 Layout and realisation

The rectifying circuit with Schottky diode HSMS-2850 is shown in Fig. 3.40. The matching circuit is constructed by a single stub  $L_5$  and a microstrip line  $L_2$ . A quarter-wavelength short stub  $L_6$  is located next to the diode. It contributes to a DC loop (Via-hole  $P_2$  - Schottky diode - Load - Via-hole  $P_4$  - Ground plane). The low pass filter consists of  $L_3$ ,  $L_4$ , and an open stub  $L_7$ . This filter rejects harmonic signals and improves the rectification process.

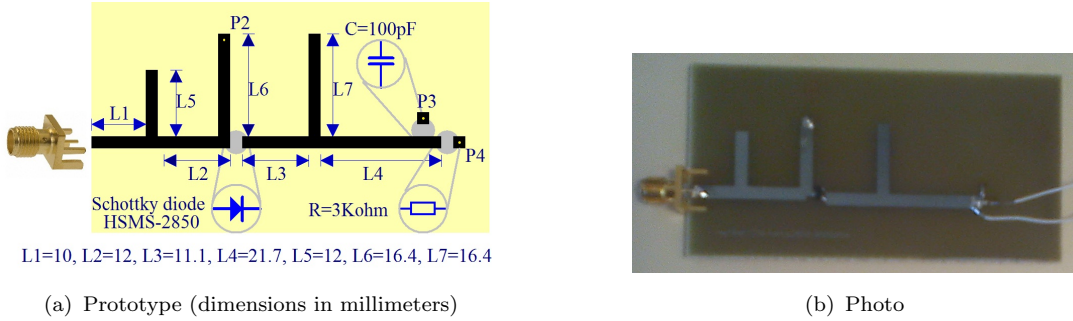


FIGURE 3.40: Configuration of a rectifying circuit with HSMS-2850

The frequency response is tested in ADS LSSP simulation and measured by a network analyser, as shown in Fig. 3.41. The simulated resonant frequency is 2.45 GHz but the measured frequency shifts to 2.4 GHz.

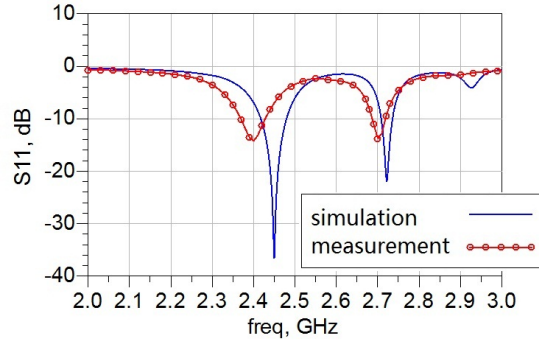


FIGURE 3.41: Simulated and measured frequency response of the rectifying circuit with HSMS-2850

The difference between simulation and measurement is mainly due to the limitation of diode modelization and the tolerance of layout fabrication. The bandwidth of -10 dB return loss is not wide. However, the DC output is not bad around the resonant frequency. In the measurement of DC voltage, the result proves this circuit produces the highest voltage at its resonant frequency, 64 mV

for  $P_{in} = -20$  dBm. Even if it is measured at 2.45 GHz, the DC voltage is about 62 mV.

### 3.4.3 DC voltage and conversion efficiency

When the rectifying circuit connects to a RF power generator, it yields DC voltage measured by a voltmeter. The DC voltages are 9.5 mV, 64 mV, 286 mV, and 968 mV when power levels are -30 dBm, -20 dBm, -10 dBm, and 0 dBm respectively, as presented in Fig. 3.42. The simulation curve shows an agreement with the measurement. The result proves that the design is quite sensitive to low power levels.

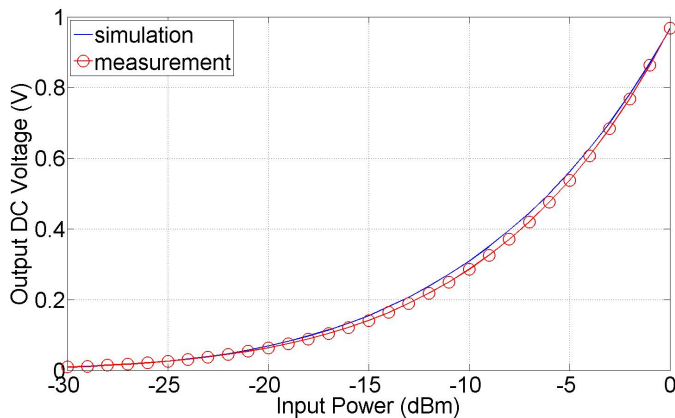


FIGURE 3.42: Simulated and measured DC voltage of the rectifying circuit with HSMS-2850

The conversion efficiencies are 3 %, 13.65 %, 27.23 %, and 31.21 % when power levels are -30 dBm, -20 dBm, -10 dBm, and 0 dBm respectively, as presented in Fig. 3.43. This design with HSMS-2850 yields very high efficiency with small load resistor 3 kΩ. It produces more DC output (64 mV and 13.65 %) then the design with HSMS-2860 (42.1 mV and 1.8 %) when the input power is -20 dBm. It is suitable in the application of power harvesting for low power levels.

The rectifying circuit with Schottky diode HSMS-2850 has been optimized for the input power of -20 dBm at ISM frequency of 2.45 GHz. The single stub matching circuit is used to match the input impedance of diodes to 50 Ω. The input band pass filter rejects harmonic signals and blocks harmonics between the connector and the diode. The harmonics participating to the rectification process improve the conversion efficiency.

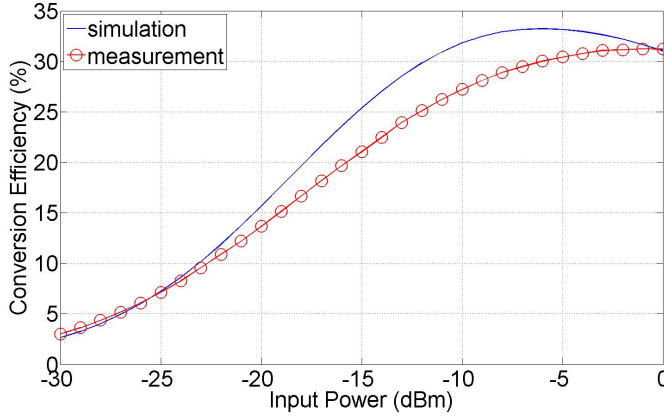


FIGURE 3.43: Simulated and measured conversion efficiency of the rectifying circuit with HSMS-2850

The output low pass filter prevents harmonics through the load.  $L7$  is a quarter-wavelength open stub which constitutes the low pass filter with  $L3$  and  $L4$ . The position of this open stub  $L7$  is optimized for the maximum efficiency, as presented in Fig. 3.44. The length of  $L3$  (11.1 mm) shows the optimal distance between this open stub and the diode.

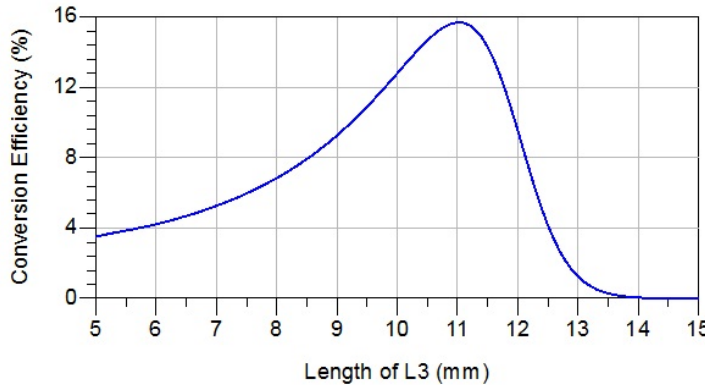


FIGURE 3.44: Simulated conversion efficiency of the rectifying circuit with HSMS-2850 against the length of  $L3$

As well as distributed components,  $L3$  for example, the resistive load is relative to the conversion efficiency, as shown in Fig. 3.45, and determines the rectifying performance [83]. When the load resistance equals to the optimal value,  $3100 \Omega$  in our case, the maximal efficiency about 13.6 % is achieved. The DC modelization of rectifying circuits and the power management based on MPPT (maximum power point tracking) will be discussed in the following section.



FIGURE 3.45: Simulated conversion efficiency of the rectifying circuit with HSMS-2850 against the load

## 3.5 Power management

### 3.5.1 DC modelization

DC modelizaton of rectifying circuits is an idea associated with the equivalent circuit model of Schottky diodes. When rectifying circuits are supplied by a RF power generator, DC currents flow through the load resistor  $R_L$ . With the help of an input band pass filter and an output low pass filter, harmonics generated by diodes are rejected. The matching technique improves the overall performance. Fig. 3.46 shows a rectifying circuit with series single diode.

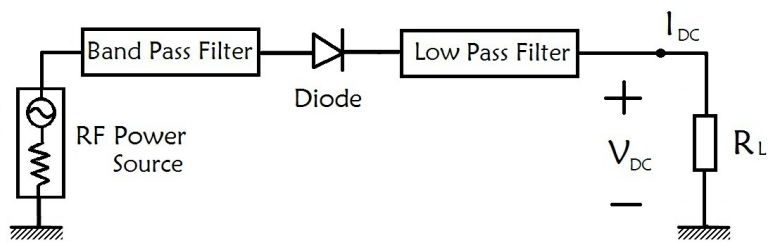


FIGURE 3.46: Single serial diode configuration of rectifying circuits

According to the maximum power transfer theorem, to obtain maximum external power from a source with a finite internal resistance, the resistance of the load must be equal to the resistance of the source as viewed from the output terminals [84].

Take the rectifying circuit with Schottky diode HSMS-2860 for example. The simulated current-voltage curves present that the rectifying circuit acts as a voltage

source with an internal resistance, as shown in Fig. 3.47. The output voltage of rectifying circuits can be expressed by the equation (3.1). The load resistance is the derivative of DC voltage and DC current in a local region. As shown by the equation (3.2), the internal resistance equals to the load when the maximal power is transferred.

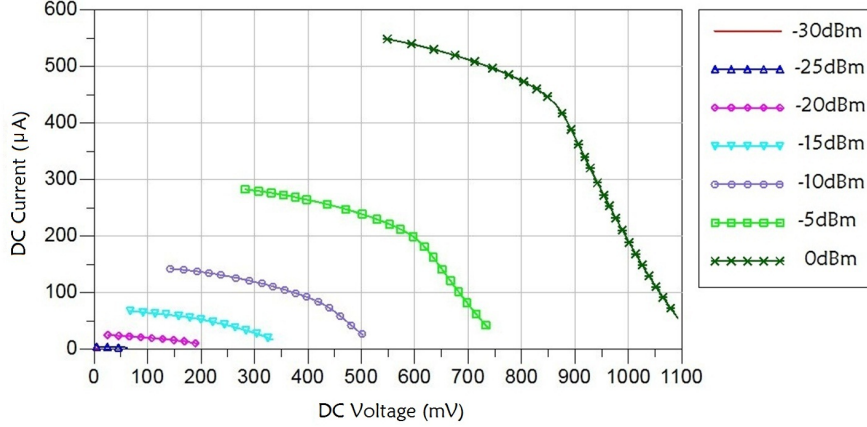


FIGURE 3.47: Simulated DC current-voltage curves of diodes HSMS-2860 for different power levels

$$V_{DC} = E - R_{source} \times I_{DC} \quad (3.1)$$

$$R_{source} = \frac{d(V_{DC})}{d(I_{DC})} \mid_{area=P_{max}} \quad (3.2)$$

The I-V curves are not quite straight lines. They are varying corresponding to the value of external load resistances. Moreover, a certain point on the I-V curve, its projective points on the x-axis and on the y-axis, and the origin point compose a rectangular. The occupied area of this rectangular presents the output DC power at this point, which is corresponding to an external load. That is to say, the maximum power point, composing the largest rectangular, is corresponding to the internal resistance, as seen in the equation (3.3).

$$P_{max} = V_{DC} \times I_{DC} \mid_{R_L=R_{source}} \quad (3.3)$$

The I-V curves are different for each power level due to the non-linear characteristic of Schottky diodes. The derivatives of I-V curves are not the same value for different power levels when the external load is the same. It means that the equivalent internal resistance is the function of incident power levels.

Although the maximum power point are not obviously seen in the I-V curves, Fig. 3.48 gives the link between simulated efficiencies and loads. The maximum power points are located where the derivative of efficiency curves equals to zero. Equivalent internal resistances at ISM 2.45 GHz are 9500  $\Omega$ , 4700  $\Omega$ , 3500  $\Omega$ , 2500  $\Omega$ , and 1800  $\Omega$  when incident power levels are -20 dBm, -15 dBm, -10 dBm, -5 dBm, and 0 dBm respectively. The internal resistance is quite large when the input power is -25 dBm. The lower the power level is, the larger the internal resistance is.

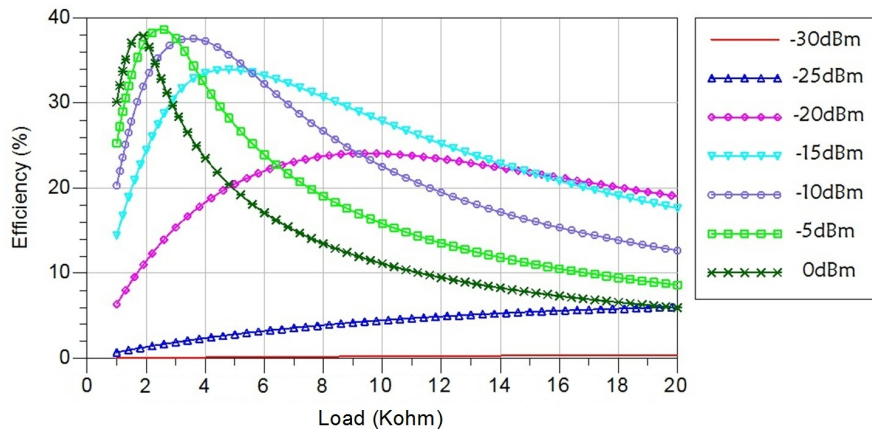


FIGURE 3.48: Simulated efficiencies of diodes HSMS-2860 in terms of load resistances for different power levels

The optimal load resistances are different for each power level owing to the variation of equivalent internal resistances inside rectifying circuits. Furthermore, the rectifying circuit designed for low power levels needs a large load resistance in order to obtain a good efficiency [85].

Compared with Schottky diodes HSMS-2860, the diode HSMS-2850 also operates as a voltage source with an internal resistance in the simulation of DC current-voltage characteristic, as presented in Fig. 3.49. An equivalent internal resistance can be calculated as the derivative of DC voltage and DC current for each power level.

The I-V curves are almost straight lines. The equivalent internal resistance does not change much with the variation of the external load. It is noticed that

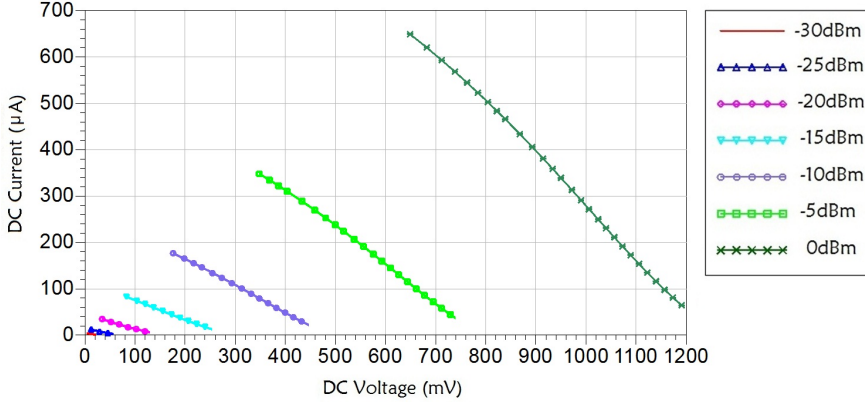


FIGURE 3.49: Simulated DC current-voltage curves of diodes HSMS-2850 for different power levels

the internal resistance varies when the input power increases. In that case, the power management of maximum power tracking is easy to be accomplished for different power levels.

Fig. 3.50 presents the relation between conversion efficiencies and external load resistances. According to the maximum power transfer theorem, the maximal DC output is achieved when the external load equals to the internal resistance.

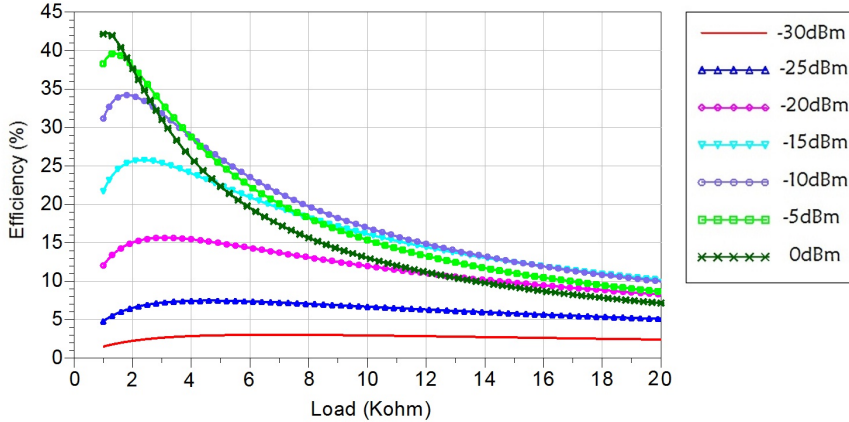


FIGURE 3.50: Simulated efficiencies of diodes HSMS-2850 in terms of load resistances for different power levels

Therefore, equivalent internal resistances can be seen in Fig. 3.50. They are  $6800\ \Omega$ ,  $4600\ \Omega$ ,  $3100\ \Omega$ ,  $2300\ \Omega$ ,  $1800\ \Omega$ ,  $1400\ \Omega$ , and  $1100\ \Omega$  respectively, when input power levels are  $-30\text{ dBm}$ ,  $-25\text{ dBm}$ ,  $-20\text{ dBm}$ ,  $-15\text{ dBm}$ ,  $-10\text{ dBm}$ ,  $-5\text{ dBm}$ , and  $0\text{ dBm}$  at ISM frequency of  $2.45\text{ GHz}$ . The peak of conversion efficiency are  $3\%$ ,  $7.5\%$ ,  $15.6\%$ ,  $25.7\%$ ,  $34.2\%$ ,  $39.6\%$ , and  $42.3\%$  respectively, corresponding to incident power levels.

On the purpose of designing a rectifying circuit with high conversion efficiency for low power levels, the design of -20 dBm input power is optimized with Schottky diode HSMS-2850 and a load resistance of  $3000\ \Omega$ . Under the condition of different power levels, the optimal load for the maximal efficiency varies. This is a difficult point for the power management based on a strategy of MPPT.

### 3.5.2 MPPT

MPPT is initially introduced by the development of photovoltaic systems. It is a technique that grid-tie inverters, solar battery chargers and similar devices to get the maximum possible power from one or more photovoltaic devices, typically solar panels, though optical power transmission systems can benefit from similar technology [86]. Solar cells have a complex relationship between solar irradiation, temperature and total resistance that produces a non-linear output efficiency. It is the purpose of the MPPT system to sample the output of the cells and apply the proper resistance load to obtain maximum power for any given environmental conditions. MPPT devices are typically integrated into an electric power converter system that provides voltage or current conversion, filtering, and regulation for driving various loads, including power grids, batteries, or motors.

As well as photovoltaic generation systems, the I-V characteristic of rectennas is non-linear and varies with incident power levels. The DC output and the conversion efficiency are characterized as a function of DC load, circuit topology, RF frequency, input power, polarization, and incidence angle. Theoretically, the maximum power point is a unique point on the I-V curve. At this point, the entire rectenna system operates with maximum efficiency and produces its maximum output power. Practically, rectennas capture the microwave energy at the power densities on the order of  $10^{-5}$  to  $10^{-1}\text{ mW/cm}^2$ . The location of the maximum power point is unknown but can be located. Therefore, MPPT techniques help rectennas operating at the maximum power point by using calculation models and search algorithms.

Many MPPT techniques have been proposed in the literatures, such as the perturb and observe method [87], the incremental conductance method [88], the load I or V maximization method [89], the artificial neural network method [90],

the fuzzy logic method [91]. These techniques are beneficial in many aspects, including simplicity, convergence speed, hardware implementation, sensors required, cost, range of effectiveness, and need for parametrization.

When a rectenna module is connected to a power converter, maximizing the output power of the DC-to-DC converter or load is to increase the power generated by the rectenna module. The controller measures the link between incremental resistance and DC power change. Once the maximum power point is computed by comparison of the voltage and current, the controller maintains this resistance until the environmental condition changes and the process is repeated.

### 3.6 Conclusion of the design of rectifying circuit

Different configurations of rectifying circuits are proposed in this chapter. From the choice of non-linear element and lumped components (such as Schottky diodes, capacitors, and load resistors), distributed components (microstrips lines and stubs for example) have been optimized in circuit simulations and in momentum. Frequency responses are shown by SP, LSSP, and HBS simulations. Impedance matching techniques are relative to the return loss in the frequency response. DC voltages and conversion efficiencies are simulated in HBS simulations. The results are analysed in the frequency domain and in the power domain in order to obtain an optimal layout.

For the application of power transmission for high power levels, the rectifying circuit with Schottky diode HSMS-2820 and double stubs matching circuit produces maximal DC voltage of 11 V and conversion efficiency of 55% over a resistive load of  $820\ \Omega$  for the power level of 20 dBm.

In the application of energy harvesting for low power levels, the rectifying circuit with HSMS-2860 and single stub matching circuit yields DC voltage of 42.1 mV and the efficiency of 1.8 % over a resistive load of  $10\ k\Omega$  for the power level of -20 dBm. In the anechoic chamber measurement, the captured power by a receiving antenna is around -15 dBm. In this case, the DC voltage is 146.1 mV and the efficiency is 6.7 %.

Due to the low forward voltage drop of HSMS-2850, the rectifying circuit with single stub matching circuit is proposed for power harvesting at low power

densities. This circuit produces DC voltage of 64 mV and conversion efficiency of 13.65 % over a resistive load of  $3 \text{ k}\Omega$  when the incident power is -20 dBm. With the condition of the chamber measurement, the DC voltage is 141.3 mV and the efficiency is 20.05 % at the power level of -15 dBm.

Based on the theory of DC modelization, rectifying circuits have been analysed as an equivalent voltage source with an internal resistance. According to the maximum power transfer theorem, the power management can be accomplished by a strategy of MPPT.



# Chapter 4

## Antenna Design for Energy Harvesting

### 4.1 Characteristics of antennas

An anechoic chamber is designed to reduce reflection and external noise in radio frequencies and used to test antennas, radars, or electromagnetic interference. In the thesis, all the experiments of antennas and rectennas have been done in an anechoic chamber, for example, the set-up of an antenna measurement [92], as presented in Fig. 4.1.

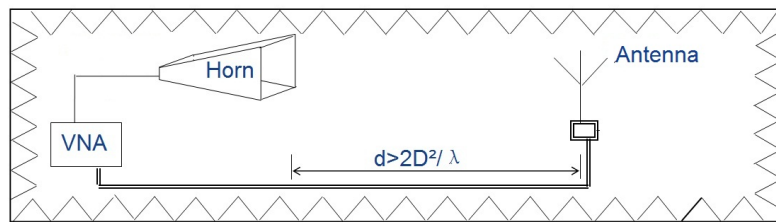


FIGURE 4.1: Experimental set-up of an antenna

#### 4.1.1 Microwave transmission equation

The Friis transmission equation describes the microwave transmission from an emitting antenna to a receiving antenna [93]. Given two antennas, the ratio of power available at the input of the receiving antenna,  $P_r$ , to output power to the transmitting antenna,  $P_t$ , is given by

$$\frac{P_r}{P_t} = G_t G_r \left( \frac{\lambda}{4\pi d} \right)^2 \quad (4.1)$$

where  $G_t$  and  $G_r$  are the antenna gains (with respect to an isotropic radiator) of the transmitting and receiving antennas respectively.

$\lambda$  is the wavelength of the radio wave.

$d$  is the distance between the antennas.

The Friis equation is modified to the equation (4.2) if the gain is in dBi.

$$P_r = P_t + G_t + G_r + 20 \log_{10} \left( \frac{\lambda}{4\pi d} \right) \quad (4.2)$$

The antenna pattern is the response of the antenna to a plane wave incident from a given direction , under the reciprocity principle. A reference antenna is connected to a RF power generator and fixed on the wall inside an anechoic chamber. An AUT (Antenna Under Test) is fixed on a positioning mast that is controlled by a computer. The computer drives the antenna to rotate from -180° to 180°. By this way, the AUT is tested in the relative direction between -180° and 180° towards the reference antenna. This rotation motion is equivalent to the theoretical configuration of AUT in the center, as shown in Fig. 4.2.

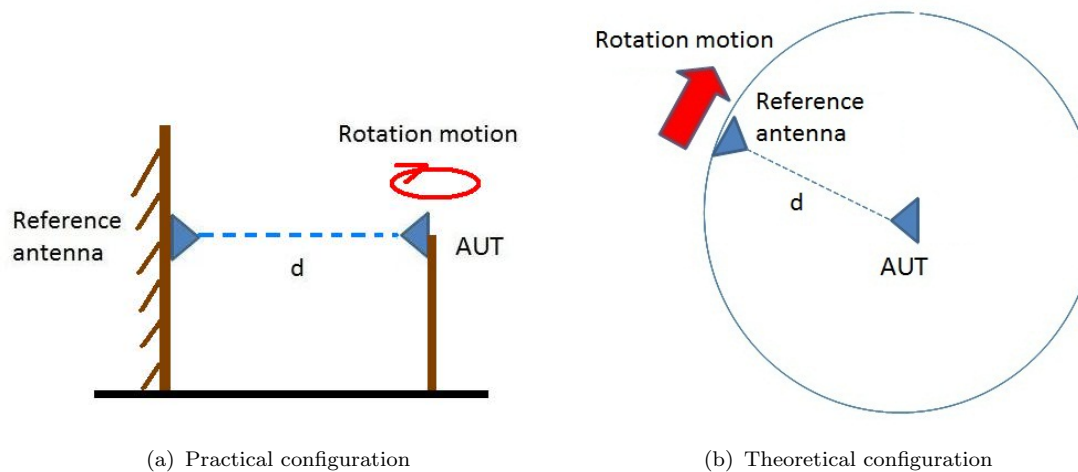


FIGURE 4.2: Scheme of antenna measurements

In order to observe an antenna's radiation patterns in the far-field region, a distance between the emitting antenna and the receiving antenna should be larger than the Fraunhofer distance, that is the far-field distance, as the value of

$$d_f = \frac{2D^2}{\lambda} \quad (4.3)$$

where  $D$  is the largest physical linear dimension of the radiator or the diameter of the emitting antenna.

The Fraunhofer distance provides the limit between the near and far field. If the emitting antenna has the aperture 14 cm and operates at 2.45 GHz, then its far-field distance is 0.32 m.

#### 4.1.2 Emitting antenna

An horn antenna, as shown in Fig. 4.3, is used as an emitting antenna in the experiments. I.M.C. (Israel Microwave Components LTD.) dual polarized antenna model IDPH-2018, is a broadband antenna which provides simultaneously horizontal and vertical polarizations in order to get a high degree of precision [94]. This antenna is fabricated using electro-forming techniques.

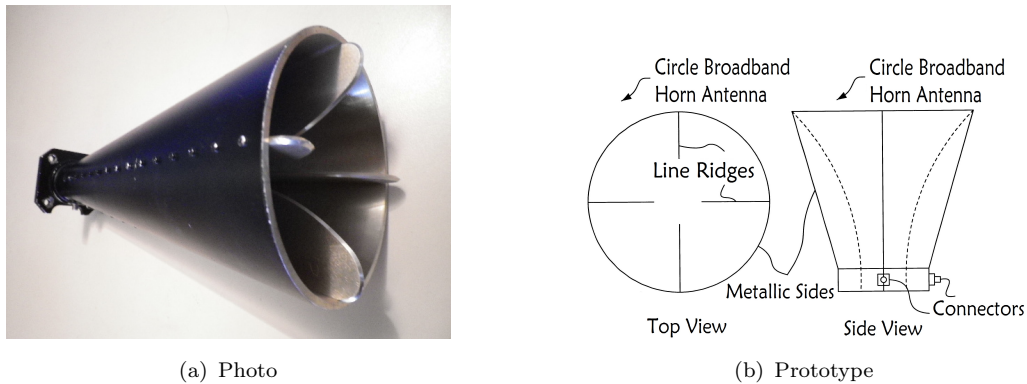


FIGURE 4.3: Emitting horn antenna

According to the mechanical specifications, as shown in Table 4.1, the far-field distance is 0.32 m at ISM 2.45 GHz. Suppose a testing antenna is located in a far-field region where the transferring distance is 5.586 m, the free-space path loss

Electrical		Phase tracking between ports	$\pm 17^\circ$ max
Frequency range	2 to 18 GHz	V.S.W.R.	2.5:1 max
Gain	5 to 18 dBi	Power handling	10 Watts C.W.
Polarization	Simultaneously horizontal and vertical	Mechanical	
Beam width of 3 dB	60° to 10°	Connectors	S.M.A. female
Isolation between ports	25 dB min	Size	140 mm aperture 305 mm long
Amplitude tracking between ports	$\pm 1.3$ dB max	Weight	2 Kg

TABLE 4.1: IDPH-2018 specifications

is inevitable, as presented in the equation (4.4). The attenuation in free-space is 55.16 dB when the microwave frequency is 2.45 GHz.

$$\alpha = -20 \log_{10} \left( \frac{\lambda}{4\pi d} \right) = -20 \log_{10} \left( \frac{c}{4\pi df} \right) \quad (4.4)$$

According to the specifications of the horn antenna, the gain is from 5 to 18 dBi when the frequency range is from 2 to 18 GHz. Gain is the very important figure-of merit parameter of an antenna. Thus the absolute-gain measurements is used to extract the horn gain at desired frequencies [95].

Two identical horn antennas are under test. One is transmitting and the other is receiving. Assuming that the antennas are well matched in terms of impedance and polarization.

$$(G)_{dB} = \frac{1}{2} \left[ 20 \log_{10} \left( \frac{4\pi d}{\lambda} \right) + 10 \log_{10} \left( \frac{P_R}{P_T} \right) \right] \quad (4.5)$$

where  $d$  is the antenna separation.

$P_R$  is the received power.

$P_T$  is the transmitted power.

If the antennas are not well matched, the mismatching factor is introduced in the former equation.

$$T_{12} = \frac{P_R}{P_T} = G_1 * G_2 * FSL * (1 - S_{11_1}^2)(1 - S_{11_2}^2) \quad (4.6)$$

where  $FSL$  is the free-space loss. This attenuation is  $20\log_{10}\left(\frac{4\pi d}{\lambda}\right)$  in dB.

$S_{11_1}$  and  $S_{11_2}$  are the reflection coefficients of these two antennas. These parameters can be measured separately by a network analyser.

Thus the gain equation of the antenna under test is modified by

$$(G)_{dB} = \frac{1}{2}[20\log_{10}\left(\frac{4\pi d}{\lambda}\right) + 10\log_{10}\left(\frac{P_R}{P_T}\right) - 10\log_{10}(1 - S_{11_1}^2)(1 - S_{11_2}^2)] \quad (4.7)$$

This two-antenna method is used to obtain the gain of the broadband horn antenna either in horizontal polarization or in vertical polarization. The measured curves of the horn gain are presented in vertical and horizontal polarization in Fig. 4.4. The frequency range is from 1 to 12 GHz. And the values of antenna gain at 2.45 GHz are 4.55 dBi in vertical polarization and 3.138 dBi in horizontal polarization respectively.

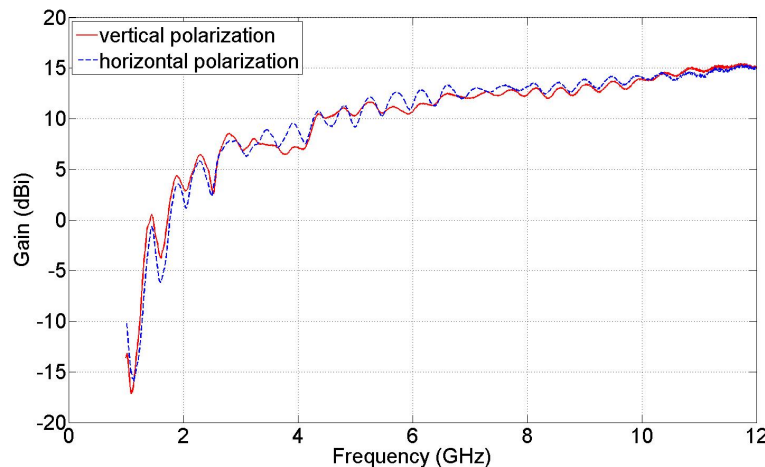


FIGURE 4.4: Measured gain of the emitting horn antenna

The gain of the horn antenna is extracted by the two-antenna method. Then take the horn antenna as the reference. The three-antenna technique is used to measure the gain of antennas under test [96]. The gain of the AUT is obtained by the gain-comparison measurements. In this technique, the gain of the horn antenna is the reference gain. Two sets of measurements are performed. First, the standard gain antenna is in receiving mode, and the received power  $P_S$  is recorded as the calibration process. Second, the standard gain antenna is replaced by the testing antenna, and its received power  $P_T$  is measured. The geometrical arrangement is kept intact and the transmitted power is maintained same.

$$(G_T)_{dB} = (G_S)_{dB} + 10\log_{10}\left(\frac{P_T}{P_S}\right) \quad (4.8)$$

where  $G_T$  is the gain of the test antenna.

$G_S$  is the gain of the standard antenna.

### 4.1.3 Description of the received power

In order to observe an antenna's operation, the power at the location of the receiving antenna is expressed by two concepts. One is the total received power which can be measured at the output of the antenna by a power meter. Taking into account the antenna gain, this value can be verified by the equation (4.2).

The other concept is the power density (power per unit area). Take an isotropic radiator as the reference. It is a theoretical, lossless, omnidirectional antenna. And it radiates uniformly in all directions. If the power is radiated from an isotropic antenna, it will have a uniform power density in all directions. The power density at any distance from an isotropic antenna is simply the transmitted power divided by the surface area of a sphere ( $4\pi d^2$ ) at that distance. The surface area of the sphere increases by the square of the radius, thus the power density decreases by the square of the radius.

The power density from an isotropic antenna is given by

$$p_{iso} = \frac{P_t}{4\pi d^2} \quad (4.9)$$

where  $P_t$  is the transmitted power.  $P_t$  is either peak or average power depending on how  $p_{iso}$  is to be specified.

$d$  is the range from an antenna, that is the radius of a sphere.

Directional antennas are used to control most of the radiated power in a particular direction. The gain of an antenna is the ratio of power radiated in the desired direction as compared to the power radiated from an isotropic antenna. Thus the power density at a distant point from a directional antenna with a gain  $G_t$  is the power density from an isotropic antenna multiplied by the directional antenna gain. The power density from an emitting antenna is estimated by

$$p = \frac{P_t G_t}{4\pi d^2} \quad (4.10)$$

The definition of power density is only relative to the radiation of an emitting antenna and to the position of a receiving antenna. However, the received power is determined by an effective capture area of a receiving antenna. The effective area is a measure of how effective an antenna is at the power of radio waves. The received power available at the antenna terminal is the power density times the effective capture area of the receiving antenna.

For a given regular antenna, the capture area is constant no matter how far it is from the transmitter. As illustrated in Fig. 4.5, the received signal power decreases by 1/4 as the distance doubles. In that case, the received power is easily calculated or tested by a power meter.

The effective capture area is not always directly correlated to the physical area. It is a function of antenna gain and operating wavelength [97]. It is determined by the voltage available across a load matching the antenna feed impedance for a given electromagnetic field strength density. If the antenna is placed in an electromagnetic field of a certain intensity, a certain amount of power will appear in the load at antenna terminals. The area of space around the antenna that

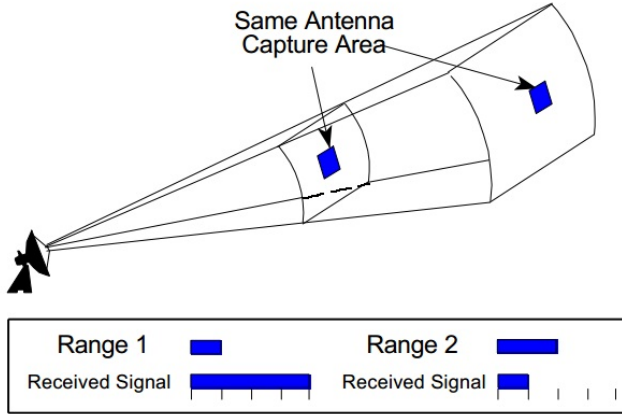


FIGURE 4.5: Power density versus range

provided this amount of power is the effective capture area. The physical size determines the effective area as it might affect gain of an antenna, as well as the shape, the mode, and the coupling effect [98, 99].

Hence, the effective area represents how much power is captured from the plane wave and delivered by the antenna. A general relation for the effective area in terms of the peak antenna gain  $G_a$  of any antenna is given by

$$A_e = \frac{\lambda^2 G_a}{4\pi} \quad (4.11)$$

## 4.2 Patch antenna

The technical constraints lead us to choose printed antennas which is easily fabricated and integrated with rectifying circuits. Some antenna types satisfies our requirement, including patch antenna, monopole antenna, dipole antenna and so on.

The microstrip patch antenna is a popular printed resonant antenna for narrowband microwave wireless applications. Due to its planar configuration, low cost, and easy integration with microstrip technology, the microstrip patch antenna has been widely studied as elements for an array and it is becoming increasingly useful because of being printed directly onto a circuit board [100].

### 4.2.1 Dimension of the patch

All the parameters in a rectangular patch antenna design ( $L$ ,  $w$ ,  $h$ , and  $\varepsilon_r$ ) control the properties of the antenna, as presented in Fig. 4.6. Firstly the length of a patch controls the resonant frequency. In general, even for more complicated microstrip antennas, the length of the longest path on the microstrip controls the lowest frequency of operation. The equation (4.12) gives the relationship between the resonant frequency and the patch length [98].

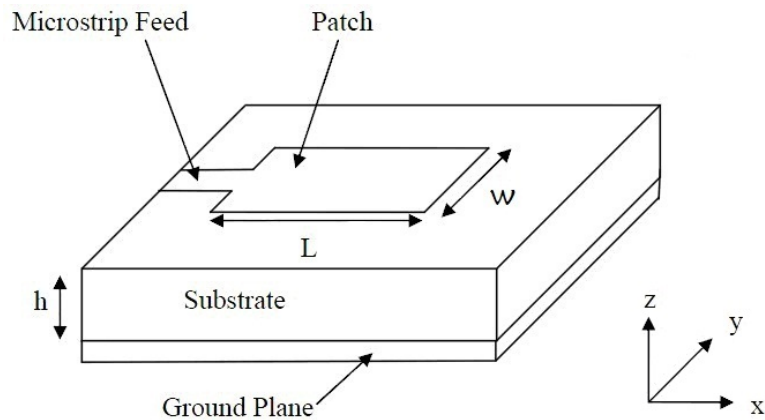


FIGURE 4.6: Microstrip patch antenna

$$L = \frac{\lambda_0}{2\sqrt{\varepsilon_{eff}}} \quad (4.12)$$

$$w = \frac{\lambda_0}{2} \cdot \left( \frac{\varepsilon_r + 1}{2} \right)^{-1/2} \quad (4.13)$$

$$\text{with } \varepsilon_{eff} = \frac{\varepsilon_r + 1}{2} + \frac{\varepsilon_r - 1}{2} \left( 1 + \frac{10h}{w} \right)^{-0.555} \quad (4.14)$$

where  $L$  is the length of the patch.

$h$  is the thickness of the substrate.

$w$  is the width of the patch.

$\lambda_0$  is the wavelength in free-space.

$\varepsilon_r$  and  $\varepsilon_{eff}$  are relative and effective dielectric constant of the PCD material.

The radiation from a rectangular patch is equivalent to the radiation of two rectangular apertures, as shown in Fig. 4.7. A stationary wave appears when a microstrip line of a length  $\lambda/2$  ends with open circuit at two sides. The electric field is maximal at the ends and zero in the center. So it is in phase opposition inside a substrate, but the leaky fields are in phase at the ends. Electric fields add up in phase, extend further away from the patch, and produce the radiation of the microstrip antenna.

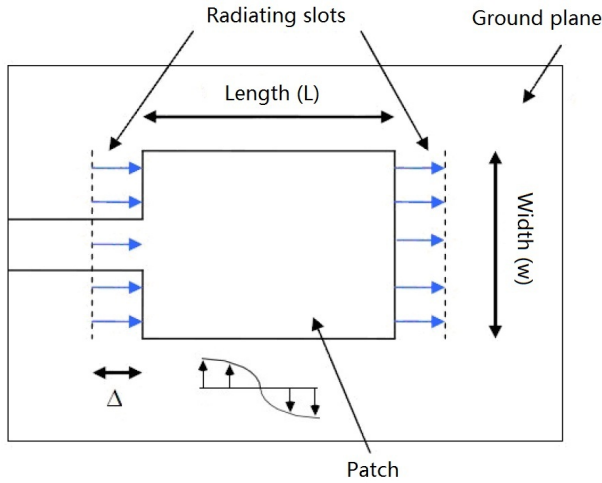


FIGURE 4.7: Top view of patch antenna

Consequently the effective length of a patch is greater than its real length. The real length must be smaller than a half-wavelength. The equation of antenna length is modified to the equation (4.15), which includes a first order correction for the edge extension due to the fringing fields [98]. In general fabrication, the width is chosen as 0.8 time wide as the length in order to avoid the resonance in the y-axis.

$$L = \frac{\lambda_0}{2\sqrt{\varepsilon_{eff}}} - 2\Delta \quad (4.15)$$

$$\text{with } \Delta = 0.412h \frac{(\varepsilon_{eff} + 0.3)(w/h + 0.262)}{(\varepsilon_{eff} - 0.258)(w/h + 0.813)} \quad (4.16)$$

### 4.2.2 Impedance of the patch

The transmission line model represents the rectangular patch as a parallel-plate transmission line connecting two radiating apertures. In the cavity model, the dominant TM<sub>10</sub> mode has a uniform field distribution along the x-axis at the the slots. These slots show high-impedance terminations from both sides of the patch. The equivalent circuit of a slot is constructed as a parallel BG circuit, as shown in Fig. 4.8.

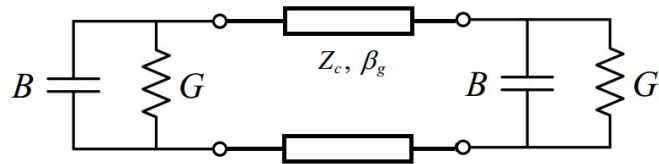


FIGURE 4.8: Equivalent circuit of rectangular patch antenna

The equivalent circuit includes two radiating slots connected by a transmission line.  $G$  represents the radiation loss while  $B$  represents the capacitance of the slot. The equivalent conductance  $G$  is obtained from the theory of uniform apertures while the equivalent susceptance  $B$  is related to the fringe capacitance.  $Z_c$  is the characteristic impedance of the line and  $\beta_g$  is its propagation constant. Thus the input impedance of the patch fed in the middle of the edge is computed as follows.

$$Y_{in} = 2 \cdot (G + jB) \quad (4.17)$$

$$\text{with } G = 1/R = \frac{\pi w}{\eta \lambda_0} \left[ 1 - \frac{(\beta_g h)^2}{24} \right] \quad (4.18)$$

$$B = j\omega C = 0.01668 \cdot \frac{\Delta}{h} \frac{w}{\lambda_0} \varepsilon_{eff} \quad (4.19)$$

where  $R$  is the radiation loss.

$B$  is a rectangular capacitor with dimensions  $\Delta \cdot w$  on a substrate of thickness  $h$ . It is equivalent to a lumped element  $C$ .

$\eta$  is the medium impedance.  $\eta_0$  is  $120\pi$  in the vacuum.

The two slots are separated by an electrical distance of  $180^\circ$ . Ideally the resonant input impedance of the patch for the dominant  $\text{TM}_{10}$  mode is entirely resistive and equal to half the transformed resistance of each slot [98].

$$Z_{in} = \frac{1}{Y_{in}} = \frac{1}{2G} \quad (4.20)$$

For patch antenna fed at the edge, the input impedance is greater than the characteristic impedance of the microstrip feeding line (typically  $50\ \Omega$ ). Inset-feed and probe-feed techniques are widely used to achieve the impedance match.

A linearly polarized microstrip patch antenna ( $27.76\ \text{mm} \times 23.73\ \text{mm}$ ) is designed to associate with previous rectifying circuits in order to obtain integrated rectennas [101]. The antenna simulation is carried out using the full wave electromagnetic simulator HFSS [102], as shown in Fig. 4.9.

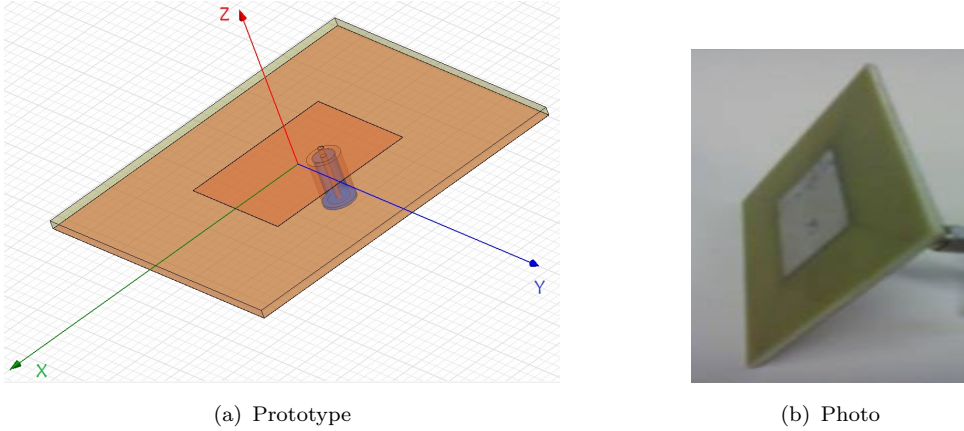


FIGURE 4.9: Configuration of the patch

If the patch is fed at the edge, it yields a high input impedance,  $309.7\ \Omega$  in this case. Since the current is low at the ends of half-wavelength patch and increases in magnitude towards the center, the input impedance should reduce if the patch is fed closer to the center. The input resistance depends on the feeding point  $x$  [103].

$$R_{in} = \frac{1}{2G} S \sin^2 \frac{\pi x}{L} \quad (4.21)$$

The impedance matching can be achieved by choosing a suitable feeding point and tuning the input impedance to the desired value. Simulated by HFSS, the patch antenna is fed from the bottom layer via a probe. The center conductor of a coaxial cable serves as the feeding probe to couple the electromagnetic energy in or out of the patch. The feeding point is 5 mm far from the center of the patch in order to match the antenna to  $50 \Omega$ . The patch is printed on Bernier FR4 substrate with  $\epsilon_r = 4.6$  and 1.58 mm thickness.

### 4.2.3 Frequency response of the patch

Some noteworthy observations are apparent from Fig. 4.10. The measured return loss by VNA shows agreement with the simulated one. The resonant frequency of the patch antenna is located at 2.45 GHz. The -10 dB bandwidth is 50 MHz from 2.42 GHz to 2.47 GHz. Rectangular patch antennas are notoriously narrowband. Even if the patch is optimized for the wideband property, the increment of bandwidth is in a small range. However, some antennas are broadband such as dipole and monopole [104].

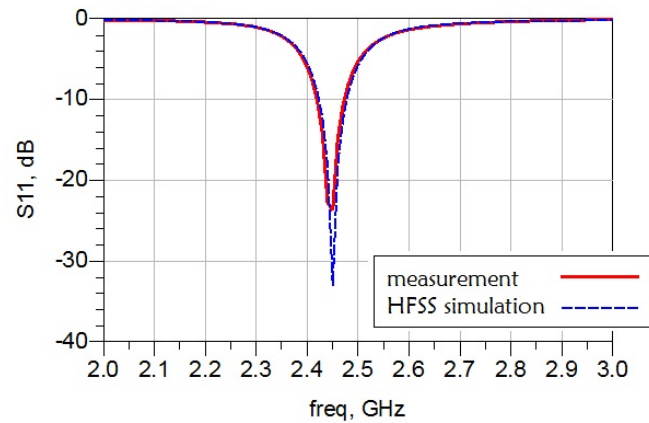


FIGURE 4.10: Simulated and measured return loss of the patch

### 4.2.4 Radiation patterns and gain

Simulated radiation patterns at 2.45 GHz are shown in Fig. 4.11, and measured ones are in Fig. 4.12. The radiation pattern shows the transmission coefficient between the emitting antenna and the patch. It means that the antenna radiates more power in a certain direction than another directions. The given

patterns present high directivity in co-polarization on the E-plane and on the H-plane. The directivity decreases when the antenna moves away from broadside towards lower elevations. The measured patterns are normalised and their sharps of co-polarization agree the simulated ones.

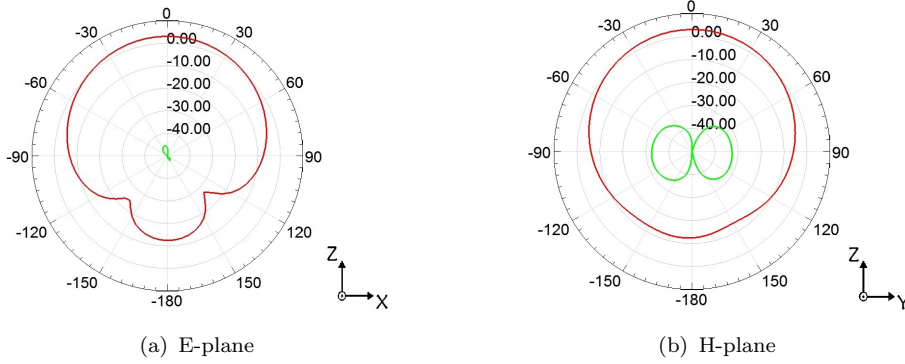


FIGURE 4.11: Simulated radiation patterns of E-plane and H-plane in co-polarization (red line) and cross-polarization (green line) of the patch

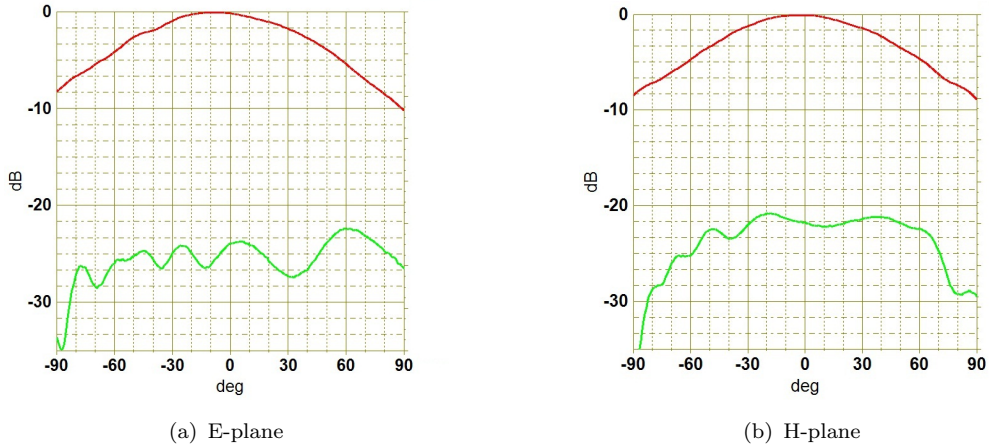


FIGURE 4.12: Measured radiation patterns of E-plane and H-plane in co-polarization (red line) and cross-polarization (green line) of the patch

In the measurement inside an anechoic chamber, the directivity is 5.61 dBi on the E-plane and 5.56 dBi on the H-plane. HPBW (Half Power Beam Width) is  $98^\circ$  on the E-plane and  $94^\circ$  on the H-plane. The co-polarization level is more than 20 dB higher than the cross-polarization level. It means that the patch antenna owns linearly polarization.

The antenna has a -10 dB bandwidth of 50 MHz from 2.42 to 2.47 GHz. This frequency dependency also shows in radiation patterns, as presented in Fig. 4.13. The received power is seen by its amplitude in dB versus the rotation angle as the x-axis and versus the operating frequency as the y-axis.

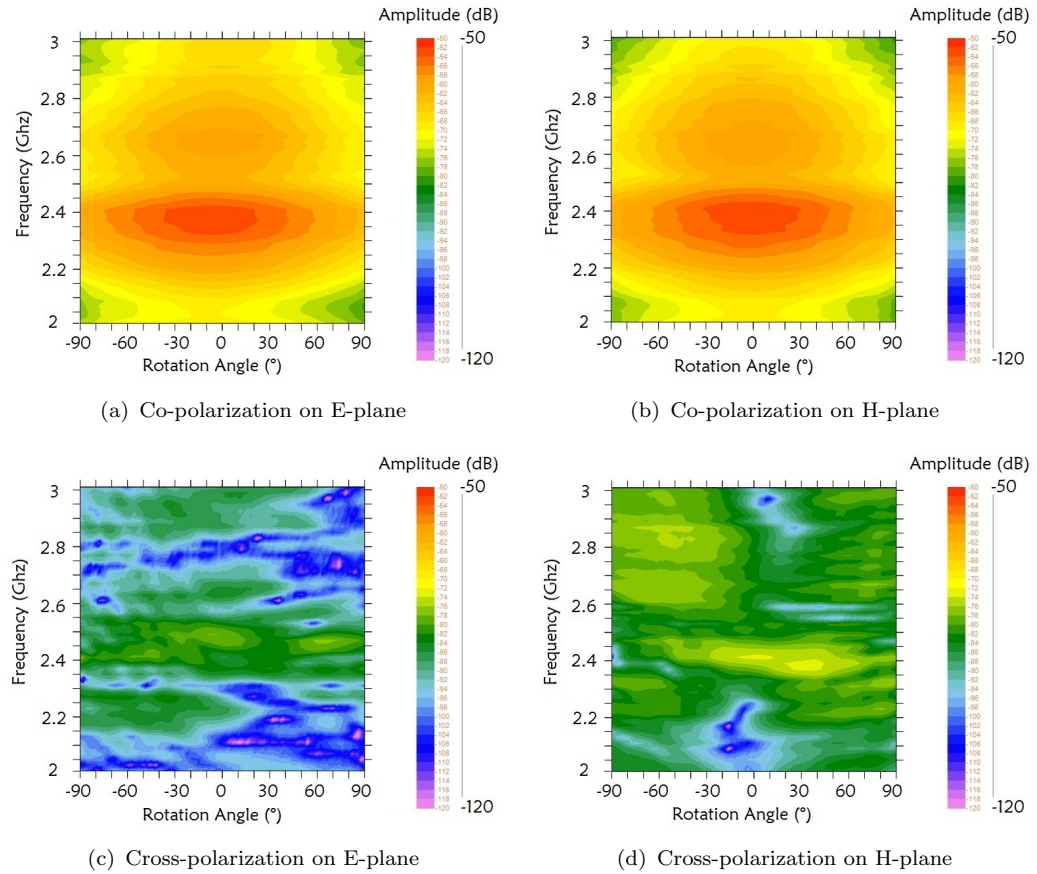


FIGURE 4.13: Radiation patterns of the patch with frequency sweep

When operating frequencies are too high or too low, the antenna cannot have good radiation performance. It operates around the resonant frequency and at a range of rotation angles. When the antenna operates around its resonant frequency, it absorbs lots of energy in a wide range of rotation angles. The radiation pattern of cross-polarization is regarded as a reference for the one of co-polarization. The transmission coefficient is so small that the energy distribution cannot be seen in radiation patterns of cross-polarization.

The antenna gain is defined as the antenna directivity times a factor representing the radiation efficiency. This efficiency is defined as the ratio of the radiated power to the input power. The input power is transformed into radiated power and surface wave power while a small portion is dissipated due to conductor and dielectric losses of the materials. Surface waves are guided waves captured within the substrate and partially radiated and reflected back at the substrate edges. Surface waves are more easily excited when materials with higher dielectric constants or thicker materials.

Bernier FR4 substrate with  $\varepsilon_r = 4.6$  and 1.58 mm thickness is used to fabricate the patch. Thus the surface wave is not important. HFSS provides a 3D gain simulation, as shown in Fig. 4.14. The total gain is 3.1 dBi in the simulation.

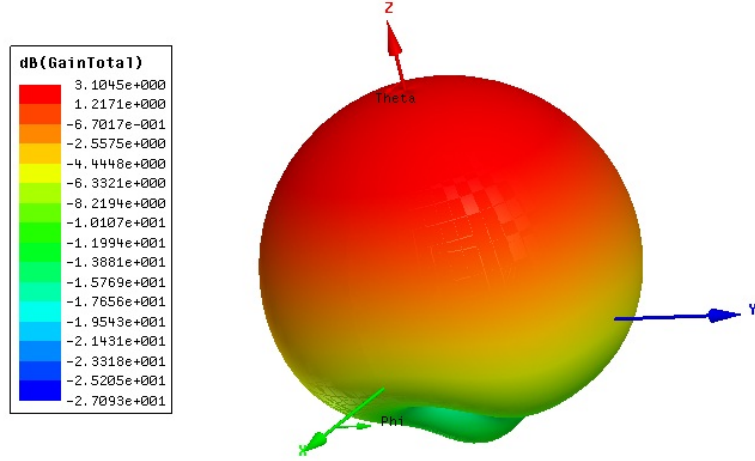


FIGURE 4.14: Simulated 3D gain of the patch

The patch's radiation at the fringing fields can be viewed as two radiating slots placed above a ground plane. The 3D gain shows high levels of radiation towards the front side and low levels of radiation towards the back side. This front-to-back ratio is highly dependent on the size and shape of ground plane in practical cases. Here the ground plane (63.19 mm  $\times$  59.16 mm) is chosen based on the hypothesis of an infinite ground plane.

### 4.3 Monopole antenna

Since the length of the patch, half-wavelength, is about the same as the length of a resonant dipole, some properties of a patch antenna with radiation characteristics are similar to those of a resonant dipole. In order to minimize the occupied area of antennas, a monopole antenna printed over a finite ground plane is proposed to replace the patch. The quarter-wavelength monopole improves the impedance bandwidth. Moreover, it is easy to increase the bandwidth of monopole antenna by the way of several techniques in terms of bandwidth enhancement.

### 4.3.1 Prototype of the monopole

A monopole antenna is a class of radio antenna consisting of a straight rod-shaped conductor, mounted perpendicularly or parallel over some type of conductive surface. The monopole is a resonant antenna and the rod functions as a resonator for radio waves with oscillating standing waves of voltage and current along its length [105, 106]. This kind antenna owns wide geometry which enhances the bandwidth.

The conventional wideband monopole has been widely used in the broadcast communication applications, but it is not suitable for some high frequency applications due to its solid structure and un-integration. Replacing a conventional wire monopole, a planar monopole can provide almost the same bandwidth and radiating performance with much smaller volume. However, they all need a perpendicular ground plane as a result of increasing of the antenna volume and inconvenience for integration. Printed with a ground plane on the same or opposite side of a substrate, printed monopole antennas are more popular due to easier integration and less occupied volume.

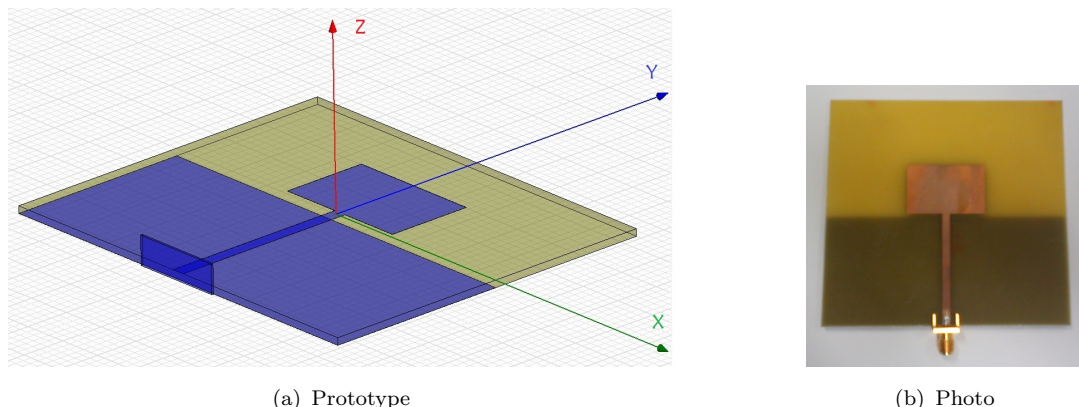


FIGURE 4.15: Configuration of the monopole

Based on the study of patch antennas, a prototype of quarter-wave printed monopole antenna is analysed for a broad bandwidth in Ansoft HFSS. As shown in Fig. 4.15, a rectangular monopole feeding by  $50 \Omega$  microstrip line is printed on the dielectric substrate (Bernier FR4 substrate with  $\epsilon_r = 4.6$  and 1.58 mm thickness). The dimensions of the monopole and the ground plane, the height of the feed gap between the feed point and the ground plane are the parameters affecting the antenna operation. All the parameters are mechanically tuned and

analysed by HFSS till a broad bandwidth around 2.45 GHz and a good matching level with  $50\ \Omega$  feed line are obtained.

The length and the width of the monopole are 19.2 mm and 30.2 mm, about 29 % and 46 % of the guided wavelength. On the other side of the substrate, the length and the width of the ground plane are 41 mm and 91.8 mm. The height of the feed gap between the feed point and the ground plane is 1 mm.

### 4.3.2 Frequency response of the monopole

The simulated return loss and the measured one of the monopole are shown in Fig. 4.16. The measured -10 dB return loss bandwidth is 1.91 GHz from 1.9 to 3.81 GHz, while the simulated one is 1.56 GHz from 1.97 to 3.53 GHz. The measured result is even better than the simulated one. Because the dielectric loss increases when the frequency increases. Then the Q factor reduces and the bandwidth enlarges.

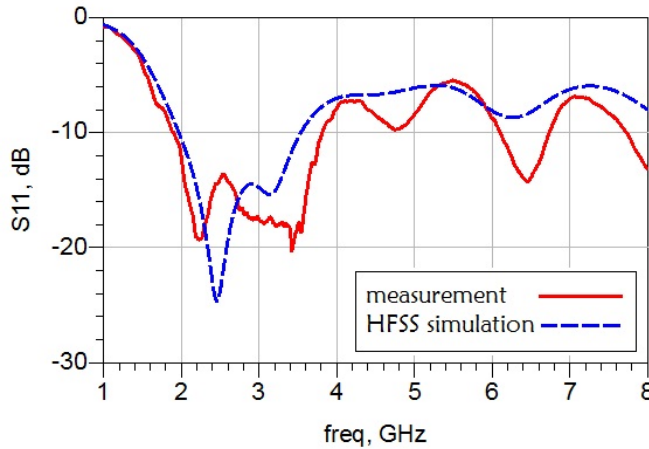


FIGURE 4.16: Simulated and measured return loss of the monopole

The measurement confirms the broadband characteristic of monopole antennas, as predicted in the simulation. Although rectifying circuits is very narrow bandwidth, monopole antennas have a wide bandwidth and this advantage simplifies the difficulty of the impedance match between antennas and rectifying circuits in rectenna systems.

### 4.3.3 Radiation patterns and gain

The radiation patterns have been simulated in HFSS and measured by Rohde&Schwarz VNA (Vector Network Analyser) [107] inside an anechoic chamber. Fig. 4.17 presents the measured and simulated normalized radiation pattern at 2.45 GHz.

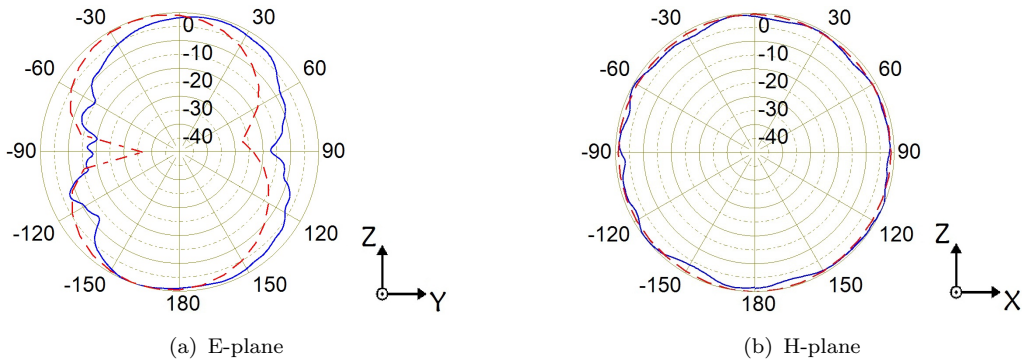


FIGURE 4.17: Simulated (red line) and measured (blue line) radiation patterns of the monopole

The measured H-plane pattern is close to the one obtained in the simulation. The measured E-plane pattern follows the shape of the simulated one, though the agreement is not as good as the H-plane. The distortion on the measured curve may be caused by the feed connector and the coaxial cable. The monopole has a directivity of 6.01 dBi in co-polarization on the E-plane, while the directivity on the H-plane is 1.51 dBi. It is noticed that the monopole has a quasi omnidirectional property in the position of vertical polarization on the azimuthal plane.

The monopole antenna has a wide bandwidth from 1.9 GHz to 3.81 GHz. This frequency dependency also shows in radiation patterns, as presented in Fig. 4.18. The colour bar represents the received power in dB. The y-axis is operating frequencies of the emitting antenna in unit GHz. The x-axis is rotation angles from  $-180^\circ$  to  $180^\circ$ .

When operating frequencies are inside the bandwidth of -10 dB return loss, the monopole has good radiating performance on the whole H-plane, as well as on the E-plane except for certain angles. The radiation patterns of cross-polarization do not show strong radiating effect, about -70 dB compared with -50 dB in co-polarization. Thus the co-polarization on the H-plane is recommended as the operating style of this monopole.

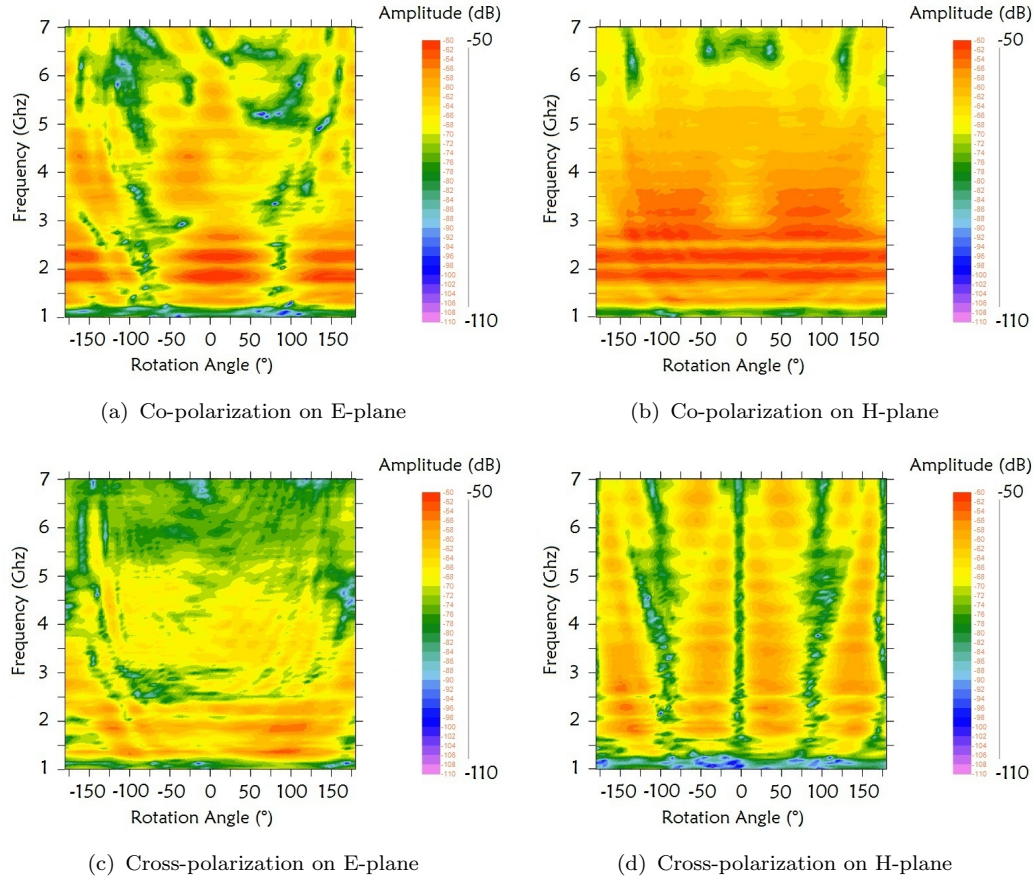


FIGURE 4.18: Radiation patterns of the monopole with frequency sweep

Based on the gain-comparison method, the gain of antenna under test is analysed by the software ANT32-ANA. By this way, the gain of the monopole is measured as shown in Fig. 4.19. Generally the antenna gain depends on its directivity and its efficiency at operating frequencies. The gain is satisfied when the monopole is well matched. The maximum value of monopole gain is 3.01 dBi in the chamber measurement.

In general, the pattern of an antenna is 3-dimensional, so is the gain. Since it is impractical to measure a 3-D gain, HFSS simulation provides a gain of three dimensions, as shown in Fig. 4.20. It shows a typical shape of radiation patterns of a monopole antenna. The total gain is 2.32 dBi in the simulation.

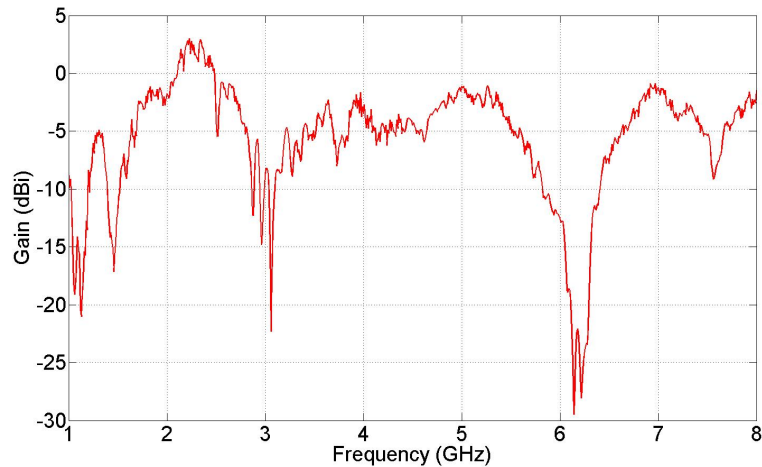


FIGURE 4.19: Measured gain of the monopole

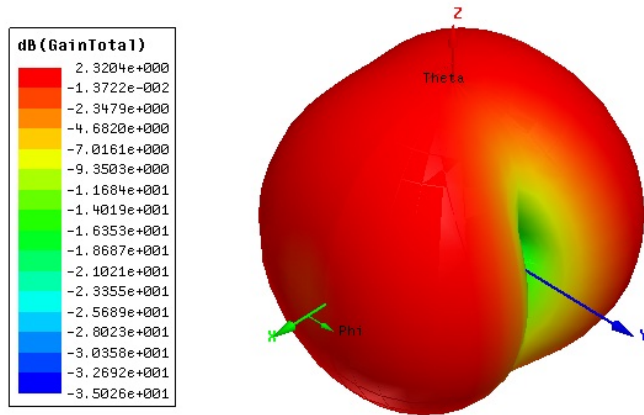


FIGURE 4.20: Simulated 3D gain of the monopole

## 4.4 Monopole with a shorting pin

The printed monopole, as the same as the patch, has a variety of beneficial properties including mechanical durability, conformability, compactness, and cheap manufacturing costs. The monopole features wide operating bandwidth, satisfactory radiation properties, simple structure, and easy fabrication. In the aim of integrating monopole antennas with rectifying circuits, antennas are modified to contribute to a DC loop which is an important part of rectifying circuits. A shorting pin is introduced inside the planar structure of printed monopole by an inspiration of PIFA (Planar Inverted-F Antenna) [108].

#### 4.4.1 Prototype of the modified monopole

A prototype of the modified monopole antenna is simulated for a broad bandwidth in HFSS. The dimensions of the monopole and the ground plane, the height of the feed gap between the feed point and the ground plane, and the position of the short circuited point are important parameters that affect antenna characteristics. All the parameters are analysed in order to understand the performance of antennas.

As shown in Fig. 4.21, a rectangular monopole and a  $50\ \Omega$  microstrip feed line are printed on the same side of the dielectric substrate (Bernier FR4 substrate with  $\epsilon_r = 4.6$  and 1.58 mm thickness). The length and the width of the monopole are 17 mm and 33.5 mm, about 26 % and 51 % of the guided wavelength.

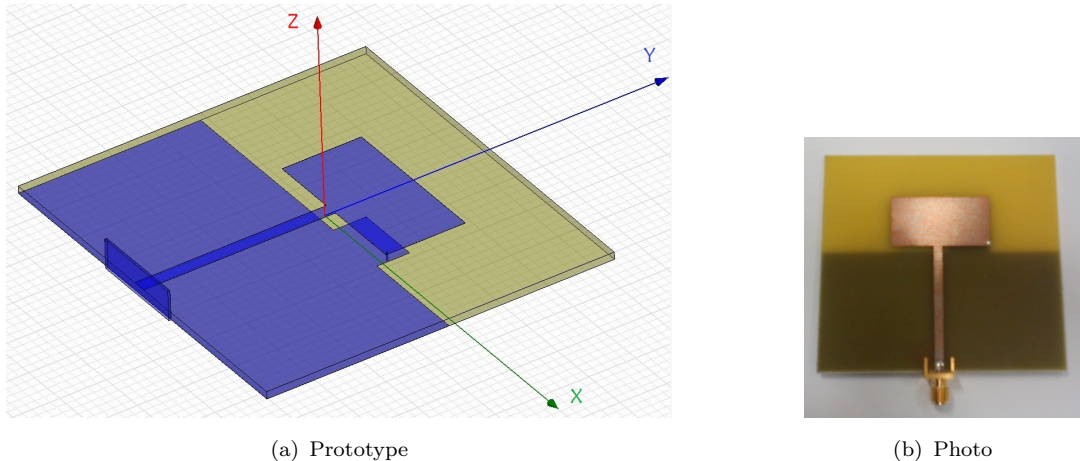


FIGURE 4.21: Configuration of the monopole with a shorting pin

On the other side of the substrate, besides the rectangular ground plane as the same as the former antenna, a small rectangular pad covers the right-lower corner of the monopole. The length and the width of the ground plane are 39 mm and 80 mm. The height of the feed gap between the feed point and the ground plane is 2 mm. The length and the width of the pad, where the shorting pin is located, are 7 mm and 14 mm. The shorting pin is 0.5 mm away from the right edge and the lower edge of the right-lower corner on the monopole. The via-hole of a shorting pin is 0.4 mm diameter.

#### 4.4.2 Frequency response of the modified monopole

The simulated return loss and the measured one of the monopole with a shorting pin are shown in Fig. 4.22. The measurement agrees the broadband characteristic of the modified monopole simulated by HFSS. The measured -10 dB return loss bandwidth is 1.07 GHz from 1.61 to 2.68 GHz, while the simulated one is 1.05 GHz from 1.7 to 2.75 GHz.

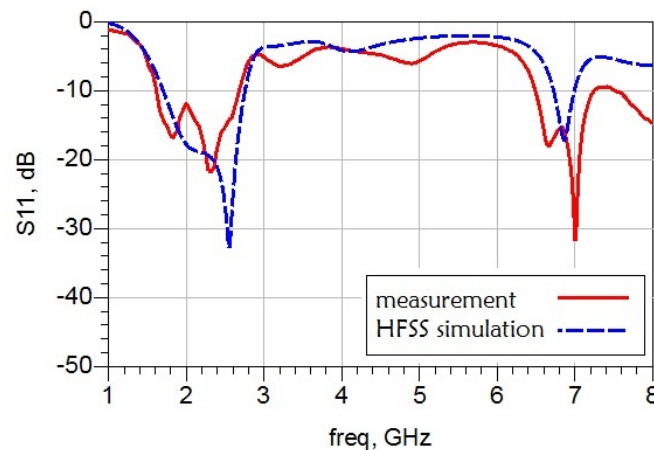


FIGURE 4.22: Simulated and measured return loss of the monopole with a shorting pin

The difference between simulation and measurement is mainly due to the modelization of the via-hole and the tolerance of fabrication. All in all, the modified monopole is wideband as well as the monopole mentioned in the last section. Their bandwidths are obviously much broader than the bandwidth of the patch.

#### 4.4.3 Radiation patterns and gain

The radiation patterns have been simulated in HFSS and compared with the measured ones. Fig. 4.23 exhibits the measured and simulated normalized radiation pattern of co-polarization at 2.45 GHz. The measured E-plane and H-plane patterns follow the shape of the ones obtained in the simulation. The measured curve may be influenced by the interference of the feed connector and the coaxial cable. The monopole has a directivity of 5.82 dBi in the position of horizontal polarization on the E-plane, while the directivity is 2.92 dBi in the position of vertical polarization on the azimuthal plane.

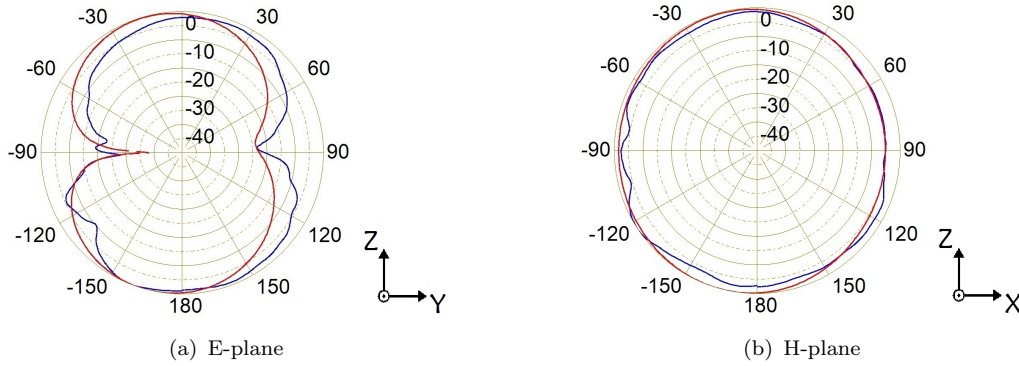


FIGURE 4.23: Simulated (red line) and measured (blue line) radiation patterns of the monopole with a shorting pin

In the radiation pattern on the H-plane, the directivity is higher on  $-90^\circ$  than  $0^\circ$ . It is noticed that the modified monopole gets more directional when the emitting antenna is on the right side of the monopole.

Radiation patterns on the H-plane are not symmetrical owing to the special design of a shorting pin. A narrow wire is used to connect the monopole and the ground plane through the via-hole. It may introduce an unexpected effect of inductance. This asymmetric structure lead to a variable behaviour of rectennas if rectifying circuits are integrated with the modified monopole. However, the short circuited structure can replace the short stub and reduce the surface of matching circuits. This modified monopole offers an embryonic form of compact rectennas.

The modified monopole has a -10 dB bandwidth from 1.61 to 2.68 GHz. This frequency dependency also shows in radiation patterns, as presented in Fig. 4.24. The received power in dB is swept against the rotation angle from  $-180^\circ$  to  $180^\circ$  as the x-axis and against the operating frequency from 1 to 7 GHz as the y-axis.

When operating frequencies are beyond the bandwidth of -10 dB return loss, the antenna do not show good radiating performance. The antenna captures much energy if the operating frequency is inside the matching band, in the main direction for example. But it absorbs less energy in certain directions. There is no strong radiating effect in radiation patterns of cross-polarization, about -70 dB. Compared with the original monopole, the configuration of a shorting pin influences radiation patterns of the modified monopole. The asymmetric structure changes the quasi omnidirectional property on the azimuthal plane.

Based on the gain-comparison method, the gain of the modified monopole is analysed by the software ANT32-ANA. Fig. 4.25 presents the measured gain

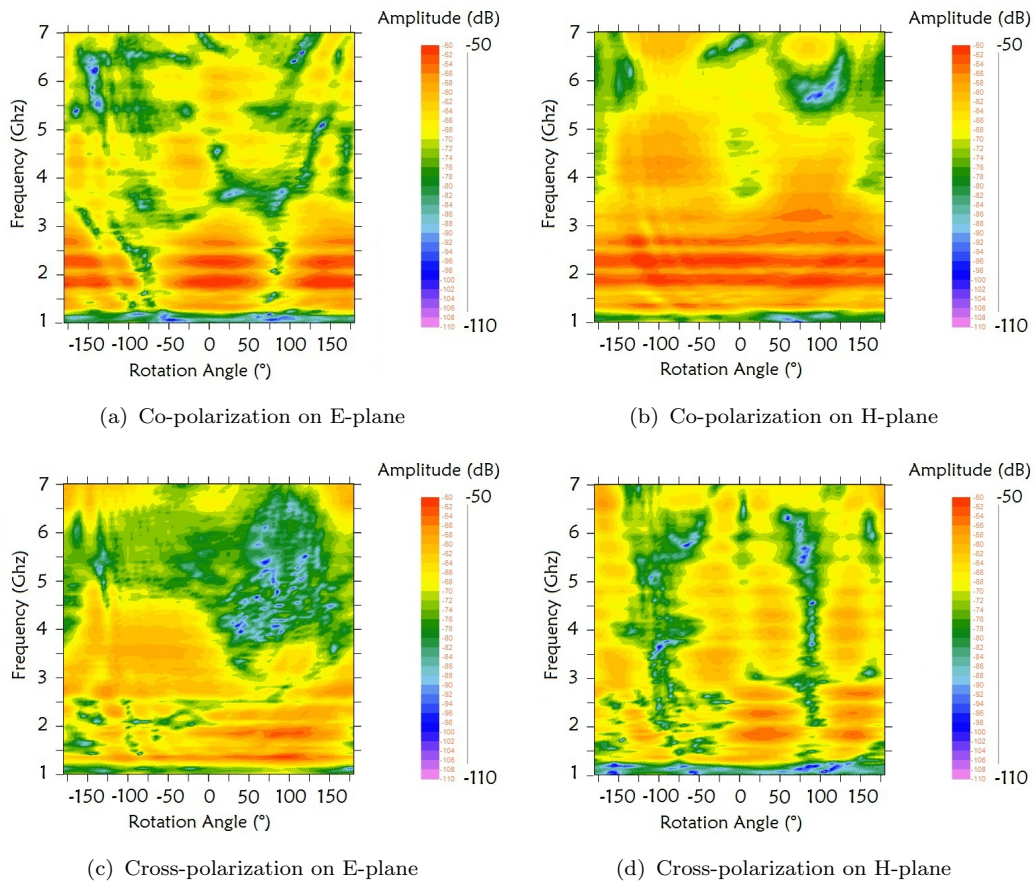


FIGURE 4.24: Radiation patterns of the modified monopole with frequency sweep

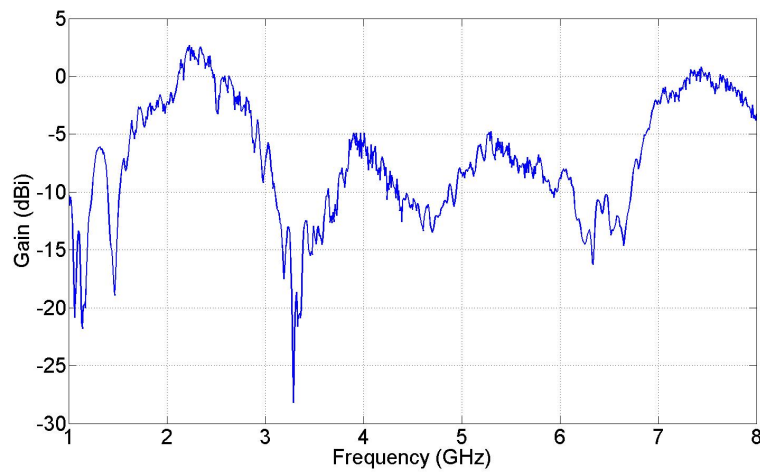


FIGURE 4.25: Measured gain of the monopole with a shorting pin

of this antenna. The gain is satisfied when the monopole is well matched. The gain where it is not desired is due to its directivity and its efficiency at operating frequencies. The maximum gain is 2.71 dBi in the chamber measurement.

The measurement in an anechoic chamber gives the gain versus operating frequency, while the simulation provides a 3D gain, as shown in Fig. 4.26. The total gain is 2.55 dBi in the simulation.

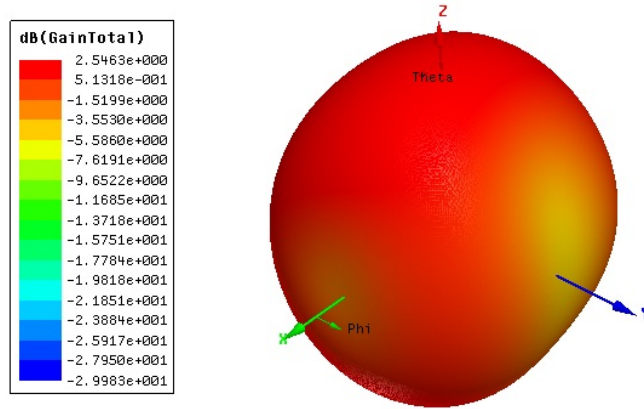


FIGURE 4.26: Simulated 3D gain of the monopole with a shorting pin

#### 4.4.4 Analysis of the received power

Fig. 4.27 illustrated the received power of the modified monopole in the vertical polarization in the chamber measurement, when the microwave propagation direction is perpendicular to the monopole. The output power of the VNA is 0 dBm. The emitting power goes from the VNA, through a power amplifier of 35 dB gain, and to an emitting antenna.

The emitting horn operates from 2 to 18 GHz, and its gain varies from 5 to 18 dBi. If the operating frequency is too low or too high, the received power is low owing to the frequency range and the gain of antennas. Besides, the monopole is well matched from 1.7 to 2.75 GHz. The received power is high if the monopole operates in a good matching level. The power curve ripples a little due to the variation of the output power from the emitting antenna. Another factor is the free-space attenuation. According to the Friis equation, the higher the frequency is, the more the attenuation is, then the lower the received power is. As seen in Fig. 4.27, the received power is around -15 dBm at 2.45 GHz.

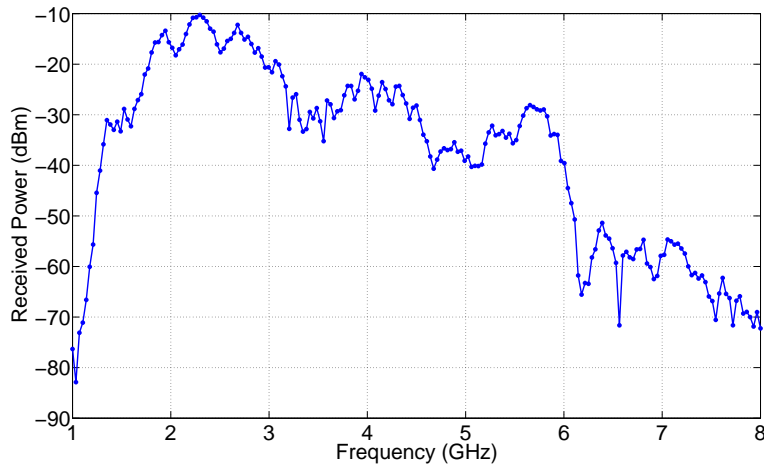


FIGURE 4.27: Measured received power of the monopole with a shorting pin against the frequency

By using Servo-controller, the AUT rotates in an anechoic chamber in order to observe the radiation performance of the antenna. The emitting antenna in co-polarization with AUT is fixed on the wall of the chamber. It is always in the main direction. That means the received power in different angles does not depend on radiation patterns of the emitting antenna. The received power shows in Fig. 4.28 against all the directions. Owing to the irregular configuration of the modified monopole, it gets more directional at  $0^\circ$ ,  $-60^\circ$ , and  $-90^\circ$ . On the contrary, it gets less directional at  $-50^\circ$ ,  $40^\circ$ , and  $70^\circ$ . This is link to the radiating property of the modified monopole.

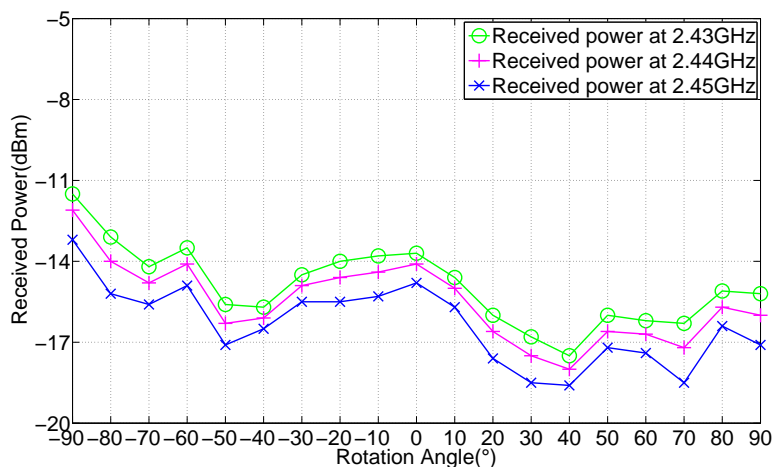


FIGURE 4.28: Measured received power of the monopole with a shorting pin against the rotation angle

## 4.5 Conclusion of the antenna design

The design of the receiving subsystem is a key link in the rectenna configuration. This subsystem cooperates with the rectifying device and decides incident power levels for which rectifying circuits operate. Generally in the rectification process, the higher the power level is, the larger the DC voltage is, and then the better the conversion efficiency is. When energy harvesting antennas own high gains, the efficiency of rectifying parts can be high even if these rectennas are located at low power densities. What's more, radiating properties of antennas are important in the rectenna design. The innovation of antennas provides an opportunity to construct rectennas in compact structures.

All the antennas have been designed in HFSS simulations. Prototypes of patch, monopole, and modified monopole antennas are analysed according to our requirements. For each prototype, the structure and the dimension are optimized around the resonant frequency of 2.45 GHz.

First of all, the patch antenna has been designed owing to its simple structure. Its resonant frequency is located at 2.45 GHz with narrow bandwidth of -10 dB return loss. It is linearly polarized and has simulated 3D gain of 3.1 dBi.

The monopole antenna has been proposed as a length of about quarter-wavelength based on the design of half-wavelength patch antenna. It owns wide bandwidth (1.91 GHz) of -10 dB return loss around the resonant frequency (2.45 GHz). The printed monopole has a quasi omnidirectional property in vertical polarization on the azimuthal plane. The total gain is 3.01 dBi in the chamber measurement.

Inspirited by PIFA configurations, a shorting pin is introduced inside the planar structure of printed monopole. The monopole is modified as a part of matching circuit on the purpose of integrating the antenna with rectifying circuits in a compact structure. The modified monopole owns broad bandwidth (1.07 GHz) of -10 dB return loss around the resonant frequency. It gets more directional on certain degrees of the H-plane in vertical polarization due to its asymmetrical structure. A total gain of 2.71 dBi is obtained in an anechoic chamber.

The modified monopole with a shorting pin is studied in terms of frequency response, radiation patterns, and 2D or 3D gain. And the received power is analysed in the frequency domain and against rotation angles. This antenna is used to

integrate rectifying circuits on a coplanar structure. Then the compact rectenna will be proposed for the application of energy harvesting at low power densities.



# Chapter 5

## Combination and Integration of Rectenna

### 5.1 Design for high power levels

People have designed some rectennas which are applicable with high conversion efficiencies for high power levels at frequency bands of ISM or GSM. These rectennas participate in power transmission systems and recharge wireless devices at high power densities [109–111].

#### 5.1.1 Rectenna experiment

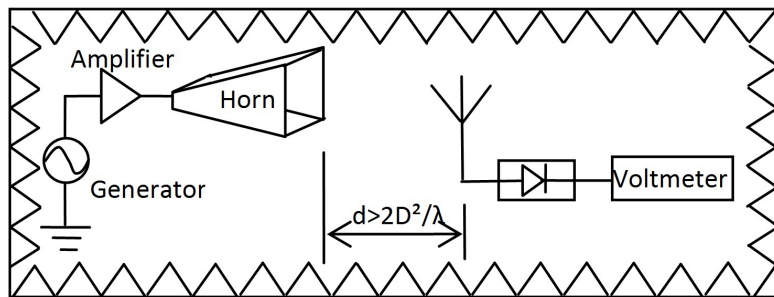


FIGURE 5.1: Rectenna experiment set-up with a movable position

The rectenna experiment has been carried out in an anechoic chamber to measure the DC output with a transmitter-receiver configuration, as shown in Fig. 5.1. An horn antenna, having a gain of 5 dBi, has been used to transmit the

power from the generator. The location of the rectenna has been kept away from the horn in a far field distance.

The conversion efficiency, defined as the ratio of the output DC power to the received RF power, is an important parameter to show the rectification performance. The output DC power is proportional to the square of the output DC voltage and it is inversely proportional to the load resistance.

$$\eta = \frac{P_{DC}}{P_r(d)} \times 100\% = \frac{U_L^2}{R_L P_r(d)} \times 100\% \quad (5.1)$$

where  $U_L$  is the output DC voltage.

$R_L$  is the load resistance.

$P_r(d)$  is the received energy by antennas. It decreases with the distance between the emitting and receiving antennas.

The relation between conversion efficiencies and input power levels intuitively estimates the rectifying characteristic of rectennas. If the effective capture area of an antenna is given, the received power can be obtained in terms of power densities where the antenna is located. On the other hand, if the received power can be measured by a power sensor, power densities can be calculated in terms of the received power.

In practical cases, the received power from an integrated rectenna is not always known, particularly with an irregular layout. In this case, figures of output DC voltages against power densities are used to show the rectification performance of rectennas, instead of the link between conversion efficiencies and input power levels.

### 5.1.2 Rectifying circuit with HSMS-2820

By using the simulation software ADS, rectifying circuits with Schottky diode HSMS-2820 have been optimized for high power levels around 10 dBm at the ISM frequency of 2.45 GHz. Aiming at low-cost devices for energy harvesting, their layouts have been realised on FR4 substrate with  $\varepsilon_r = 4.6$  and 1.58 mm thickness.

The measured output DC voltage and conversion efficiency are maximized to 11 V and 55 %. Besides, a patch antenna with probe feeding has been designed for a resonant frequency 2.45 GHz in HFSS and printed on FR4 substrate. Its directivity is 5.56 dBi in vertical polarization.

Then rectifying circuits have been modified to integrate with the microstrip patch antenna. A connector is connecting the input of rectifying circuits and the output of the patch, as seen in Fig. 5.2. Two short wires connect the two ends of the load resistor in order to easily extract the value of DC voltage. This modification decreases the maximum value of conversion efficiency to 30 %.

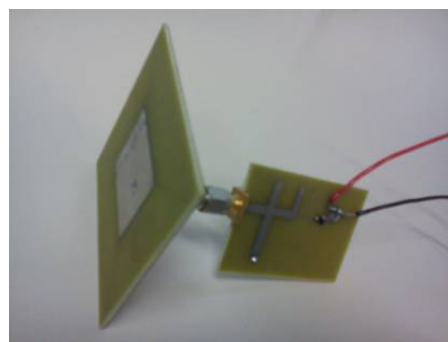


FIGURE 5.2: Modified rectifying circuit with a patch antenna

A preliminary testing on the rectifying circuit has been done by measuring DC output voltages against input power levels. Then the modified rectifying circuit connected with a patch has been measured in an anechoic chamber. We have studied two relative distances between the emitting antenna and the rectenna. The position of  $d=0.3$  m is close to the Fraunhofer distance (0.32 m) while the position of  $d=0.5$  m is in a far field distance from an emitting antenna.

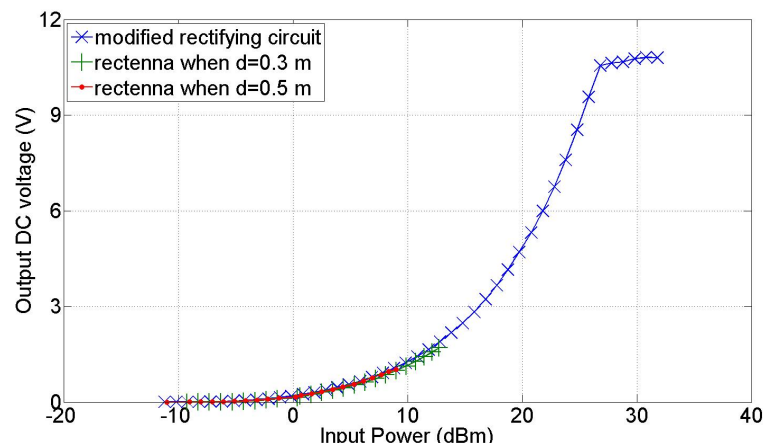


FIGURE 5.3: Output DC voltage of the rectenna integrated with a patch

The measured curves of the rectenna fit the measurement of the modified rectifying circuit, as shown in Fig. 5.3 and Fig. 5.4. The rectenna receives the power from -11 dBm to 13 dBm and obtains the maximum conversion efficiency close to 20 %. The attenuation in the cables and also in the space reduces the received power of the rectenna. The values of free-space attenuation are 29.77 dB and 34.2 dB when the distances are 0.3 m and 0.5 m respectively. However, the rectenna can capture more energy if an antenna array is used. In the application of energy harvesting for sensor networks, we do not consider antenna arrays due to more occupied volume.

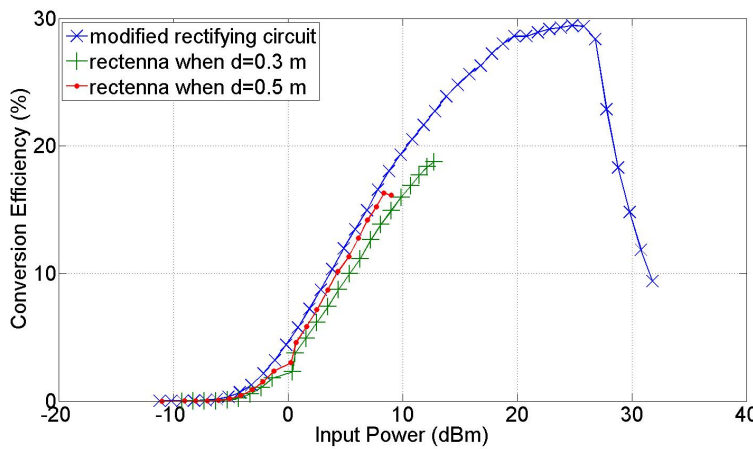


FIGURE 5.4: Conversion efficiency of the rectenna integrated with a patch

Fig. 5.5 and Fig. 5.6 show the measured DC voltages and conversion efficiencies of the rectenna at high power densities. Fig. 5.3 and Fig. 5.5 are the curves of output DC voltages against power densities and against input power levels respectively. They give the same description of rectenna performance.

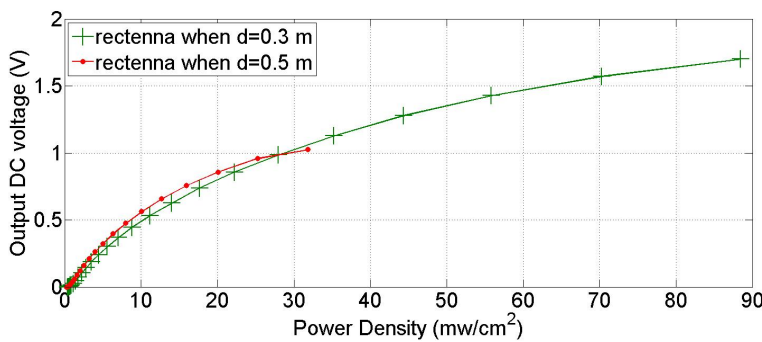


FIGURE 5.5: Output DC voltage of the rectenna integrated with a patch against power densities

The DC voltage is 1.025 V and the conversion efficiency is 16.13 % at the power density of 31.83 mW/cm<sup>2</sup>. And the DC output is 1.7 V and the efficiency

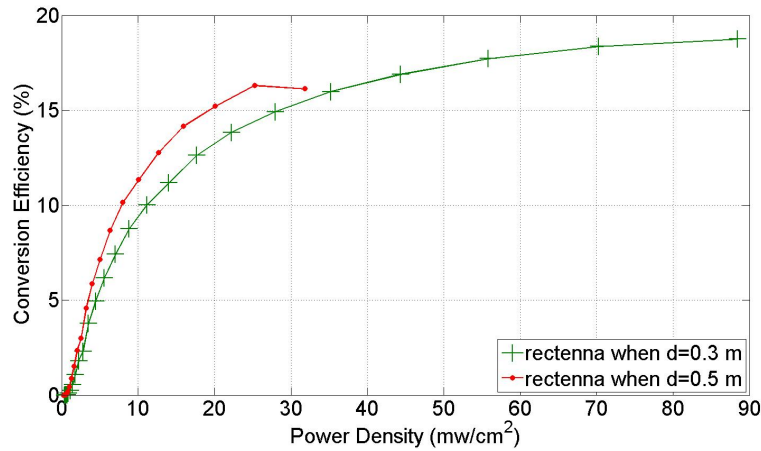


FIGURE 5.6: Conversion efficiency of the rectenna integrated with a patch against power densities

is 18.75 % at the power density of 88.42 mW/cm<sup>2</sup>. This global efficiency may be increased by controlling each step of the design. But the attenuation in the space is so large as to influence the practicability of this device.

## 5.2 Design for low power levels

Based on an investigation of ambient environment, the microwave power density in energy harvesting for RFIDs [112, 113] or for battery-free transponders is on the order of 10<sup>-2</sup> mW/cm<sup>2</sup> [114]. The rectenna mentioned in the last section is not suitable for the application of energy harvesting at low power densities.

### 5.2.1 Rectifying circuit with HSMS-2860

Rectifying circuits with Schottky diode HSMS-2860 have been simulated in ADS. The matching circuit has been optimized for low power levels around -20 dBm at the ISM frequency of 2.45 GHz. The layouts have been printed on FR4 substrate with  $\epsilon_r = 4.6$  and 1.58 mm thickness. The measured efficiency is 5 % to 10 % when input power levels are -20 dBm to -15 dBm. Analysed in HFSS and printed on the same substrate, the monopole is modified with a shorting pin. It has 1.07 GHz bandwidth of -10 dB return loss and 2.92 dBi gain in vertical polarization. The rectifying circuit and the antenna have been tested separately.

Then these two parts are connected by connectors and cables in order to constitute the rectenna system.

### 5.2.2 Measurement in an anechoic chamber

The experiment has been carried out with a transmitter-receiver configuration in an anechoic chamber, as seen in Fig. 5.7. The antenna is located 5.586 m far away from an emitting horn of 5 dBi gain. A power amplifier of 35 dB gain is connected to the VNA output and to the horn input since each port of the VNA is limited to 20 dBm RF power. The amplifier is available from 2 to 4 GHz, and the maximum output power is 35 dBm. It is fed by 15 V and 3.5 A from a DC power supply.

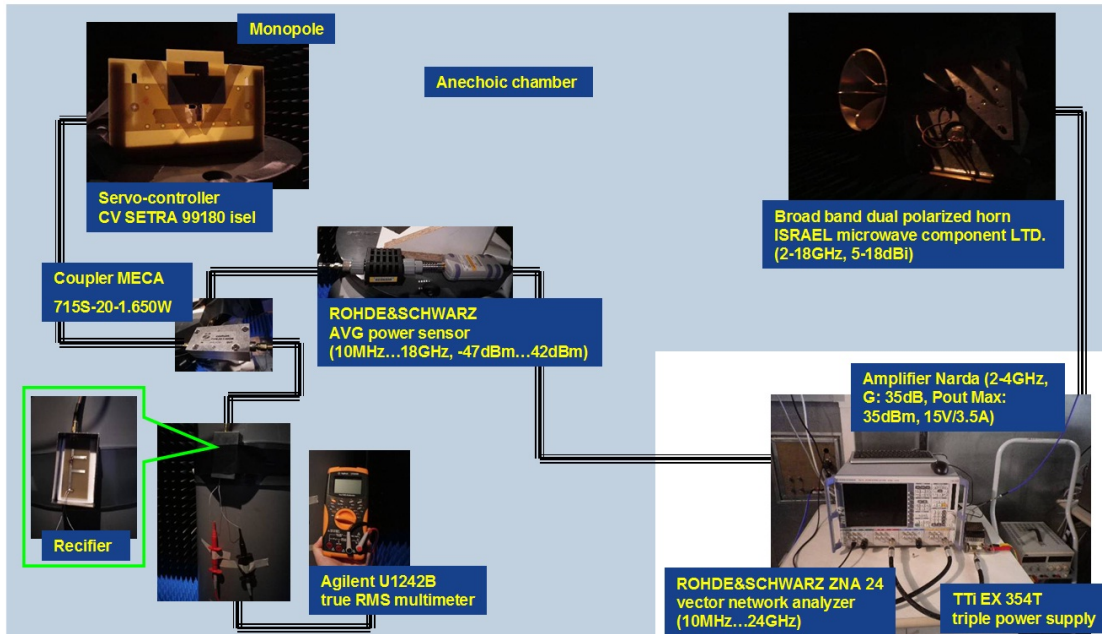


FIGURE 5.7: Experimental set-up of the rectifying circuit with the antenna

At the output terminal, the antenna is fixed on a positioning shelf which is made by epoxy and wood, as shown in Fig. 5.8. The rectifying circuit is protected by a metallic box in the aim of weakening the radiation of the circuit itself. A coupler transfers the received power to the rectifying circuit. The coupler's output of 20 dB attenuation is connected to a Rohde & Schwarz power sensor. From the power sensor, the VNA obtains the received power including the attenuation of the coupler and the loss of cables. The output DC voltage across the load resistor has been measured by a voltmeter against the received power.

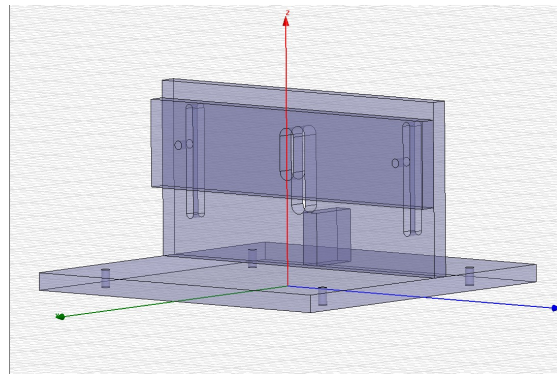


FIGURE 5.8: Antenna shelf

To observe the cooperation of the rectifying circuit and the monopole, the rectifying circuit has operated with a RF power generator, and then the circuit has operated with the proposed antenna. Fig. 5.9 presents the DC output voltage against the incident power at the input of rectifying circuits. These two curves show an agreement. It is noticed that the rectifying circuit operates well no matter if it connects to a RF generator directly or to an antenna which absorbs the microwave energy from an ambient environment.

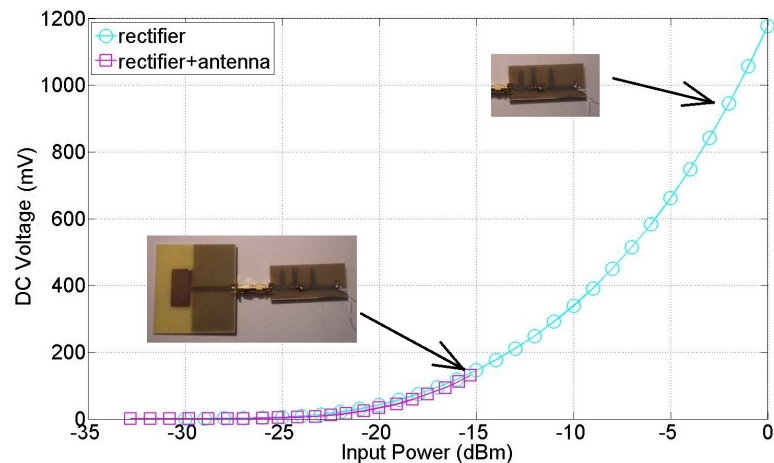


FIGURE 5.9: Vout comparison between the rectifying circuit and the circuit with the monopole

In the comparison between the rectifying circuit with a power generator and the circuit with the monopole, the conversion efficiency of the simple rectifying circuit is slightly higher than the one cooperated with the monopole due to the mismatch between the rectifying circuit and the monopole, as well as the loss inside connectors, as shown in Fig. 5.10. The integration of antennas and rectifying circuits will probably suppress this loss.

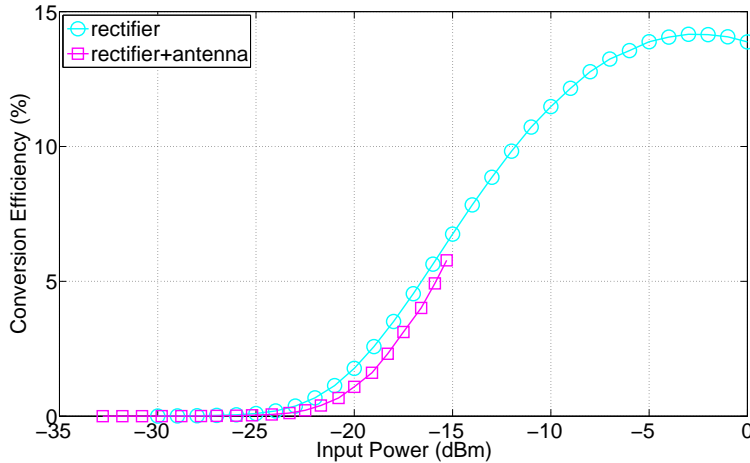


FIGURE 5.10: Efficiency comparison between the rectifying circuit and the circuit with the monopole

Output DC voltages and conversion efficiencies of rectifying circuits increase with the increment of input power levels. The rectifying circuit yields DC voltages more than 1.178 V and the maximum efficiency 14.2 % for an incident power of -5 dBm. However, it products maximal DC voltage of 130.6 mV and conversion efficiency of 5.8 % cooperatively with the monopole, when the input power is around -15 dBm. If incident power levels increase, the rectenna combined by the rectifying circuit and the monopole may obtain conversion efficiency up to 14 %, as good as the results when the rectifying circuit operating alone.

As we know, the output DC voltage goes up when the incident power of the rectifying circuit increases. The conversion efficiency shows the same trend with input power levels. Following the shape of power level absorbed by the antenna, Fig. 5.11 presents the variation of DC voltage against the direction which the antenna faces to. The circuit has better DC output at  $-90^\circ$ ,  $-60^\circ$ , and  $90^\circ$  than the one at  $0^\circ$ , mainly owing to power levels captured by the antenna at each angle.

The situation of conversion efficiency is more complicated than the one of DC voltage. The efficiency is not only in direct proportion to the square of DC voltage but also in inverse proportion of the received power. Moreover, even if the power density is the same in a certain distance away from the emitting antenna, the DC voltage and the efficiency are not the same value at different directions. Because the receiving antenna gets more directional in some degrees. It captures and transfers more energy to the rectifying circuit. It is noticed that the conversion efficiency varies heavily with the increment of input power levels when the input

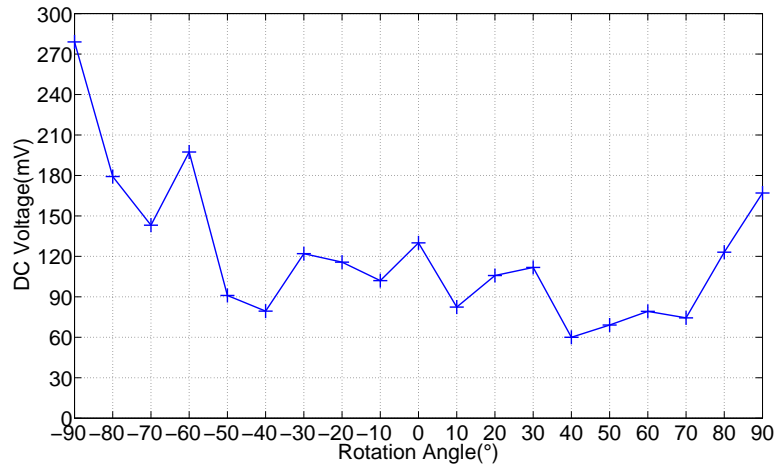


FIGURE 5.11: Output DC voltage of the rectifying circuit with the antenna against the rotation angle

power is from -20 dBm to -10 dBm in Fig. 5.10. Thus, the efficiency varies a lot versus different directions in Fig. 5.12. To fix the antenna, as possible as we can, in a certain angle where it captures more energy is beneficial to the rectification performance.

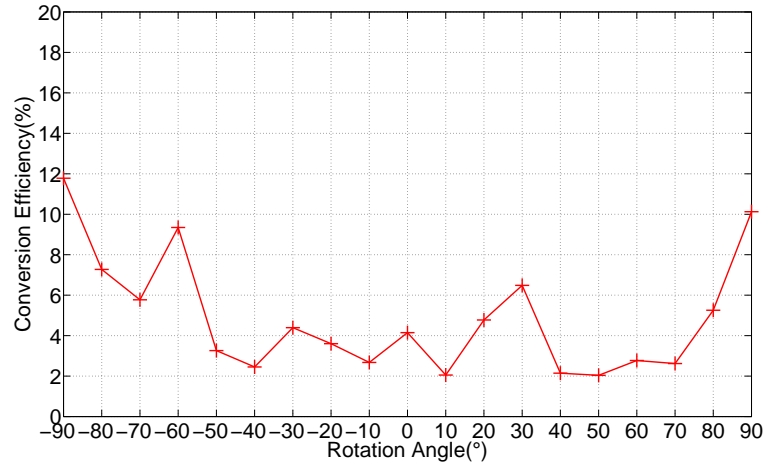


FIGURE 5.12: Conversion efficiency of the rectifying circuit with the antenna against the rotation angle

### 5.3 Rectenna integration

The rectenna system has been studied for high and low power levels. The antenna for energy harvesting has broad bandwidth around the desired frequency. And the rectifying circuits operate RF-to-DC conversion. The key of improving

the overall performance is to increase the conversion efficiency of rectifying circuits and to reduce the losses. The rectifying circuit with Schottky diode HSMS-2820 has conversion efficiency of 55 % at power levels around 20 dBm while the rectifying circuit with HSMS-2860 gets an efficiency of 1.8 % at power levels of -20 dBm. These circuits are applicable to integrate with antennas by smart matching techniques. Then compact rectennas with good efficiency and less surface can supply DC energy for wireless devices.

### 5.3.1 Integrated monopole rectenna: rectenna I

The proposed monopole rectenna is illustrated in Fig. 5.13. A rectangular monopole and a rectifying circuit are printed on the same side of the dielectric substrate.  $L_2$  and  $L_1$  denote the length and the width of the monopole. The single stub matching circuit,  $L_6$  and  $L_4$ , is designed to match the input impedance of the diode with the monopole for the incident power -20 dBm at 2.45 GHz.

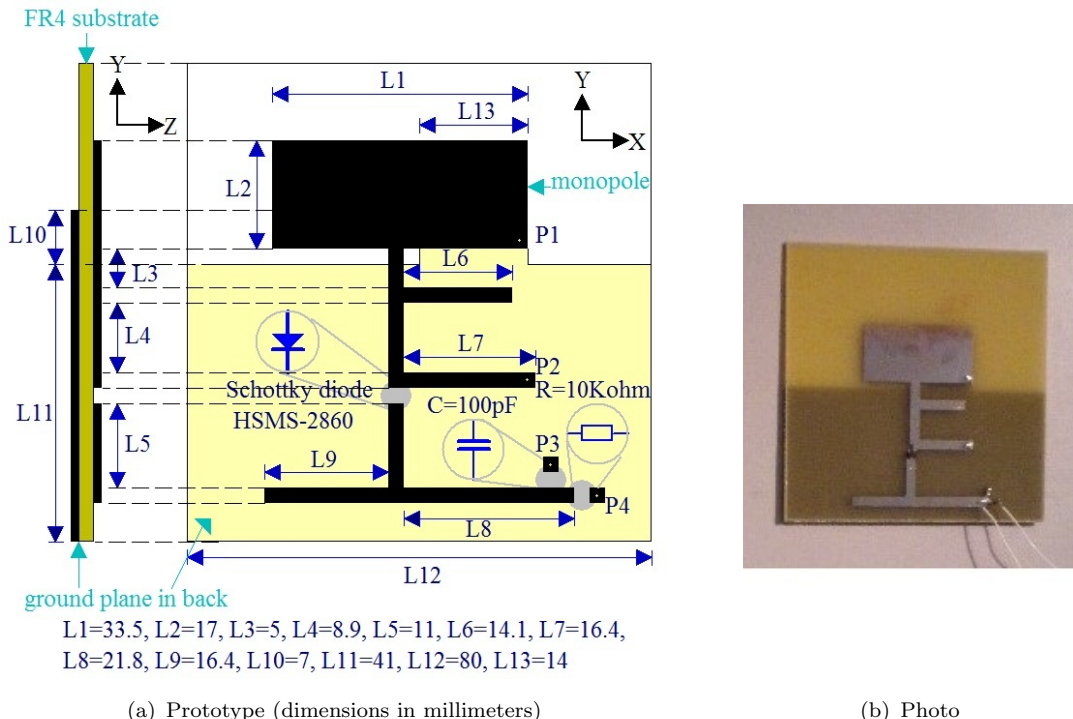


FIGURE 5.13: Configuration of the rectenna I

A short stub  $L_7$  of quarter-wavelength is introduced to constitute a DC loop (Via-hole  $P_2$  - Schottky diode - Load - Via-hole  $P_4$  - Ground plane). The input band pass filter ( $L_7$ ,  $L_4$ , and  $L_6$ ) protects the fundamental frequency and prevents

harmonic signals. An output low pass filter is composed by a quarter-wavelength open stub  $L9$  and by a half-wavelength transmission line ( $L5 + L8$ ) in order to arrange lumped elements and reject harmonic signals.

On the other side of the substrate, the conducting ground plane only covers the section of the rectifying circuit and a shorting pin  $P1$  of the monopole.  $L10$  and  $L13$  are the length and the width of the pad where the shorting pin is located. The pin is 0.5 mm each from the right and lower fringes of the monopole's right-lower corner. The height of the feed gap between the feed point and the ground plane is 2 mm.

The dimensions of the monopole and the ground plane, the height of the feed gap between the feed point and the ground plane, and the short circuited point are the parameters affecting the antenna operation. A total gain of 2.71 dBi and a -10 dB return loss bandwidth of 1.07 GHz are achieved for an optimal design. The advantage of such a broadband monopole simplifies the matching technique between antennas and narrow bandwidth rectifying circuits. Monopole antennas absorb RF energy from all the directions and the energy is converted by rectifying circuits.

### 5.3.2 Integration of DC loop: rectenna II

As an inspiration from prototypes of a printed monopole and a planar inverted-F antenna, a short circuited structure is introduced with the purpose of DC loop. The via-hole contributes to the DC loop instead of the short stub  $L7$  of the rectifying circuit. As presented in Fig. 5.14, the single stub matching circuit includes an open stub  $L6$  and a serial microstrip line  $L4$ . This design decreases the rectenna surface and it is an important step towards the conception of compact structures. The DC loop is changed from the rectenna I (Via-hole  $P2$  - Schottky diode - Load - Via-hole  $P4$  - Ground plane) to the rectenna II (Via-hole  $P1$  - Schottky diode - Load - Via-hole  $P4$  - Ground plane).

In comparison of the performance of integrated rectennas with and without a short stub, some harmonic signals rejected by the short stub  $L7$  inside the rectenna I may not be rejected completely by the rectenna II. Harmonics reflect to the antenna and join in the radiation. Therefore, the input impedance of the

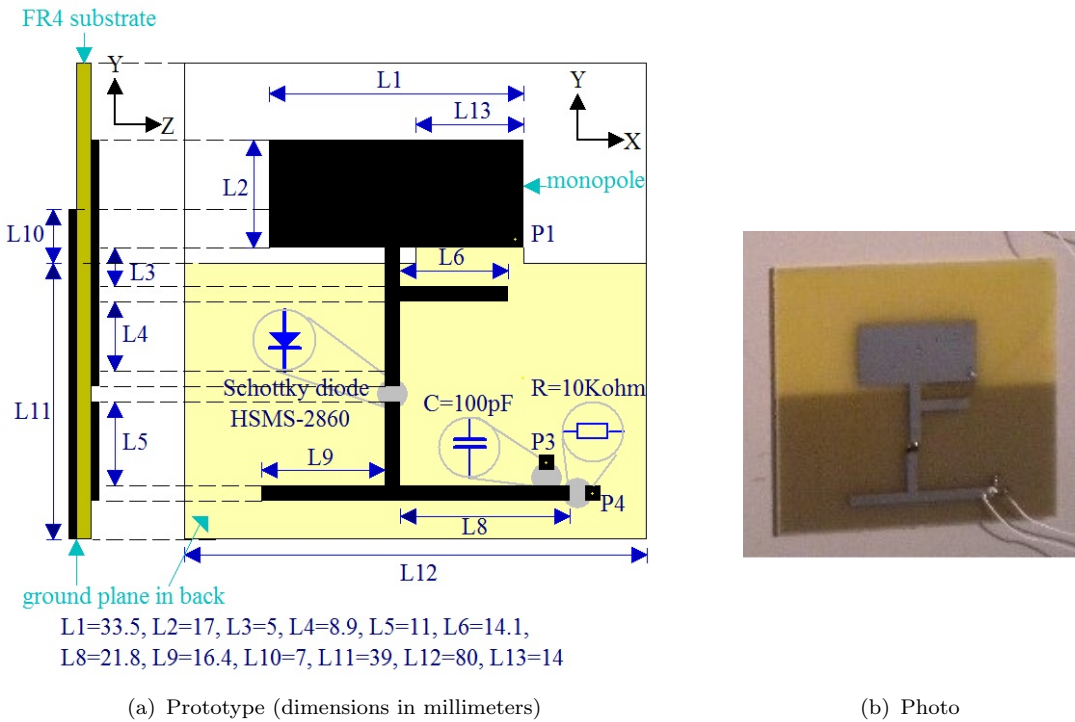


FIGURE 5.14: Configuration of the rectenna II

rectifying circuit changes, which may affect the matching level between the circuit and the antenna.

### 5.3.3 Anechoic chamber experiment

The integrated rectennas are fixed on a positioning shelf in an anechoic chamber, as in Fig. 5.15. The distance between the horn and the rectenna is  $5.856\text{ m}$ . The VNA output transfers the RF energy through a 35 dB gain amplifier to an emitting antenna. The rectenna receives the RF power and converts it into DC voltage which is measured by a voltmeter.

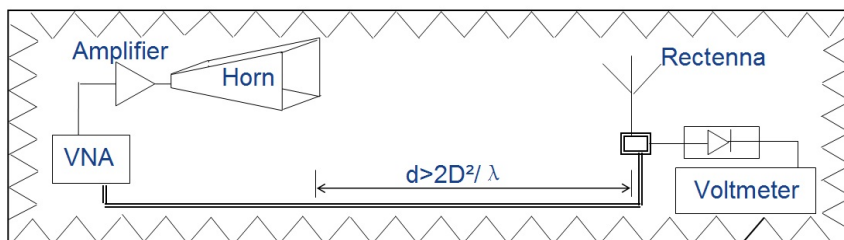


FIGURE 5.15: Experimental set-up of a rectenna

According to the Friis transmission equation, the power density at the rectenna position is determined. The measured DC voltage increases with an increment of power density, as shown in Fig. 5.16. When the monopole and the rectennas are in vertical polarization and perpendicular to the propagation direction, they capture microwave energy at low power densities. The rectifying circuit connected with the monopole products maximal DC voltage of 130 mV at the power density  $2.1 \mu\text{W/cm}^2$ , compared with 20 mV by the rectenna I and 40 mV by the rectenna II.

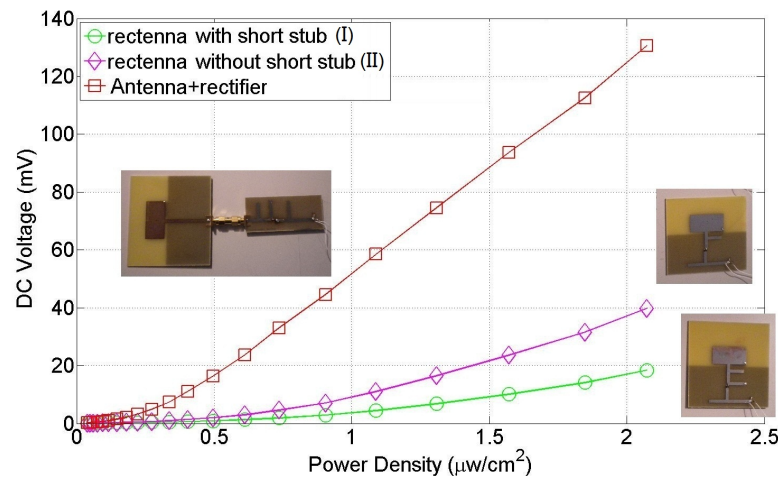


FIGURE 5.16: Measured DC voltage of the rectennas I and II against the power density at  $0^\circ$

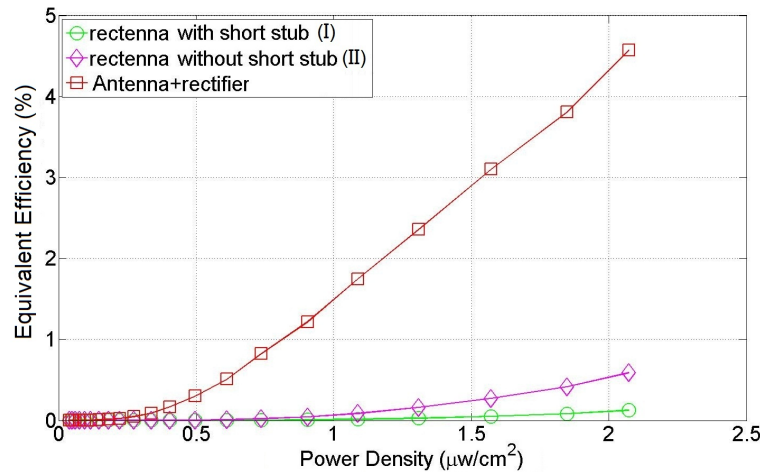


FIGURE 5.17: Equivalent efficiency of the rectennas I and II against the power density at  $0^\circ$

In the case of the monopole integrated with rectifying circuits by connectors, the receiving antenna captures the RF power around -15 dBm and the equivalent efficiency of the rectifying circuit is close to 5 %. However, the integrated rectennas

I and II operate at the power levels less than -20 dBm. It is estimated that these rectennas have efficiencies less than 1 %, as shown in Fig. 5.17.

An unavoidable problem caused by coplanar integration is the interference of distributed elements inside rectifying circuits. In the case of the monopole connected with rectifying circuits, there is no coupling effect between antennas and rectifying circuits. And these two parts are well matched according to the simulating analysis.

Due to the compactness of integrated rectennas, the matching level changes in the cases of the rectennas I and II. This leads to worse performance than the monopole connected with rectifying circuits. It is impossible to extract the matching level between antennas and rectifying circuits in the cases of integrated rectennas by ADS co-simulation analysis.

While the rectenna is vertical polarized on the direction -90° compared with the main direction 0°, the rectifying circuit connected with the monopole products maximal DC voltage of 279 mV at the power density  $2.1 \mu\text{W}/\text{cm}^2$ , compared with 250 mV by the rectenna I at 2.44 GHz and 100 mV by the rectenna II at 2.45 GHz, as presented in Fig. 5.18.

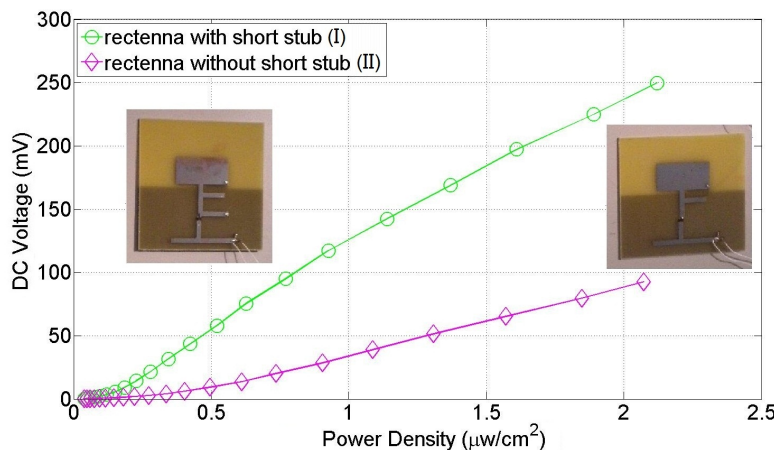


FIGURE 5.18: Measured DC voltage of the rectennas I and II against the power density at -90°

In this case, the received power by the monopole is around -10 dBm and the equivalent efficiency of the rectifying circuit is 21 %. Furthermore, the rectenna I has an equivalent efficiency around 16 % and better performance than the rectenna II with an equivalent efficiency of 3 %, as shown in Fig. 5.19. The idea of rectenna II reduces the rectenna surface by 30 % and gives the possibility of integration.

The choice of the best rectenna is difficult to be decided. Because the relative position between ambient sources and sensors is unknown in practical cases. The rectenna performance is link to the location of sensors.

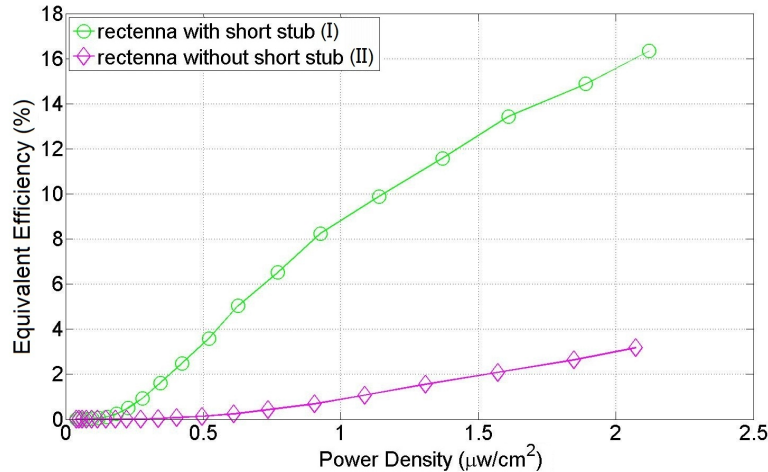


FIGURE 5.19: Equivalent efficiency of the rectennas I and II against the power density at  $-90^\circ$

All in all, rectenna configurations have been optimised with modified monopole antennas and rectifying circuits. Matching circuits between antennas and diodes ameliorate the overall conversion performance. Due to radiation patterns of the modified monopole in vertical polarization, the antenna has outstanding behaviours when it is parallel to the propagation direction. Cooperating with the monopole, rectifying circuits yield 279 mV at the power density  $2.1 \mu\text{W}/\text{cm}^2$ . Under the same condition, the rectenna I and II product 250 mV and 100 mV respectively. Consequently, about 10 % microwave energy can be recycled at this low power level.

## 5.4 Rectenna with high efficiency

In the application of energy harvesting at low power densities, rectifying circuits with Schottky diode HSMS-2860 have been integrated to monopole antennas. These rectennas have been measured on their main direction by a network analyser in an anechoic chamber. The rectenna I produces 20 mV and the rectenna II yields 40 mV at the power density of  $2.1 \mu\text{W}/\text{cm}^2$ . A better performance is obtained at  $-90^\circ$ . The value of DC output is low compared to practical cases.

The modelization of diodes and the optimization of layouts have been done to improve the conversion efficiency. However, the performance of diodes HSMS-2860 does not satisfy our goal. The following choice is to look for other diodes designed for low power levels.

### 5.4.1 Rectifying circuit with HSMS-2850

The Schottky diode HSMS-2850 has been introduced for the application of low power levels due to its low forward voltage drop, although the series resistance is large. The rectifying circuit with single stub matching circuit produces DC voltage of 64 mV and obtains conversion efficiency of 13.65 % when the incident power is -20 dBm. Its efficiency is 7.6 times more than the one with HSMS-2860.

This rectifying circuit has been combined with the modified monopole by a right angle connector, as shown in Fig. 5.20. The rectifying system is regarded as the reference in the chamber measurement. It will be discussed with the integrated rectennas III and IV in the following part.

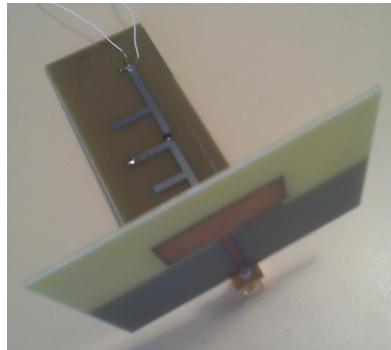


FIGURE 5.20: Rectifying circuit with HSMS-2850 connected with the modified monopole

This rectenna has been measured with a transmitter-receiver configuration in an anechoic chamber. It obtains the maximum DC output for RF energy harvesting at 2.35 GHz on the main direction. The radiation property of the rectenna determines incident power levels of rectifying circuits. The DC voltages are 9.5 mV, 64 mV, 286 mV, and 968 mV when input power levels are -30 dBm, -20 dBm, -10 dBm, and 0 dBm. In this case, the conversion efficiencies are 3 %, 13.65 %, 27.23 %, and 31.21 % respectively.

### 5.4.2 Integrated rectenna with HSMS-2850: rectenna III

As presented in Fig. 5.21, the rectenna III has been printed on FR4 substrate with  $\epsilon_r = 4.6$  and 1.58 mm thickness. A short circuit is introduced into the monopole antenna. It consists of a printed monopole ( $L2 \times L1$ ) with short circuited structure  $P1$ . The rectifying circuit is designed with single series Schottky diode HSMS-2850 and single stub matching circuit ( $L6$  and  $L4$ ).

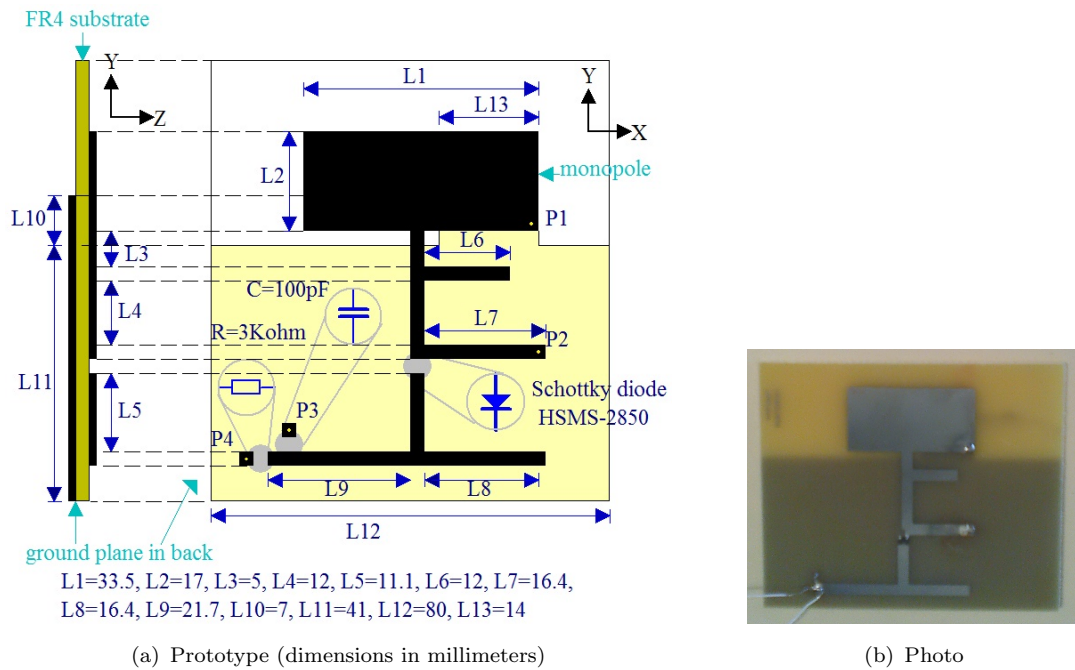


FIGURE 5.21: Configuration of the rectenna III

A quarter-wavelength  $L7$  contributes to a DC loop (Via-hole  $P1$  - Schottky diode - Load - Via-hole  $P4$  - Ground plane). The load resistance is optimized as  $3\text{ k}\Omega$  and the capacitor in parallel is  $100\text{ pF}$ . The output low pass filter consists of a quarter-wavelength  $L8$  and microstrip lines,  $L5$  and  $L9$ . It rejects harmonic signals generated by diodes and locks the harmonics in rectifying cycle.

On the other side of the substrate, the ground plane only covers the section of the rectifying circuit and a shorting pin  $P1$ . The pad ( $L10 \times L13$ ) is located just to connect the shorting pin and to cover the right-lower corner of the monopole. The feed gap is 2 mm height between the feed point and the ground plane.

The dimensions of the monopole and the ground plane, the height of the feed gap, and the position of the shorting pin have been simulated in Ansoft HFSS. The modified monopole is wideband and has a total gain of 2.71 dBi in the chamber

measurement. It may bring a little distortion if the rectifying circuit is coplanar and joins to the radiation. The layouts of rectennas are optimized to let rectifying circuits not change the antenna properties as much as possible. The rectenna produces the maximum DC output for RF energy harvesting at 2.35 GHz.

### 5.4.3 Integrated rectenna with new DC loop: rectenna IV

Based on the study of the rectenna I and the rectenna II for energy harvesting at low power densities, and the rectenna III for high conversion efficiency, the rectenna IV is proposed with an advantage of surface reduction. As presented in Fig. 5.22, the monopole ( $L2 \times L1$ ) is integrated with a rectifying circuit through a feed line of 5 mm. The matching circuit ( $L6$  and  $L4$ ) is used to match the input impedance of diodes to the antenna impedance. The output low pass filter ( $L5$ ,  $L9$ , and a quarter-wavelength open stub  $L8$ ) protects DC signals and rejects harmonics. The layout shows clearly that a quarter-wavelength short stub is suppressed comparing with the rectenna III. Thus the DC loop is formed by the via-hole  $P1$ , Schottky diode, the load, and the via-hole  $P4$ .

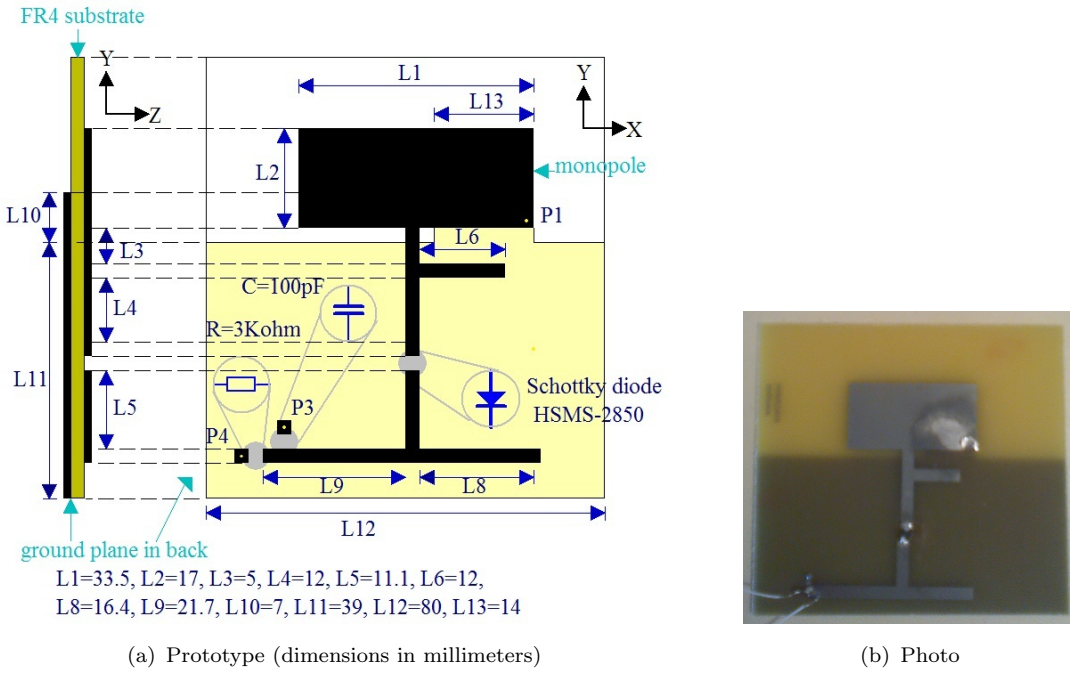


FIGURE 5.22: Configuration of the rectenna IV

On the other side of the substrate, the conducting ground plane ( $L11 \times L12$ ), the pad ( $L10 \times L13$ ) connected to the monopole, and a shorting pin  $P1$  at the right-lower corner of the monopole are optimized in HFSS simulations. The height of

the feed gap between the feed point and the ground plane is tuned to 2 mm. The layout has been realised on FR4 substrate with  $\varepsilon_r = 4.6$  and 1.58 mm thickness. This rectenna yields the maximum DC output for energy harvesting at 2.42 GHz.

#### 5.4.4 DC voltage and equivalent efficiency

The modified monopole combined with a rectifying circuit has been measured in an anechoic chamber. The monopole captures microwave energy and transfers it to Schottky diodes. The rectifying circuit with HSMS-2850 converts RF energy into DC power. Thanks to the characteristic of this diode, this rectifying system has good conversion efficiency.

The rectenna III consists of a modified monopole and a rectifying circuit on a coplanar structure. It produces high DC voltage at low power densities. As presented in Fig. 5.23, the DC voltage is 208.4 mV at the power density of 2.1  $\mu\text{W}/\text{cm}^2$ , compared with the non-planar configuration (210.6 mV).

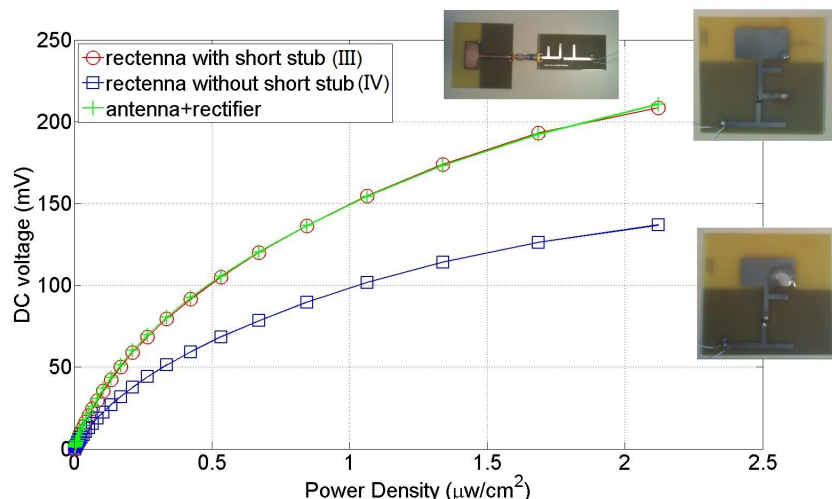


FIGURE 5.23: Measured DC voltage of the rectennas III and IV against the power density at 0°

Supposing that the radiation of the monopole is not disturbed by rectifying circuits, the equivalent efficiency is about 31 %, as shown in Fig. 5.24 and the captured power is estimated to -13.3 dBm. These two rectennas are based on the same antenna subsystem. Rectifying circuits are similar but the connecting methods are different. Matching circuits are well designed and thus the results of DC voltage are similar at the main direction.

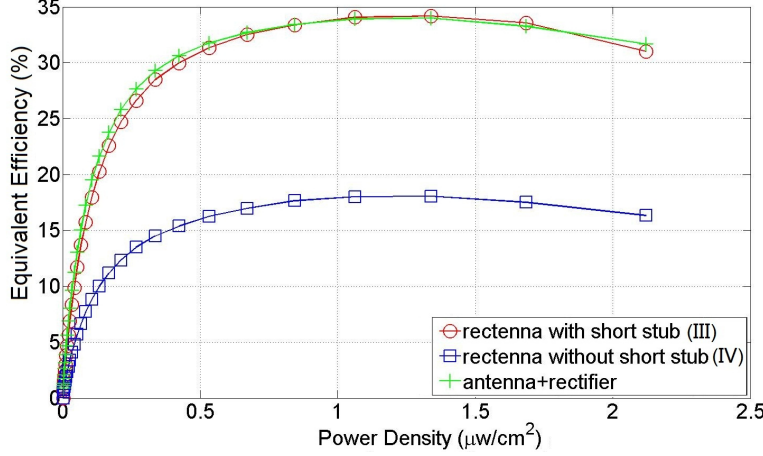


FIGURE 5.24: Equivalent efficiency of the rectennas III and IV against the power density at  $0^\circ$

Based on the coplanar configuration of the rectenna III, the rectenna IV has an improvement of DC loop which decreases the layout surface. However, the quarter-wavelength short stub  $L7$  inside the rectenna III not only contributes to the DC loop but also prevents harmonic signals. The rectenna IV without this  $\lambda/4$  short stub may lead to mismatched harmonics. In this case, the radiating property of the monopole is influenced by harmonic reflection to the antenna, and the DC voltage of rectifying circuits is reduced. The rectenna IV yields 136.8 mV DC voltage at the power density  $2.1 \mu\text{W}/\text{cm}^2$ . The equivalent efficiency is about 16 % and the estimated input power is -14 dBm.

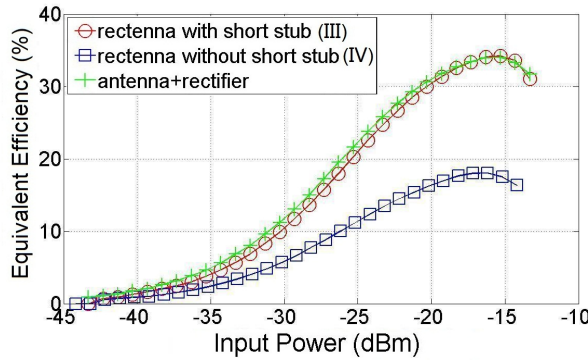


FIGURE 5.25: Equivalent efficiency of the rectennas III and IV against the incident power at  $0^\circ$

The equivalent efficiency is maximal to 34 % by the rectenna III and 18 % by the rectenna IV at the power density  $1.3 \mu\text{W}/\text{cm}^2$ . Due to the filtering function of the monopole, the rectenna performance is improved. As presented in Fig. 5.25,

the equivalent efficiency is 30 % at an input power of -20 dBm, 10 % at -30 dBm input power, and 2 % at -38 dBm input power, respectively.

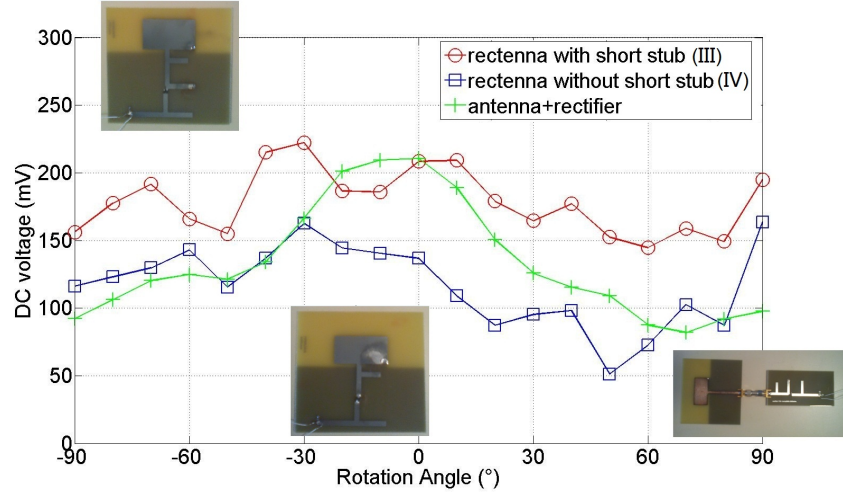


FIGURE 5.26: Measured DC voltage of the rectennas III and IV against the rotation angle

Fig. 5.26 presents measured DC voltages of these rectennas against the rotation angle. On the main direction, the rectenna III shows an agreement with the non-planar structure of the monopole and rectifying circuits. However, on other directions, the results of these two rectennas do not fit owing to the radiating effect of coplanar rectifying circuits. Fig. 5.27 presents the directional property of these rectennas in the domain of equivalent efficiency.

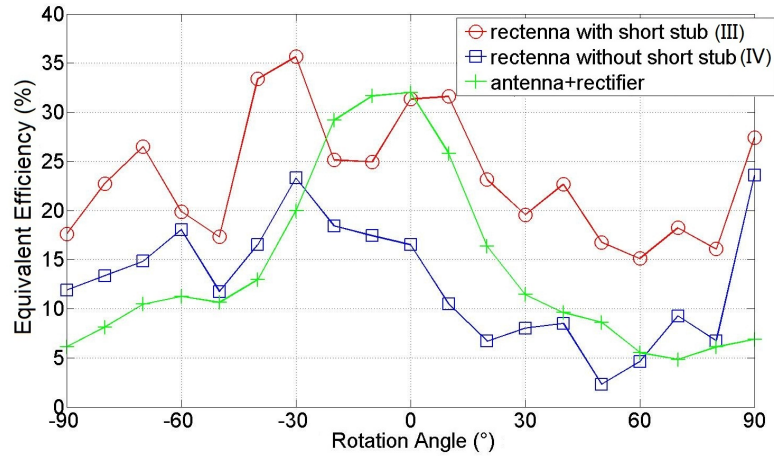


FIGURE 5.27: Equivalent efficiency of the rectennas III and IV against the rotation angle

The rectenna with non-planar configuration yields maximal DC output (210.6 mV and 32 %) on the main direction. It shows worse performance (82 mV and

4.85 %) on the direction -90°. The rectenna III produces better DC output (222.3 mV and 35.65 %) at -30° but worse DC output (144.7 mV and 15.11 %) at 60°. The rectenna IV is also directional on the figure of DC voltage against the rotation angle. Better DC voltage is 163.6 mV at -30 ° and the equivalent efficiency is 23.6 %. Worse DC voltage is 51.2 mV at 50° and the efficiency is about 2.31 %.

In practical cases, the relative position between ambient sources and sensors is not known and any direction may be concerned. Therefore, we introduce an average criterion in order to define the rectenna performance on all the directions. The average level of DC voltage 178.8 mV and the equivalent efficiency 23 % at the power density  $2.1 \mu\text{W}/\text{cm}^2$  are considered as the performance of the rectenna III. Under the same condition as the rectenna III, the rectenna IV yields the average DC voltage of 116.6 mV and the equivalent efficiency of 13 %.

## **5.5 Conclusion of rectenna design**

Various configurations of rectennas are proposed in this chapter, as presented in Table 5.1. The rectenna layout consists of the radiating part and the rectifying part. Generally these two parts are designed separately. The radiating part includes antennas and distributed components which can radiate or receive RF energy. Moreover, the rectifying part is composed by diodes, load resistors, matching circuits, and filters. Based on the study of rectifying circuits, antennas are combined with these circuits on a coplanar configuration. The short circuited monopole integrated with rectifying circuits, by using the shorting pin inside the monopole instead of the short stub inside rectifying circuits, provides a compact structure.

For the application of power transmission at high power densities, the rectenna with Schottky diode HSMS-2820 has been designed for an incident power of 20 dBm. A patch antenna with probe feeding operates with good linearly polarization. A double stubs matching circuit is used to well match the input impedance of diodes to the antenna. The DC voltage is 1.025 V and the conversion efficiency is 16.13 % at the power density of  $31.83 \text{ mW}/\text{cm}^2$ . And the DC output is 1.7 V and the efficiency is 18.75 % at the power density of  $88.42 \text{ mW}/\text{cm}^2$ . This rectenna has good DC output at high power densities.

Design	Patch rectenna with diode HSMS-2820	Integrated monopole rectenna with diode HSMS-2860 (rectenna I)	Monopole rectenna with integrated DC loop and diode HSMS-2860 (rectenna II)	Integrated monopole rectenna with diode HSMS-2850 (rectenna III)	Monopole rectenna with integrated DC loop and diode HSMS-2850 (rectenna IV)
Load	$820\Omega$	$10k\Omega$	$10k\Omega$	$3k\Omega$	$3k\Omega$
Freq	2.45GHz	2.44GHz	2.45GHz	2.35GHz	2.42GHz
Effective area	$13\text{cm}^2$	$18\text{cm}^2$	$13\text{cm}^2$	$22\text{cm}^2$	$18\text{cm}^2$
Equivalent $\eta_{max}$	16%	16%	3%	34%	18%
Power density	$32\text{mW/cm}^2$	$2.1\mu\text{W/cm}^2$	$2.1\mu\text{W/cm}^2$	$1.3\mu\text{W/cm}^2$	$1.3\mu\text{W/cm}^2$
Equivalent $P_{in}$	9dBm	-14.2dBm	-15.7dBm	-15.3dBm	-16.2dBm
Mean $\eta$ ( $p=2.1\mu\text{W/cm}^2$ )				23%	13%
Common and difference	ISM, high power	ISM, low power	ISM, low power	ISM, low power	ISM, low power

TABLE 5.1: Measured results of rectenna design

For the application of energy harvesting at low power densities, the rectennas with HSMS-2860 have been optimized for an input power of -20 dBm. The rectenna I with the monopole antenna produces DC voltage of 20 mV and the rectenna II with the modified monopole yields 40 mV at the power density of  $2.1\mu\text{W/cm}^2$  on the main direction. Furthermore, the rectenna I produces DC voltage of 250 mV and the rectenna II yields 100 mV at the power density of  $2.1\mu\text{W/cm}^2$  on  $-90^\circ$ . In this case, about 10 % of microwave energy can be recycled at low power levels.

In the aim of obtaining high conversion efficiency at low power densities, the rectennas with HSMS-2850 have been introduced due to the perfect characteristic of this diode for low power levels. The rectenna III with the monopole produces DC voltage of 208.4 mV and the rectenna IV yields 136.8 mV at the power density of  $2.1\mu\text{W/cm}^2$  on the main direction. The rectenna III achieves the maximal efficiency 34% when the incident power is -15.3 dBm, compared to the rectenna proposed by S. Rivière [115–117] with conversion efficiency 29% at an input power

-15 dBm. Taking into account the relative location between the rectennas and the ambient sources in practical cases, the rectenna III produces the average DC voltage of 178.8 mV and the equivalent efficiency of 23 % at the power density of  $2.1 \mu\text{W/cm}^2$ . Under the same condition, the rectenna IV yields the average DC voltage of 116.6 mV and the equivalent efficiency of 13 %.

# Chapter 6

## Conclusion and Perspective

### 6.1 Conclusion

Wireless power transmission technology transmits electromagnetic microwave power through free-space. The power level, sometimes high or low, depends upon the location of wireless sensors, the distance between the base station and sensors, and the intensity of emitting energy. Furthermore, network sensors are rechargeable by the technology of energy harvesting. The rectenna is a kind of wireless battery instead of the traditional battery. It captures microwave energy from ambient environments and converts it into useful DC energy. Usually the power density is low due to the safety standard.

First of all, we did the bibliography study about rectifying circuits, antennas, and rectennas. In the aim of minimizing the conduction loss of diodes and optimizing the output DC voltage, single serial diode configurations are chosen for the rectification process. Rectifying elements, particularly Schottky diodes, are studied by some methods, including equivalent circuit model, ADS simulated model, SPICE parameters, and diode modelization.

ADS simulating approaches are used in diode modelization and rectifying circuit simulations. SP and LSSP analyse scattering parameters in the frequency domain. Associated with multiple parameter sweeps, HBS shows the non-linear behaviour of diodes and gives scattering parameters in the power domain. Rectifying circuits are designed based on Hybrid optimization and tuning methodology.

Co-simulation verifies the result of circuit simulation by taking into account the precise simulating model, the coupling effect, and the dielectric and metallic losses.

In the chapter of RF/DC conversion, various rectifying circuits are discussed for the application of power transmission of high and low power levels. For example, the rectifying circuit with Schottky diode HSMS-2820 produces maximum DC voltage of 11 V and conversion efficiency of 55 % over a load resistor of 820  $\Omega$  when the input power is 20 dBm. Another example is the rectifying circuit with Schottky diode HSMS-2860. It yields DC voltage of 42.1 mV and conversion efficiency of 1.8 % over a load resistor of 10 k $\Omega$  for the power level of -20 dBm. All the circuits are optimized for certain power level according to our requirement. RF power is harvested with high efficiency for high power levels and with low efficiency for low power levels.

On the purpose of energy scavenging at low power densities, the rectifying circuit with Schottky diode HSMS-2850 achieves DC voltage of 64 mV and conversion efficiency of 13.65 % over a resistive load 3 k $\Omega$  when the incident power is -20 dBm. This circuit with high efficiency for low power levels contributes to the application of power converting from low radiation sources.

In the chapter of antenna design for energy harvesting, different layouts of antennas are considered in order to capture maximum RF energy. The patch antenna is easily realized, linear polarized, and narrowband. The monopole antenna is printed on PCB, less area occupied, and wideband. Inspired by the structure of PIFA, the monopole with a shorting pin is broadband and has good radiation properties. It provides an opportunity to design a compact rectenna.

In the chapter of combination and integration of rectenna, we proposed several rectenna structure coplanar or non-planar. The rectenna with patch antenna and HSMS-2820 produces maximum DC voltage of 1.7 V and the efficiency of 18.75 % at the power density of 88.42 mV/cm<sup>2</sup>. The rectenna with monopole antenna and HSMS-2860 yields maximal DC voltage of 250 mV at the power density of 2.1  $\mu$ W/cm<sup>2</sup>. Around 10 % RF energy can be recycled at this low power level.

In the best case with high efficiency for low power levels, the rectenna with monopole and HSMS-2850 produces DC voltage of 208.4 mV and equivalent efficiency of 31 % at the power density of 2.1  $\mu$ W/cm<sup>2</sup>. Under the condition of unexpected distance between sensors and ambient sources, the average value of DC voltage is 178.8 mV and equivalent efficiency is 23 %. More than 20 % of

Design	Aperture coupled patch rectenna	Dual-frequency rectenna	Rectifier with high Q resonators	Spiral rectenna	Integrated monopole rectenna with diode HSMS-2850
Author	S.Rivière	Z.Saddi	T.Ungan	D.Bouchouicha	Y.Zhou
Year of publication	2010	2013	2009	2010	2013
$\eta$	29%	10.5%	22%	0.7%	34%
$p$	$5.37\mu\text{W}/\text{cm}^2$ (-15dBm)	0.13 and 0.248 $\mu\text{W}/\text{cm}^2$ (-20dBm)	-30dBm	$3.55\text{nW}/\text{cm}^2$ (-38dBm)	$1.3\mu\text{W}/\text{cm}^2$ (-15.3dBm)
Freq	2.45GHz	1.8 and 2.35GHz	24MHz	1.85GHz	2.35GHz
Cons	ISM, low power	GSM and ISM, low power	Medium wave, low power	GSM, low power	ISM, low power

TABLE 6.1: Comparison of rectenna designs

microwave energy is harvested by these proposed rectennas at the power density between  $0.75 \mu\text{W}/\text{cm}^2$  and  $2.4 \mu\text{W}/\text{cm}^2$ , a majority of power range in COPIC investigation. In the comparison, as presented in Table 6.1, the integrated monopole rectennas with diode HSMS 2850 own good performance in low power applications at ISM frequency. Consequently, they can be used in point-to-point power transmission of low power levels or for a long distance. Besides, batteries of wireless devices can be charged by these rectennas which captures RF energy from low ambient radiation sources.

The minimum power density given by COPIC is  $5.2 \text{nW}/\text{cm}^2$ . In this case, the rectenna with HSMS-2850 provides maximal DC voltage  $2.34 \text{ mV}$ . This voltage is too low to supply wireless devices. The estimated received power is less than -30 dBm and the equivalent efficiency is poor. However, the rectenna with Schottky diode HSMS-2850 can operate well at the electric field  $3 \text{ V/m}$  ( $2.4 \mu\text{W}/\text{cm}^2$ ) in the urban zone. The available power output is approximately 10 % of the consumption of a sensor ( $100 \mu\text{W}$ ).

## 6.2 Perspective

In the applications of power transmission and energy harvesting, no matter whether the power level is high or low, the main objective with the rectenna design is to achieve high conversion efficiency. Thus the design can be improved in the field of RF energy reception and rectification, including some aspects as follows.

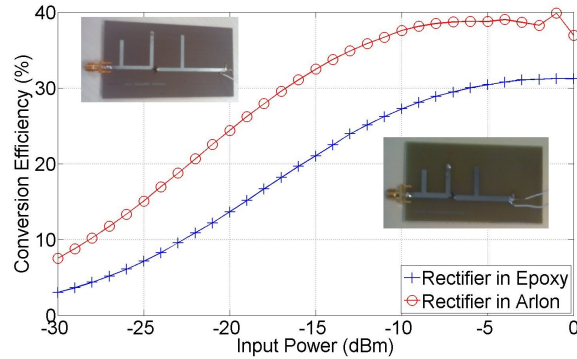


FIGURE 6.1: Conversion efficiency of rectifying circuits in Epoxy and in Arlon

The proposed rectennas in the thesis are printed on Bernier FR4 substrate with  $\epsilon_r = 4.6$ ,  $\tan\delta=0.02$ , and 1.58 mm thickness. The loss tangent of the used FR4 dielectric is relatively high compared to other dielectric materials, for example, Arlon Diclad 527 substrate with  $\epsilon_r = 2.55$ ,  $\tan\delta=0.0025$ , and 0.762 mm thickness. The use of low-loss materials decreases the dielectric loss, and consequently it is beneficial for the efficiency.

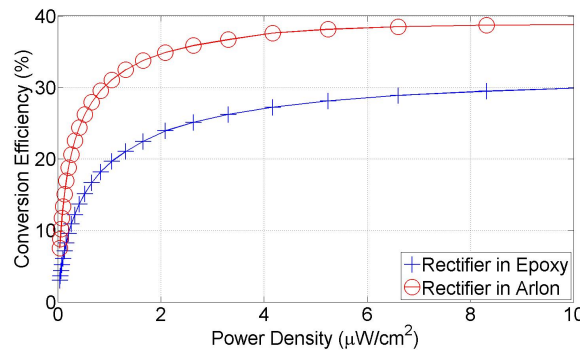


FIGURE 6.2: Conversion efficiency of circuits in Epoxy and in Arlon against the equivalent power density with 3 dBi antenna

As presented in Fig. 6.1, the rectifying circuit in Arlon produces conversion efficiency about 10 % higher than the circuit in Epoxy. In terms of the equivalent power density with 3 dBi gain antenna, as shown in Fig. 6.2, the circuit in Arlon obtains maximum efficiency close to 40 % at low power densities. However, we

choose the low-cost substrate Epoxy in the aim of rectenna design for sensor networks.

In the energy receiving process, maximum power should be collected and delivered to the rectifying circuit. Several broadband antennas, circularly polarized antennas, and large antenna arrays can be used as receiving antennas. The broadband antenna enables more RF power to be captured from various sources. And the circularly polarized antenna receives RF power with less polarization mismatch. These antennas are good ideas to harvest RF energy effectively. Taking into account the compromise between the antenna size and the radiation gain, antenna arrays increase the incident power of rectification by the way of enlarging antenna aperture and gain. Small or multi-layer antennas are interesting to meet the requirement of antenna size.

In the energy converting process, the improvement of conversion efficiency inside rectifying circuits is the key to increase the overall efficiency of rectenna systems. A non-linear rectifying element, such as Schottky diode, determines the performance of rectifying circuits. RF characteristics of diodes decide the operating frequency range and available power levels of rectification process.

For example, Schottky diodes HSMS-2820 and HSMS-2860 have small series resistances and large breakdown voltages. These diodes support high power levels and they are suitable for power transmission with less conduction loss. Another example is Schottky diodes HSMS-2850 and SMS7630. These diodes own small threshold voltage and they are applicable for energy harvesting for low power levels. Though they own large series resistance, the conduction loss is not a dominant factor when the forward current is low at low power densities. The spindiode is also interesting due to zero bias resistance.

With the development of semiconductor device, the ambition is to search for a diode which owns good characteristics at ISM or GSM frequencies and for low power levels. Most important of all, it has small threshold voltage and small series resistance. The rectenna with such diode can operate at low power densities, and supply wireless devices under various environments.

Besides, the band pass filter between the antenna and the diode rejects the harmonics generated by the diode and re-radiated from the antenna as power losses. The low pass filter between the diode and the load prevents the harmonics from transmitting to the load and reflects them to participate in a new cycle

of rectification. The matching circuit between the antenna and the rectifying circuit increase the conversion efficiency by minimizing the mismatch loss. A higher output voltage can increase the applicability of the rectenna. All in all, the efficiency can be improved by optimizing the circuit construction.

# Bibliography

- [1] S. Roundy, D. Steingart, L. Frechette, P. Wright, and J. Rabaey. *Wireless Sensor Networks*, volume 2920, chapter Power sources for wireless sensor networks. Springer Berlin Heidelberg, January 2004.
- [2] J. C. Lin. Wireless power transfer for mobile applications, and health effects [telecommunications health and safety]. *IEEE Antennas and Propagation Magazine*, 55(2):250–253, April 2013.
- [3] D. M. Rowe. *Thermoelectrics Handbook: Macro to Nano*, chapter Thermo-electric power generation: efficiency and compatibility. CRC Press, 2006.
- [4] K. Bullis. Free power for cars - automakers look to thermoelectrics to help power tomorrow’s vehicles. Technical report, MIT Technology Review, December 2005.
- [5] P. J. Marron, S. Karnouskos, D. Minder, and A. Ollero. *The Emerging Domain of Cooperating Objects*, chapter State of the art in cooperating objects research. Springer Berlin Heidelberg, 2011.
- [6] S. P. Beeby, M. J. Tudor, and N. M. White. Energy harvesting vibration sources for microsystems applications. *Measurement Science and Technology*, 17(12):175–195, December 2006.
- [7] J. Granstrom, J. Feenstra, H. Sodano, and K. Farinholt. Energy harvesting from a backpack instrumented with piezoelectric shoulder straps. *Smart Materials and Structures*, 16(5):1810–1820, October 2007.
- [8] F. Yildiz. Potential ambient energy-harvesting sources and techniques. *The Journal of Technology Studios*, 35(1):40–48, 2009.

- [9] A. H. Epstein. Millimeter-scale, micro-electro-mechanical systems gas turbine engines. *Engineering for Gas Turbines and Power*, 126(2):205–226, June 2004.
- [10] J. B. Lee, Z. Chen, M. G. Allen, A. Rohatgi, and R. Ayra. A high voltage solar cell array as an electrostatic mems power supply. In *Proceedings of the IEEE Workshop on Micro Electro Mechanical Systems*, pages 331–336, January 1994.
- [11] M. Freunek and L.M. Reindl. Maximum efficiencies of indoor photovoltaic devices. *IEEE Journal of Photovoltaics*, 3(1):59–64, November 2012.
- [12] Y. Q. Wang and X. X. Yang. Design of a high-efficiency circularly polarized rectenna for 35 GHz microwave power transmission system. In *Proceedings of the Asia-Pacific Power and Energy Engineering Conference*, pages 1–4, March 2012.
- [13] J. J. Schlesak, A. Alden, and T. Ohno. A microwave powered high altitude platform. In *Proceedings of the IEEE MTT-S International Microwave Symposium Digest*, pages 283–286, May 1988.
- [14] A. J. Reid and M. D. Judd. A novel self-powered condition monitoring sensor for harsh environments - feasibility study. In *Proceedings of the 15th International Symposium on High Voltage Engineering*, August 2007.
- [15] T. Von Buren, P. D. Mitcheson, T. C. Green, E. M. Yeatman, A. S. Holmes, and G. Troster. Optimization of inertial micropower generators for human walking motion. *IEEE Sensors Journal*, 6(1):28–38, February 2006.
- [16] T. Starner and J. A. Paradiso. Human generated power for mobile electronics. Technical report, College of Computing Georgia Tech, July 2004.
- [17] P. S. Hall and Y. Hao. *Antennas and propagation for body-centric wireless communications*, chapter Introduction to body-centric wireless communications. Artech House, Inc., 2006.
- [18] J. B. Hagen. *Radio-frequency electronics circuits and applications*, chapter Power supplies. Cambridge University Press, 1996.
- [19] T. K. Sarkar, M. C. Wicks, and M. Salazar-Palma. *Smart Antennas*, chapter A survey of various propagation models for mobile communication. John Wiley & Sons, Inc., 2003.

- [20] G. Liu, N. Mrad, G. Xiao, Z. Li, and D. Ban. RF-based power transmission for wireless sensors nodes. In *Proceedings of the International Workshop on Smart Materials, Structures and NDT in Aerospace*, November 2011.
- [21] W. C. Brown. The history of power transmission by radio waves. *IEEE Transactions on Microwave Theory and Techniques*, 32(9):1230–1242, September 1984.
- [22] H. Takhedmit, L. Cirio, B. Merabet, B. Allard, F. Costa, C. Vollaire, and O. Picon. Efficient 2.45 GHz rectenna design including harmonic rejecting rectifier device. *Electronics Letters*, 46(12):811–812, June 2010.
- [23] B. Strassner and K. Chang. Highly efficient C-band circularly polarized rectifying antenna array for wireless microwave power transmission. *IEEE Transactions on Antennas and Propagation*, 51(6):1347–1356, June 2003.
- [24] International Commission on Non-Ionizing Radiation Protection. Guidelines for limiting exposure to time-varying electric, magnetic, and electromagnetic fields (up to 300 GHz). *Health Physics*, 74(4):494–522, 1998.
- [25] *IEEE Standard for Safety Levels with Respect to Human Exposure to Radio Frequency Electromagnetic Fields, 3 kHz to 300 GHz*. Institute of Electrical and Electronics Engineers, IEEE Std C95.1 edition, 1999.
- [26] World Health Organization. What are electromagnetic fields? Technical report, WHO Regional Office for Europe, 1999.
- [27] Diminution de l'exposition aux ondes électromagnétiques émises par les antennes relais de téléphonie mobile. Technical report, 2013. URL [http://www.developpement-durable.gouv.fr/IMG/pdf/rapport\\_COPIC\\_31\\_juillet\\_2013.pdf](http://www.developpement-durable.gouv.fr/IMG/pdf/rapport_COPIC_31_juillet_2013.pdf).
- [28] T. Uungan, X. Le Polozec, W. Walker, and L. Reindl. Rf energy harvesting design using high Q resonators. In *Proceedings of the IEEE MTT-S International Microwave Workshop on Wireless Sensing, Local Positioning, and RFID*, pages 1–4, September 2009.
- [29] D. Bouchouicha, M. Latrach, F. Dupont, and L. Ventura. An experimental evaluation of surrounding RF energy harvesting devices. In *Proceedings of the 40th Microwave Conference*, pages 1381–1384, September 2010.

- [30] W. C. Brown. Experiments in the transportation of energy by microwave beam. *IRE International Convention Record*, 12:8–17, March 1964.
- [31] W. C. Brown. Experiments involving a microwave beam to power and position a helicopter. *IEEE Transactions on Aerospace and Electronic Systems*, AES-5(5):692–702, September 1969.
- [32] H. Geng and I. Park. *Semiconductor manufacturing handbook*, chapter IC Design. McGraw-Hill, Inc., 2005.
- [33] S. M. Sze. *Physics of semiconductor devices*, chapter P-n Junction diode. John Wiley & Sons, Inc., 2nd edition, 1981.
- [34] T. Yoo and K. Chang. Theoretical and experimental development of 10 and 35 GHz rectennas. *IEEE Transactions on Microwave Theory and Techniques*, 40(6):1259–1266, June 1992.
- [35] J. O. McSpadden, T. Yoo, and Chang K. Theoretical and experimental investigation of a rectenna element for microwave power transmission. *IEEE Transactions on Microwave Theory and Techniques*, 40(12):2359–2366, December 1992.
- [36] J. Zbitou, M. Latrach, and S. Toutain. Hybrid rectenna and monolithic integrated zero-bias microwave rectifier. *IEEE Transactions on Microwave Theory and Techniques*, 54(1):147–152, January 2006.
- [37] J. J. Nahas. Modeling and computer simulation of a microwave-to-dc energy conversion element. *IEEE Transactions on Microwave Theory and Techniques*, 23(12):1030–1035, December 1975.
- [38] S. A. Maas. *Nonlinear microwave and RF circuits*, chapter Solid-state device modeling for quasistatic analysis. Artech House, Inc., 2nd edition, 2003.
- [39] H. Takhedmit. *Modélisation et conception de circuits de réception complexes pour la transmission d'énergie sans fil à 2.45 GHz*. PhD thesis, L'École Centrale de Lyon, 2010.
- [40] B. R. Franciscatto, V. Freitas, J. M. Duchamp, C. Defay, and T. P. Vuong. Circuit de conversion RF-DC à 2.45 GHz à fort rendement pour les applications de récupération d'énergie RF. In *Proceedings of the 18èmes Journées Nationales Microondes*, May 2013.

- [41] W. Storr. Electronic tutorial about power diodes as rectifiers. Technical report, Basic Electronics Tutorials, 2013.
- [42] F. Losee. *RF systems, components, and circuits handbook*, chapter Semiconductor diodes and their circuits. Artech House, Inc., 1997.
- [43] J. Zbitou. *Étude, conception et réalisation d'un système de conversion RF-DC*. PhD thesis, L'École Polytechnique de l'Université de Nantes, January 2005.
- [44] *HSMS-282x surface mount RF Schottky barrier diodes*. Avago Technologies, 2008. Data Sheet.
- [45] J. Singh. *Semiconductor devices - basic principles*, chapter Metal-semiconductor junctions. John-Wiley & Sons, Ltd., 2001.
- [46] R. M. Kielkowski. *Inside SPICE - overcoming the obstacles of circuit simulation*, chapter Understanding circuit simulation. McGraw-Hill, Inc., 1994.
- [47] B. Merabet, L. Cirio, H. Takhedmit, F. Costa, C. Vollaire, B. Allard, and O. Picon. Low-cost converter for harvesting of microwave electromagnetic energy. In *Proceedings of the IEEE Energy Conversion Congress and Exposition*, pages 2592–2599, 2009.
- [48] S. Vaja and S. Halabi. *Agilent ADS tutorial*, 2011.
- [49] D. Bouchouicha. *Etude de faisabilité de la récupération d'énergie électromagnétique ambiante*. PhD thesis, L'Université François - Rabelais de Tours, November 2010.
- [50] *Surface mount microwave Schottky detector diodes*. Hewlett Packard, 1999. Technical Data.
- [51] Y. Q. Wang and X. X. Yang. Design of a high-efficiency circularly polarized rectenna for 35 GHz microwave power transmission system. In *Proceedings of the Asia-Pacific Power and Energy Engineering Conference*, pages 1–4, March 2012.
- [52] G. Andia Vera, A. Georgiadis, A. Collado, and S. Via. Design of a 2.45 ghz rectenna for electromagnetic (EM) energy scavenging. In *Proceedings of the IEEE Radio and Wireless Symposium*, pages 61–64, January 2010.

- [53] *Surface mount mixer and detector Schottky diodes*. Alpha Industries. Data Sheet.
- [54] *MA4E1317, MA4E1318, MA4E1319-1, MA4E1319-2, MA4E2160 GaAs flip chip Schottky barrier diodes*. M/A-COM Products. Data Sheet.
- [55] J. Heikkinen and M. Kivikoski. Low-profile circularly polarized rectifying antenna for wireless power transmission at 5.8 GHz. *IEEE Microwave and Wireless Components Letters*, 14(4):162–164, April 2004.
- [56] Y. J. Ren and K. Chang. 5.8-GHz circularly polarized dual-diode rectenna and rectenna array for microwave power transmission. *IEEE Transactions on Microwave Theory and Techniques*, 54(4):1495–1502, April 2006.
- [57] A. Douyere, J. D. Lan Sun Luk, and F. Alicalapa. High efficiency microwave rectenna circuit: modelling and design. *Electronics Letters*, 44(24):1409–1410, November 2008.
- [58] J. Heikkinen and M. Kivikoski. A novel dual-frequency circularly polarized rectenna. *IEEE Antennas and Wireless Propagation Letters*, 2(1):330–333, February 2003.
- [59] M. Latrach and B. Brosset. Experimental and theoretical study of rectifier power at 2.45 GHz. In *Proceedings of the 4th International Seminar on Wireless Power Transportation*, May 2001.
- [60] B. Merabet, H. Takhedmit, B. Allard, L. Cirio, F. Costa, O. Picon, and C. Vollaire. Integrated rectenna circuit for microwave power scavenging. In *Proceedings of the 6th International Conference on Integrated Power Electronics Systems*, pages 1–6, March 2010.
- [61] V. Marian, C. Vollaire, J. Verdier, and B. Allard. Conception de topologies de rectennas pour des applications d'alimentation sans fil. In *Proceedings of the 17èmes Journées Nationales Microondes*, May 2011.
- [62] D. Karolak, T. Taris, Y. Deval, J. B. Béguéret, and A. Mariano. Comparaison de conception de redresseurs à faible puissance dédiés à la récupération d'énergie RF. In *Proceedings of the 18èmes Journées Nationales Microondes*, May 2013.

- [63] B. Merabet, F. Costa, H. Takhedmit, C. Vollaire, B. Allard, L. Cirio, and O. Picon. A 2.45-GHz localized elements rectenna. In *Proceedings of the 3rd IEEE International Symposium on Microwave, Antenna, Propagation and EMC Technologies for Wireless Communications*, pages 419–422, October 2009.
- [64] H. Takhedmit, B. Merabet, L. Cirio, B. Allard, F. Costa, C. Vollaire, and O. Picon. Design of a 2.45 GHz rectenna using a global analysis technique. In *Proceedings of the 3rd European Conference on Antennas and Propagation*, pages 2321–2325, March 2009.
- [65] H. Takhedmit, B. Merabet, L. Cirio, B. Allard, F. Costa, C. Vollaire, and O. Picon. A 2.45-GHz low cost and efficient rectenna. In *Proceedings of the 4th European Conference on Antennas and Propagation*, pages 1–5, April 2010.
- [66] J. A. G. Akkermans, M. C. van Beurden, G. J. N. Doodeman, and H. J. Visser. Analytical models for low-power rectenna design. *IEEE Antennas and Wireless Propagation Letters*, 4:187–190, June 2005.
- [67] J. A. C. Theeuwes, H. J. Visser, M. C. Van Beurden, and G. J. N. Doodeman. Efficient, compact, wireless battery design. In *Proceedings of the European Conference on Wireless Technologies*, pages 233–236, October 2007.
- [68] T. C. Yo, C. M. Lee, C. M. Hsu, and C. H. Luo. Compact circularly polarized rectenna with unbalanced circular slots. *IEEE Transactions on Antennas and Propagation*, 56(3):882–886, March 2008.
- [69] J. Y. Park, S. M. Han, and T. Itoh. A rectenna design with harmonic-rejecting circular-sector antenna. *IEEE Antennas and Wireless Propagation Letters*, 3(1):52–54, December 2004.
- [70] Z. Saddi, W. Haboubi, H. Takhedmit, S. E. Adami, O. Picon, J. D. Lan Sun Luk, F. Costa, B. Allard, C. Vollaire, and L. Cirio. Rectenna à faible niveau de puissance pour la récupération et la conversion d'énergie électromagnétique à 1.8 et 2.45 GHz. In *Proceedings of the 18èmes Journées Nationales Microondes*, June 2013.
- [71] W. C. Brown. All electronic propulsion - key to future spaceship design. *Microwave Power Transmission Systems*, July 1988.

- [72] L. Besser and R. Gilmore. *Practical RF circuit design for modern wireless systems*, volume 1: Passive circuits and systems, chapter Impedance matching techniques. Artech House, Inc., 2003.
- [73] C. Bowick. *RF circuit design*, chapter Impedance matching. Newnes, 1982.
- [74] A. Georgiadis, G. Andia, and A. Collado. Rectenna design and optimization using reciprocity theory and harmonic balance analysis for electromagnetic (em) energy harvesting. *IEEE Antennas and Wireless Propagation Letters*, 9:444–446, May 2010.
- [75] Y. Zhou. Design and realization of a receiver rectifier antenna. Master’s thesis, L’École Polytechnique de l’Université de Nantes, July 2010.
- [76] R. Ludwig and P. Bretchko. *RF circuit design - theory and applications*, chapter Introduction. Prentice-Hall, Inc., 2000.
- [77] Y. Zhou, B. Froppier, and T. Razban. Study of a matching circuit effect on a microwave rectifier. In *Proceedings of the 11th Mediterranean Microwave Symposium*, pages 29–33, September 2011.
- [78] D. M. Pozar. *Microwave engineering*, chapter Transmission line theory. John Wiley & Sons, Ltd., 2005.
- [79] G. Matthaei, L. Young, and E. M. T. Jones. *Microwave filters, impedance-matching networks, and coupling structures*, chapter Stepped-impedance transformers and filter prototypes. Artech House, Inc., 1980.
- [80] C. Coleman. *An introduction to radio frequency engineering*, chapter Transmission lines and scattering matrices. Cambridge University Press, 2004.
- [81] *HSMS-286x series surface mount microwave Schottky detector diodes*. Avago Technologies, 2009. Data Sheet.
- [82] *HSMS-285x series surface mount zero bias Schottky detector diodes*. Avago Technologies, 2009. Data Sheet.
- [83] H. Takhedmit, B. Merabet, L. Cirio, B. Allard, F. Costa, C. Vollaire, and O. Picon. A 2.45-GHz dual-diode RF-to-DC rectifier for rectenna applications. In *Proceedings of the European Microwave Conference*, pages 37–40, September 2010.

- [84] A. Douyere. *Méthodologie de synthèse et d'optimisation de radiopile bornée à un domaine de fonctionnement*. PhD thesis, L'Université de La Reunion, 2008.
- [85] Y. Zhou, B. Froppier, and T. Razban. Schottky diode rectifier for power harvesting application. In *Proceedings of the IEEE International Conference on RFID-Technologies and Applications*, pages 429–432, November 2012.
- [86] T. Tafticht and K. Agbossou. Development of a mppt method for photovoltaic systems. In *Proceedings of the Canadian Conference on Electrical and Computer Engineering*, volume 2, pages 1123–1126, 2004.
- [87] N. Femia, G. Petrone, G. Spagnulol, and M. Vitelli. Optimization of perturb and observe maximum power point tracking method. *IEEE Transactions on Power Electronics*, 20(4):963–973, July 2005.
- [88] M. Lokanadham and K. V. Bhaskar. Incremental conductance based maximum power point tracking (MPPT) for photovoltaic system. *International Journal of Engineering Research and Applications*, 2(2):1420–1424, April 2012.
- [89] A. N. A. Ali, M. H. Saied, M. Z. Mostafa, and T. M. Abdel-Moneim. A survey of maximum PPT techniques of PV systems. In *Proceedings of the IEEE Energytech*, pages 1–17, May 2012.
- [90] B. Amrouche, M. Belhamel, and A. Guessoum. Artificial intelligence based PO MPPT method for photovoltaic systems. *Revue des Energies Renouvelables ICRESD-07 Tlemcen*, pages 11–16, 2007.
- [91] M. S. Aït Cheikh, C. Larbes, G. F. Tchoketch Kebir, and A. Zerguerras. Maximum power point tracking using a fuzzy logic control scheme. *Revue des Energies Renouvelables*, 10(3):387–395, September 2007.
- [92] C. Corbel. *Procédure de mesures de SER en chambre anéchoïque*. IETR, May 2011.
- [93] J. D. Kraus. *Antennas*, chapter Basic antenna concepts. McGraw-Hill, Inc., 2nd edition, 1988.
- [94] *Basics of dual-polarized antennas*. The International Engineering Consortium.

- [95] M. Hillbun. *Antenna measurements*. Practical Antenna.
- [96] H. C. Lu and T. H. Chu. Antenna gain and scattering measurement using reflective three-antenna method. In *Proceedings of the IEEE Antennas and Propagation Society International Symposium*, volume 1, pages 374–377, July 1999.
- [97] L. W. Epp, A. R. Khan, H. K. Smith, and R. P. Smith. A compact dual-polarized 8.51-GHz rectenna for high-voltage (50 V) actuator applications. *IEEE Transactions on Microwave Theory and Techniques*, 48(1):111–120, January 2000.
- [98] C. A. Balanis. *Antenna theory analysis and design*, chapter Fundamental parameters of antennas. John Wiley & Sons, Inc., 2005.
- [99] H. J. Visser. *Array and phased array antenna basics*, chapter Antenna parameters. John Wiley & Sons, Ltd., 2005.
- [100] K. L. Wong. *Planar antennas for wireless communications*, chapter Antennas for wireless applications. John Wiley & Sons, Inc., 2003.
- [101] Y. Zhou, B. Froppier, and T. Razban. Design and realization of a rectenna. In *Proceedings of the First Sino-French Workshop on Research Collaborations in Information and Communication Technologies*, May 2011.
- [102] O. El Mrabet. *High frequency structure simulator (HFSS) tutorial*. IETR, 2006.
- [103] J. R. James and P. S. Hall. *Handbook of microstrip antennas*, chapter Microstrip antenna feeds. Peter Peregrinus, Ltd., 1989.
- [104] K. L. Wong. *Compact and broadband microstrip antennas*, chapter Broadband microstrip antennas. John Wiley & Sons, Inc., 2002.
- [105] I. Pelé. *Étude et conception d'antennes large bande et d'antennes multistandards pour les communications mobiles*. PhD thesis, L’École Polytechnique de l’Université de Nantes, December 2005.
- [106] J. Liang, C. C. Chiau, X. Chen, and C. G. Parini. Study of a printed circular disc monopole antenna for UWB systems. *IEEE Transactions on Antennas and Propagation*, 53(11):3500–3504, November 2005.

- [107] *Understanding the fundamental principles of vector network analysis.* Hewlett Packard. Application Note 1287-1.
- [108] Z. N. Chen and Y. W. Chia. *Broadband planar antennas design and applications*, chapter Planar inverted-L/F antennas. John Wiley & Sons, Ltd., 2006.
- [109] X. X. Yang, C. Jiang, A. Z. Elsherbeni, and Y. Q. Wang. A novel compact printed rectenna for data communication systems. *IEEE Transactions on Antennas and Propagation*, 61(5):2532–2539, May 2013.
- [110] R. K. Yadav, S. Das, and R. L. Yadava. Rectennas design, development and applications. *International Journal of Engineering Science and Technology*, 3(10):7823–7841, 2011.
- [111] S. Drabowitch, A. Papiernik, H. D. Griffiths, J. Encinas, and B. L. Smith. *Modern antennas*, chapter Receiving antennas. Springer, 2005.
- [112] B. Glover and H. Bhatt. *RFID essentials*, chapter RFID architecture. O'Reilly Media, Inc, 2006.
- [113] K. Finkenzeller. *RFID handbook - fundamentals and applications in contactless smart cards and identification*, chapter Examples applications. John Wiley & Sons, Ltd., 2nd edition, 2003.
- [114] J. A. Hagerty, F. B. Helmbrecht, W. H. McCalpin, R. Zane, and Z. B. Popovic. Recycling ambient microwave energy with broad-band rectenna arrays. *IEEE Transactions on Microwave Theory and Techniques*, 52(3):1014–1024, March 2004.
- [115] A. Douyère, S. Rivière, J. Rivière, F. Alicalapa, and J. D. Lan Sun Luk. Conception et réalisation d'un convertisseur rf/dc dédié à la collecte de faibles niveaux de puissance. In *18èmes Journées Nationales Microondes*, May 2013.
- [116] S. Rivière, F. Alicalapa, A. Douyère, and J. D. Lan Sun Luk. A compact rectenna device at low power level. *Electromagnetics Research C*, 16:137–146, May 2010.
- [117] A. Douyère, A. Celeste, C. Descharles, and J. D. Lan Sun Luk. Non linear Schottky diode characterization used in a high efficiency rectenna design methodology. In *International Astronautical Conference*, November 2005.



# Résumé en français

La demande d'autonomie croissante des terminaux de communication, l'utilisation de capteurs et de réseaux de capteurs inaccessibles après leur mise en place et la volonté de minimiser l'impact énergétique d'une communication amènent à définir une stratégie de gestion de la ressource énergétique. Cela passe par une gestion de la consommation d'énergie en fonction de la qualité du canal de communication, mais également par la possibilité pour un terminal de communication de récupérer de l'énergie de manière autonome, c'est-à-dire sans être connecté à un réseau énergétique filaire. Il s'agit alors de récupérer l'énergie environnante, qui peut être soit mécanique (vibration), thermique, hydraulique, éolienne ou électromagnétique, comme indiqué sur la figure 6.3.

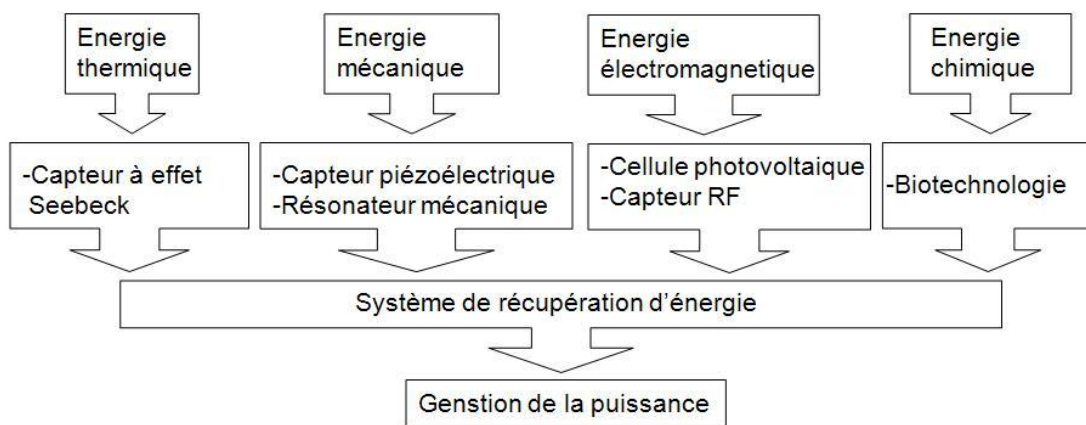


FIGURE 6.3: Schéma du système de récupération d'énergie

Pour la récupération de l'énergie électromagnétique, on distingue deux grands domaines, celui proche du spectre visible (capteur photovoltaïque) et celui de la bande radio fréquence. C'est uniquement à ce dernier cas que nous nous intéressons. La récupération de l'énergie de la bande radio fréquence consiste à réaliser un convertisseur radio fréquence - continu. L'élément le plus simple pour réaliser cette fonction est un redresseur constitué d'une diode et d'une charge RC.

## Introduction

La multiplication du nombre d'objets communicants fait de l'autonomie des terminaux de communication sans fil une problématique majeure. L'énergie électromagnétique, au travers de l'utilisation d'une rectenna (antenne redresseuse) est un moyen fiable pour augmenter la durée de vie des capteurs et d'une manière générale des terminaux consommant peu de puissance. La rectenna est composée d'une antenne de réception et d'un circuit de redressement. Elle capte l'énergie électromagnétique environnante et la convertit en énergie DC utile.

Les conceptions actuelles de rectenna permettent d'obtenir, pour la plupart, un haut rendement de conversion à des niveaux de puissance élevés et ce dans des bandes de fréquence libres ISM, ou les bandes de téléphonie mobile GSM et UMTS. Ce type de rectenna est plus particulièrement adapté au transfert d'énergie sans fil. Dans ce cas, l'énergie électrique est transformée en énergie radio fréquence, puis transmise par des antennes à travers l'espace en direction d'un point éloigné. L'énergie RF est ensuite recueillie et convertie en courant continu au point de réception par des rectennas.

Le rendement global du système de transmission d'énergie est nécessairement le produit des rendements individuels associés aux processus des systèmes d'émission, de réception et de conversion d'énergie. La mise en place d'un tel système est liée, soit à la présence d'un fort niveau de puissance dans l'espace, soit à la possibilité de déployer un réseau d'antenne. Une chaîne de transmission de puissance en espace libre a besoin d'atteindre les objectifs de haut rendement, de faible coût, de grande fiabilité et de faible encombrement.

Par exemple, une rectenna à haut rendement basée sur un convertisseur à double diodes Schottky et avec un filtre de rejet d'harmonique à 2,45 GHz présente une efficacité de 83 % à  $0,31 \text{ mW/cm}^2$  [22]. Un autre article présente un réseau d'antenne redresseuse à polarisation circulaire à gain élevé et à haut rendement en technologie coplanaire. Chaque antenne a un gain de 11 dBi et chaque élément de rectenna atteint 81 % d'efficacité de conversion à 5,71 GHz [23].

Cependant, des niveaux élevés de densité de puissance ne sont pas disponibles partout. Dans le domaine de la transmission de puissance à partir d'une station de base, l'atténuation de l'énergie micro-ondes est inévitable sur une longue distance.

De plus, les communications terrestres doivent respecter des faibles densités de puissance à l'égard de la norme de santé. Selon les directives d'exposition par l'ICNIRP (International Commission on Non-Ionizing Radiation Protection), les densités de puissance sont limitées à  $0,45 \text{ mW/cm}^2$  à 900 MHz et  $0,9 \text{ mW/cm}^2$  à 1,8 GHz pour les fréquences de téléphonie mobile, et  $1 \text{ mW/cm}^2$  à 2,45 GHz pour la fréquence du four à micro-ondes. Annoncés par l'OMS (World Health Organization), les niveaux d'expositions typiques maximales sont  $10 \mu\text{W/cm}^2$  pour les émetteurs de radio et de télévision et de la station de base de téléphonie mobile,  $20 \mu\text{W/cm}^2$  pour les radars, et  $50 \mu\text{W/cm}^2$  pour le four à micro-ondes.

Dans ces conditions, le dispositif de récupération d'énergie pour des faibles niveaux de puissance est limité par le comportement de la diode. Par un exemple, un article [28] présente un redresseur, réalisé avec un résonateur à fort coefficient de qualité (quartz), qui atteint une tension continue de 1 V avec un rendement de conversion supérieur à 22 % pour une puissance d'entrée de -30 dBm. Malheureusement, du fait du résonateur à quartz, le redresseur fonctionne à la fréquence de 24 MHz. Un autre exemple de redresseur fonctionnant à faible niveau de puissance est une rectenna, réalisée avec une antenne en spirale, avec un rendement de conversion 0,7 % pour une densité de puissance de  $3,55 \text{ nW/cm}^2$  à 1,85 GHz [29]. L'état de l'art nous montre donc des rectennas à haut rendement lorsque la densité de puissance est forte ou la fréquence est basse, mais le rendement est très faible dans la bande de fréquence 400MHz - 3GHz pour les faibles niveaux de densité puissance.

Dans cette thèse, nous présentons l'étude de rectenna en vue de récupération d'énergie à faible densité de puissance RF. Le redresseur est constitué d'une diode Schottky. La partie rayonnante est une antenne patch à bande étroite ou une antenne monopôle large bande. Intégré à l'antenne sur une même carte les circuits de redressement sont proposés avec une seule diode Schottky pour la conversion RF/DC. Les circuits d'adaptation sont optimisés pour améliorer le rendement de conversion en augmentant la puissance à la fréquence fondamentale, et en rejetant les signaux harmoniques. Les paramètres qui déterminent la performance de la rectenna ont été simulés dans Agilent ADS (Advanced Design System) et Ansoft HFSS (High Frequency Structure Simulator).

Les rectennas fonctionnant à faible niveau de puissance peuvent être utilisées dans la transmission de puissance point-à-point en respectant les standards de densité de puissance. Elles sont également adaptées à la récupération d'énergie

ambiante aux fréquences ISM, tels que Wi-Fi, Bluetooth et Zig-Bee. Les batteries d'appareils sans fil peuvent alors être rechargées par des rectennas qui captent l'énergie RF à partir de sources de rayonnement ambiant à des faibles densités de puissance.

## Principes

L'antenne redresseuse a été inventée par W. C. Brown et a été utilisée en démonstration pour des applications telles que l'hélicoptère télé alimenté en puissance micro-ondes ou des projets comme les stations spatiales solaires de puissance. Elle constitue l'élément le plus important dans les systèmes de transmission de puissance micro-ondes. L'objectif principal de la conception de rectenna est d'obtenir un rendement de conversion élevé. Ceci nécessite premièrement de recevoir le maximum de puissance RF et ensuite de convertir efficacement l'énergie captée en courant continu.

La clé pour améliorer l'efficacité de conversion RF/DC est le circuit de redressement. Le circuit typique comprend une diode Schottky, une résistance de charge et des filtres. La performance du circuit est déterminée par la propriété non linéaire de diode Schottky, par les pertes induites par la barrière de potentiel et la résistance série. Il est difficile de prédire l'efficacité de conversion d'un système de rectenna optimisé. Certaines méthodes théoriques ont été proposées pour analyser le processus de conversion dans le domaine temporel et dans le domaine fréquentiel.

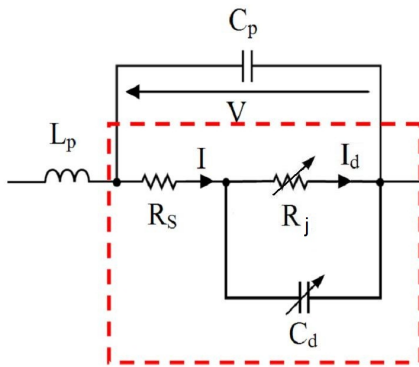


FIGURE 6.4: Modèle électrique d'une diode Schottky avec les éléments parasites du boîtier

Le comportement non linéaire de diode Schottky est modélisé grâce à deux éléments: une résistance de jonction non linéaire  $R_j$  et un condensateur de jonction

$C_d$ , tel que présenté sur la figure 6.4. Ces deux éléments variables sont soumis à la tension aux bornes de la barrière de la diode Schottky  $V_d$ . La résistance série  $R_s$  est également un élément non linéaire. Mais elle est généralement considérée comme une résistance linéaire en raison de ses faibles variations sous polarisation directe. L'incrément de  $R_s$  influence négativement le rendement global du circuit en raison de l'augmentation de la perte de conduction. L'encapsulation de la diode fait apparaître  $L_p$  l'inductance parasite et  $C_p$  la capacité parasite.

Construit par une jonction métal-semiconducteur au lieu de la jonction P-N, les diodes Schottky sont caractérisées par un temps de commutation rapide, la faible chute de tension en direct, et la faible capacité de jonction. Le courant qui passe à travers la résistance de jonction, est calculé par l'équation (6.1).

$$I_d = I_s(e^{\frac{qV_d}{NkT}} - 1) \quad (6.1)$$

où  $I_s$ : courant de saturation ( $1 \times 10^{-12}$  A typiquement)

$q$ : charge électrique ( $1,6 \times 10^{-19}$  Coulomb)

$N$ : facteur d'idéalité (généralement entre 1 et 2)

$k$ : constante de Boltzmann ( $1,38 \times 10^{-23}$  JK $^{-1}$ )

$T$ : température en Kelvin

D'après l'analyse spectrale des courants et des tensions à travers les diodes, les courants sont distribués en composante continue, en fréquence fondamentale et en fréquences harmoniques. En prenant la tension thermique  $kT/q$  égale à 26 mV à la température ambiante, le facteur d'idéalité est égal à 1 et  $V_0$  égal à 1 V, alors le signal DC et la seconde harmonique sont dominants dans l'équation de  $I_d$ . En détails, la composante DC représente 34,07 % du courant total. La première et la deuxième harmonique représentent respectivement 7,05 % et 45,31 % du courant total. La troisième et la quatrième harmonique représentent 2,34 % et 11,24 % du courant total.

Cette analyse montre tout l'intérêt des filtres passe-bande et passe-bas utilisés en entrée et en sortie du redresseur pour bloquer les signaux harmoniques. Les harmoniques sont alors réfléchies et converties encore dans un nouveau cycle de

Diodes Schottky	HSMS-2810	HSMS-2820	HSMS-2850	HSMS-2860
$BV(V)$	25	15	3,8	7
$I_{BV}(A)$	10E-5	10E-4	10E-4	10E-5
$C_{j0}(\text{pF})$	1,1	0,7	0,18	0,18
$E_G(\text{eV})$	0,69	0,69	0,69	0,69
$I_s(A)$	4,8E-9	2,2E-8	3E-6	5E-8
$N$	1,08	1,08	1,06	1,08
$R_s(\Omega)$	10	6	25	5
$V_j(V)$	0,65	0,65	0,35	0,65
$X_{TI}$	2	2	2	2
$M$	0,5	0,5	0,5	0,5
$V_f$	400mV ( $I_f=1\text{mA}$ ) 1V ( $I_f=35\text{mA}$ )	340mV( $I_f=1\text{mA}$ ) 0,5V( $I_f=10\text{mA}$ ) 0,7V( $I_f=30\text{mA}$ )	150mV ( $I_f=0,1\text{mA}$ ) 250mV ( $I_f=1\text{mA}$ )	350mV( $I_f=1\text{mA}$ ) 0,6V( $I_f=30\text{mA}$ )
Niveau de puissance	faible bruit de scintillation	>-20dBm	<-20dBm	$P_{in} < -20\text{dBm}$ ( $\text{freq} > 1,5\text{GHz}$ ) $P_{in} > -20\text{dBm}$ ( $\text{freq} > 4\text{GHz}$ )
Bande de fréquence	RF	RF	<1,5GHz	915MHz-5,8GHz

TABLE 6.2: Les paramètres typiques des diodes Schottky de la série HSMS-28xx

conversion. Le rendement de conversion augmente en conséquence en raison du redressement des signaux à la fréquence fondamentale ainsi que des harmoniques.

Le rendement dépend des caractéristiques des diodes. Chaque série de diode a un ensemble de caractéristiques communes qui sont différentes des autres séries. Elles peuvent être comparées facilement entre elles en consultant les paramètres SPICE donnés sur leurs fiches. Le tableau 6.2 présente les paramètres typiques de diode Schottky de la série HSMS-28xx.

$BV$  est la tension de claquage inverse.  $I_{BV}$  est le courant à cette tension de claquage.  $C_{j0}$  est la capacité de jonction à polarisation nulle.  $V_j$  est le potentiel de jonction.  $M$  est le coefficient de variation de jonction.  $E_G$  est l'énergie de bande interdite.  $X_{TI}$  est l'exposant de la température de courant de saturation (3 pour la jonction P-N, 2 pour Schottky).  $V_f$  est la chute de tension en direct.

La série HSMS-281x dispose d'un très faible bruit de scintillement. La série HSMS-282x présente une faible résistance série, une faible tension directe, et de bonnes caractéristiques RF. La série HSMS-285x est une série de diode de

détection sans polarisation pour les applications de petit signal ( $P_{in} < -20$  dBm) à des fréquences inférieures à 1,5 GHz. Cette diode semble être le meilleur choix pour les faibles puissances, mais pas dans la bande de fréquence souhaitée. Aux fréquences plus élevées, HSMS-286x peut être envisagée.

## Conversion RF/DC

Un circuit de redressement est généralement constitué par une diode, une résistance de charge, un filtre d'entrée et un filtre de sortie, comme indiqué dans la figure 6.5. Le filtre passe-bande d'entrée rejette les harmoniques créés par la diode. Le filtre passe-bas de sortie empêche les harmoniques d'atteindre la charge. De plus, des circuits d'adaptation d'impédance doivent être conçus entre les antennes de réception et les circuits de redressement afin d'éviter la perte due à la désadaptation.

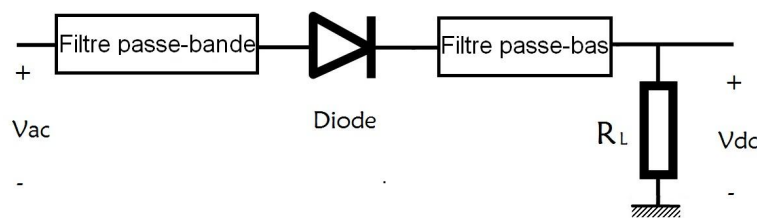


FIGURE 6.5: Schéma d'un circuit de redressement

### ● Simulations et analyses

Prenons une configuration avec une seule diode série par exemple. La structure de redresseur est présentée sur la figure 6.6. Nous avons choisi une diode de type HSMS-2820 afin de maximiser le rendement, du fait de sa faible résistance série ( $6 \Omega$ ), et d'avoir une variation de la puissance d'entrée importante, du fait de la valeur élevée (15 V) de la tension de claquage inverse.

L'étape suivante est le choix de charge de manière à optimiser le rendement du redresseur, indépendamment du circuit d'accès. Le rendement global du système  $\eta$  est défini par l'équation (6.2). On définit le rendement effectif du redresseur  $\eta_{eff}$  par l'équation (6.3), qui est égal au rapport de la puissance continue dans la charge sur la puissance réellement transmise au redresseur, c'est-à-dire le rendement sans tenir compte des pertes par désadaptation.

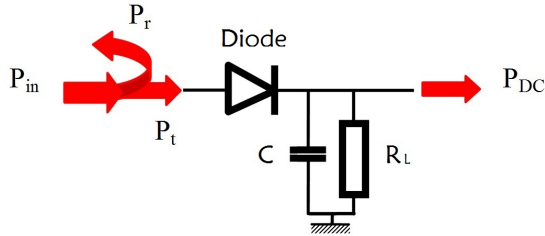


FIGURE 6.6: Schéma d'un circuit redresseur de diode série

$$\eta = \frac{P_{DC}}{P_{in}} \times 100\% = \frac{V_{DC}^2/R_L}{P_{in}} \times 100\% \quad (6.2)$$

$$\eta_{eff} = \frac{P_{DC}}{P_t} \times 100\% = \frac{V_{DC}^2/R_L}{P_t} \times 100\% \quad (6.3)$$

où  $R_L$ : résistance de charge

$V_{DC}$ : tension redressée aux bornes de la charge  $R_L$

$P_{in}$ : puissance d'entrée

$P_t$ : puissance effectivement transmis à l'intérieur de la diode

$P_{DC}$ : puissance DC aux bornes de la charge  $R_L$

Si le filtre passe-bande d'entrée est bien conçu, la puissance incidente est transférée totalement à la diode de redresseur. Dans ce cas, le rendement global peut être élevé et proche du rendement effectif. Au contraire, le rendement global peut être faible en raison de la désadaptation entre l'impédance d'entrée de la diode et l'impédance de sortie du dispositif d'alimentation.

Sur la base des méthodes de simulation Agilent ADS, tels que SP (Scattering Parameter), LSSP (Large Signal Scattering Parameter), HBS (Harmonic Balance Simulation), et des séries de simulation avec des paramètres multiples, le modèle de simulation est construit en prenant en compte d'une désadaptation d'entrée. En supposant que toute la puissance participe au processus de redressement, le rendement global est proche du rendement effectif, rapport de la puissance continue de sortie sur la puissance allant à l'intérieur de la diode.

En vue de trouver la diode la plus appropriée pour une application donnée, le rendement effectif est étudié en fonction de certains paramètres SPICE typiques de la diode, dont la tension de claquage, la capacité de jonction à polarisation nulle, la résistance série, et le courant de saturation. Prenons les paramètres SPICE de la diode Schottky HSMS-2820 comme référence. Le modèle est simulé par la méthode HBS avec plusieurs balayages de paramètres afin d'avoir une vue globale de l'efficacité dans le domaine fréquentiel et dans le domaine de l'énergie. L'objectif est d'obtenir la meilleure valeur du rendement effectif pour améliorer la performance globale.

### ● Conception pour les niveaux de puissance élevés

La diode HSMS-2820, encapsulée dans un boîtier SOT23, est optimisée pour la détection sans polarisation dans les applications RF. En outre, la résistance série parasite de ce produit est faible,  $6\ \Omega$ , entraînant de faibles pertes de conduction et un haut rendement de redressement. De plus, la tension de claquage élevée à 15 V permet d'avoir une puissance de sortie élevée. Suite à l'étude des diodes, le choix de la charge se fait alors en optimisant la valeur du rendement effectif. La valeur optimale du rendement est obtenue pour une valeur de charge proche de  $1000\ \Omega$ . La variation suivant la valeur du condensateur est négligeable à partir du moment où la valeur de la capacité reste supérieure à 30 pF. L'optimisation conduit à la charge suivante:  $R = 820\ \Omega$  et  $C = 82\ pF$ .

Afin de concevoir simplement le circuit d'adaptation, du fait de la non linéarité du circuit, nous choisissons arbitrairement d'adapter le circuit pour une puissance transmise 10 dBm. En utilisant l'optimisation ADS hybride, le circuit redresseur est alors identifié à l'impédance ramenée en entrée de la diode à la fréquence de 2,45 GHz. Pour permettre un réglage aisément après simulation, nous choisissons une structure d'adaptation de type double stub.

Comme le montre la figure 6.7, le circuit d'adaptation est constitué de deux tronçons ouverts ( $L4, L5$ ) et de deux lignes micro-ruban ( $L2, L3$ ) reliant ces stubs et la diode. Il transforme l'impédance d'entrée de la section de rectification à l'impédance de  $50\ \Omega$ . Un stub court-circuité quart d'onde est introduit à côté de la ligne d'alimentation. Elle contribue à la boucle DC (Via-trou  $P2$  - diode Schottky - Charge - Via-trou  $P3$  - Plan de masse) et également au rejet d'harmoniques. Les

effets de discontinuité dans des lignes de transmission de largeurs différentes sont pris en compte dans la simulation.

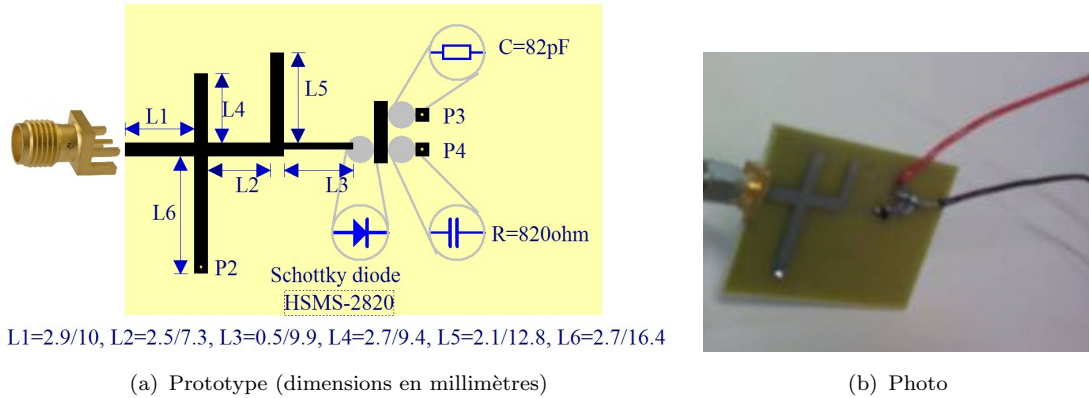


FIGURE 6.7: Circuit de redressement pour les niveaux de puissance élevés

Le circuit est gravé sur un substrat Bernier FR4 de permittivité relative  $\epsilon_r = 4,6$ , de hauteur  $h = 1,58$  mm et d'une tangente de perte  $\tan\delta = 0,02$ . Ensuite, le paramètre  $S_{11}$  est mesuré par un analyseur de réseau. La réponse en fréquence présente une bande passante 80 MHz et la réponse en puissance montre une bande passante de 14 dBm sur la figure 6.8. Ces résultats limitent donc les points de fonctionnement du redresseur. Cette première étude sur un convertisseur RF/DC montre que l'adaptation est un point critique pour obtenir une bonne performance.

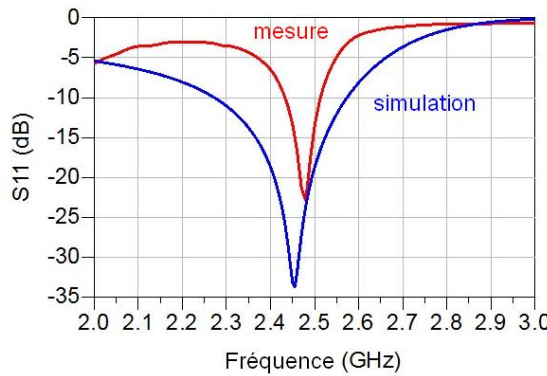


FIGURE 6.8:  $S_{11}$  en fonction de la fréquence pour la conception de niveaux de puissance élevés

La tension DC en sortie est mesurée aux bornes de la résistance de charge. La figure 6.9 décrit la tension en sortie en fonction du niveau de la puissance injectée par un générateur de signaux à l'entrée du circuit. Dans l'intervalle -10 dBm à 25 dBm, le modèle ADS de la diode HSMS-2820 est respecté, par conséquent les résultats de la simulation et de la mesure ont la même allure. Une tension de 11 V

à la puissance 25 dBm a été obtenue. Le rendement maximum  $\eta$  avant l'adaptation est inférieur à 25 %, il atteint 60 % après l'adaptation.

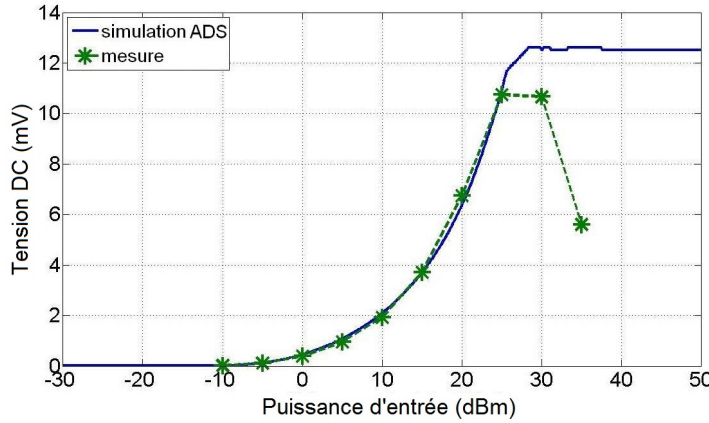


FIGURE 6.9: Tension DC de sortie pour la conception de niveaux de puissance élevés

Les résultats de mesure et de simulation du rendement de conversion RF/DC sont présentés sur la figure 6.10. L'efficacité de conversion maximale mesurée est de 55 % pour la puissance RF 20 dBm à l'entrée du circuit. L'efficacité de la diode augmente avec la tension directe à ses bornes et atteint son maximum lorsque cette tension est proche de la tension de claquage.

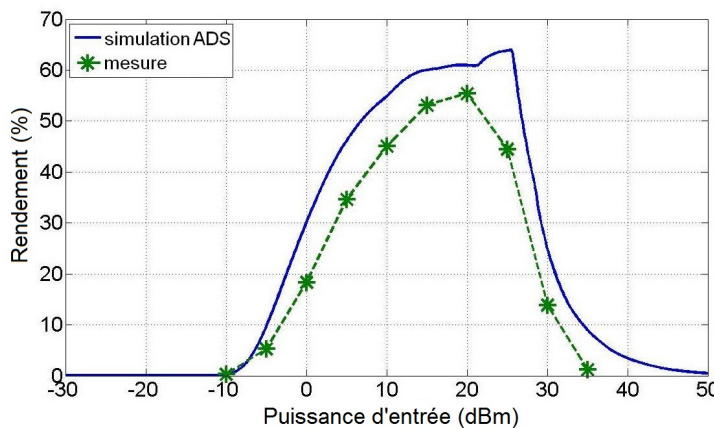


FIGURE 6.10: Rendement mesuré et simulé pour la conception de niveaux de puissance élevés

Même si le rendement maximum  $\eta$  avant l'adaptation est inférieur à 25 %, il atteint 60 % après l'adaptation. Les résultats de mesure et de simulation du rendement de conversion RF/DC sont présentés sur la figure 6.10, l'efficacité de conversion maximale mesurée est 55 % pour la puissance RF 20 dBm à l'entrée du circuit. L'efficacité de la diode augmente avec la tension directe à ses bornes et atteint son maximum lorsque cette tension est proche de la tension de claquage.

## ● Conception pour les faibles niveaux de puissance

Basé sur l'étude des circuits redresseurs à diode Schottky HSMS-2820 pour les applications de forte puissance, cette diode n'est, de toute évidence, pas adaptée aux niveaux de puissance inférieure à -20 dBm. Nous proposons une autre diode HSMS-2860 pour les applications de faible puissance.

Selon les paramètres SPICE sur la fiche produit, HSMS-2860 possède un grand courant de saturation, 50 nA, une petite résistance série de  $5 \Omega$  et une faible capacité de jonction de 0,18 pF à polarisation nulle. Comparé aux autres diodes, cette diode permet une meilleure efficacité pour les faibles niveaux de puissance, comme le prouve dans le modèle de diode. En outre, la configuration à une seule diode série est sensible à un signal faible niveau en raison de la faible tension de seuil de 0,35 V. Elle est donc adaptée pour des applications de récupération d'énergie à faibles densités de puissance. Toutefois, en raison de la faible tension de claquage 7 V, cette diode doit être maintenue dans des faibles niveaux de puissance afin d'éviter sa destruction.

Le circuit d'adaptation est optimisé par la méthode hybride. Nous proposons trois circuits de redressement avec différentes configurations de circuit d'adaptation, comme le stub unique, tel que présenté dans la figure 6.11, les stubs radiales, et la structure compacte. Ces circuits redresseurs sont imprimés sur un substrat Bernier FR4. Chaque circuit contient une diode Schottky HSMS-2860 dans un boîtier SOT23.

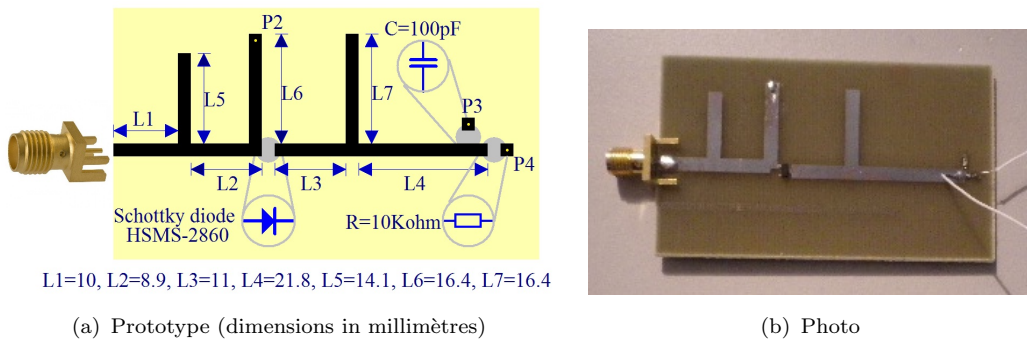


FIGURE 6.11: Circuit de redressement pour la conception de faibles niveaux de puissance

Un prototype avec un circuit d'adaptation à simple stub est optimisé pour la puissance incidente -20 dBm à 2,45 GHz à l'aide du critère de meilleur rendement de conversion. La longueur de la ligne micro-ruban  $L2$  et la longueur du

tronçon ouvert  $L_5$  sont optimisées pour l'adaptation d'impédance entre la diode et l'alimentation. Un stub court-circuité quart d'onde  $L_6$  est proposé à l'entrée de la diode de manière à constituer la boucle DC (Via-trou  $P_2$  - diode Schottky - Charge - Via-trou  $P_4$  - Plan de masse) et à rejeter les signaux harmoniques générés par le processus de redressement.

Un stub ouvert quart d'onde  $L_7$  est ajoutée au filtre passe-bas de sortie pour empêcher les signaux harmoniques de passer vers la charge. La valeur de charge résistive est également optimisée à  $10 \text{ k}\Omega$  pour obtenir le meilleur rendement. La précision de la simulation est améliorée en tenant compte de l'effet de bout de ligne et de l'inductance équivalente du via.

Le circuit de redressement a été réalisé et testé à l'aide d'un VNA Rohde & Schwarz. La figure 6.12 montre que les résultats mesurés sont en accord avec les courbes spost simulées. Dans la réponse en fréquence de 2 GHz à 3 GHz, une fréquence de résonance se situe autour de 2,45 GHz avec une bande passante étroite.

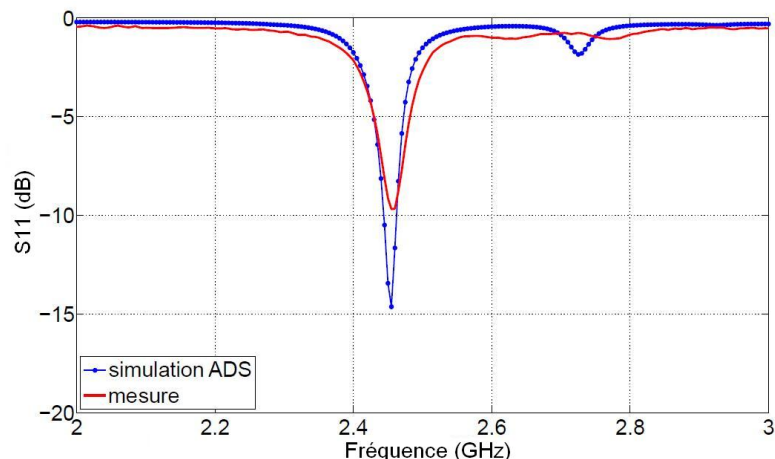


FIGURE 6.12:  $S_{11}$  en fonction de la fréquence pour la conception de faibles niveaux de puissance

Sur la réponse en puissance, de -30 dBm à -10 dBm sur la figure 6.13, le niveau d'adaptation est correcte quand la puissance d'entrée est inférieure à -20 dBm. La variation entre les résultats simulés et mesurés est principalement due à la limitation de la modélisation de la diode et aux tolérances du processus de fabrication.

La mesure de la tension continue en sortie permet de déterminer le rendement de conversion du circuit de redressement. Lorsque l'entrée de ce circuit est reliée

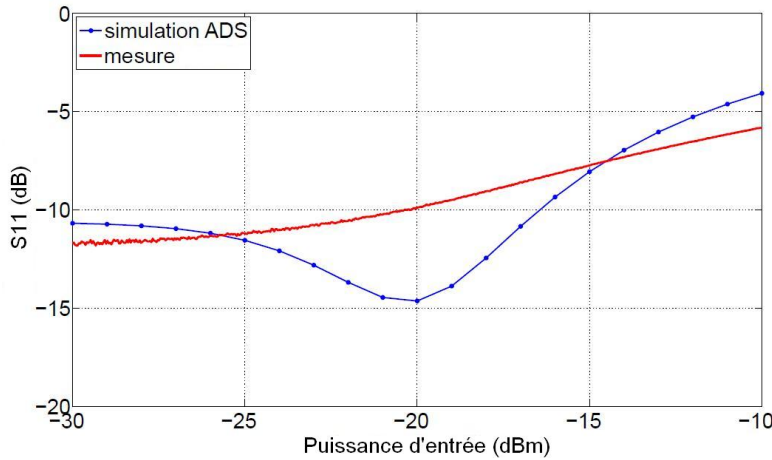


FIGURE 6.13:  $S_{11}$  en fonction de la puissance pour la conception de faibles niveaux de puissance

à un générateur de puissance RF, la tension de sortie est testée par un voltmètre. Comme indiqué sur la figure 6.14, les tensions DC sont mesurées 42,1 mV, 146,1 mV, et 338,8 mV, où les niveaux de puissance sont -20 dBm, -15 dBm, et -10 dBm respectivement.

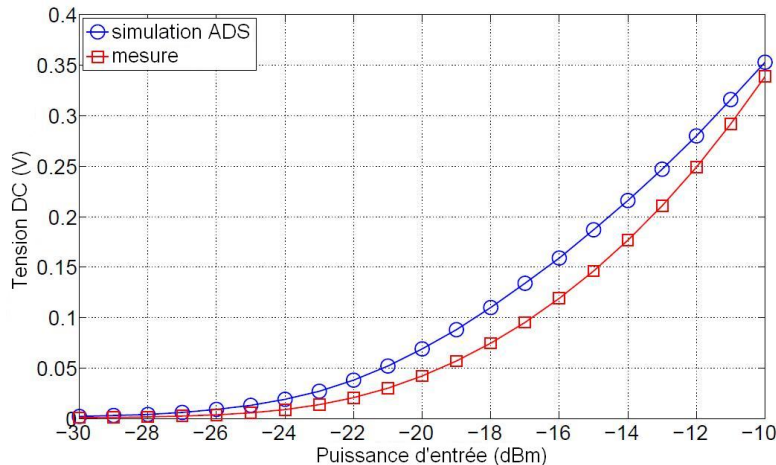


FIGURE 6.14: Tension DC de sortie pour la conception de faibles niveaux de puissance

Comme on voit sur la figure 6.15, les rendements mesurés sont 1,8 %, 6,7 %, et 11,5 % pour  $P_{in} = -20$  dBm, -15 dBm, et -10 dBm respectivement. Cette efficacité de conversion est faible à cause des pertes intrinsèques de la diode, des pertes diélectrique et métallique, des pertes de rayonnement et des pertes introduites par les câbles et les connecteurs. Ce sont les facteurs d'influence sur le rendement total à faibles niveaux de puissance.

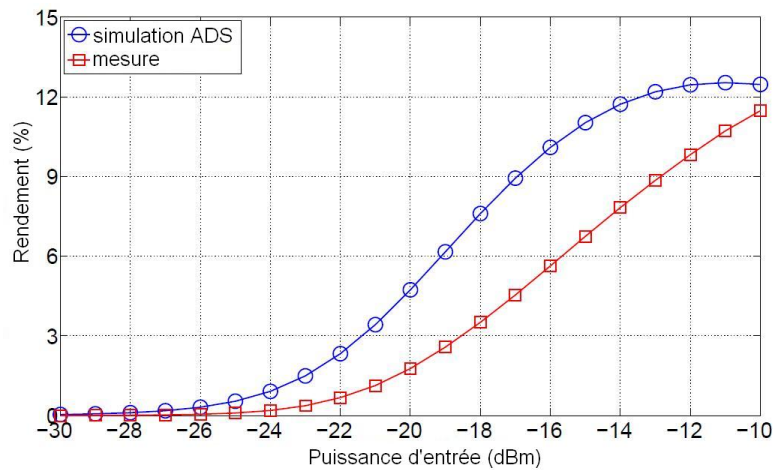


FIGURE 6.15: Rendement mesuré et simulé pour la conception de faibles niveaux de puissance

Autrement dit, si l'énergie RF n'est pas transférée efficacement aux récepteurs, elle est perdue. Si 5 % à 10 % de celle-ci peut être recyclée en énergie DC utile, alors ce dispositif contribue à réduire les coûts et à un environnement écologique.

### ● Conception à haute efficacité

Les circuits mentionnés ci-dessus peuvent être utilisés dans des applications de transmission de puissance dans lesquelles le niveau de puissance est suffisamment élevé. Mais dans les applications liées à la récupération de l'énergie, les puissances mises en jeu sont plus faible. Dans ce cas, le circuit de redressement conçu produit une faible efficacité en raison des caractéristiques de la diode. Avec l'objectif de rendement élevé à faible densité de puissance, un autre modèle a été pris en considération pour l'application de récupération d'énergie.

La diode HSMS-2850 encapsulée dans un boîtier SOT23, possède une petite capacité de jonction à polarisation nulle et un grand courant de saturation. Ainsi, le temps de commutation est court et le redressement peut donner un rendement plus élevé. Cette diode a une faible hauteur de barrière, une faible potentiel de jonction et une faible chute de tension directe. La tension directe est 150 mV où le courant direct est égal à 0,1 mA, et 250 mV où  $I_f = 1$  mA. Sa faible tension directe est donc tout à fait appropriée pour la conception de faibles niveaux de puissance. Cependant, la diode possède une grande résistance série. Cela signifie une perte importante de conduction à l'intérieur de la diode pour des niveaux de puissance élevés. Elle n'est pas recommandée pour les applications de niveaux

de puissance élevés. Bien que cette diode ne soit recommandée pour la bande de fréquence que l'on utilise, sa forte sensibilité nous a poussé à l'utiliser.

Par la méthode ADS hybride, le circuit de redressement a été optimisé pour un bon niveau d'adaptation autour de 2,45 GHz, comme montré sur la figure 6.16. Dans le même temps, la résistance de charge est choisie à  $3\text{ k}\Omega$  pour la meilleure efficacité au niveau de puissance -20 dBm. Le condensateur en parallèle avec la charge est 100 pF, ce qui est suffisamment grand pour le courant continu de sortie.

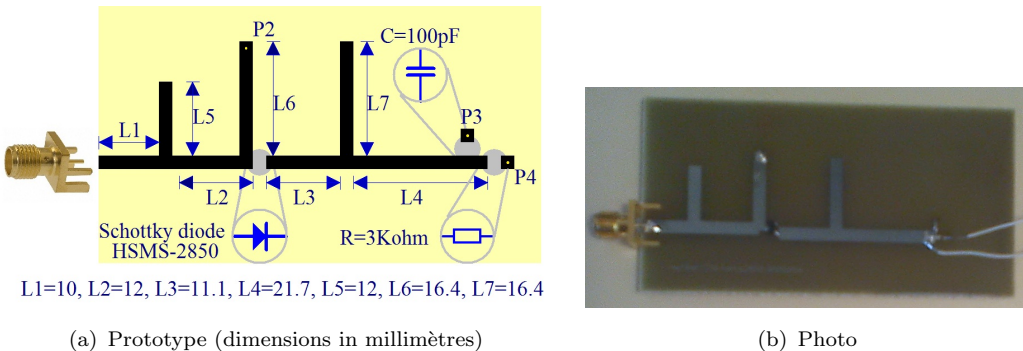


FIGURE 6.16: Circuit de redressement pour la conception à haute efficacité

Le circuit d'adaptation est constitué par un seul tronçon  $L5$  et une ligne micro-ruban  $L2$ . Un stub court-circuité quart d'onde  $L6$  est situé à côté de la diode. Elle contribue à la boucle DC (Via-trou  $P2$  - diode Schottky - Charge - Via-trou  $P4$  - Plan de masse). Le filtre passe-bas se compose de  $L3$ ,  $L4$  et un tronçon ouvert  $L7$ . Ce filtre rejette les signaux harmoniques et améliore le processus de redressement.

La réponse en fréquence est testée en simulation LSSP et mesurée par un analyseur de réseau, comme indiqué dans la figure 6.17. La fréquence de résonance simulée est 2,45 GHz mais la fréquence mesurée décale à 2,4 GHz. La différence entre la simulation et la mesure est principalement due à la limitation de la modélisation de la diode et la tolérance de fabrication. La bande passante de -10 dB n'est pas large. Cependant, la tension de sortie correspond à ce qui est attendu autour de la fréquence de résonance. Dans la mesure de la tension continue, le résultat prouve que ce circuit produit la tension la plus élevée à sa fréquence de résonance, 64 mV pour  $P_{in} = -20\text{ dBm}$ . Même si elle est mesurée à 2,45 GHz, la tension DC est environ 62 mV.

Lorsque le circuit redresseur est connecté à un générateur de puissance RF, on obtient des tensions DC mesurées par un voltmètre. Les tensions de sortie

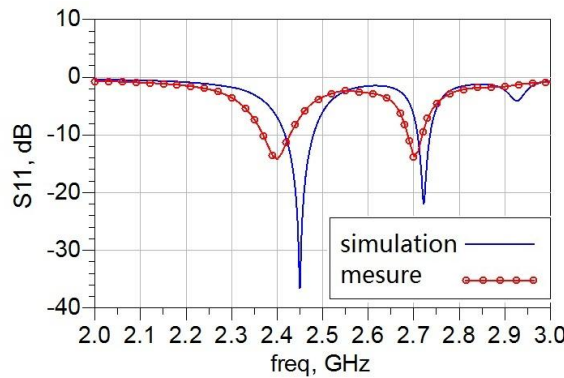


FIGURE 6.17:  $S_{11}$  en fonction de la fréquence pour la conception à haute efficacité

sont 9,5 mV, 64 mV, 286 mV, et 968 mV quand les niveaux de puissance sont -30 dBm, -20 dBm, -10 dBm, et 0 dBm respectivement, telles que présentées sur la figure 6.18. La courbe de simulation montre un très bon accord avec la mesure. Le résultat prouve que cette conception est tout à fait sensible à des faibles niveaux de puissance.

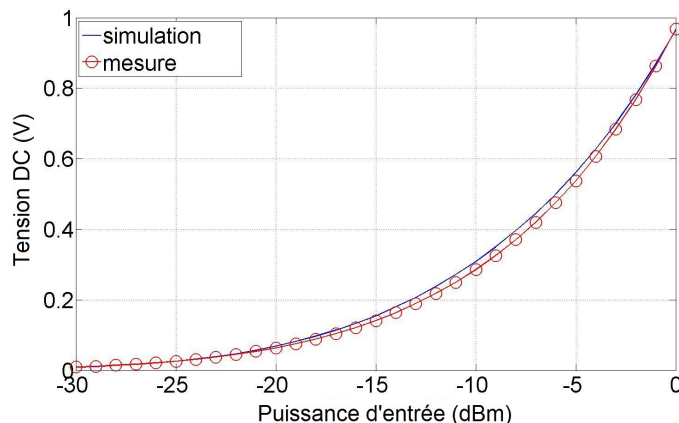


FIGURE 6.18: Tension DC de sortie pour la conception à haute efficacité

Les rendements de conversion sont 3 %, 13,65 %, 27,23 %, et 31,21 % lorsque les niveaux de puissance sont -30 dBm, -20 dBm, -10 dBm, et 0 dBm respectivement, tel que présenté sur la figure 6.19. Le rendement au niveau de puissance -20 dBm est plus élevé que le circuit de redressement avec HSMS-2860. Il est adapté à l'application de récupération d'énergie pour des faibles niveaux de puissance.

Les filtres d'entrée et de sortie rejettent les signaux harmoniques et bloquent les harmoniques entre le connecteur et la diode. Les harmoniques participant au processus de rectification améliorent le rendement de conversion.  $L7$  est un tronçon ouvert quart d'onde qui constitue le filtre passe-bas avec  $L3$  et  $L4$ . La

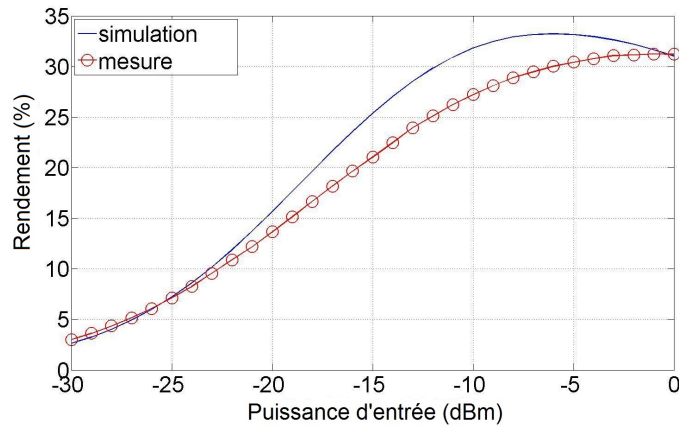


FIGURE 6.19: Rendement mesuré et simulé pour la conception à haute efficacité

position de cette ligne  $L7$  est optimisée pour une efficacité maximale, tel que présenté dans la figure 6.20. La longueur de  $L3$  (11,1 mm) représente la distance optimale entre ce tronçon ouvert et la diode.

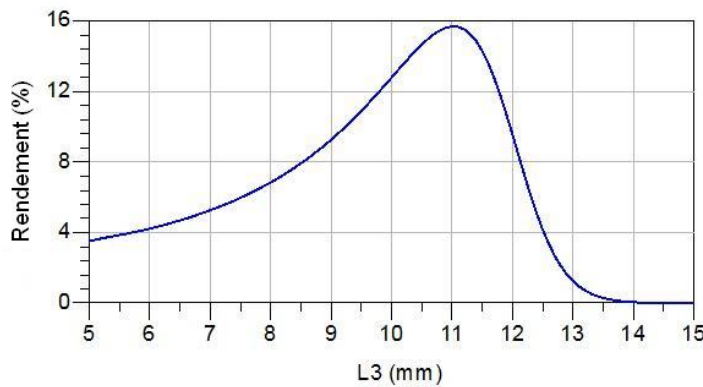


FIGURE 6.20: Rendement simulé en fonction de la longueur  $L3$

Ainsi que les composants distribués,  $L3$  par exemple, les composants localisés déterminent la performance de rectification. Le rendement de conversion dépend fortement de la résistance de charge, comme le montre la figure 6.21. Lorsque la résistance de charge est égale à la valeur optimale, 3100  $\Omega$  dans notre cas, l'efficacité maximale d'environ 13,6 % est atteinte. La modélisation DC du circuit redresseur est réalisée sur la base MPPT (Maximum Power Point Tracking) afin de gérer la puissance DC de sortie.

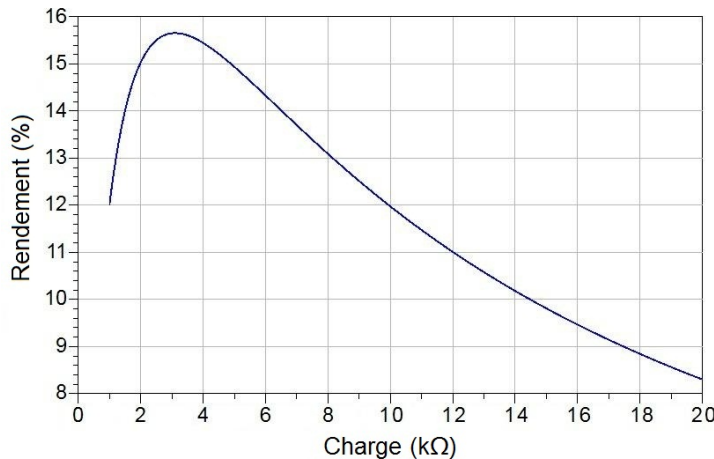


FIGURE 6.21: Rendement simulé en fonction de la résistance de charge

## Antennes pour la récupération d'énergie

La conception d'antenne de réception est un maillon clé dans la configuration de rectenna. Cette partie coopère avec le dispositif de redressement et décide des niveaux de puissance d'incidence pour lesquels les circuits redresseurs opèrent. En général, dans le processus de rectification, plus le niveau de puissance est élevée, plus la tension DC est grande, et ce en régime normal avec un rendement de conversion plus élevé. Lorsque l'antenne de récupération d'énergie possède un gain élevé, le rendement de la partie de redressement peut être élevé même si cette antenne est exposée à des faibles densités de puissance. De plus, les propriétés de rayonnement des antennes sont importantes dans la conception de l'ensemble antenne et redresseur appelé antenne redresseuse ou en anglais "rectifier antenna" (rectenna).

Toutes les antennes ont été simulées avec le simulateur HFSS. Des prototypes d'antenne patch, d'antenne monopôle et de monopôle modifié sont analysés selon nos besoins. Pour chaque prototype, la structure et les dimensions sont optimisées autour de la fréquence de résonance de 2,45 GHz.

### • Antenne patch rectangulaire

L'antenne patch micro-ruban est une antenne imprimée résonnante à bande étroite pour les applications micro-ondes. Grâce à sa configuration planaire, son

faible coût, et son intégration facile avec la technologie PCB, l'antenne patch a été largement étudiée.

Une antenne patch micro-ruban ( $27,76 \text{ mm} \times 23,73 \text{ mm}$ ) à polarisation linéaire est conçue pour être associée au circuit redresseur pour obtenir la rectenna intégrée. Le plan de masse ( $63,19 \text{ mm} \times 59,16 \text{ mm}$ ) est choisi en fonction de l'hypothèse d'un plan de masse infini. Simulé par HFSS, présentée figure 6.22, l'antenne à plaque est alimentée par une sonde. Le conducteur central d'un câble coaxial sert de sonde d'alimentation pour coupler l'énergie électromagnétique dans ou hors du patch. Le point d'alimentation est à 5 mm du centre du patch, afin d'adapter l'antenne à  $50 \Omega$ . Le patch est imprimé sur un substrat Bernier FR4 de permittivité relative  $\varepsilon_r = 4,6$ , de hauteur  $h = 1,58 \text{ mm}$  et d'une tangente de perte  $\tan\delta = 0,02$ . Le  $S_{11}$  mesuré montre un bon accord avec le résultat simulé (figure 6.23). La fréquence de résonance de l'antenne patch est située à 2,45 GHz.

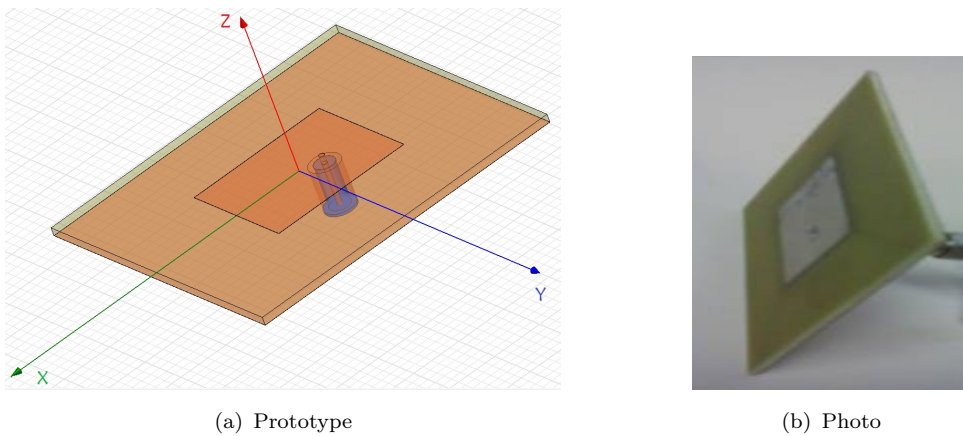


FIGURE 6.22: Antenne patch rectangulaire

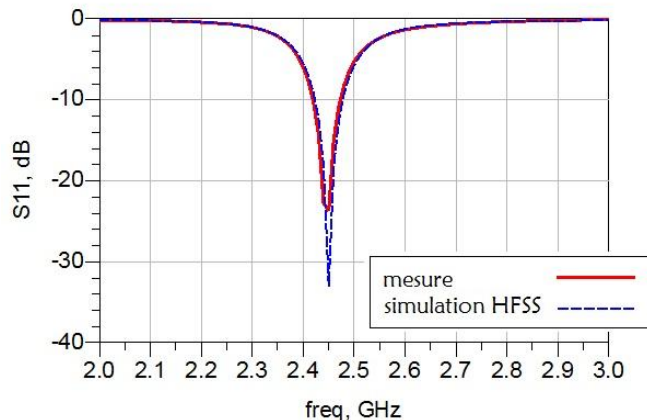


FIGURE 6.23:  $S_{11}$  en fonction de la fréquence pour l'antenne patch

La largeur de bande de -10 dB est 50 MHz entre 2,42 GHz et 2,47 GHz. L'antenne patch rectangulaire est connue pour sa bande étroite. Même si le patch peut être optimisé pour augmenter sa largeur de bande, l'augmentation de la bande passante reste dans une gamme réduite. Cependant, certaines antennes sont naturellement à large bande passante, comme les dipôles et monopôles.

Les diagrammes de rayonnement simulés à 2,45 GHz sont présentés sur la figure 6.24, et ceux mesurés sur la figure 6.25. Les mesures sont effectuées dans une chambre anéchoïque. Les diagrammes donnés présentent un rayonnement quasi-omnidirectionnel dans le plan supérieur de l'antenne. Les résultats mesurés sont en bon accord avec ceux simulés. La directivité est 5,61 dBi dans le plan E, et 5,56 dBi dans le plan H. L'angle d'ouverture ou HPBW (Half Power Beam Width) est 98° dans le plan E, et 94° dans le plan H. Le niveau de co-polarisation est 20 dB plus élevé que le niveau de polarisation croisée. Cela signifie que l'antenne patch possède une polarisation linéaire.

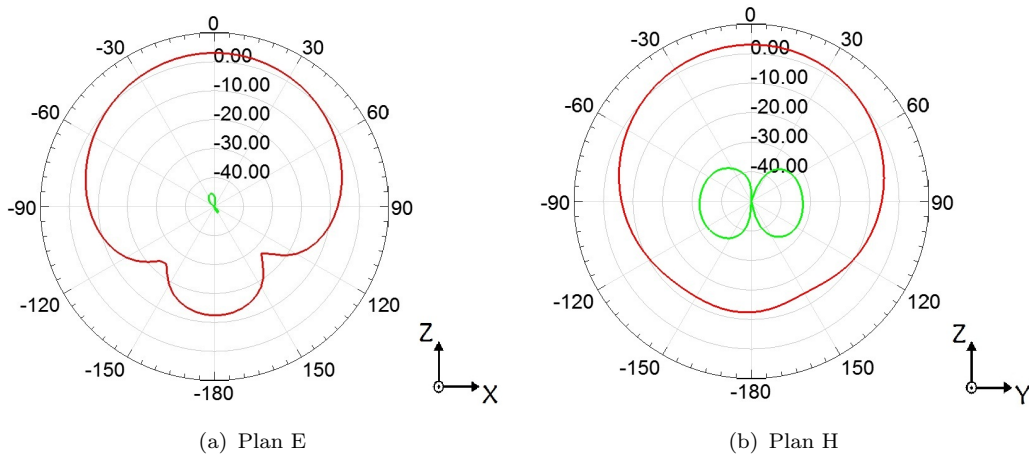


FIGURE 6.24: Les diagrammes de rayonnement simulés sur le plan E et sur le plan H en co-polarisation (courbe rouge) et en polarisation croisée (courbe verte) pour l'antenne patch

L'antenne a une bande passante de 50 MHz entre 2,42 GHz et 2,47 GHz. Cette dépendance de la fréquence est également présentée dans les diagrammes de rayonnement sur la figure 6.26. La puissance reçue est vue par son amplitude en dB par rapport à l'angle de rotation sur l'axe x et par rapport à la fréquence de fonctionnement sur l'axe y. Le gain 3D montre des niveaux élevés de rayonnement vers l'avant et de faibles niveaux de rayonnement vers l'arrière. Ce rapport avant-arrière est fortement dépendant de la taille et la forme du plan de masse dans des cas pratiques. Le gain total est 3,1 dBi dans la simulation HFSS.

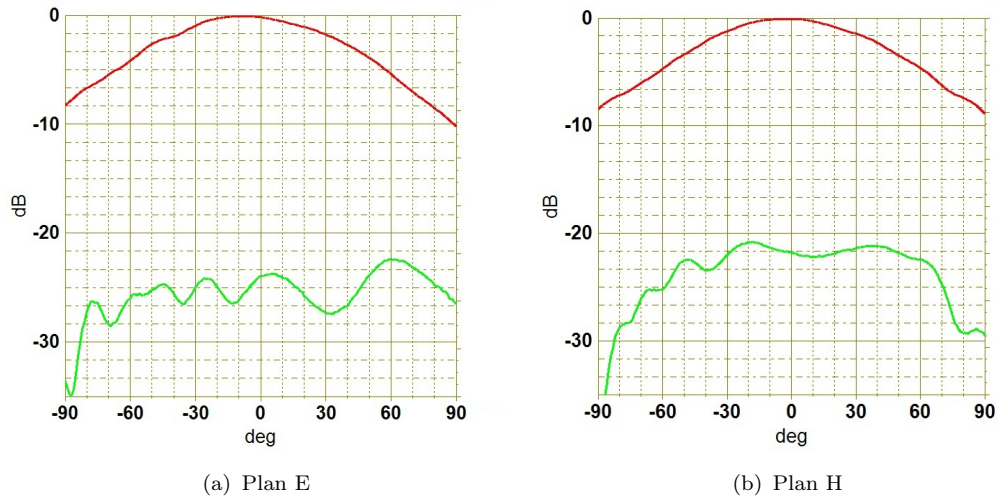


FIGURE 6.25: Les diagrammes de rayonnement mesurés dans le plan E et dans le plan H en co-polarisation (courbe rouge) et en polarisation croisée (courbe verte) pour l'antenne patch

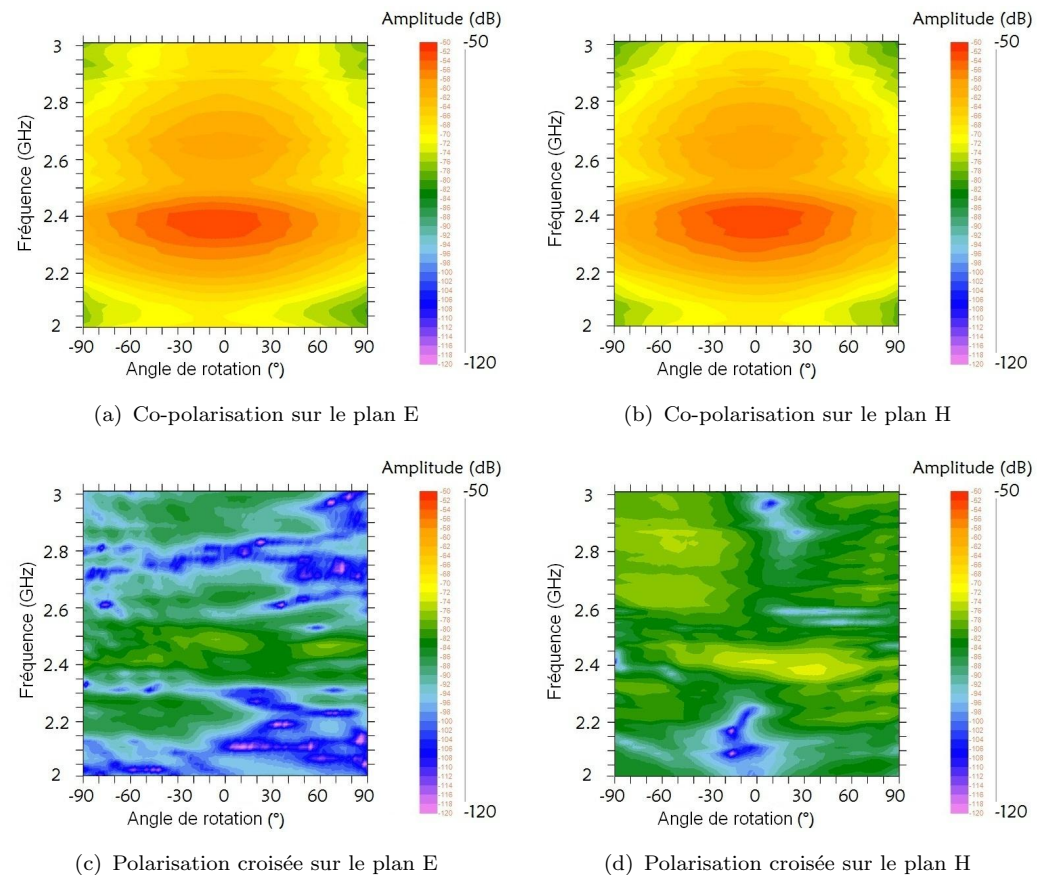


FIGURE 6.26: Les diagrammes de rayonnement en fonction de la fréquence et de l'angle de rotation pour l'antenne patch

## ● Antenne monopôle

Etant donné que la longueur du patch, une demi longueur d'onde, est environ la même que la longueur d'un dipôle résonant, certaines caractéristiques de rayonnement d'une antenne patch sont similaires à celles d'un dipôle résonant. Afin de minimiser la zone occupée d'antennes, une antenne monopôle imprimée sur un plan de masse fini est proposée pour remplacer le patch. Le monopôle quart d'onde possède une largeur de bande plus importante.

Comme le montre la figure 6.27, un monopôle rectangulaire alimenté par la ligne micro-ruban  $50\ \Omega$  est imprimé sur le substrat diélectrique Bernier FR4. Les dimensions de l'antenne monopôle et le plan de masse et la distance entre le point d'alimentation et le plan de masse sont les paramètres affectant la performance de l'antenne. Tous les paramètres sont réglés mécaniquement et analysés par HFSS jusqu'à obtenir une large bande passante autour 2,45 GHz et un bon niveau d'adaptation avec la ligne d'alimentation  $50\ \Omega$ .

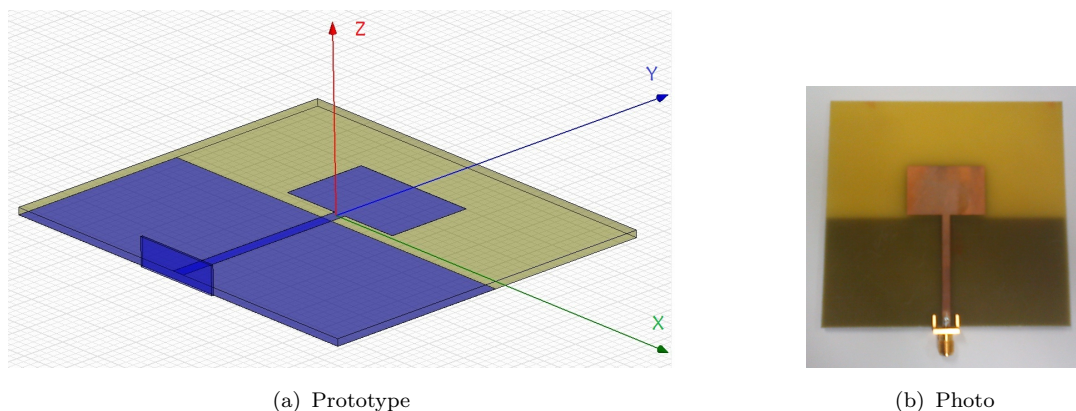


FIGURE 6.27: Antenne monopôle

La longueur et la largeur de l'antenne monopôle sont 19,2 mm et 30,2 mm, environ 29 % et 46 % de la longueur d'onde guidée. De l'autre côté du substrat, la longueur et la largeur du plan de masse sont 41 mm et 91,8 mm. La distance entre le point d'alimentation et le plan de masse est de 1 mm.

Le paramètre  $S_{11}$  simulé et celui mesuré du monopôle sont présentés sur la figure 6.28. La bande passante mesurée est 1,91 GHz de 1,9 GHz à 3,81 GHz, tandis que celle simulée est 1,56 GHz de 1,97 GHz à 3,53 GHz. Le résultat mesuré est mieux que celui simulé. La mesure confirme la caractéristique large bande d'antenne monopôle comme prévue dans la simulation. Bien que le circuit redresseur ait une bande passante très étroite, l'antenne monopôle a une large bande

passante. Cet avantage simplifie donc la difficulté de l'adaptation d'impédance entre l'antenne et le circuit de redressement dans le système de rectenna.

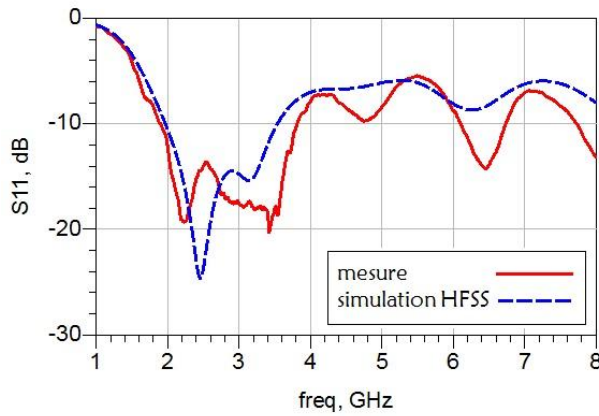


FIGURE 6.28:  $S_{11}$  simulé et mesuré d'antenne monopôle

Les diagrammes de rayonnement ont été simulés par HFSS et mesurés par VNA Rohde & Schwarz dans une chambre anéchoïque. La figure 6.29 présente les diagrammes de rayonnement normalisés mesurés et celles simulés à 2,45 GHz.

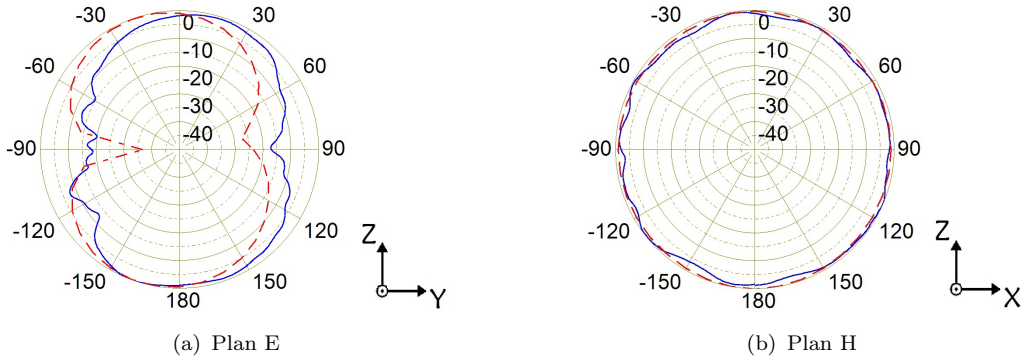


FIGURE 6.29: Les diagrammes de rayonnement simulés (courbe rouge) et mesurés (courbe bleue) d'antenne monopôle

Le diagramme du plan H mesuré est proche de celui obtenu dans la simulation. Le diagramme du plan E mesuré suit la forme de celui simulé, bien que l'accord ne soit pas aussi bon que celui du plan H. La distorsion de la courbe mesurée peut être causée par le connecteur et le câble coaxial. Le monopôle a une directivité 6,01 dBi en co-polarisation dans le plan E, alors que la directivité dans le plan H est 1,51 dBi. On remarque que le monopôle a une propriété quasi omnidirectionnelle dans la position de la polarisation verticale sur le plan azimutal.

L'antenne monopôle a une grande largeur de bande de 1,9 GHz à 3,81 GHz. Cette dépendance de la fréquence est présentée aussi dans les diagrammes de

rayonnement sur la figure 6.30. La barre de couleur représente la puissance reçue en dB. L'axe y est lié aux fréquences de l'antenne émettrice et l'axe x représente les angles de rotation de  $-180^\circ$  à  $+180^\circ$ .

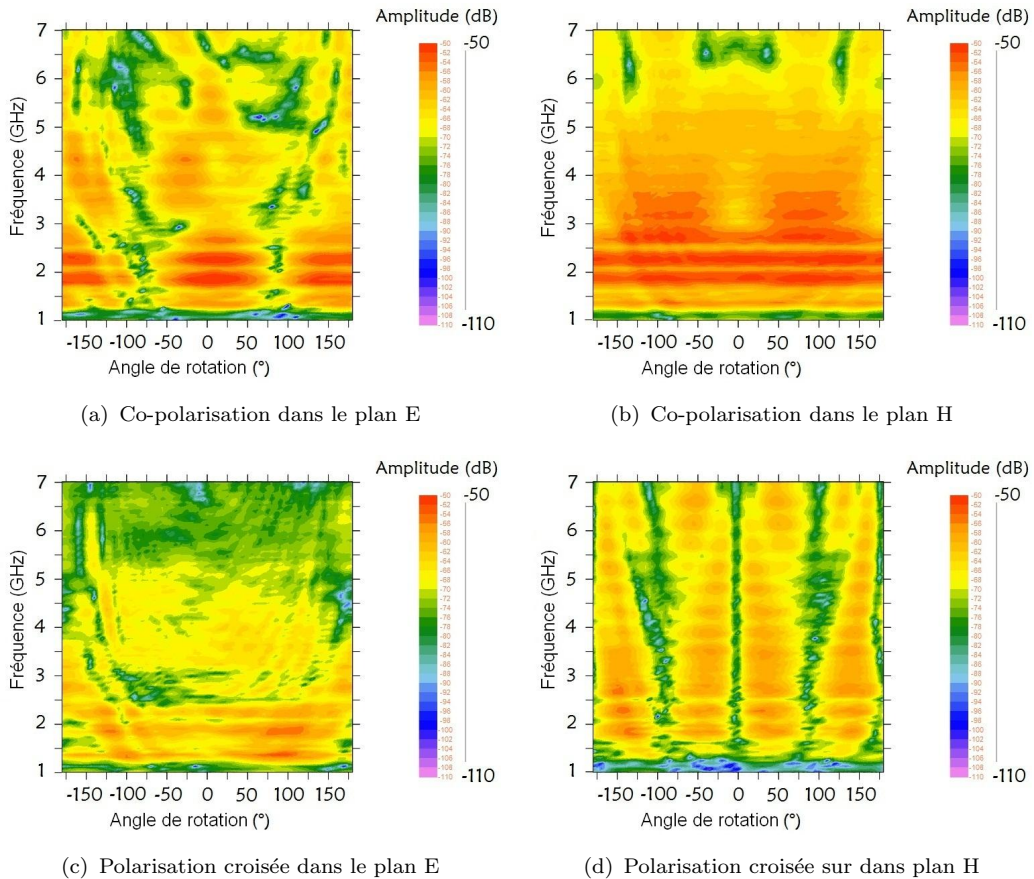


FIGURE 6.30: Les diagrammes de rayonnement en fonction de la fréquence et de l'angle de rotation pour l'antenne monopôle

Basé sur la méthode de comparaison de gain, le gain de l'antenne sous test est analysé par le logiciel ANT32-ANA. De cette manière, le gain du monopôle est mesuré, comme illustré dans la figure 6.31. Généralement, le gain de l'antenne dépend de sa directivité et de son efficacité à des fréquences de fonctionnement. Le gain est maximal lorsque le monopôle est bien adapté. La valeur maximale du gain du monopôle est 3,01 dBi dans la mesure de la chambre.

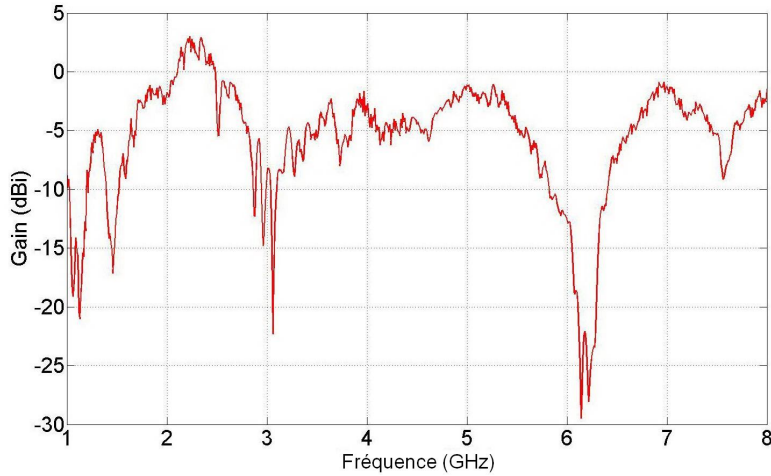


FIGURE 6.31: Gain mesuré de l'antenne monopôle

### ● Antenne monopôle court-circuitée

Le monopôle dispose d'une large bande passante, des propriétés de rayonnement quasi omnidirectionnel, d'une structure simple et d'une conception facile. Dans le but d'intégrer l'antenne monopôle et le circuit redresseur, l'antenne est modifiée de façon à intégrer la boucle DC, qui est une partie importante de circuit redresseur. Avec pour inspiration les antennes PIFA (Planar Inverted-F Antenna), un court-circuit est introduit à l'intérieur de la structure planaire du monopôle imprimé.

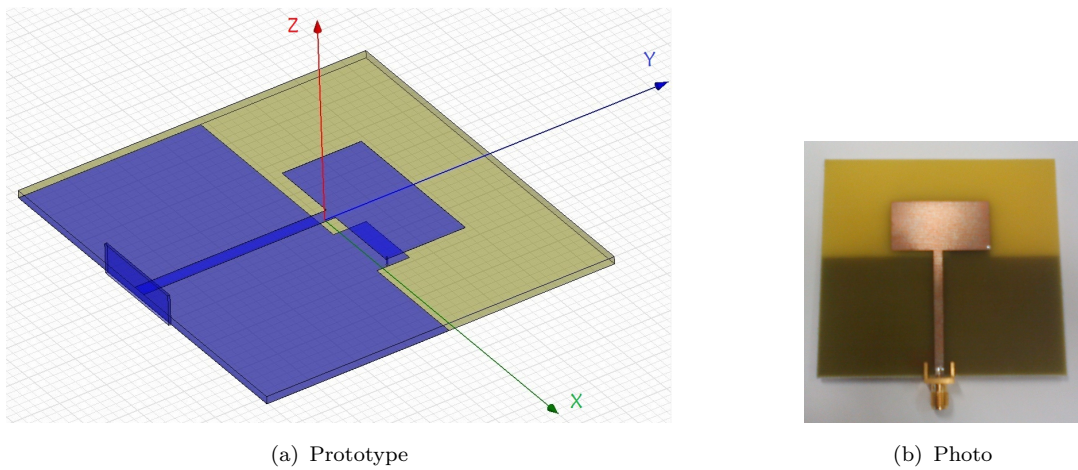


FIGURE 6.32: Antenne monopôle court-circuitée

Comme le montre la figure 6.32, un monopôle rectangulaire et une ligne d'alimentation micro-ruban d'impédance  $50 \Omega$  sont imprimés sur la face supérieure du substrat diélectrique Bernier FR4. La longueur et la largeur du monopôle sont 17 mm et 33,5 mm, environ 26 % et 51 % de la longueur d'onde guidée.

De l'autre côté du substrat, outre le plan de masse sous le linge d'accès, un petit bloc rectangulaire couvre le coin droit inférieur du monopôle. La longueur et la largeur du plan de masse sont 39 mm et 80 mm. La distance entre le point d'alimentation et le plan de masse est de 2 mm. La longueur et la largeur du bloc, où est situé le via, sont 7 mm et 14 mm. Le court-circuit est à 0,5 mm du bord droit et du bord inférieur du monopôle. Le trou d'interconnexion est de 0,4 mm de diamètre.

La figure 6.33 montre que la mesure est en accord avec la caractéristique large bande du monopôle simulée par HFSS. La bande passante mesurée est 1,07 GHz de 1,61 GHz à 2,68 GHz, tandis que celle simulée est 1,05 GHz de 1,7 GHz à 2,75 GHz. La différence entre la simulation et la mesure est due principalement à la modélisation du trou d'interconnexion et la tolérance de fabrication.

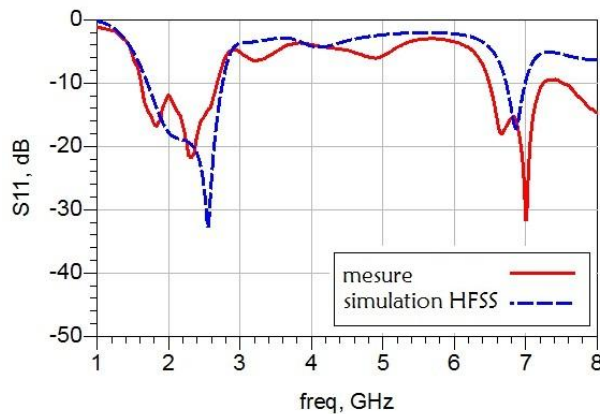


FIGURE 6.33:  $S_{11}$  simulé et mesuré d'antenne monopôle court-circuitée

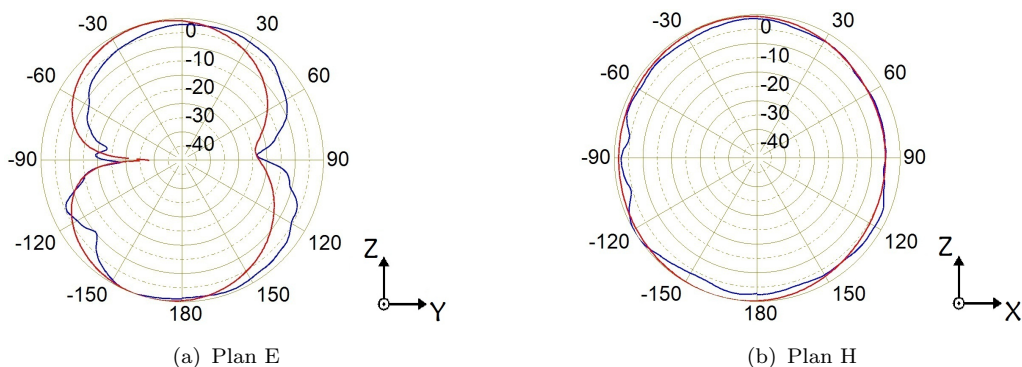


FIGURE 6.34: Les diagrammes de rayonnement simulés (courbe rouge) et mesurés (courbe bleue) d'antenne monopôle court-circuitée

La figure 6.34 présente les diagrammes de rayonnement normalisés mesurés et simulés en co-polarisation à 2,45 GHz. Les diagrammes mesurés dans le plan E et

dans les plans H suivent la forme des diagrammes obtenus dans la simulation. La courbe de mesure peut être influencée par l'interférence du connecteur et le câble coaxial. Le monopôle a la directivité 5,82 dBi en polarisation horizontale dans le plan E, alors que la directivité est 2,92 dBi en polarisation verticale dans le plan azimutal.

Sur le diagramme de rayonnement en plan H, la directivité est plus élevée dans la direction  $-90^\circ$  que  $0^\circ$ . Le diagramme de rayonnement dans le plan H n'est pas symétrique en raison de la conception spéciale du court-circuit.

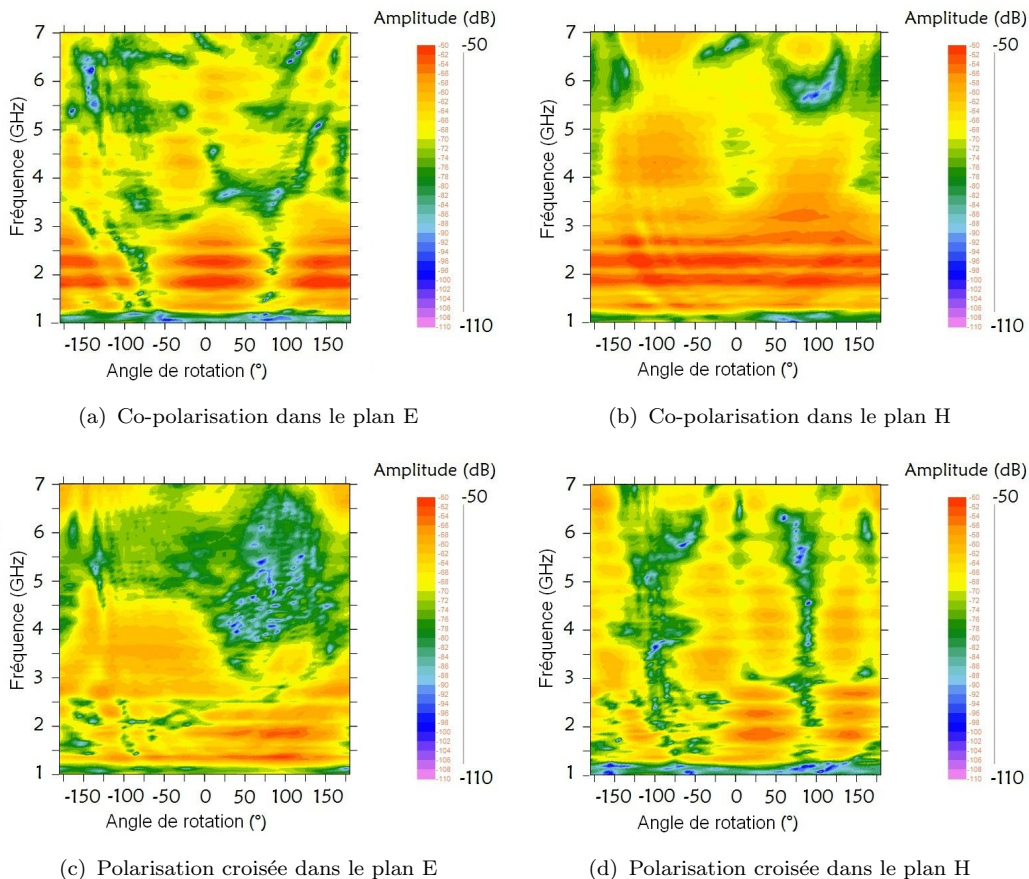


FIGURE 6.35: Les diagrammes de rayonnement en fonction de la fréquence et de l'angle de rotation pour l'antenne monopôle court-circuitée

Le monopôle modifié a une bande passante de  $-10$  dB de  $1,61$  GHz à  $2,68$  GHz. Cette dépendance en fréquence est aussi présentée dans les diagrammes de rayonnement, tel que présenté dans la figure 6.35. L'antenne capte beaucoup plus d'énergie si la fréquence de fonctionnement est située dans la bande d'adaptation, dans la direction principale par exemple. Mais elle absorbe moins d'énergie dans certaines directions. En comparaison avec le monopôle originel, la configuration

asymétrique avec le court-circuit influence la propriété de rayonnement dans le plan azimutal.

En utilisant la méthode de comparaison de gain, la figure 6.36 présente le gain mesuré de cette antenne. Le gain est maximal lorsque le monopôle est bien adapté. Le gain maximal est 2,71 dBi dans la mesure de la chambre anéchoïque.

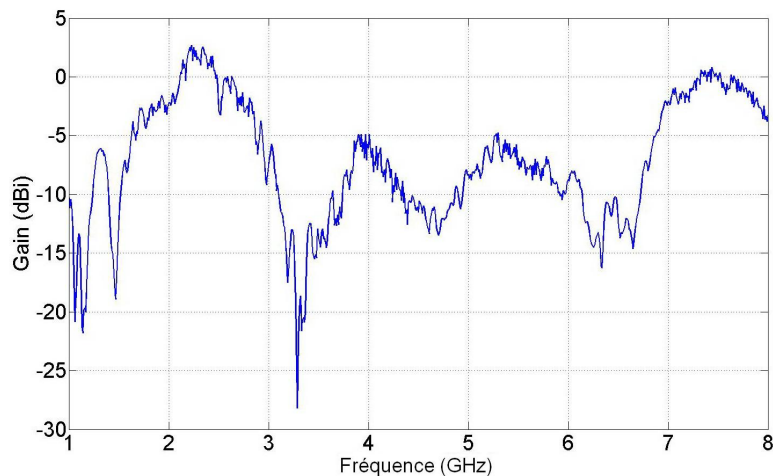


FIGURE 6.36: Gain mesuré de l'antenne monopôle court-circuitee

## Association et intégration de rectenna

Différentes configurations de rectenna sont proposées dans cette thèse. La rectenna est constituée de la partie rayonnante et de la partie de rectification. Basé sur l'étude des circuits de redressement, les antennes sont combinées avec ces circuits dans une configuration planaire. Le monopôle large bande et le monopôle court-circuité sont intégrés et fournissent une structure compacte.

### ● Rectenna pour les niveaux de puissance élevés

Pour l'application de transmission de puissance à haute densité de puissance, l'antenne redresseuse avec une diode Schottky HSMS-2820 a été conçue pour une puissance incidente 10 dBm. Une antenne patch, avec une bonne polarisation linéaire, alimentée par une sonde coaxiale est utilisée. Comme on le voit sur la figure 6.37, un circuit d'adaptation double stubs est utilisé pour adapter l'impédance d'entrée de diode à l'antenne. Un connecteur relie l'entrée du circuit de redressement et la sortie du patch.

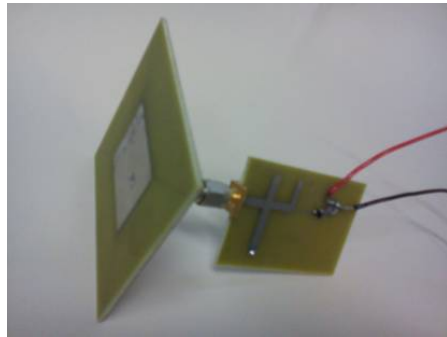


FIGURE 6.37: Rectenna pour des niveaux de puissance élevés

La mesure de l'antenne redresseuse a été effectuée dans une chambre anéchoïque. La tension continue de sortie est mesurée avec la configuration d'émetteur récepteur présentée sur la figure 6.38. Les rectennas intégrées sont fixées sur un plateau de positionnement. Une antenne cornet de gain 5 dBi, a été utilisée pour transmettre la puissance du générateur. La sortie de VNA transfère l'énergie RF à travers un amplificateur de gain 35 dB vers l'antenne d'émission. L'antenne redresseuse et le cornet sont placés à une distance de champ lointain. La rectenna reçoit la puissance RF et la convertit en une tension DC qui est mesurée par un voltmètre.

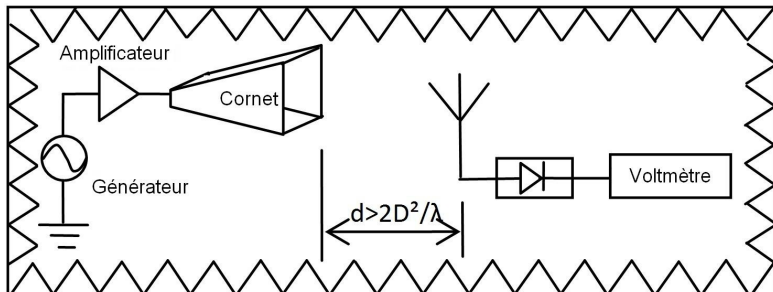


FIGURE 6.38: Montage expérimental de la rectenna avec une position mobile

La figure 6.39 et la figure 6.40 montrent les tensions redressées et les rendements de conversion de l'antenne redresseuse à fortes densités de puissance. La distance de 0,3 m est proche de la distance de Fraunhofer (0,32 m) alors que la position  $d = 0,5$  m se situe à une distance de champ lointain.

L'antenne redresseuse reçoit une puissance de -11 dBm à +13 dBm et génère la tension DC maximale de 1,7 V et un rendement de conversion maximal proche de 20 %. L'atténuation dans les câbles et les pertes d'espace réduit la puissance reçue de l'antenne redresseuse. Les valeurs d'atténuation d'espace libre sont 29,77 dB et 34,2 dB lorsque les distances sont respectivement de 0,3 m et 0,5 m. La rectenna peut évidemment capter plus d'énergie si un réseau d'antennes est utilisé.

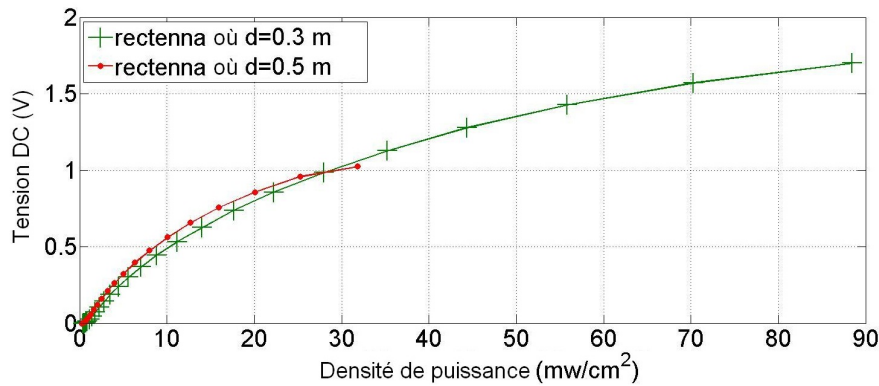


FIGURE 6.39: Tension DC de sortie de la rectenna pour les niveaux de puissance élevés

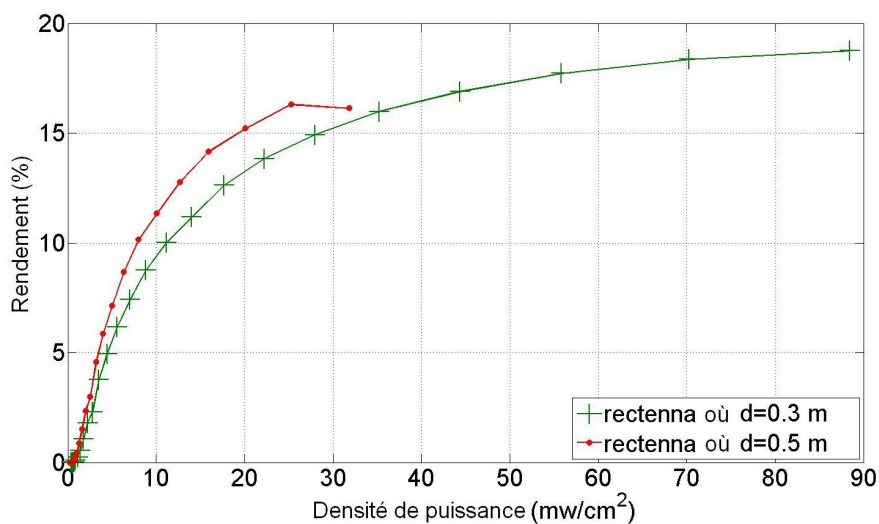


FIGURE 6.40: Rendement mesuré et simulé de la rectenna pour les niveaux de puissance élevés

### • Rectenna pour les faibles niveaux de puissance

Pour l'application de récupération d'énergie à faibles densités de puissance, la rectenna avec HSMS-2860 a été optimisée pour une puissance d'entrée -20 dBm. Les schémas ont été imprimés sur un substrat Bernier FR4 de permittivité relative  $\epsilon_r = 4,6$ , de hauteur  $h = 1,58$  mm et d'une tangente de perte de 0,02. Le rendement mesuré est de 5 % à 10 % lorsque les niveaux de puissance d'entrée sont de -20 dBm à -15 dBm. L'antenne redresseuse monopôle est illustrée sur la figure 6.41. Le monopôle rectangulaire et le circuit de redressement sont imprimés sur la même face du substrat diélectrique.  $L2$  et  $L1$  représentent la longueur et la largeur du monopôle. Le circuit d'adaptation simple stub,  $L6$  et  $L4$ , est conçu pour adapter

l'impédance d'entrée de la diode à celle du monopôle pour une puissance incidente -20 dBm à 2,45 GHz.

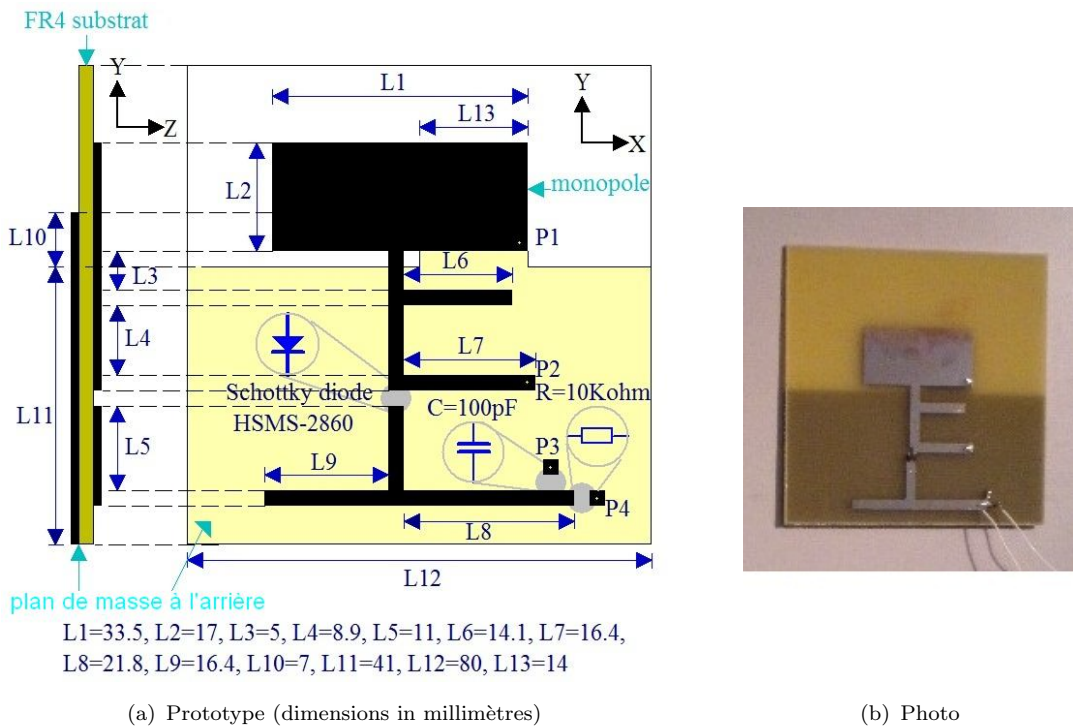


FIGURE 6.41: Rectenna I pour les faibles niveaux de puissance

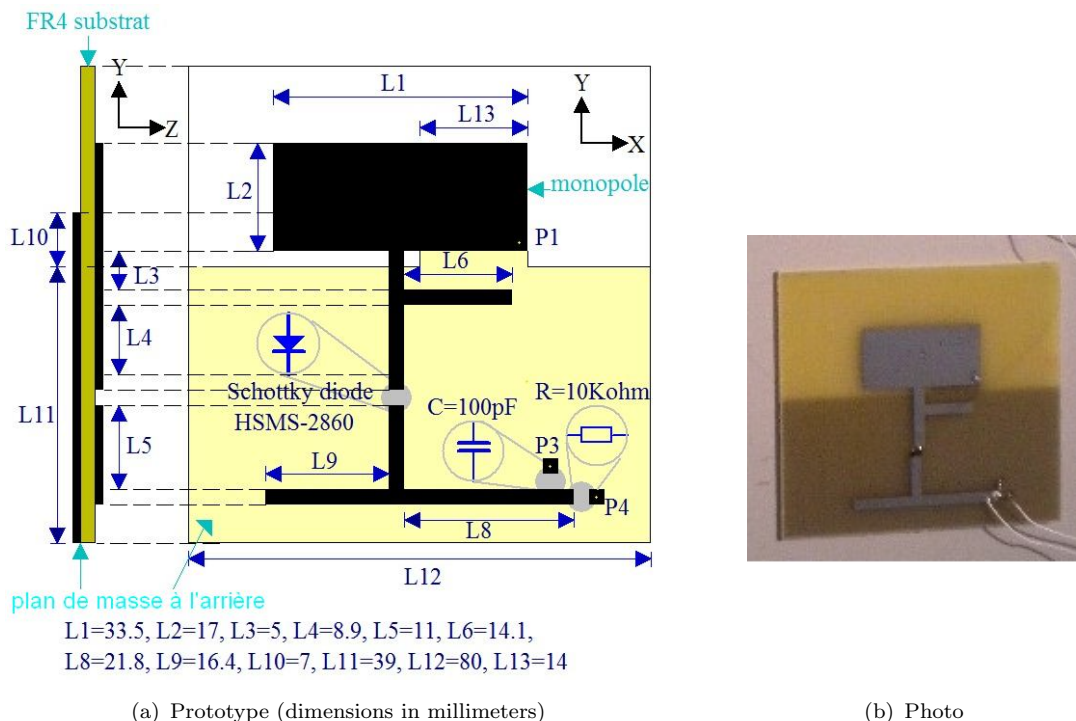
Un stub quart d'onde court-circuité  $L7$  est introduit pour constituer la boucle DC (Via-trou  $P2$  - diode Schottky - Charge - Via-trou  $P4$  - Plan de masse). Le filtre passe-bande d'entrée ( $L7$ ,  $L4$  et  $L6$ ) protège la fréquence fondamentale et stoppe les signaux harmoniques. Un filtre passe-bas de sortie est constitué par un tronçon ouvert quart d'onde  $L9$  et par une ligne de transmission demi longueur d'onde ( $L5$  et  $L8$ ).

De l'autre côté du substrat, le plan de masse ne couvre que la partie du circuit de redressement et le via de court-circuit  $P1$  du monopôle.  $L10$  et  $L13$  sont la longueur et la largeur du plan de masse situé sous le court-circuit. Le via est situé à 0,5 mm du coin inférieur droit du monopôle. La distance entre le point d'alimentation et le plan de masse égale à 2 mm.

Les dimensions du monopôle et du plan de masse, la distance entre le point d'alimentation et le plan de masse et le point de court-circuit sont les paramètres qui affectent le fonctionnement de l'antenne. Un gain de 2,71 dBi et une largeur de bande de 1 GHz sont atteints pour une conception optimale. Le monopôle large

bande permet de relâcher les contraintes sur le circuit d'adaptation entre l'antenne et le circuit redresseur à bande passante étroite.

Afin d'obtenir une rectenna plus compacte, nous utilisons le court circuit de l'antenne au lieu du stub court-circuité. Tel que présenté sur la figure 6.42, le circuit d'adaptation simple stub comprend un tronçon ouvert  $L_6$  et une ligne micro-ruban série  $L_4$ . Cette conception réduit la surface de la rectenna et c'est une étape pour la structure compacte. La boucle DC est modifiée de la rectenna I (Via-trou  $P_2$  - diode Schottky - Charge - Via-trou  $P_4$  - Plan de masse) à la rectenna II (Via-trou  $P_1$  - diode Schottky - Charge - Via-trou  $P_4$  - Plan de masse).



(a) Prototype (dimensions in millimeters)

(b) Photo

FIGURE 6.42: Rectenna II pour les faibles niveaux de puissance

En comparaison de la performance des rectennas intégrées avec ou sans stub court-circuité, certains signaux harmoniques rejetés dans la rectenna I ne sont pas rejetés complètement par le circuit d'adaptation de la rectenna II. Les harmoniques ne sont plus réfléchis et sont alors rayonné. Par conséquent, l'impédance d'entrée des circuits redresseurs change, ce qui peut influer sur le niveau d'adaptation entre le circuit et l'antenne.

Les rectennas intégrées sont positionnées à une distance de 5,856 m de l'antenne cornet dans la chambre anéchoïque. Selon l'équation de transmission de Friis, la densité de puissance à la position de la rectenna est déterminée. Les tensions DC

mesurées augmentent avec une augmentation de la densité de puissance, comme le montre la figure 6.43. Lorsque le monopôle et les rectennas sont en polarisation verticale, et perpendiculaire à la direction de propagation, elles captent l'énergie micro-ondes à de faibles densités de puissance. Le circuit de redressement connecté au monopôle produit la tension DC maximale 130 mV pour une densité de puissance de  $2,1 \mu\text{W}/\text{cm}^2$ , contre 20 mV par la rectenna I et 40 mV par la rectenna II.

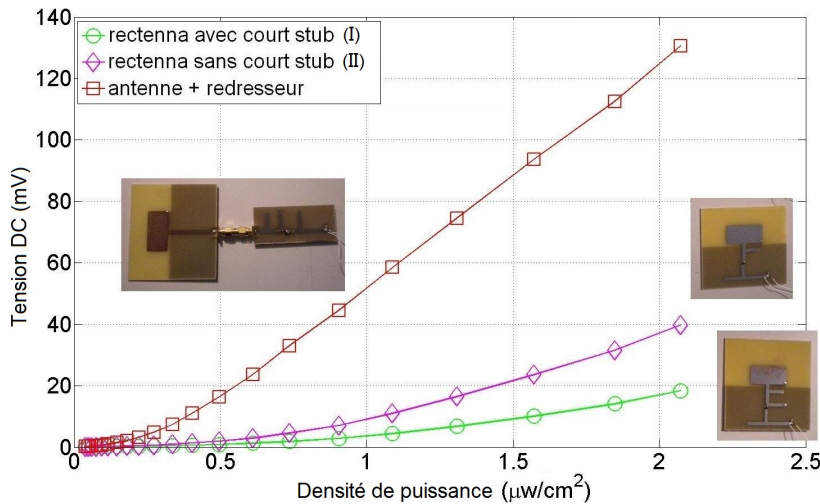


FIGURE 6.43: Tension DC de sortie des rectennas I et II en fonction de la densité de puissance à  $0^\circ$

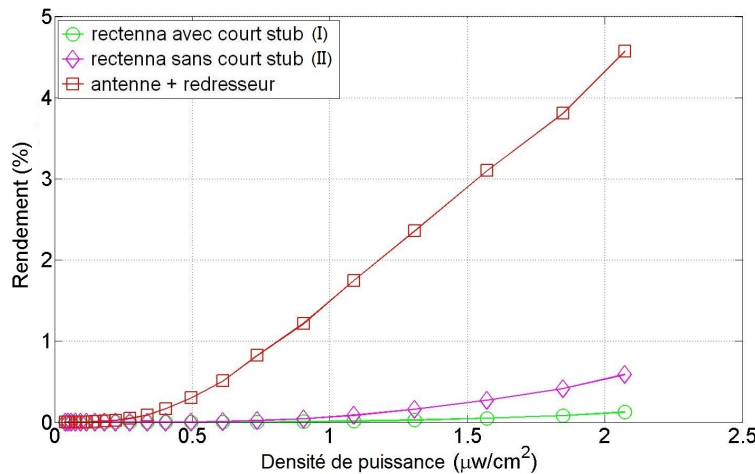


FIGURE 6.44: Rendement équivalent des rectennas I et II en fonction de la densité de puissance à  $0^\circ$

Dans le cas de l'antenne monopôle associé au circuit de redressement par un connecteur, l'antenne de réception reçoit une puissance RF autour de -15 dBm et le rendement du circuit redresseur est d'environ 5 %. Toutefois, lorsque les

rectennas intégrées I et II fonctionnent à des niveaux de puissance inférieurs à -20 dBm, il est estimé que ces rectennas présentent des rendements inférieurs à 1 %.

Dans le cas des rectennas intégrées, rectennas I et II, les niveaux d'adaptation changent. Cela conduit à des moins bonnes performances que le monopôle lié au circuit de redressement par un connecteur. Il est actuellement impossible d'extraire le niveau d'adaptation entre les antennes et les circuits de redressement dans les cas des rectennas intégrées, même par l'analyse en co-simulation avec ADS.

Lorsque la polarisation de l'onde est parallèle à la surface de l'antenne et qu'elle vient de la direction -90° par rapport à la direction principale, le circuit de redressement connecté au monopôle produit la tension maximale 279 mV à la densité de puissance  $2,1 \mu\text{W/cm}^2$  comparativement à 250 mV pour la rectenna I et à 100 mV pour la rectenna II, comme montré sur la figure 6.45.

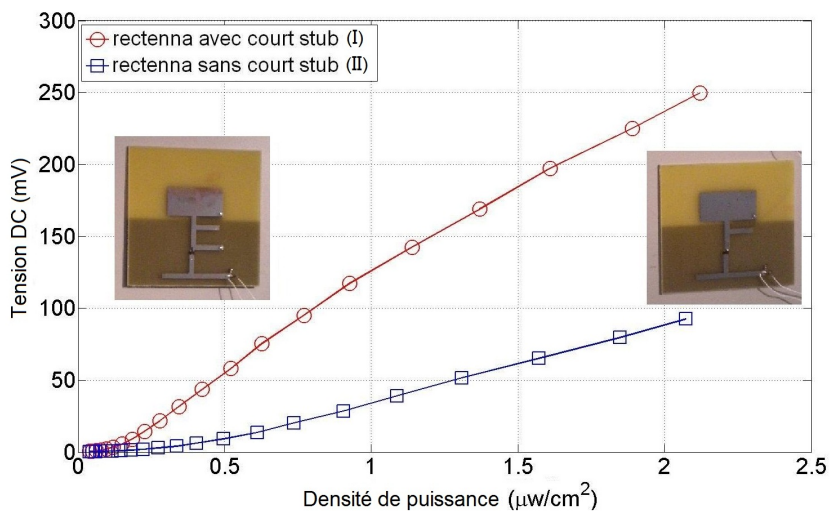


FIGURE 6.45: Tension DC de sortie des rectennas I et II en fonction de la densité de puissance à -90°

Dans ce cas, la puissance reçue par le monopôle est environ -10 dBm et le rendement du circuit redresseur est 21 %. En outre, la rectenna I présente un rendement équivalent d'environ 16 %, soit une meilleure performance que la rectenna II qui a un rendement équivalent de 3 %. L'idée de la rectenna II réduit la surface de rectenna et donne une possibilité d'intégration. Le choix de la rectenna la plus performante est difficile à déterminer. En effet, en pratique la position relative entre les sources ambiantes et des capteurs est inconnue. La performance de rectenna est alors liée à l'emplacement et à l'orientation des capteurs.

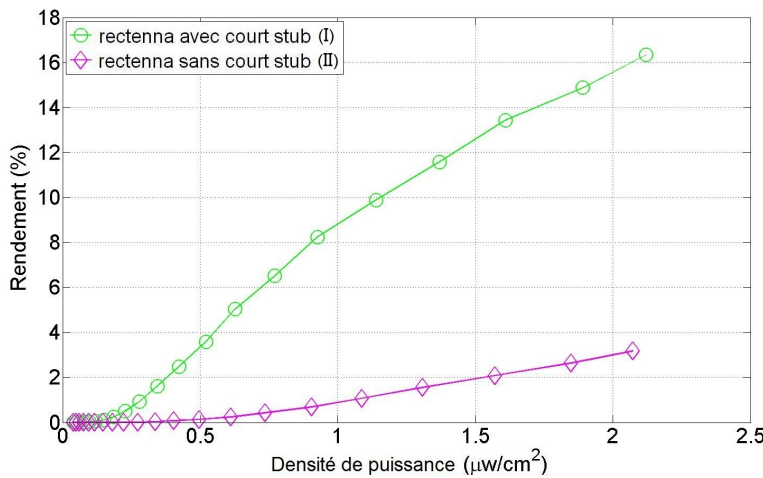


FIGURE 6.46: Rendement équivalent des rectennas I et II en fonction de la densité de puissance à -90°

### ● Rectenna à haute efficacité

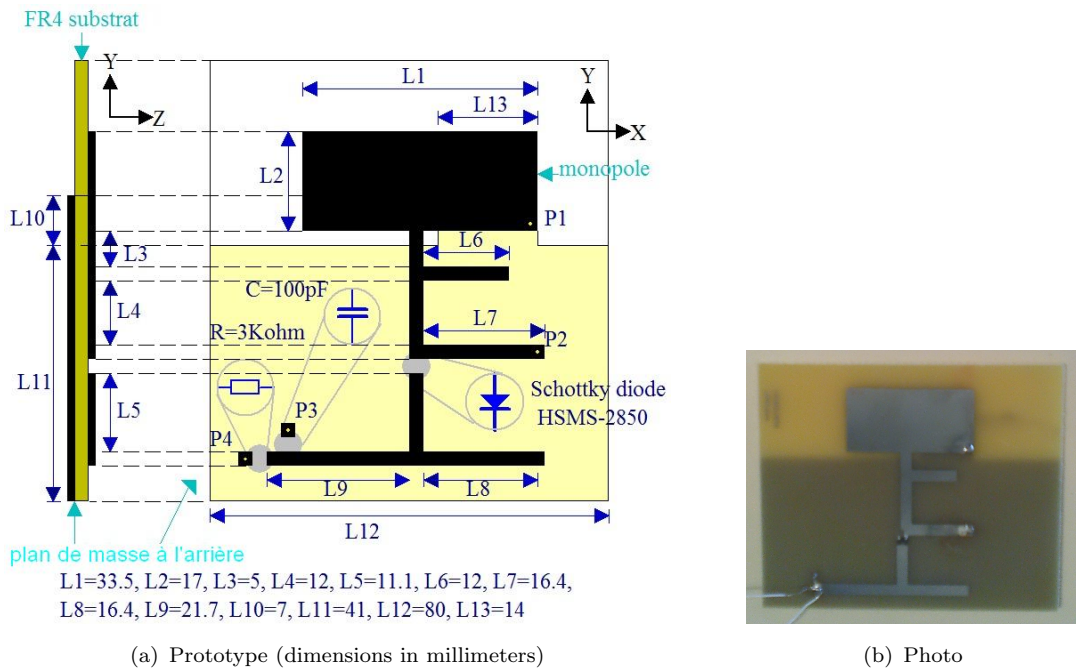


FIGURE 6.47: Rectenna III à haute efficacité

Dans le but d'obtenir un rendement de conversion élevé à faibles densités de puissance, l'antenne redresseuse avec une diode HSMS-2850 a été introduite en raison de la très bonne sensibilité de cette diode pour des faibles niveaux de puissance, en dépit de non recommandation pour cette bande de fréquence. Le circuit de redressement avec la diode HSMS-2850 a été imprimé avec le monopôle

modifié sur un substrat Bernier FR4, tel que présenté sur la figure 6.47. Un court-circuit est introduit dans l'antenne monopôle. Le monopôle modifié se compose d'un monopôle imprimé ( $L2 \times L1$ ) avec la structure à court circuit  $P1$ .

Le circuit de redressement est conçu avec la diode Schottky HSMS-2850 et le circuit d'adaptation de stub unique ( $L6$  et  $L4$ ). Un stub quart d'onde  $L7$  contribue à la boucle DC (Via-trou  $P1$  - diode Schottky - Charge - Via-trou  $P4$  - Plan de masse). La résistance de charge est optimisée à  $3\text{ k}\Omega$  avec une capacité en parallèle est  $100\text{ pF}$ . Le filtre passe-bas de sortie est constitué par un stub quart d'onde  $L8$  et des lignes micro-ruban,  $L9$  et  $L5$ .

De l'autre côté du substrat, le plan de masse couvre uniquement la partie du circuit de redressement et la via  $P1$ . Le pad ( $L10 \times L13$ ) est situé en dessous pour connecter le via au plan de masse. La distance entre le point d'alimentation et le plan de masse est de 2 mm.

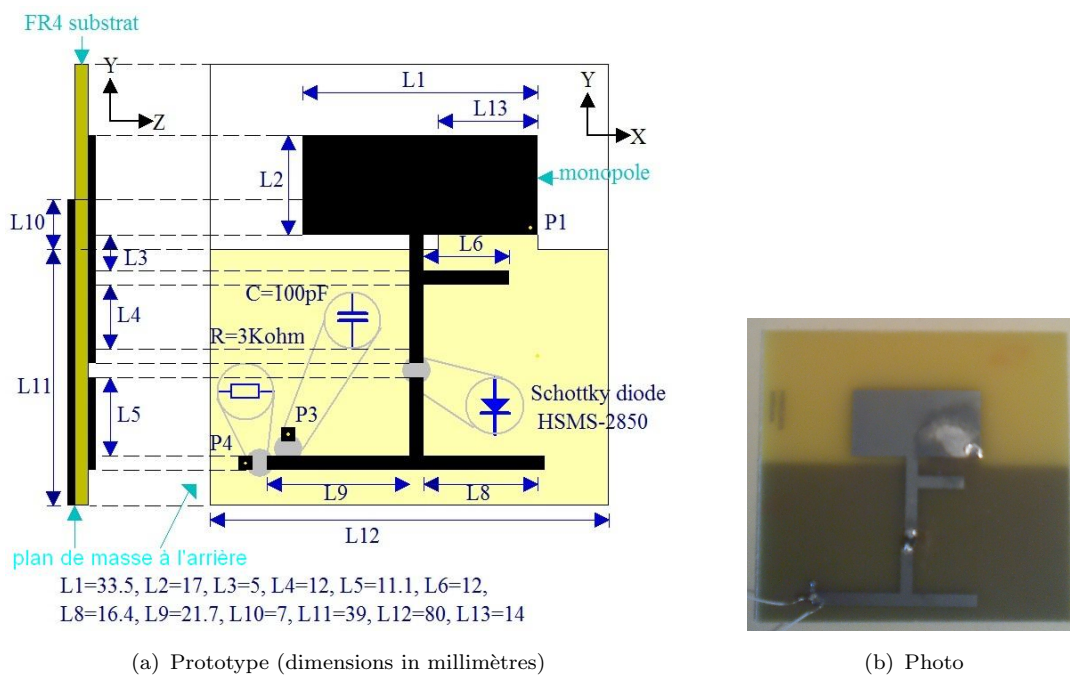


FIGURE 6.48: Rectenna IV à haute efficacité

Basé sur l'étude de la rectenna I et la rectenna II pour la récupération d'énergie à des densités de puissance faibles, et la rectenna III pour un rendement de conversion élevé, la rectenna IV est proposée avec un avantage de réduction de la surface. Tel que présenté dans la figure 6.48, le monopôle ( $L2 \times L1$ ) est intégré à un circuit de redressement avec une ligne d'alimentation de 5 mm. Le circuit d'adaptation ( $L6$  et  $L4$ ) est utilisé pour adapter l'impédance d'entrée de la diode à l'impédance

de l'antenne. Le filtre passe-bas ( $L5$ ,  $L9$ , et le tronçon ouvert quart d'onde  $L8$ ) protège le signal DC et rejette les harmoniques. Le plan indique clairement qu'un court tronçon quart d'onde est supprimé par comparaison avec la rectenna III. Ainsi, la boucle de courant continu est formée à travers le trou d'interconnexion  $P1$ , une diode Schottky, la charge, et le trou d'interconnexion  $P4$ .

De l'autre côté du substrat, le plan de masse ( $L11 \times L12$ ) et le bloc ( $L10 \times L13$ ) relié au monopôle, par le via  $P1$  sont optimisés dans des simulations HFSS. La distance entre le point d'alimentation et le plan de masse est identique. Cette rectenna a été gravée sur un substrat Bernier FR4.

Le monopôle modifié associé avec un circuit de redressement, et les rectennas III et IV sont été mesurés en chambre anéchoïque. La rectenna III produit une tension continue élevée à de faibles densités de puissance. Tel que présenté dans la figure 6.49, la tension DC est 208,4 mV à la densité de puissance  $2,1 \mu\text{W/cm}^2$ , par rapport à la configuration non intégré (210,6 mV).

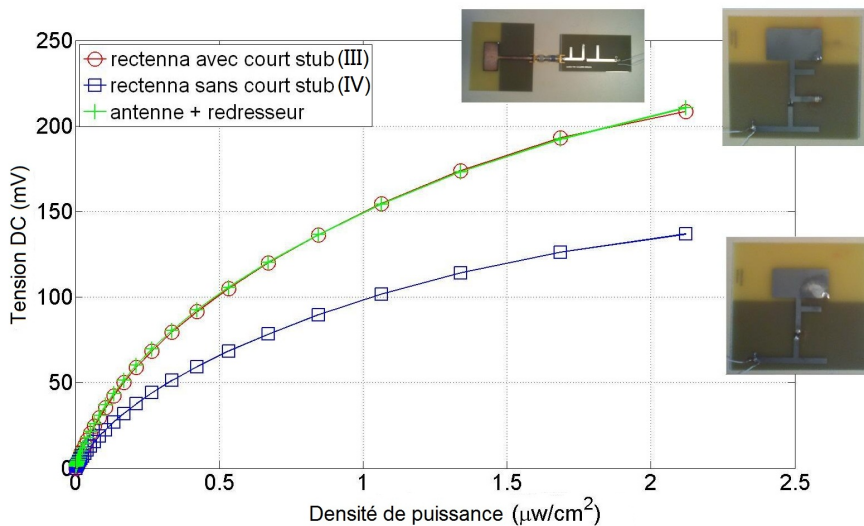


FIGURE 6.49: Tension DC de sortie des rectennas III et IV en fonction de la densité de puissance à  $0^\circ$

En supposant que le rayonnement du monopôle ne soit pas perturbée par le circuit de redressement, l'efficacité équivalente est d'environ 31 % et la puissance captée est estimée à -13,3 dBm. Ces deux antennes redresseuses sont basées sur la même configuration. Les circuits redresseurs sont similaires, mais les méthodes d'intégration sont différentes.

Sur la base de la configuration planaire de la rectenna III, la rectenna IV est une amélioration de la boucle DC qui diminue la surface de la rectenna. Toutefois,

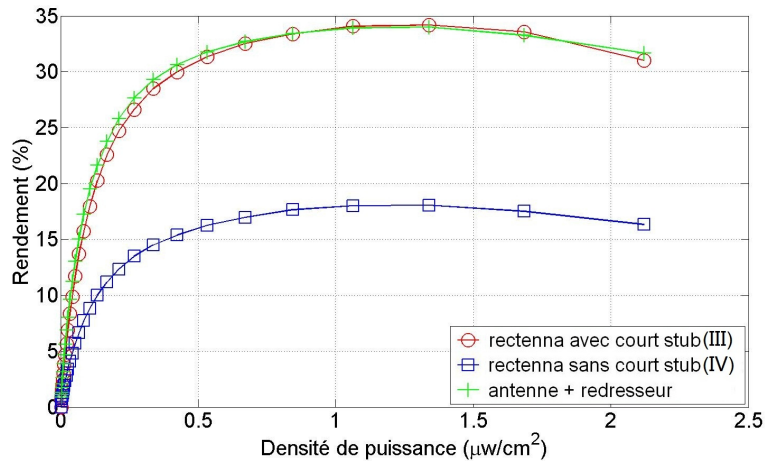


FIGURE 6.50: Rendement équivalent des rectennas III et IV en fonction de la densité de puissance à 0°

le stub court-circuité quart d'onde L7 à l'intérieur de la rectenna III contribue non seulement à la boucle DC mais aussi bloque les signaux harmoniques. La rectenna IV sans ce stub est influencée par la réflexion des harmoniques et la tension DC du circuit de redressement est réduite. La rectenna IV donne une tension DC 136,8 mV pour un niveau de densité de puissance 2,1  $\mu\text{W}/\text{cm}^2$ . L'efficacité équivalente est d'environ 16 % et la puissance d'entrée est estimée à -14 dBm.

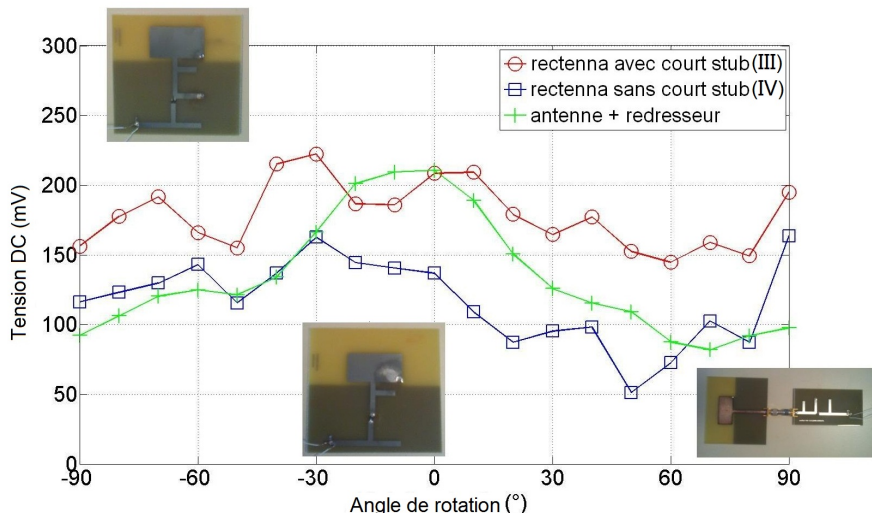


FIGURE 6.51: Tension DC de sortie des rectennas III et IV en fonction de l'angle de rotation

La figure 6.51 présente les tensions DC mesurées de ces rectennas en fonction de l'angle de rotation. La rectenna avec la configuration non planaire donne une tension de sortie et un rendement maximal (210,6 mV et 32 %) dans la direction principale. La rectenna III donne une tension de sortie et un rendement meilleur

Design	Rectenna avec patch et diode HSMS-2820	Rectenna I (monôpole et diode HSMS-2860)	Rectenna II (monôpole court-circuité et diode HSMS-2860)	Rectenna III (monôpole et diode HSMS-2850)	Rectenna IV (monôpole et diode HSMS-2850)
Charge	$820\Omega$	$10k\Omega$	$10k\Omega$	$3k\Omega$	$3k\Omega$
Fréq	2,45GHz	2,44GHz	2,45GHz	2,35GHz	2,42GHz
$A_e$	$13\text{cm}^2$	$18\text{cm}^2$	$13\text{cm}^2$	$22\text{cm}^2$	$18\text{cm}^2$
$\eta_{max}$	16%	16%	3%	34%	18%
$p$	$32\text{mW/cm}^2$	$2,1\mu\text{W/cm}^2$	$2,1\mu\text{W/cm}^2$	$1,3\mu\text{W/cm}^2$	$1,3\mu\text{W/cm}^2$
$P_{in}$	9dBm	-14,2dBm	-15,7dBm	-15,3dBm	-16,2dBm
$\eta_{moyen}$				23%	13%
Cons	ISM, high power	ISM, low power	ISM, low power	ISM, low power	ISM, low power

TABLE 6.3: Les résultats mesurés des rectennas

(222,3 mV et 35,65 %) dans la direction -30°. La valeur la plus faible est obtenue dans la direction 60° avec une tension de 144,7 mV et un rendement de 15,11 %. La rectenna IV donne également des valeurs de tension et de rendement différentes suivant l'angle de rotation. La plus forte tension est de 163,6 mV à -30° et le rendement équivalent est de 23,6 %. La plus faible tension est de 51,2 mV à 50° et le rendement est d'environ 2,31 %.

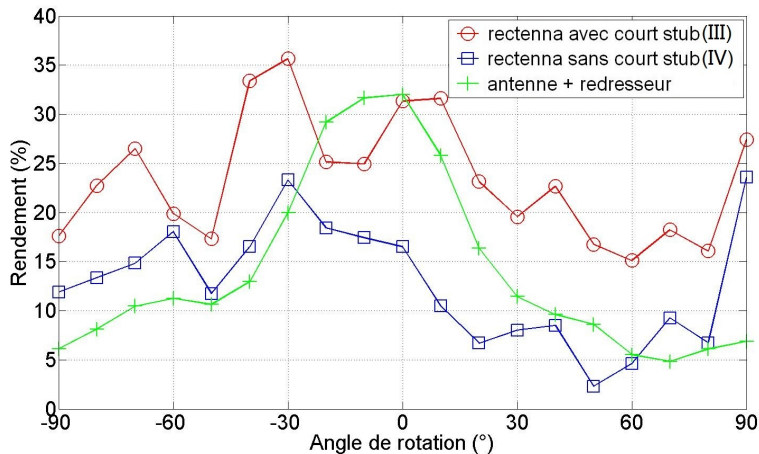


FIGURE 6.52: Rendement équivalent des rectennas III et IV en fonction de l'angle de rotation

Dans les cas pratiques, la position relative entre les sources ambiantes et les capteurs n'est pas connue et n'importe quelle direction peut être concernée. Le rendement moyen et la tension moyenne peuvent dans ce cas définir le critère de performance de la rectenna. Nous obtenons dans ce cas une tension DC moyenne

de 178,8 mV et un rendement équivalent de 23 % pour une densité de puissance  $2,1 \mu\text{W}/\text{cm}^2$ . Tel que présenté dans le tableau 6.3, plus de 20 % de l'énergie micro-ondes est récoltée par les rectennas proposées.

## Conclusions

Dans la transmission d'énergie sans fil et de la récupération d'énergie, le niveau de puissance peut être faible ou élevé en fonction de l'emplacement des capteurs sans fil, de la distance entre la station de base et les capteurs et la puissance d'émission. Dans le cadre de la récupération d'énergie, l'antenne redresseuse est une sorte de batterie sans fil au lieu d'une batterie traditionnelle. Elle capte l'énergie des micro-ondes à partir du rayonnement ambiant, et la transforme en énergie DC utile. Généralement la densité de puissance est faible en raison des normes sanitaires.

Tout d'abord, nous avons fait l'étude bibliographique des circuits de redressement, des antennes et des rectennas. Dans le but de minimiser la perte de conduction des diodes et d'optimiser la tension DC de sortie, la configuration à diode unique en série est choisie pour le processus de rectification. Les éléments de redressement, en particulier des diodes Schottky, sont étudiés à l'aide des outils de simulation. Le modèle de circuit équivalent est décrit soit avec les paramètres SPICE de la diode soit avec le modèle de simulation ADS. Les approches de simulation ADS sont utilisées dans la modélisation de la diode et la simulation du circuit de redressement. Les outils SP et LSSP analysent les paramètres S dans le domaine fréquentiel. Associé à des analyses paramétriques, HBS montre le comportement non linéaire de la diode et donne les paramètres S en fonction de la puissance. Les circuits de redressement sont conçus sur la base d'optimisation hybride.

Les différentes configurations d'antennes sont analysées en simulation à l'aide de HFSS dans l'objectif de capter le maximum d'énergie RF. Le choix s'est porté sur l'antenne patch, simple à réaliser, à polarisation linéaire et à bande étroite. Puis l'antenne monopôle a été choisie afin de réduire les dimensions et d'augmenter la bande passante. Inspiré par les structures d'antennes PIFA, le monopôle court-circuité à une large bande passante et des bonnes propriétés de rayonnement. Il offre la possibilité de concevoir une antenne redresseuse compacte.

Design	Rectenna patch à base d'une ouverture couplé	Rectenna bi-bande à anneau hybride à double fente circulaire	Redresseur réalisé avec un résonateur à quartz	Rectenna à base d'une antenne spirale	Rectenna III (monopôle et diode HSMS-2850)
Auteur	S.Rivière	Z.Saddi	T.Ungan	D.Bouchouicha	Y.Zhou
Année	2010	2013	2009	2010	2013
$\eta$	29%	10,5%	22%	0,7%	34%
$p$	$5,37\mu\text{W}/\text{cm}^2$ (-15dBm)	0,13 and 0,248 $\mu\text{W}/\text{cm}^2$ (-20dBm)	-30dBm	$3,55\text{nW}/\text{cm}^2$ (-38dBm)	$1,3\mu\text{W}/\text{cm}^2$ (-15,3dBm)
Fréq	2,45GHz	1,8 and 2,35GHz	24MHz	1,85GHz	2,35GHz
Cons	ISM, low power	GSM and ISM, low power	Medium wave, low power	GSM, low power	ISM, low power

TABLE 6.4: Comparaison des rectennas

Dans le chapitre sur l'association et l'intégration de rectenna, nous avons proposé plusieurs structures des rectennas coplanaires ou non planaires. La rectenna avec l'antenne patch et la diode Schottky HSMS-2820 produit la tension maximale 1,7 V et le rendement 18,75 % pour une densité de puissance de  $88,42 \text{ mV}/\text{cm}^2$ . La rectenna avec l'antenne monopôle et la diode Schottky HSMS-2860 donne la tension maximale 250 mV pour une densité de puissance  $2,1 \mu\text{W}/\text{cm}^2$ . Environ 10 % de l'énergie RF peut être recyclée à ce niveau de puissance faible.

Un rendement élevé pour de faibles niveaux de puissance est obtenu avec la rectenna constituée du monopôle et de la diode Schottky HSMS-2850. Elle produit une tension DC de 208,4 mV et un rendement équivalent de 31 % pour une densité de puissance de  $2,1 \mu\text{W}/\text{cm}^2$ . La position arbitraire entre les capteurs et les sources ambiantes, nous a conduits à introduire la valeur moyenne de la tension DC et de rendement pour caractériser les rectennas. Une tension moyenne de 178,8 mV et un rendement moyen de 23 % sont obtenus. Tel que présenté dans le tableau 6.4, les rectennas proposées possèdent une bonne performance dans la demande de faible puissance à la fréquence ISM. Par conséquent, elles peuvent être utilisées dans la transmission d'énergie point-à-point de faibles niveaux de puissance ou sur une longue distance. En outre, les batteries d'appareils sans fil peuvent être chargées par ces rectennas qui captent l'énergie RF à partir de sources ambiantes

à faible rayonnement. La puissance disponible en sortie représente environ 10 % de la consommation d'un capteur (100  $\mu$ W).

## Perspectives

Dans les applications de transmission de puissance et la récupération d'énergie, peu importe si le niveau de puissance est élevé ou faible, l'objectif principal de la conception de rectenna est d'obtenir un rendement de conversion élevé. Ainsi, la conception peut être améliorée dans la manière de la récupérer et de redresser l'énergie RF.

Dans le processus de réception d'énergie, la puissance maximale doit être collectée et transférée au circuit de redressement. Des antennes larges bandes et des grands réseaux d'antennes peuvent être utilisés pour capter l'énergie RF. L'antenne large bande permet de récupérer la puissance RF à partir de diverses sources. Une antenne à polarisation circulaire peut permettre de maximiser le rendement quel que soit l'orientation de la rectenna. En tenant compte du compromis entre la taille et le gain de l'antenne, les réseaux d'antenne augmentent la puissance incidente pour le redressement.

Dans le processus de conversion d'énergie, l'amélioration de l'efficacité de conversion à l'intérieur du circuit de redressement est la clé pour augmenter l'efficacité globale du système de rectenna. Un élément de redressement non linéaire tel que la diode Schottky, détermine la performance du circuit redresseur. Les caractéristiques RF de diode déterminent la gamme de fréquence de fonctionnement et les niveaux de puissance disponibles dans le processus de rectification.

Par exemple, les diodes Schottky HSMS-2820 et HSMS-2860 ont les petites résistances en série et les grandes tensions de claquage. Ces diodes soutiennent des niveaux de puissance élevés et elles sont adaptées à la transmission de puissance avec moins de perte de conduction. Les autres exemples sont les diodes Schottky HSMS-2850 et SMS7630. Ces diodes possèdent des petites tensions de seuil et elles sont appropriées aux applications de récupération d'énergie à faibles niveaux de puissance. Bien qu'ils possèdent de grandes résistances séries, la perte de conduction n'est pas un facteur dominant lorsque le courant direct est très faible, notamment à faible densité de puissance.

Avec le développement des dispositifs semi-conducteur, l'ambition est de rechercher une diode qui possède des bonnes caractéristiques aux fréquences ISM et de télécommunication mobile. Le plus important est qu'elle ait une faible tension de seuil et une faible résistance série. L'antenne redresseuse avec une telle diode peut fonctionner à faibles densités de puissance, et alimenter des appareils sans fil dans des divers environnements.

Les rectennas proposées dans ma thèse sont imprimées sur un substrat Bernier FR4 de permittivité relative  $\varepsilon_r = 4,6$ , de hauteur  $h = 1,58$  mm et d'une tangente de perte  $\tan\delta = 0,02$ . La tangente de perte du substrat diélectrique utilisé est relativement élevé par rapport à d'autres matériaux diélectriques, par exemple Arlon Diclad 527 substrat de permittivité relative  $\varepsilon_r = 2,55$ , de hauteur  $h = 0,762$  mm et d'une tangente de perte  $\tan\delta = 0,0025$ . L'utilisation des matériaux à faible perte diminue la perte diélectrique, et par conséquent un nouveau substrat à faible tangente de perte est bénéfique pour le rendement de conversion.

**Mot clés:** Récupération d'énergie électromagnétique, rectenna, conversion RF/DC, diode Schottky, antenne.



# Thèse de Doctorat

**Yuwei ZHOU**

**Contribution à la récupération de l'énergie électromagnétique ambiante pour les objets communicants autonomes**

**Contribution to electromagnetic energy harvesting for wireless autonomous devices**

## Résumé

Les travaux de cette thèse sont axés sur la récupération de l'énergie électromagnétique ambiante en vue d'améliorer la durée de vie des objets communicants autonomes.

Les émissions radiofréquences de la téléphonie mobile et sans fil, du wifi et éventuellement de la radio et la télévision peuvent être captées et transformées en tension continue pour alimenter des systèmes nomades tels que les téléphones portables, les capteurs sans fils de données environnementales, les ordinateurs, etc. Une antenne large bande ou multi-bande associée à un circuit de redressement haute fréquence, à base de diode Schottky doit être optimisée pour la réception et le redressement des puissances faibles de ces émissions (de l'ordre de quelques micro watt par cm<sup>2</sup>). Un travail important sur l'optimisation à la fois dans le domaine de fréquence et surtout dans le domaine de puissance est effectué dans cette thèse. Les simulateurs hautes fréquences circuit ADS et électromagnétique HFSS sont utilisés pour concevoir les antennes redresseuses. Les rendements de conversion obtenus suite aux travaux de cette thèse placent le laboratoire au niveau de l'état de l'art international.

## Mots clés

Récupération d'énergie électromagnétique, Antenne, Diode Schottky, Redresseur, Rectenna.

## Abstract

The research works of this thesis are focused on the ambient electromagnetic energy harvesting to improve the life time of wireless autonomous devices. The waves produced by cellular telephones, Wireless Internet and also radio and television transmissions may be captured and rectified to produce a continuous voltage able to supply mobile phones, environment data sensors, computers, etc. Broadband or multiband antennas, combined to a high frequency rectifying circuits with Schottky diodes must be optimized for the reception and rectifying of a very low level electromagnetic power (about a few micro watts per cm<sup>2</sup>). In this thesis, an important optimization work is done in frequency domain and especially in power domain. The high frequency circuit simulator ADS and high frequency electromagnetic simulator HFSS, are used to design the rectenna. The obtained conversion efficiencies place our laboratory in the international state of the art in electromagnetic energy harvesting.

## Key Words

Energy harvesting, Antenna, Schottky diode, Rectifier, Rectenna.